Heinrich Heine
Universität
Düsseldorf

Receptor signaling specificity in plants

Inaugural-Dissertation

zur Erlangung des Doktorgrades
der Mathematisch-Naturwissenschaftlichen Fakultät
der Heinrich-Heine-Universität Düsseldorf

vorgelegt von

Patrick Blümke, geb. Schultz

aus Rüdesheim am Rhein

Düsseldorf, November 2020

aus dem Institut für Entwicklungsgenetik
der Heinrich-Heine-Universität Düsseldorf

Gedruckt mit der Genehmigung der
Mathematisch-Naturwissenschaftlichen Fakultät der
Heinrich-Heine-Universität Düsseldorf

Berichterstatter:

1. Prof. Dr. Rüdiger Simon
2. Prof. Dr. Georg Groth

Tag der mündlichen Prüfung: 18.02.2021

Eidesstattliche Versicherung zur Dissertation mit dem Titel:

Receptor signaling specificity in plants

Ich versichere an Eides Statt, dass die Dissertation von mir selbständig und ohne unzulässige fremde Hilfe unter Beachtung der „Grundsätze zur Sicherung guter wissenschaftlicher Praxis an der Heinrich-Heine-Universität Düsseldorf“ erstellt worden ist.

Außerdem versichere ich, dass ich diese Dissertation nur in diesem und keinem anderen Promotionsverfahren eingereicht habe und dass diesem Promotionsverfahren kein gescheitertes Promotionsverfahren vorausgegangen ist.

Düsseldorf, 26.11.2020

Ort, Datum

Unterschrift

Index

Aims of the study

Plants communicate via dynamically regulated information systems, which typically comprise mobile signaling molecules, plasma membrane (PM)-located receptors, and intracellular target proteins. This study aims to contribute to the understanding of signal transduction through CLAVATA family (CLVf) receptor pathways in the model organism *Arabidopsis thaliana*.

CLVf receptors are crucial for various aspects of plant life like stem cell homeostasis, vascular development, and pathogen interactions. To perceive peptide ligands of the CLV3/EMBRYO SURROUNDING REGION-related (CLE) family, different CLVf receptors and other proteins, e.g. co-receptors or the CLAVATA2 (CLV2) / CORYNE (CRN) heteromer, form complexes at the PM. Depending on the cellular context, the same repertoire of CLVf receptors mediates distinct signaling outputs. However, it is not clear how CLE peptides signals are integrated after receptor activation to confer specificity to each pathway. Furthermore, downstream targets of the CLVf receptors are not known, either. Therefore, this study addresses two major open questions within CLVf receptor research, i.e. downstream signaling and signaling specificity.

Chapter I provides a recent literature overview on how receptor pathways in plants gain specificity despite a high degree of shared signaling elements.

Chapter II comprises the identification and characterization of novel CLVf receptor interactors. Protein-protein interaction studies and genetic analyses will be applied to test the capability of the receptor-like cytoplasmic kinase (RLCK) MAZZA (MAZ) and its homologs to act as downstream mediators of CLVf receptor signaling. Furthermore, a new role of CLVf receptor pathways in stomatal development will be accessed.

Chapter III addresses the role of CRN and CLV2 within root meristem differentiation, where CRN is mandatory for CLE peptide perception, potentially by guiding PM-localization of CLVf receptors. A dissection of the *CRN* expression domain will reveal the spatial impact of the protein within distinct cell files of the root meristem and if CLE peptides act non-cell-autonomously to trigger differentiation processes.

Chapter IV resolves a specific CRN function in developing phloem files of the root. Applying competitive *in vivo* interaction analyses will demonstrate how CRN interaction with a CLVf receptor and OCTOPUS, a protein with subcellular polarity, defines pathway-specific CLE peptide responses.

Chapter V displays a screen to enlarge the range of suitable fluorophore combinations to perform state of the art Förster resonance energy transfer (FRET)-based fluorescence-lifetime imaging microscopy (FLIM). This can improve protein-protein interactions studies and, thus, is important to understand complex signaling networks.

In the following, multifaceted approaches will be described, which aim to decipher mechanisms of signal perception, signal specification, and signal integration within CLVf receptor pathways. Considering that many elements of CLVf receptor signaling are conserved in crop plants, new insights into the underlying molecular principles can contribute to crop breeding programs.

Chapter I

Emerging mechanisms to fine-tune receptor kinase signaling specificity

The following manuscript was published in Current Opinion in Plant Biology in October 2020.

https://doi.org/10.1016/j.pbi.2020.05.010

Authors:

Sergio Galindo-Trigo[1*], Patrick Blümke[2*], Rüdiger Simon[2] and Melinka A Butenko[1]

Affiliations:

[1] Section for Genetics and Evolutionary Biology, Department of Biosciences, University of Oslo, 0316 Oslo, Norway

[2] Institute for Developmental Genetics, Heinrich Heine University, Universitätsstraße 1, 40225 Düsseldorf, Germany

* These authors contributed equally.

Author contributions:

All authors wrote the manuscript.

Available online at www.sciencedirect.com

ScienceDirect

Current Opinion in Plant Biology

Emerging mechanisms to fine-tune receptor kinase signaling specificity

Sergio Galindo-Trigo[1,3], Patrick Blümke[2,3], Rüdiger Simon[2] and Melinka A Butenko[1]

Organisms need to constantly inform their cellular machinery about the biochemical and physical status of their surroundings to adapt and thrive. While some external signals are also sensed intracellularly, a considerable share of external information is registered already at the plasma membrane (PM). Receptor kinases (RKs) are crucial for plant cells to integrate such cues from the environment, from microbes, or from other cells to coordinate their physiological response and their development. Early studies on RK signaling depicted the path from external signal to internal response in a linear fashion, but recent findings show that these cellular information highways are highly interconnected and pass signals through molecular intersections. In this review, we first discuss how individual RKs simultaneously contribute to the transduction and deconvolution of a multitude of signals by controlled assembly into diverse RK complexes, exemplified by FERONIA signaling versatility. We then elaborate on how cells can exert highly localized control over the assembly, interaction and composition of such complexes in order to attain essential cellular output specificity.

Addresses
[1] Section for Genetics and Evolutionary Biology, Department of Biosciences, University of Oslo, 0316 Oslo, Norway
[2] Institute for Developmental Genetics and Cluster of Excellence on Plant Sciences, Heinrich Heine University, Universitätsstraße 1, 40225 Düsseldorf, Germany

Corresponding author: Butenko, Melinka A (m.a.butenko@ibv.uio.no)
[3] These authors contributed equally to this review.

Current Opinion in Plant Biology 2020, **57**:41–51

This review comes from a themed issue on **Cell signaling and gene regulation**

Edited by **Ross Sozanni**

https://doi.org/10.1016/j.pbi.2020.05.010

General introduction

Land plants depend on their receptor inventory and developmental plasticity to cope with the external conditions from which they cannot escape, and RK families have undergone a remarkable expansion in gene number since plants started their conquest of land [1–3]. Early characterization of, for instance, ERECTA (ER), CLAVATA1 (CLV1), HAESA (HAE) or FLAGELLIN SENSING2 (FLS2) as regulators of stomata and meristem development, abscission, or defense to pathogens, respectively [4–7], depicted linear RK pathways that involved ligand perception, coreceptor binding, intracellular phosphorylation cascades, regulation of transcription factors, and modulation of transcription. The utilization of identical signaling components by different signaling systems could pose a way to facilitate coordination between pathways at multiple levels. Here, we discuss recent studies that illustrate a new understanding of how signaling specificity is safeguarded in a cellular environment that is crowded with interacting RKs and peptides.

Lessons learned from FERONIA signaling versatility

FER is a convergence point for extracellular signals

Ligands interact with the extracellular domain of RKs with high affinities, but not in an exclusive one-to-one manner. Instead, there are examples where individual ligands can be recognized by different receptors, and individual receptors can be activated by different ligands. FERONIA (FER), belonging to the *Catharanthus roseus* RLK1-like (*Cr*RLK1L) family in *Arabidopsis thaliana* (Arabidopsis), was initially described as a regulator of fertility but partakes in diverse receptor complexes and acts at the crossroad of signal perception and activation of multiple signal transduction cascades [8]. The ectodomain of FER and other *Cr*RLK1Ls comprises two malectin-like domains through which small rapid alkalinization factor (RALF) peptides, cell wall components like pectin, and apoplastic proteins like leucine-rich repeat (LRR) extensins (LRXs) can be sensed [9–13,14•]. Several RALFs trigger responses via FER: RALF1 triggers apoplast alkalinization, stomatal closure and impairs root growth; RALF23 quenches immune responses by hindering FER from scaffolding immunity receptor complexes, while RALF17 enhances immunity via FER (Figure 1a) [9,10,15]. Furthermore, several *Cr*RLK1Ls can be activated by RALF34, which regulates lateral root primordia formation via THESEUS1 and binds pollen tube growth regulators ANXUR1 and 2 (ANX1/2) and BUDDHA'S PAPER SEAL1 and 2 (BUPS1/2) to promote pollen tube burst by disrupting autocrine signaling of the RALF4/19 pair (Figure 1b) [11,12,16]. Additionally, direct interactions between the ectodomain of FER and LRXs coordinate cell wall status and vacuolar size

Figure 1

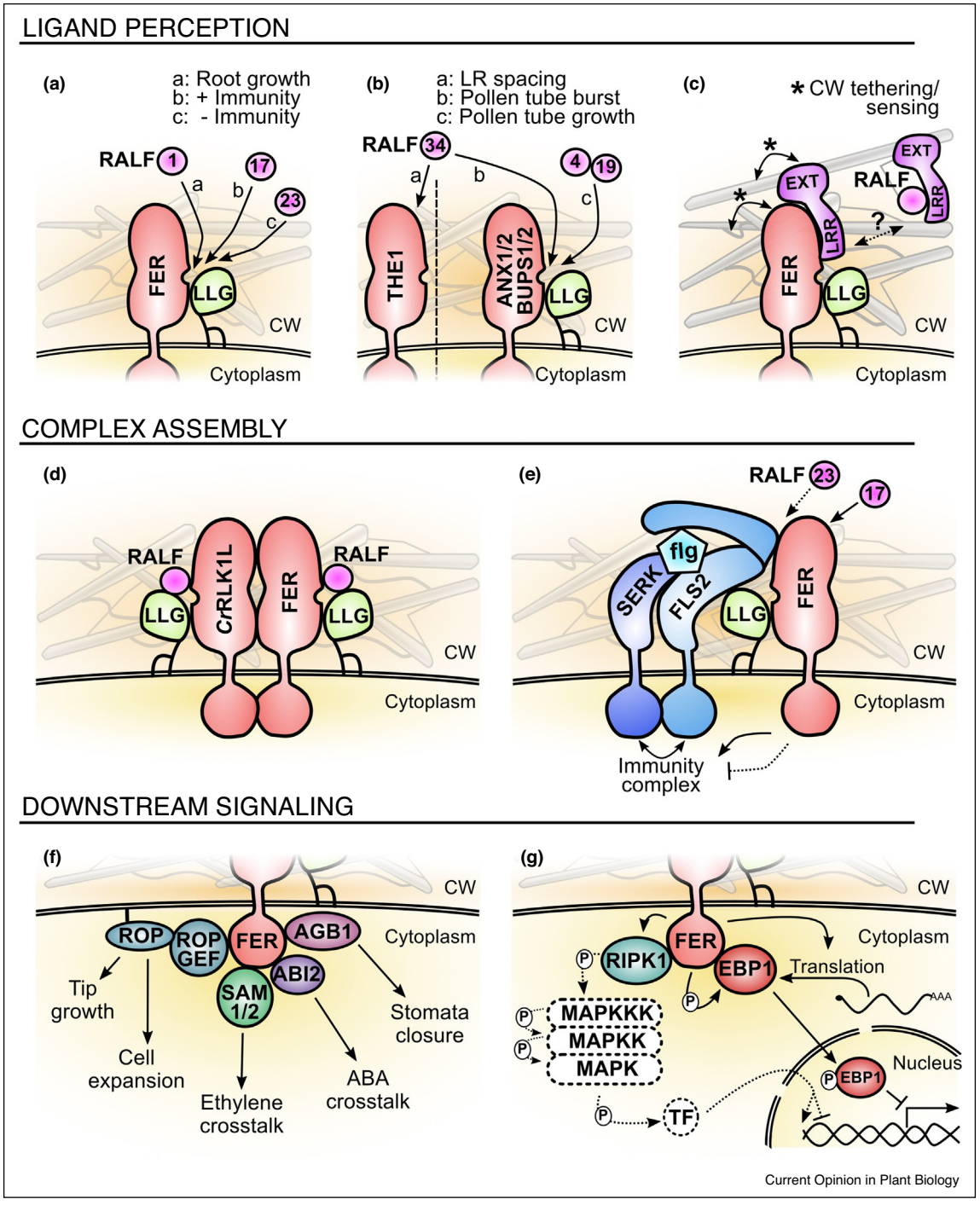

FER and *Cr*RLK1L signaling.
(a) Different RALF peptides can be recognized by a single *Cr*RLK1L. **(b)** A single RALF peptide can bind more than one *Cr*RLK1L to trigger diverse responses. **(c)** FER dual tethering to cell wall components via direct interaction with pectin and through LRX proteins. LRXs are able to bind RALF peptides and, as demonstrated during pollen tube growth, they can be essential for the activity of the peptides [12,17]. The relationship between LRX-RALF complexes and *Cr*RLK1L-LLG perception of RALFs remains unexplored. **(d)** A model for *Cr*RLK1L signaling through heterodimers of *Cr*RLK1L-LLG units. **(e)** Function of FER as a RALF-dependent scaffold of immune complex formation. **(f)** Diverse direct downstream effectors connect FER with multiple developmental responses. **(g)** EBP1 translation-transcription loop to mediate FER-RALF1 transcriptional changes and a speculative alternative method for gene expression regulation via RIPK1 activation of the MAPK cascade. RALF, rapid alkalinization factor; FER, FERONIA; LLG, LORELEI-LIKE GLYCOSYLPHOSPHATIDYLINOSITOL ANCHORED PROTEIN; CW, cell wall; LR, lateral root; THE1, THESEUS1;

regulation, guarding cell integrity during fast elongation in roots [14•]. LRX proteins also bind RALF peptides and are essential for RALF4/19 to exert their function during pollen tube growth; nevertheless, whether *Cr*RLK1Ls and LRXs constitute a RALF4/19 sensing complex in pollen tubes or whether they affect two separate steps of RALF4/19 signaling remains to be elucidated (Figure 1c) [12,17].

Ligand-receptor partner plurality is not exclusive to RALFs and the *Cr*RLK1Ls: the CLAVATA3/ESR-RELATED9/10 (CLE9/10) peptides regulate asymmetric cell division in the stomatal lineage through an RK complex of HAESA-LIKE1 (HSL1) and SOMATIC EMBRYOGENESIS RECEPTOR KINASES (SERKs), and xylem lineage cell division via BARELY ANY MERISTEM1 (BAM1) [18•]. The RKs controlling Casparian strip and embryonic cuticle formation, GASSHO1/SCHENGEN3 (GSO1/SGN3) and GSO2, act with SERKs and bind not only CASPARIAN STRIP INTEGRITY FACTOR1 (CIF1) and 2, but an additional pair of related peptides named CIF3 and 4, and the sulfated peptide TWISTED SEED1 (TWS1) [19–21,22•].

Selective partnering at the plasma membrane

PM receptors cluster into complexes that enhance the ligand-receptor binding affinity and promote downstream signaling via transphosphorylation of the receptor kinase domains. The RALF peptide receptor complex has been structurally determined as a heterodimer between FER and a LORELEI-LIKE GLYCOSYLPHOSPHATIDYLINOSITOL-ANCHORED PROTEIN (LLG) [23••]. LLGs are small membrane-anchored proteins that act as coreceptors for *Cr*RLK1Ls and assist the delivery of receptors to the PM [24–27]. To regulate fertilization, FER associates with the LLG protein LORELEI (LRE) and the pair of functionally redundant *Cr*RLK1Ls HERCULES RECEPTOR KINASE1 (HERK1) and ANJEA (ANJ), which also associate with LRE [24]. Similarly, ANX1/2 and BUPS1/2 interact with each other and with LLG2/3 to maintain pollen tube growth, suggesting that RALFs may be perceived by multipartite receptor complexes comprising two sets of *Cr*RLK1L-LLG heterodimers (Figure 1d) [25,26].

Effective immunity in Arabidopsis relies on detection of bacterial-derived epitopes like flagellin22 (flg22) by the FLS2-BRASSINOSTEROID INSENSITIVE1 (BAK1)/SERK3 (hereon referred to as SERK3) receptor complex, which is scaffolded by FER [6,10,28]. While interaction has been reported between ANX1 and the FLS2–SERK3 complex in response to flg22, the FLS2–SERK3 interaction is impaired when *ANX1* is overexpressed, thus repressing immunity [29]. It remains to be determined if ANX1 association with FLS2 and SERK3 regulates FLS2–SERK3 complex formation. Understanding how the two *Cr*RLK1Ls associate with the same components in response to the same stimuli to yield opposed responses requires further investigation, although competition for immune receptor complex members and recruitment of different downstream signaling components could explain the response divergence. Interestingly, LLG1 was independently reported to positively influence immunity by interacting with FLS2, prompting us to wonder whether different *Cr*RLK1L–LLG–LRR–RK complexes could regulate developmental processes currently linked to *Cr*RLK1L-LLG dimers alone (Figure 1e) [30].

Diversity downstream of FER

FER has been long established as a regulator of development beyond fertility and immunity, including root hair and trichome development, root and petiole elongation or abiotic stress responses (see Ref. [8] for in-depth review). Recently, FER has been linked to two additional processes: flowering time and auxin transport during root gravitropism [31,32]. In several of these processes, FER relies on RHO OF PLANTS (ROP) proteins to activate PM NADPH oxidases for reactive oxygen species (ROS) production, trigger Ca^{2+} flux changes and inhibit H^+-ATPases to increase apoplastic pH [9,33–35]. Besides, FER crosstalks with other plant hormones by phosphorylating *S*-ADENOSYL METHIONINE SYNTHASE1 and 2 to negatively regulate ethylene production, and protein phosphatase ABSCISIC ACID-INSENSITIVE2 to dampen abscisic acid signaling (Figure 1f) [36,37]. Interestingly, FER kinase activity is dispensable for the control of pollen tube reception in ovules and for root growth, revealing context-dependent molecular mechanisms of FER downstream signaling [38–40]

Additional direct targets of FER keep emerging. FER acts as a receptor for Gβ-protein1 (AGB1) to induce RALF1-mediated stomatal closure [15,41]. The ErbB3-binding protein1 (EBP1) takes part in a RALF1-FER transcription-translation feedback loop, where FER first stimulates translation of *EBP1* mRNA upon RALF1 treatment. EBP1 is then phosphorylated by FER, and subsequently transported to the nucleus to repress RALF1-responsive genes [42•]. These findings shed light on a so far poorly understood mechanism in plants and present a communication shortcut between PM signaling and transcriptional change [43]. Often, RKs utilize a

ANX1/2, ANXUR1 and 2; BUPS1/2, BUDDHA'S PAPER SEAL1 and 2; LRR-EXT, LRR extensin; *Cr*RLK1L, *C. roseus* receptor-like 1-like; SERK, SOMATIC EMBRYOGENESIS RECEPTOR KINASE; FLS2, FLAGELLIN SENSING2; flg, flagellin22; ROP, RHO OF PLANTS; ROPGEF, ROP GUANINE EXCHANGE FACTOR; SAM1/2, *S*-ADENOSYLMETHIONINE SYNTHASE1 and 2; ABI2, ABA INSENSITIVE2; AGB1, Gβ-protein 1; RIPK1, RPM1-INDUCED PROTEIN KINASE; EBP1, ErbB3-binding protein 1. Circled P represents phosphorylation events.

module of mitogen activated protein kinases (MAPKs) that comprises the phosphorylation cascade of MAP kinase kinase kinases (MAPKKKs), MAP kinase kinases (MAPKKs) and MAPKs, which ultimately leads to transcriptional adjustments (see Ref. [44] for review). Additional research is required to elucidate how specificity is maintained through this phosphorylation cascade since multiple extracellular inputs can activate the same small subset of MAPKs to phosphorylate transcription factors that yield strikingly diverse transcriptional outputs [45]. Recently, members of the receptor-like cytoplasmic kinase (RLCK)-VII clade were found to relay immunity-related RK signals onto the MAPK cascade by phosphorylating and activating MAPKKK3/5, thus creating a link between immunity-related RKs and MAPK cascade activation [46]. Interestingly, the clade VII RLCK protein RPM1-INDUCED PROTEIN KINASE (RIPK) is directly phosphorylated by FER after RALF1 sensing during root growth [47], suggesting that, parallel to EBP1 activation, *Cr*RLK1Ls could utilize RIPK or related RLCKs to activate the canonical MAPK cascade to induce transcriptional changes (Figure 1g). However, FER and related *Cr*RLK1Ls ANX1/2 can also signal via MARIS (MRI), a membrane-localized RLCK belonging to the subfamily VIII required for pollen tube and root hair tip growth. Contrasting FER-RIPK physical interaction and phosphorylation, MRI appears to act further downstream following *Cr*RLK1L-mediated ROS production [48].

Some of the FER interactors are integral components of networks with remarkably high dimensions. For instance, SERK3 belongs to the LRR(II)-RK group of coreceptors [49], which interact with RKs containing larger LRR ectodomains. Receptor ligand complexes engaging SERKs as coreceptors include FLS2 during immune responses, BRASSINOSTEROID INSENSITIVE1 (BRI1) perceiving brassinosteroids (BRs), ER binding EPIDERMAL PATTERNING FACTORS (EPFs) during stomatal patterning, or HAE and HAESA-LIKE2 (HSL2) relaying a signal from INFLORESCENCE DEFICIENT IN ABSCISSION (IDA) to control cell separation [28,50–54]. Recent evidence demonstrated the participation of SERKs in CIFs recognition by GSO1/2 and in CLE9/10 sensing by HSL1 [18•,19]. Furthermore, other LRR(II)-RKs, namely CLAVATA3 INSENSITIVE KINASES (CIKs), are coreceptors of CLV1, CLV2, RPK2 and BAM1/2 relaying CLE signals in meristem termination, as well as in cell specification during anther development [55•,56,57]. It is conceivable that, in some instances, pathway crosstalk could be facilitated by these coreceptors through competition, sequestration, and sharing. Nevertheless, in the context of the antagonism between FLS2 and BRI1 signaling pathways (both of which use SERK3 as coreceptor; see Ref. [58] for review) it has been shown that the amount of SERK3 is not rate limiting and that inhibition of immunity by BRs is independent of this coreceptor [59,60].

Extensive studies of receptors like FER suggest that intricate RK signaling scenarios are the rule rather than the exception. This was recently documented in a high-throughput assay where the extracellular domains of 200 LRR RKs were tested for interaction, resulting in the identification of cell-surface interaction networks [61•]. While tight control over the spatiotemporal expression of ligands and receptors represents an efficient strategy to generate specificity at the cellular level, further mechanisms are required for the cell to integrate diverse signals and balance plant development with defense.

How to gain signaling specificity

Multi-functionality of signaling elements requires discrimination between independent signaling inputs. There are various mechanisms by which specificity of signaling can be obtained.

Structural determinants of receptor specificity

How members of the SERK family of coreceptors can generate a wide range of different cellular responses resides in part in their structure. The *bak1-5* (*serk3*) mutant exhibits severe immunity defects but shows normal BR signaling [62]. The difference in signaling output resided in a conserved phosphosite within the cytoplasmic domain of SERK3, the phosphorylation of which is mandatory for FLS2-based immune responses, while dispensable for BRI1 signaling showing that BRI1 and FLS2 use different phosphorylation sites on SERK3 for receptor activation [63••]. In addition, other SERK3 interactors like PEP1 RECEPTOR1 (PEPR1), PEPR2, ER, HAE or HSL*2* require the phosphorylation of a kinase subdomain VIa tyrosine (Tyr-VIa) residue with analogous positioning at their respective complex interface with SERK3. Conversely, this tyrosine is not conserved in BRI1, leading to the classification of SERK-interacting receptors as Tyr-VIa-dependent or Tyr-VIa-independent and to a model of phosphocode-based dichotomy for SERK function [63••].

Structural features can also provide the basis for difference in signaling output by changes in interaction affinities. The BR signaling capability of BRI1 is counteracted by BAK1-INTERACTING RECEPTOR-LIKE KINASEs (BIRs), which inhibit the formation of BRI1-SERK heterodimers by interacting with the ectodomains of SERKs [64]. This negative regulation by BIR proteins is also found in other SERK-dependent pathways. For example, BIR2 and BIR3 restrain SERK3 from complex formation with FLS2 in the resting state and only release the coreceptors upon ligand perception [65,66]. In contrast, the short LRR-RK NUCLEAR SHUTTLE PROTEIN-INTERACTING KINASE 1 (NIK1) destabilizes the SERK3/FLS2 complex after flg22 binding.

However, NIK1 acts conceptually similar to BIRs with respect to competitive receptor binding, which is fine-tuned by the NIK1 phosphorylation status and thought to be the basis for the specificity of antibacterial and antiviral immune responses [67]. Recently, a mechanistic description of coreceptor competition was obtained for the multifaceted SERK coreceptors by structural characterization of the gain-of-function SERK3 *elongated* (SERK3^{elg}) allele. The slight structural modification at the LRR binding surface of SERK3^{elg} indirectly favors SERK-BRI1 interaction by attenuating the competitive binding of SERKs to BIRs. Furthermore, the affinity of SERK3^{elg} to other LRR receptors like HAE is strongly reduced compared to wild-type SERK3 [64]. This illustrates that signaling specificity resides in structural properties of a protein and that their modification promotes different signaling routes. In animals, it has been suggested that the binding of different ligands to the same RK could stabilize structurally distinct receptor states that can be differentially interpreted by intracellular receptor modules thereby providing functionally discrete outcomes from the same receptor [68]. It remains to be determined whether such biased agonism applies in plants.

Regulation of signaling events by dynamic protein trafficking

The spatio-temporal availability of proteins involved in a particular signaling event can determine specificity between pathways. Turnover of signaling elements is a key mechanism to dampen an activated cascade and to regulate their availability before cascade activation. The ligand induced internalization of FLS2 in intracellular vesicles by a clathrin-dependent and sterol-associated endocytic pathway terminates immune signaling by targeting FLS2 for degradation and also desensitizes cells to the same stimulus [69•,70–73]. This mechanism is shared by pattern recognition receptors and appears to be a general feature of plant immunity [70]. In addition, endosomal signaling can potentially also contribute to signaling specificity. Whereas blocking BRI1 endocytosis in the PM enhances BR signaling output, a decrease in FLS2 endocytosis affects only the activation of a subset of the flg22-triggered signaling. This indicates that early FLS2 signaling events are possibly triggered at the PM level and, after internalization, intracellular signaling events continue to control late responses until the receptor is degraded. The sum of early and late responses leads to a complete immune response [74].

Related peptides can specify signaling output by establishing differential subcellular dynamics of a single receptor. ERECTA-LIKE1 (ERL1), the major receptor restricting stomatal differentiation, shows distinct subcellular dynamics in response to different signal inputs. ERL1 is continuously recycled, but undergoes a TOO MANY MOUTHS (TMM)-dependent rapid internalization upon EPF1 perception, while its antagonist Stomagen/EPFL9 triggers retention of ERL1 to the endoplasmic reticulum, thereby inhibiting signaling [75].

In general, internalization limits the availability of RK at the PM. Receptor endocytosis followed by degradation or recycling via the endoplasmic trafficking pathway rely on tightly regulated vesicular transport. For example, BR signaling depends on members of the BIG subfamily of ADP-ribosylation factor (ARF) GTPases that mediate BRI1 endocytosis [76]. However, the most prominent trigger of protein turnover is the ubiquitylation of target proteins via specific E3 ubiquitin ligases, as shown for various RK signaling pathways [77,78]. The power of PLANT U-BOX (PUB) ubiquitin ligases to dynamically fine-tune receptor signaling is reflected, for example, by the flg22-induced FLS2 degradation via PUB12/13. After ligand binding SERK3 phosphorylates and activates PUB12/13 and thereby promotes FLS2 polyubiquitylation [79]. Downstream of FLS2, again, turnover events are carefully balanced, as apparent by the antagonizing action of heterotrimeric G-proteins and the calcium-dependent protein kinase CPK28 controlling PUB25/26 activity. This differential PUB25/26 regulation determines the degradation of the downstream effector BOTRYTIS-INDUCED KINASE1 (BIK1) [80]. *Vice versa*, the stabilization of a signaling module by impairing receptor ubiquitylation can prolong signaling. Such mode of action is found in the case of the atypical LRR-RK SCRAMBLED/STRUBBELIG (SCM) that regulates cell fate in the root epidermis [81•]. SCM is thought to support the movement of the transcription factor CAPRICE through plasmodesmata to promote the development of root hairs. This system is modulated by QUIRKY (QKY), a SCM interactor that prevents its ubiquitylation. QKY therefore reinforces SCM stability and can be regarded as a negative regulator of receptor turnover. Similarly, ubiquitin-specific proteases like UBIQUITIN-SPECIFIC PROTEASE12 and 13 in the case of ROOT MERISTEM GROWTH FACTOR1 receptor in root meristem homeostasis can enhance signal specificity [82].

Another example of endocytosis dependent regulation of RK localization is presented by the oxidative state dependent turnover of the ARABIDOPSIS CRINKLY4 (ACR4) RK in the root stem cell niche [83]. Here, a ROS gradient along the root meristem directly affects stem cell maintenance by controlling the amount of ACR4 localized at the PM which regulates the differentiation state of stem cell descendants. Since ROS signaling is interconnected with developmental effects of auxin and cytokinin (reviewed in Ref. [84]), receptor turnover in response to disturbed redox balance might also play a general role in hormone dependent root meristem development.

Not only receptor, but also peptide processing and availability provides a route for spatially restricted signaling. During seed development, a bilateral communication

Figure 2

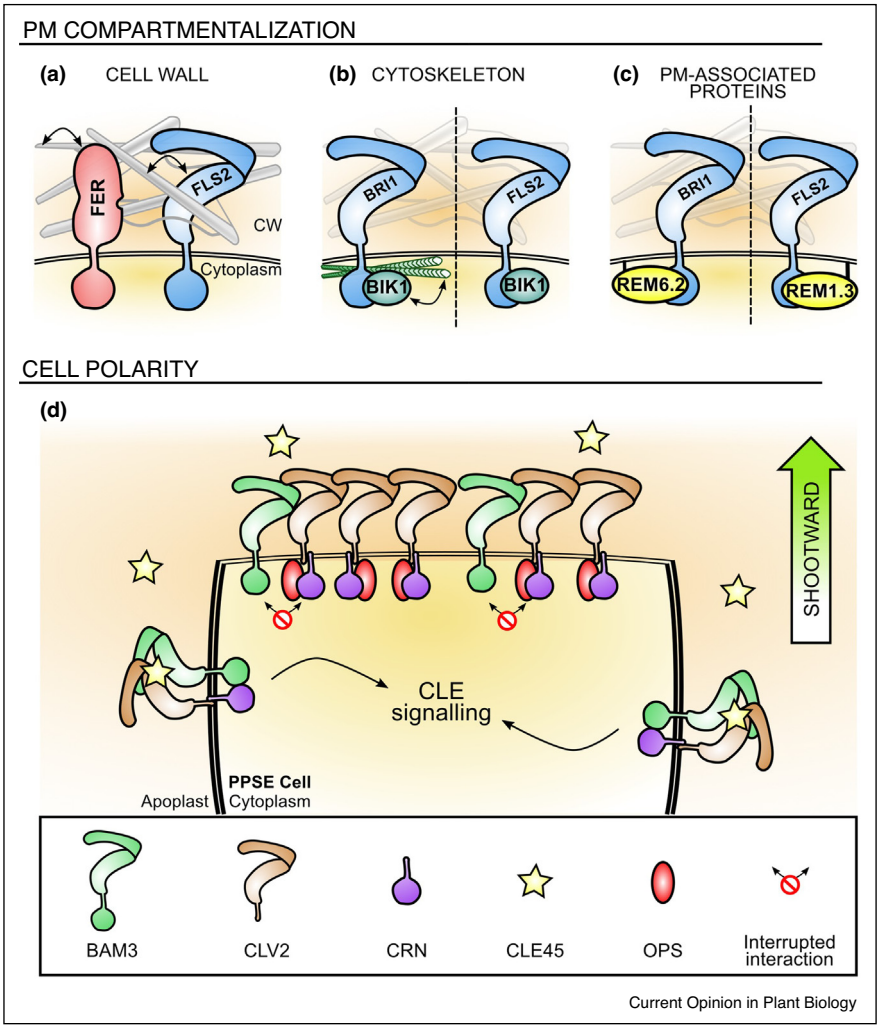

Specificity of signaling processes by distinct subcellular receptor localization.
Plant cells evolved several mechanisms to allocate signaling complexes to different subregions of the PM. **(a)** The direct or indirect interaction with cell wall components contributes to receptor localization and mobility along the PM, as studies on FER or FLS2 show [13,14•,88••]. **(b)** Intracellularly, the cytoskeleton guides proteins to their designated position. BIK1 associated with cortical microtubules preferentially co-localizes with BRI1, instead of forming BIK1–FLS2 complexes [89•]. **(c)** Members of the remorin family provide nano-environments with defined protein composition. Nanodomains contribute to receptor stabilization and separation [89•]. **(d)** Polarly localized proteins can establish PM subdomains, defined by the direction of cellular growth or neighboring cells. In developing phloem cells OPS is exclusively present at the shootward orientated side, where it is thought to interfere with BAM3/CLV2/CRN receptor complexes to dampen CLE45 signaling [97•]. CW, cell wall; FER, FERONIA; FLS2, FLAGELLIN SENSING2; BRI1, BRASSINOSTEROID INSENSITIVE1; BIK1, BOTRYTIS-INDUCED KINASE1; REM, remorin; BAM3, BARELY ANY MERISTEM3, CLV2, CLAVATA2; CRN, CORYNE; CLE45, CLAVATA3/EMBRYO SURROUNDING REGION-RELATED 45, OPS, OCTOPUS; PPSE, root protophloem sieve elements.

system is established between embryo and endosperm to control the formation of the cuticle that ultimately terminates communication between embryo and endosperm. The embryo secretes an inactive precursor of TWS1 which is processed by the ALE1 subtilase in the endosperm. The processed and active TWS1 diffuses back to the embryo where it is perceived by the GSO1/2 receptors to promote cuticle formation. Once a sufficient cuticle is formed, TWS1 can no longer reach the endosperm and signaling is terminated [22•]. The salt-stress triggered cleavage and activation of RALF22/23 by SITE-1 PROTEASE (S1P) causes FER internalization and displays another example of peptide maturation being critical for signal integration and transmission [85].

Determining the micro-environment and nano-environment of receptor signaling at the plasma membrane

Another factor potentially mediating specificity between common elements of different signaling cascades might

be their local separation and controlled interaction, although experimental data supporting this notion are still scarce. Several mechanisms guarantee a precise membrane subcompartmentalization to avoid a non-coordinated diffusion of membrane-integral and membrane-associated proteins (recently reviewed in Refs. [86,87]). Applying high resolution microscopy-based single particle tracking of fluorescence-labelled receptors like FLS2 demonstrated that the cytoskeleton and cell wall elements regulate mobility and clustering of proteins at the PM [88••]. Thus, the above-mentioned interactions of FER with the cell wall may not only help sense developmental and environmental changes [12,14•,85], but also influence receptor distribution along the PM (Figure 2a).

An impact of PM compartmentalization is suggested in a study on specificity of BRI1 and FLS2 signaling which, although sharing the same coreceptor SERK3 and downstream RLCK BIK1, trigger different outputs potentially due to local separation of receptor complexes into PM nanodomains with differential association to cortical microtubules (Figure 2b) [89•]. Control of protein localization at PM sites can be achieved by posttranslational modifications, such as attachment of GLYCOSYLPHOSPHATIDYLINOSITOL-anchors, myristoylation or *S*-acylation (reviewed in Ref. [90]). The reversibility of *S*-acylation allows the dynamic control of protein localization. *S*-acylation at the juxtamembrane domain of FLS2 and other immune receptors through the specific activity of Protein *S*-acyltransferases has been recently suggested to regulate RK nanodomain localization and function. The functional significance of *S*-acylation is still under discussion, where one study reported enhanced signaling when the ratio of *S*-acylated receptor was lowered, pointing towards an inactivation mechanism within specific membrane nanodomains [90,91].

While sequestration into nanodomains potentially control the specificity of receptor signaling, there is also a feedback from signaling on nanodomain composition. Flotillins (FLOT) and remorins (REM) are two groups of PM-associated scaffolding proteins that contribute to nanodomain formation and serve to stabilize or isolate receptors (Figure 2c; reviewed in Ref. [86]). REM phosphorylation via kinases that are involved in various signaling cascades potentially influences the properties of nanodomains [92–94]. This suggests a reciprocal modulation between signaling cascades and local membrane composition that is only starting to be understood.

Beyond nanodomains, membranes can be compartmentalized at plasmodesmata or by the polarity of a cell [95,96]. Polar localization of the membrane-associated OCTOPUS (OPS) protein along developing root protophloem sieve elements (PPSE) affects their differentiation [97•]. OPS competes with the interaction of the receptor BAM3 and the composite CLV2/CORYNE receptors, which is required for perception of the secreted peptide CLE45. The quantitative dampening of receptor signaling by OPS thus counteracts CLE45 function, thereby promoting PPSE differentiation (Figure 2d). The polar orientation of OPS could then enable the establishment of a signaling gradient along the phloem cell file.

Conclusions and perspectives

An extraordinary high number of RKs and interconnections between pathways equip plants with signaling systems of remarkable complexity. The discussed mechanisms for signaling specificity are crucial to orchestrate the selective transduction of information, and direct signal traffic even through convoluted, multilayered intersections. Not all mechanisms apply to all RK signaling pathways and it will be of interest to gain more insight into how a multifunctional receptor like FER can convey specificity in signaling output. Key discoveries came from studies on the structures and interactions of receptors and downstream signaling components, and on precise cellular localization of receptor complexes. Dynamic and superresolution imaging tools are advancing rapidly, and *in situ* structural studies on receptor complexes come within reach through breakthrough technologies in electron tomography. We are still lacking sufficiently precise sensors that report on the activities of signaling receptors with high sensitivity and good spatial resolution, but given the rapid development of novel methods in the field, we can expect exciting insights down to the single molecule scale within the next years.

Conflict of interest statement

Nothing declared.

Acknowledgements

PB was supported by the IMPRS 'Understanding complex plant traits using computational and evolutionary approaches'; research in RS lab was supported by the DFG through CEPLAS and CRC1208. We would like to thank Dr Iesling for help during the revision. SG-T and MAB were supported by the Research Council of Norway (grant 230849). SG-T was in addition supported by funding from the Ministry of Education and Research to the University of Oslo.

References and recommended reading

Papers of particular interest, published within the period of review, have been highlighted as:

- • of special interest
- •• of outstanding interest

1. Shiu SH, Bleecker AB: **Receptor-like kinases from Arabidopsis form a monophyletic gene family related to animal receptor kinases**. *Proc Natl Acad Sci U S A* 2001, **98**:10763-10768.
2. Lehti-Shiu MD, Zou C, Hanada K, Shiu SH: **Evolutionary history and stress regulation of plant receptor-like kinase/pelle genes**. *Plant Physiol* 2009, **150**:12-26.
3. Tax F, Kemmerling B: *Receptor-like Kinases in Plants: from Development to Defense*. Heidelberg; New York: Springer; 2012.
4. Clark SE, Williams RW, Meyerowitz EM: **The CLAVATA1 gene encodes a putative receptor kinase that controls shoot and floral meristem size in Arabidopsis**. *Cell* 1997, **89**:575-585.

5. Jinn TL, Stone JM, Walker JC: **HAESA, an Arabidopsis leucine-rich repeat receptor kinase, controls floral organ abscission**. *Genes Dev* 2000, **14**:108-117.

6. Gomez-Gomez L, Boller T: **FLS2: an LRR receptor-like kinase involved in the perception of the bacterial elicitor flagellin in Arabidopsis**. *Mol Cell* 2000, **5**:1003-1011.

7. Torii KU, Mitsukawa N, Oosumi T, Matsuura Y, Yokoyama R, Whittier RF, Komeda Y: **The Arabidopsis ERECTA gene encodes a putative receptor protein kinase with extracellular leucine-rich repeats**. *Plant Cell* 1996, **8**:735-746.

8. Franck CM, Westermann J, Boisson-Dernier A: **Plant malectin-like receptor kinases: from cell wall integrity to immunity and beyond**. *Annu Rev Plant Biol* 2018, **69**:301-328.

9. Haruta M, Sabat G, Stecker K, Minkoff BB, Sussman MR: **A peptide hormone and its receptor protein kinase regulate plant cell expansion**. *Science* 2014, **343**:408-411.

10. Stegmann M, Monaghan J, Smakowska-Luzan E, Rovenich H, Lehner A, Holton N, Belkhadir Y, Zipfel C: **The receptor kinase FER is a RALF-regulated scaffold controlling plant immune signaling**. *Science* 2017, **355**:287-289.

11. Ge ZX, Bergonci T, Zhao YL, Zou YJ, Du S, Liu MC, Luo XJ, Ruan H, Garcia-Valencia LE, Zhong S *et al.*: **Arabidopsis pollen tube integrity and sperm release are regulated by RALF-mediated signaling**. *Science* 2017, **358**:1596-1599.

12. Mecchia MA, Santos-Fernandez G, Duss NN, Somoza SC, Boisson-Dernier A, Gagliardini V, Martinez-Bernardini A, Fabrice TN, Ringli C, Muschietti JP *et al.*: **RALF4/19 peptides interact with LRX proteins to control pollen tube growth in Arabidopsis**. *Science* 2017, **358**:1600-1603.

13. Feng W, Kita D, Peaucelle A, Cartwright HN, Doan V, Duan QH, Liu MC, Maman J, Steinhorst L, Schmitz-Thom I *et al.*: **The FERONIA receptor kinase maintains cell-wall integrity during salt stress through Ca^{2+} signaling**. *Curr Biol* 2018, **28**:666-675.

14. • Dunser K, Gupta S, Herger A, Feraru MI, Ringli C, Kleine-Vehn J: **Extracellular matrix sensing by FERONIA and Leucine-rich repeat extensins controls vacuolar expansion during cellular elongation in *Arabidopsis thaliana***. *Embo J* 2019, **38**:e100353.
Provides direct evidence of the coordinated action of FER and LRXs in cell wall sensing for the first time. Dunser *et al.* made use of genetic assays and elegant microscopic visualization of the 3D structure of the vacuolar system of root cells to discover that the FER ectodomain interacts with the LRR domain of LRXs which together coordinate cell wall status with cellular growth rates by interfering with vacuole size. *Cr*RLK1Ls and LRXs have been shown to mediate other cell expansion processes such as pollen tube tip growth through an unknown mechanism. Testing whether the *Cr*RLK1L-LRX cooperative relay of cell wall signals also takes place during pollen tube tip growth would help clarify this key process of plant reproduction. Further research should be directed towards the identification of the molecular link between the surface receptor and the vacuolar system dynamics.

15. Yu YQ, Chakravorty D, Assmann SM: **The G protein beta-subunit, AGB1, interacts with FERONIA in RALF1-regulated stomatal movement**. *Plant Physiol* 2018, **176**:2426-2440.

16. Gonneau M, Desprez T, Martin M, Doblas VG, Bacete L, Miart F, Sormani R, Hematy K, Renou J, Landrein B *et al.*: **Receptor kinase THESEUS1 is a rapid alkalinization factor 34 receptor in Arabidopsis**. *Curr Biol* 2018, **28**:2452-2458.

17. Moussu S, Broyart C, Santos-Fernandez G, Augustin S, Wehrle S, Grossniklaus U, Santiago J: **Structural basis for recognition of RALF peptides by LRX proteins during pollen tube growth**. *bioRxiv* 2019:695874.

18. • Qian P, Song W, Yokoo T, Minobe A, Wang G, Ishida T, Sawa S, Chai J, Kakimoto T: **The CLE9/10 secretory peptide regulates stomatal and vascular development through distinct receptors**. *Nat Plants* 2018, **4**:1071-1081.
Characterization of the functional relevance of *CLE9* and *CLE10* genes in stomata and xylem development. *CLE9* and *CLE10* encode identical predicted mature peptides that signal through the HSL1 receptor to counteract stomata development. Double mutant *cle9 cle10* plants have more guard cells per cotyledon area, while exogenous application of CLE9/10 results in a decline in the number of epidermal cells entering the stomatal development lineage in a HSL1-dependent manner. Additionally CLE9/10 negatively regulate periclinal xylem cell division in roots via the BAM family of receptors. Whereas HSL1 requires the SERK coreceptors for efficient CLE9/10 reception, BAM1 does not appear to recruit SERKs upon CLE9/10 treatment thus highlighting the multiplicity in signaling mechanisms exerted by a single small peptide. Given the recent characterization of the CIKs as coreceptors for CLE peptides in diverse developmental contexts [55•,56,57], it would be interesting to test whether CIKs could also perceive CLE9/10 in roots as BAM coreceptors.

19. Okuda S, Fujita S, Moretti A, Hohmann U, Doblas VG, Ma Y, Pfister A, Brandt B, Geldner N, Hothorn M: **Molecular mechanism for the recognition of sequence-divergent CIF peptides by the plant receptor kinases GSO1/SGN3 and GSO2**. *Proc Natl Acad Sci U S A* 2020, **117**:2693-2703.

20. Tsuwamoto R, Fukuoka H, Takahata Y: **GASSHO1 and GASSHO2 encoding a putative leucine-rich repeat transmembrane-type receptor kinase are essential for the normal development of the epidermal surface in Arabidopsis embryos**. *Plant J* 2008, **54**:30-42.

21. Doblas VG, Smakowska-Luzan E, Fujita S, Alassimone J, Barberon M, Madalinski M, Belkhadir Y, Geldner N: **Root diffusion barrier control by a vasculature-derived peptide binding to the SGN3 receptor**. *Science* 2017, **355**:280-284.

22. • Doll NM, Royek S, Fujita S, Okuda S, Chamot S, Stintzi A, Widiez T, Hothorn M, Schaller A, Geldner N *et al.*: **A two-way molecular dialogue between embryo and endosperm is required for seed development**. *Science* 2020, **367**:431-435.
During seed development, a bilateral communication system is established between embryo and endosperm to control the formation of the cuticle that ultimately terminates communication between embryo and endosperm. Doll *et al.* discover a feedback regulation within embryo cuticle formation where the embryo secretes an inactive precursor of the peptide TWS1 which is processed by the ALE1 subtilase in the endosperm. The processed and activated TWS1 diffuses back to the embryo where it is perceived by the GSO1/2 receptors to promote cuticle formation. Once sufficient cuticle is formed, TWS1 can no longer reach the endosperm and signaling is terminated. The study is an interesting example of spatio-temporal regulation of signaling events, since the signaling output (cuticle formation) provides at the same time a mechanism to shut down the pathway.

23. •• Xiao Y, Stegmann M, Han Z, DeFalco TA, Parys K, Xu L, Belkhadir Y, Zipfel C, Chai J: **Mechanisms of RALF peptide perception by a heterotypic receptor complex**. *Nature* 2019, **572**:270-274.
An elegant combination of crystallography, biochemistry and genetics that provides a mechanistic framework for RALF perception via FER–LLG protein heterodimers. Xiao *et al.* solved the structure of a FER–LLG1–RALF23 protein complex and characterized the dynamics of its formation. In this complex, the N-terminus of a RALF peptide is able to bind the LLG protein and nucleate the assembly with FER ectodomain. Only members of the RALF family of small peptides with a strong similarity to RALF23 were found to interact with these receptors, indicating that different subfamilies of RALFs exert their functions in distinct ways. This report supports the fact that FER forms RALF-sensing complexes with different LLGs, and that such complexes are capable of binding several related RALFs, thus suggesting that alternative CrRLK1L-LLG combinations could sense different RALFs that are expressed in different tissues or under different conditions. In the light of the discoveries of LRXs as mediators of RALF signaling, their capacity to physically interact with RALFs and the ectodomain of FER, as well as the functional and physical interactions between FER-LRE and HERK1/ANJ-LRE to mediate fertility, higher order complexes comprising more than one CrRLK1L-LLG module to sense RALFs with the help of LRX proteins constitute an exciting avenue for future research.

24. Galindo-Trigo S, Blanco-Tourinan N, DeFalco TA, Wells ES, Gray JE, Zipfel C, Smith LM: **CrRLK1L receptor-like kinases HERK1 and ANJEA are female determinants of pollen tube reception**. *EMBO Rep* 2019:e48466.

25. Ge Z, Zhao Y, Liu MC, Zhou LZ, Wang L, Zhong S, Hou S, Jiang J, Liu T, Huang Q *et al.*: **LLG2/3 Are co-receptors in BUPS/ANX-RALF signaling to regulate Arabidopsis pollen tube integrity**. *Curr Biol* 2019, **29**:3256-3265.

26. Feng H, Liu C, Fu R, Zhang M, Li H, Shen L, Wei Q, Sun X, Xu L, Ni B *et al.*: **LORELEI-LIKE GPI-ANCHORED PROTEINS 2/3 regulate pollen tube growth as chaperones and coreceptors for ANXUR/BUPS receptor kinases in Arabidopsis**. *Mol Plant* 2019, **12**:1612-1623.

27. Li C, Yeh FL, Cheung AY, Duan Q, Kita D, Liu MC, Maman J, Luu EJ, Wu BW, Gates L *et al.*: **Glycosylphosphatidylinositol-anchored proteins as chaperones and co-receptors for FERONIA receptor kinase signaling in Arabidopsis**. *eLife* 2015, **4**:e06587.

28. Chinchilla D, Zipfel C, Robatzek S, Kemmerling B, Nurnberger T, Jones JD, Felix G, Boller T: **A flagellin-induced complex of the receptor FLS2 and BAK1 initiates plant defence**. *Nature* 2007, **448**:497-500.

29. Mang H, Feng B, Hu Z, Boisson-Dernier A, Franck CM, Meng X, Huang Y, Zhou J, Xu G, Wang T *et al.*: **Differential regulation of two-tiered plant immunity and sexual reproduction by ANXUR receptor-like kinases**. *Plant Cell* 2017, **29**:3140-3156.

30. Shen Q, Bourdais G, Pan H, Robatzek S, Tang D: **Arabidopsis glycosylphosphatidylinositol-anchored protein LLG1 associates with and modulates FLS2 to regulate innate immunity**. *Proc Natl Acad Sci U S A* 2017, **114**:5749-5754.

31. Wang L, Yang T, Lin Q, Wang B, Li X, Luan S, Yu F: **Receptor kinase FERONIA regulates flowering time in Arabidopsis**. *BMC Plant Biol* 2020, **20**:26.

32. Dong QK, Zhang ZW, Liu YT, Tao LZ, Liu HL: **FERONIA regulates auxin-mediated lateral root development and primary root gravitropism**. *Febs Lett* 2019, **593**:97-106.

33. Duan Q, Kita D, Johnson EA, Aggarwal M, Gates L, Wu HM, Cheung AY: **Reactive oxygen species mediate pollen tube rupture to release sperm for fertilization in Arabidopsis**. *Nat Commun* 2014, **5**:3129.

34. Ngo QA, Vogler H, Lituiev DS, Nestorova A, Grossniklaus U: **A calcium dialog mediated by the FERONIA signal transduction pathway controls plant sperm delivery**. *Dev Cell* 2014, **29**:491-500.

35. Duan Q, Kita D, Li C, Cheung AY, Wu HM: **FERONIA receptor-like kinase regulates RHO GTPase signaling of root hair development**. *Proc Natl Acad Sci U S A* 2010, **107**:17821-17826.

36. Chen J, Yu F, Liu Y, Du C, Li X, Zhu S, Wang X, Lan W, Rodriguez PL, Liu X *et al.*: **FERONIA interacts with ABI2-type phosphatases to facilitate signaling cross-talk between abscisic acid and RALF peptide in Arabidopsis**. *Proc Natl Acad Sci U S A* 2016, **113**:E5519-5527.

37. Mao D, Yu F, Li J, Van de Poel B, Tan D, Li J, Liu Y, Li X, Dong M, Chen L *et al.*: **FERONIA receptor kinase interacts with S-adenosylmethionine synthetase and suppresses S-adenosylmethionine production and ethylene biosynthesis in Arabidopsis**. *Plant Cell Environ* 2015, **38**:2566-2574.

38. Haruta M, Gaddameedi V, Burch H, Fernandez D, Sussman MR: **Comparison of the effects of a kinase-dead mutation of FERONIA on ovule fertilization and root growth of Arabidopsis**. *FEBS Lett* 2018, **592**:2395-2402.

39. Duan Q, Cheung AY: **Context-specific dependence on FERONIA kinase activity**. *FEBS Lett* 2018, **592**:2392-2394.

40. Kessler SA, Lindner H, Jones DS, Grossniklaus U: **Functional analysis of related CrRLK1L receptor-like kinases in pollen tube reception**. *EMBO Rep* 2015, **16**:107-115.

41. Yu YQ, Assmann SM: **Inter-relationships between the heterotrimeric G beta subunit AGB1, the receptor-like kinase FERONIA, and RALF1 in salinity response**. *Plant Cell Environ* 2018, **41**:2475-2489.

42. • Li CY, Liu XM, Qiang XN, Li XY, Li XS, Zhu SR, Wang L, Wang Y, Liao HD, Luan S *et al.*: **EBP1 nuclear accumulation negatively feeds back on FERONIA-mediated RALF1 signaling**. *Plos Biol* 2018, **16**:e2006340.
Description of a mechanism by which FER communicates with the transcription machinery upon RALF1 treatment. FER induces EBP1 translation, phosphorylation and nuclear accumulation. EBP1 then binds the promoters of RALF1 transcriptional targets as well as the RALF1 promoter to dampen its transcription and provide a transcription-translation feedback loop. This study provides evidence for a direct communication between cell-surface receptors and transcriptional modulation, a mechanism that is largely unexplored in plants. EBP1 function is deeply rooted in eukaryotic evolution as it also connects the epidermal growth factor receptor (EGFR) with transcription in mammals. Determining and comparing the structural basis for receptor-EBP1 recognition in plants and animals would aid understanding if the conservation of EBP1 function across kingdoms dwells on an invariable interaction mechanism. Further exploration of EBP1 functions could unravel similar communication avenues for additional RKs in plants as an alternative to the canonical MAPK cascade.

43. Stegmann M: **EBP1: a crucial growth regulator downstream of receptor kinases across kingdoms**. *PLoS Biol* 2018, **16**: e3000056.

44. Bigeard J, Hirt H: **Nuclear signaling of plant MAPKs**. *Front Plant Sci* 2018, **9**:469.

45. Krysan PJ, Colcombet J: **Cellular complexity in MAPK signaling in plants: questions and emerging tools to answer them**. *Front Plant Sci* 2018, **9**:1674.

46. Bi GZ, Zhou ZY, Wang WB, Li L, Rao SF, Wu Y, Zhang XJ, Menke FLH, Chen S, Zhou JM: **Receptor-like cytoplasmic kinases directly link diverse pattern recognition receptors to the activation of mitogen-activated protein kinase cascades in Arabidopsis**. *Plant Cell* 2018, **30**:1543-1561.

47. Du C, Li X, Chen J, Chen W, Li B, Li C, Wang L, Li J, Zhao X, Lin J *et al.*: **Receptor kinase complex transmits RALF peptide signal to inhibit root growth in Arabidopsis**. *Proc Natl Acad Sci U S A* 2016, **113**:8326-8334.

48. Boisson-Dernier A, Franck CM, Lituiev DS, Grossniklaus U: **Receptor-like cytoplasmic kinase MARIS functions downstream of CrRLK1L-dependent signaling during tip growth**. *Proc Natl Acad Sci U S A* 2015, **112**:12211-12216.

49. Ma X, Xu G, He P, Shan L: **SERKing coreceptors for receptors**. *Trends Plant Sci* 2016, **21**:1017-1033.

50. Nam KH, Li J: **BRI1/BAK1, a receptor kinase pair mediating brassinosteroid signaling**. *Cell* 2002, **110**:203-212.

51. Li J, Wen J, Lease KA, Doke JT, Tax FE, Walker JC: **BAK1, an Arabidopsis LRR receptor-like protein kinase, interacts with BRI1 and modulates brassinosteroid signaling**. *Cell* 2002, **110**:213-222.

52. Meng X, Chen X, Mang H, Liu C, Yu X, Gao X, Torii KU, He P, Shan L: **Differential function of Arabidopsis SERK family receptor-like kinases in stomatal patterning**. *Curr Biol* 2015, **25**:2361-2372.

53. Santiago J, Brandt B, Wildhagen M, Hohmann U, Hothorn LA, Butenko MA, Hothorn M: **Mechanistic insight into a peptide hormone signaling complex mediating floral organ abscission**. *eLife* 2016, **5**:e15075.

54. Meng X, Zhou J, Tang J, Li B, de Oliveira MVV, Chai J, He P, Shan L: **Ligand-induced receptor-like kinase complex regulates floral organ abscission in Arabidopsis**. *Cell Rep* 2016, **14**:1330-1338.

55. • Hu C, Zhu YF, Cui YW, Cheng KL, Liang W, Wei ZY, Zhu MS, Yin HJ, Zeng L, Xiao Y *et al.*: **A group of receptor kinases are essential for CLAVATA signalling to maintain stem cell homeostasis**. *Nat Plants* 2018, **4**:205-211.
A subset of uncharacterized LRR(II)-RKs named CIKs emerge as key regulators of CLE signaling in the control of meristem development. Triple and quadruple mutants between the closely related CIK1-4 phenocopy -*clavata* mutant defects in meristem morphology. *cik* mutants are resistant to exogenous application of several CLE peptides in shoot apical meristem termination and root growth, portraying these receptors as putative CLE-signaling regulators. Further genetic and biochemical assays demonstrated that CIKs form receptor complexes with the previously characterized CLE receptors CLV1, CLV2 and RPK2, albeit lacking interaction enhancement upon peptide treatment. With this study, Hu and colleagues expand the CLE receptor repertoire in Arabidopsis and highlight the relevance of performing detailed genetic screens to uncover redundancies in plant genomes. Two concomitant reports have also brought attention towards the CIKs as CLE coreceptors [56,57], providing further evidence to support that LRR(II)-RKs are multifaceted regulators of plant development.

56. Cui YW, Hu C, Zhu YF, Cheng KL, Li XN, Wei ZY, Xue L, Lin F, Shi HY, Yi J *et al.*: **CIK receptor kinases determine cell fate specification during early anther development in Arabidopsis**. *Plant Cell* 2018, **30**:2383-2401.

57. Anne P, Amiguet-Vercher A, Brandt B, Kalmbach L, Geldner N, Hothorn M, Hardtke CS: **CLERK is a novel receptor kinase required for sensing of root-active CLE peptides in Arabidopsis**. *Development* 2018, **145**:dev162354.

58. Tang D, Wang G, Zhou JM: **Receptor kinases in plant-pathogen interactions: more than pattern recognition**. *Plant Cell* 2017, **29**:618-637.

59. Albrecht C, Boutrot F, Segonzac C, Schwessinger B, Gimenez-Ibanez S, Chinchilla D, Rathjen JP, de Vries SC, Zipfel C: **Brassinosteroids inhibit pathogen-associated molecular pattern-triggered immune signaling independent of the receptor kinase BAK1**. *Proc Natl Acad Sci U S A* 2012, **109**:303-308.

60. Lozano-Duran R, Macho AP, Boutrot F, Segonzac C, Somssich IE, Zipfel C: **The transcriptional regulator BZR1 mediates trade-off between plant innate immunity and growth**. *eLife* 2013, **2**: e00983.

61. • Smakowska-Luzan E, Mott GA, Parys K, Stegmann M, Howton TC, Layeghifard M, Neuhold J, Lehner A, Kong J, Grunwald K *et al.*: **An extracellular network of Arabidopsis leucine-rich repeat receptor kinases**. *Nature* 2018, **553**:342-346.

A comprehensive study of leucine-rich repeat (LRR) receptor kinase interaction networks. Smakowska *et al.* investigated 40 000 potential extracellular domain interactions using a sensitized high-throughput interaction assay, and produced a LRR-based cell surface interaction network consisting of 567 interactions. Using results from the interaction map they found a new interaction partner; APEX, for the immune receptors PEPR1 and 2. They showed that APEX interacts with PEPR1 and PEPR2 in a ligand-independent manner, and a wild-type *APEX* dosage is required for appropriate Pep2-induced responses. Their interaction network provided evidence for coreceptors to act as regulatory scaffolds by organizing larger RKs into signaling networks and showed that network stability ensures appropriate response modulation.

62. Schwessinger B, Roux M, Kadota Y, Ntoukakis V, Sklenar J, Jones A, Zipfel C: **Phosphorylation-dependent differential regulation of plant growth, cell death, and innate immunity by the regulatory receptor-like kinase BAK1**. *PLoS Genet* 2011, **7**: e1002046.

63. •• Perraki A, DeFalco TA, Derbyshire P, Avila J, Sere D, Sklenar J, Qi XY, Stransfeld L, Schwessinger B, Kadota Y *et al.*: **Phosphocode-dependent functional dichotomy of a common co-receptor in plant signalling**. *Nature* 2018, **561**:248-252.

This study gives important insights into the mechanism of signaling specificity in the case of the highly redundantly employed SERK coreceptors. Perraki *et al.* reveal differential SERK phosphorylation that is also mirrored in the corresponding receptors, providing the structural basis for specific receptor/coreceptor interaction. Through homology analysis between 229 Arabidopsis LRR-RKs the authors identified two distinct functional receptor classes, with or without a conserved phosphorylation site, respectively.

64. Hohmann U, Nicolet J, Moretti A, Hothorn LA, Hothorn M: **The SERK3 elongated allele defines a role for BIR ectodomains in brassinosteroid signalling**. *Nat Plants* 2018, **4**:345-351.

65. Halter T, Imkampe J, Mazzotta S, Wierzba M, Postel S, Bucherl C, Kiefer C, Stahl M, Chinchilla D, Wang X *et al.*: **The leucine-rich repeat receptor kinase BIR2 is a negative regulator of BAK1 in plant immunity**. *Curr Biol* 2014, **24**:134-143.

66. Imkampe J, Halter T, Huang S, Schulze S, Mazzotta S, Schmidt N, Manstretta R, Postel S, Wierzba M, Yang Y *et al.*: **The Arabidopsis leucine-rich repeat receptor kinase BIR3 negatively regulates BAK1 receptor complex formation and stabilizes BAK1**. *Plant Cell* 2017, **29**:2285-2303.

67. Li B, Ferreira MA, Huang M, Camargos LF, Yu X, Teixeira RM, Carpinetti PA, Mendes GC, Gouveia-Mageste BC, Liu C *et al.*: **The receptor-like kinase NIK1 targets FLS2/BAK1 immune complex and inversely modulates antiviral and antibacterial immunity**. *Nat Commun* 2019, **10**:4996.

68. Trenker R, Jura N: **Receptor tyrosine kinase activation: from the ligand perspective**. *Curr Opin Cell Biol* 2020, **63**:174-185.

69. • Cui Y, Li X, Yu M, Li R, Fan L, Zhu Y, Lin J: **Sterols regulate endocytic pathways during flg22-induced defense responses in Arabidopsis**. *Development* 2018, **145** dev.165688.

This study provides a detailed analysis of ligand-induced FLS2 receptor endocytosis with special interest on sterol homeostasis. Advanced imaging techniques (variable-angle total internal reflection fluorescence, single-particle tracking, and Fluorescence correlation spectroscopy) were applied in combination with various specific inhibitor treatments to differentiate between clathrin-mediated and sterol-associated endocytic pathway, both critical for FLS2 internalization. Further, the role of flotillins and nanodomain formation in the context of sterol distribution at the PM is discussed. In the light of this study it will be interesting to investigate if other RK are influenced by sterol-associated endocytic pathways.

70. Mbengue M, Bourdais G, Gervasi F, Beck M, Zhou J, Spallek T, Bartels S, Boller T, Ueda T, Kuhn H *et al.*: **Clathrin-dependent endocytosis is required for immunity mediated by pattern recognition receptor kinases**. *Proc Natl Acad Sci U S A* 2016, **113**:11034-11039.

71. Robatzek S, Chinchilla D, Boller T: **Ligand-induced endocytosis of the pattern recognition receptor FLS2 in Arabidopsis**. *Genes Dev* 2006, **20**:537-542.

72. Salomon S, Robatzek S: **Induced endocytosis of the receptor kinase FLS2**. *Plant Signal Behav* 2006, **1**:293-295.

73. Smith JM, Salamango DJ, Leslie ME, Collins CA, Heese A: **Sensitivity to Flg22 is modulated by ligand-induced degradation and de novo synthesis of the endogenous flagellin-receptor FLAGELLIN-SENSING2**. *Plant Physiol* 2014, **164**:440-454.

74. Claus LAN, Savatin DV, Russinova E: **The crossroads of receptor-mediated signaling and endocytosis in plants**. *J Integr Plant Biol* 2018, **60**:827-840.

75. Qi X, Maes M, Zeng S, Torii KU: **The manifold actions of signaling peptides on subcellular dynamics of a receptor specify stomatal cell fate**. *bioRxiv* 2019:836437.

76. Xue S, Zou J, Liu Y, Wang M, Zhang C, Le J: **Involvement of BIG5 and BIG3 in BRI1 trafficking reveals diverse functions of BIG-subfamily ARF-GEFs in plant growth and gravitropism**. *Int J Mol Sci* 2019, **20**:2339.

77. Desaki Y, Takahashi S, Sato K, Maeda K, Matsui S, Yoshimi I, Miura T, Jumonji JI, Takeda J, Yashima K *et al.*: **PUB4, a CERK1-interacting ubiquitin ligase, positively regulates MAMP-triggered immunity in Arabidopsis**. *Plant Cell Physiol* 2019, **60**:2573-2583.

78. Zhou J, Liu D, Wang P, Ma X, Lin W, Chen S, Mishev K, Lu D, Kumar R, Vanhoutte I *et al.*: **Regulation of Arabidopsis brassinosteroid receptor BRI1 endocytosis and degradation by plant U-box PUB12/PUB13-mediated ubiquitination**. *Proc Natl Acad Sci U S A* 2018, **115**:1906-1915.

79. Lu D, Lin W, Gao X, Wu S, Cheng C, Avila J, Heese A, Devarenne TP, He P, Shan L: **Direct ubiquitination of pattern recognition receptor FLS2 attenuates plant innate immunity**. *Science* 2011, **332**:1439-1442.

80. Wang J, Grubb LE, Wang J, Liang X, Li L, Gao C, Ma M, Feng F, Li M, Li L *et al.*: **A regulatory module controlling homeostasis of a plant immune kinase**. *Mol Cell* 2018, **69**:493-504.

81. • Song JH, Kwak SH, Nam KH, Schiefelbein J, Lee MM: **QUIRKY regulates root epidermal cell patterning through stabilizing SCRAMBLED to control CAPRICE movement in Arabidopsis**. *Nat Commun* 2019, **10**:1744.

In this study the dynamic regulation underlying the movement of CPC, a R2R3 MYB-type transcription factor, to determine root hair cell fate of neighboring epidermis cells is extended by deciphering the mode of action behind SCM receptor stabilization. By slowing down ubiquitylation processes QKY prevents SCM internalization and enhances CPC mobility. By single cell transformation Song *et al.* were able to show that the QKY/SCM module functions not in CPC export, but rather in its import.

82. An Z, Liu Y, Ou Y, Li J, Zhang B, Sun D, Sun Y, Tang W: **Regulation of the stability of RGF1 receptor by the ubiquitin-specific proteases UBP12/UBP13 is critical for root meristem maintenance**. *Proc Natl Acad Sci U S A* 2018, **115**:1123-1128.

83. Qin Y, Yang L, Sun Z, Wang X, Wang Y, Zhang J, Rehman AU, Chen Z, Qi J, Wang B *et al.*: **Redox-mediated endocytosis of a receptor-like kinase during distal stem cell differentiation**

depends on its tumor necrosis factor receptor domain. *Plant Physiol* 2019, **181**:1075-1095.

84. Tognetti VB, Bielach A, Hrtyan M: **Redox regulation at the site of primary growth: auxin, cytokinin and ROS crosstalk**. *Plant Cell Environ* 2017, **40**:2586-2605.

85. Zhao CZ, Zayed O, Yu ZP, Jiang W, Zhu PP, Hsu CC, Zhang LR, Tao WA, Lozano-Duran R, Zhu JK: **Leucine-rich repeat extensin proteins regulate plant salt tolerance in Arabidopsis**. *Proc Natl Acad Sci U S A* 2018, **115**:13123-13128.

86. Jaillais Y, Ott T: **The nanoscale organization of the plasma membrane and its importance in signaling - a proteolipid perspective**. *Plant Physiol* 2020, **182**:1682-1696.

87. Yu M, Cui Y, Zhang X, Li R, Lin J: **Organization and dynamics of functional plant membrane microdomains**. *Cell Mol Life Sci* 2020, **77**:275-287.

88. •• McKenna JF, Rolfe DJ, Webb SED, Tolmie AF, Botchway SW, Martin-Fernandez ML, Hawes C, Runions J: **The cell wall regulates dynamics and size of plasma-membrane nanodomains in Arabidopsis**. *Proc Natl Acad Sci U S A* 2019, **116**:12857-12862.
Applying advanced single particle tracking microscopy, McKenna *et al.* demonstrated the impact of cell wall and cytoskeleton for nano-cluster formation, thereby suggesting an integral model of receptor localization at the PM. Precise evaluation of size and diffusion rates of FLS2 and PIN3cluster under different CW and cytoskeleton affecting conditions makes this study a technical and conceptual example for studying receptor mobility and sub compartmentalization along the PM in general.

89. • Bucherl CA, Jarsch IK, Schudoma C, Segonzac C, Mbengue M, Robatzek S, MacLean D, Ott T, Zipfel C: **Plant immune and growth receptors share common signalling components but localise to distinct plasma membrane nanodomains**. *eLife* 2017, **6**:e25114.
Focusing on mechanisms conveying specificity between FLS2 and BRI1 pathways (that share e.g. BAK1 as coreceptor or the BIK1 kinase), the authors reveal two ways of subcellular separation at the PM: (1) the specific enrichment in nanodomains composed of different members of the remorin family and (2) the preferential colocalization of microtubule-associated BIK1 with BRI1 instead of FLS2.

90. Hurst CH, Hemsley PA: **Current perspective on protein S-acylation in plants: more than just a fatty anchor?** *J Exp Bot* 2015, **66**:1599-1606.

91. Chen D, Ahsan N, Thelen JJ, Stacey G: **S-Acylation of plant immune receptors mediates immune signaling in plasma membrane nanodomains**. *bioRxiv* 2019:720482.

92. Perraki A, Gronnier J, Gouguet P, Boudsocq M, Deroubaix AF, Simon V, German-Retana S, Legrand A, Habenstein B, Zipfel C *et al.*: **REM1.3's phospho-status defines its plasma membrane nanodomain organization and activity in restricting PVX cell-to-cell movement**. *PLoS Pathog* 2018, **14**:e1007378.

93. Albers P, Ustun S, Witzel K, Kraner M, Bornke F: **A remorin from *Nicotiana benthamiana* interacts with the Pseudomonas type-III effector protein HopZ1a and is phosphorylated by the immune-related kinase PBS1**. *Mol Plant Microbe Interact* 2019, **32**:1229-1242.

94. Liang PB, Stratil TF, Popp C, Marin M, Folgmann J, Mysore KS, Wen JQ, Ott T: **Symbiotic root infections in *Medicago truncatula* require remorin-mediated receptor stabilization in membrane nanodomains**. *Proc Natl Acad Sci U S A* 2018, **115**:5289-5294.

95. Grison MS, Kirk P, Brault ML, Wu XN, Schulze WX, Benitez-Alfonso Y, Immel F, Bayer EM: **Plasma membrane-associated receptor-like kinases relocalize to plasmodesmata in response to osmotic stress**. *Plant Physiol* 2019, **181**:142-160.

96. Campos R, Goff J, Rodriguez-Furlan C, Van Norman JM: **The Arabidopsis receptor kinase IRK is polarized and represses specific cell divisions in roots**. *Dev Cell* 2020, **52**:183-195.

97. • Breda AS, Hazak O, Schultz P, Anne P, Graeff M, Simon R, Hardtke CS: **A cellular insulator against CLE45 peptide signaling**. *Curr Biol* 2019, **29**:2501-2508.
By utilizing FRET-FLIM techniques this study investigates interaction and competition dynamics between proteins at the PM. Breda *et al.* demonstrate that the polar (shootward) localized OPS protein competes with the interaction of the receptor BAM3 with the composite CLV2/CORYNE receptors, which is required for perception of the secreted peptide CLE45 during phloem development in the root. OPS thereby establishes a mechanism to influence signaling in a locally restricted manner.

Chapter II

The receptor-like cytoplasmic kinase MAZZA integrates CLAVATA-family receptor signaling to mediate stomatal patterning in *Arabidopsis thaliana*

This manuscript is in preparation for submission and was uploaded at the preprint server bioRxiv.

https://doi.org/10.1101/2020.11.12.379859

Authors:

Patrick Blümke, Jenia Schlegel, Sabine Becher, Karine Pinto, Rüdiger Simon

Affiliations:

Institute for Developmental Genetics, Heinrich Heine University, Universitätsstraße 1, 40225 Düsseldorf, Germany

Author contributions:

R.S. and P.B. conceived and planed the project. P.B. conducted experiments and data analyses, besides the following: J.S. performed shoot meristem imaging and image processing, S.B. did FLIM interaction studies of CLV1-mNeonG vs. Pti1-like homologs (Fig. 3 C), K.P. acquired initial stomatal cluster rate data (Suppl. Fig. 15). P.B. and R.S. wrote the manuscript.

The receptor-like cytoplasmic kinase MAZZA integrates CLAVATA-family receptor signaling to mediate stomatal patterning in *Arabidopsis thaliana*

Patrick Blümke, Jenia Schlegel, Sabine Becher, Karine Pinto, Rüdiger Simon*

Institute for Developmental Genetics, Heinrich Heine University, Universitätsstraße 1, 40225 Düsseldorf, Germany

* Corresponding author: ruediger.simon@hhu.de

Abstract

The receptor-like kinases (RLKs) CLAVATA1 (CLV1) and BARELY ANY MERISTEMs (BAM1 – 3) form the CLV-family (CLVf), which perceives peptides of the CLV3/EMBRYO SURROUNDING REGION (ESR)-related (CLE) family within various developmental and physiological signaling pathways of *Arabidopsis thaliana*. CLE peptide signaling, which is required for meristem size control, vascular development, pathogen responses, and long-range communication between root and shoot, involves the formation of receptor complexes at the plasma membrane (PM). These complexes comprise RLKs and co-receptors in varying compositions depending on the signaling context and regulate target gene expression, such as *WUSCHEL* (*WUS*). How the CLE signal is transmitted into the nucleus after perception at the PM is not known.

We here report on the identification of a direct interactor of CLV1, the membrane-associated receptor-like cytoplasmic kinase (RLCK) MAZZA (MAZ), which is widely expressed throughout the plant. MAZ and additional members of the Pti1-like protein family interact *in vivo* with CLVf receptors. MAZ localizes to the PM via posttranslational palmitoylation, which could enable stimulus-triggered protein re-localization. We identified a role for a CLV1/MAZ signaling module during stomatal and root development, and redundancy could potentially mask other phenotypes of *maz-1* mutants. We propose that RLCKs such as MAZ mediate CLVf signaling in a variety of developmental contexts, paving the way towards understanding the intracellular processes after CLE peptide perception.

Introduction

Plant communication and sensing of environmental cues rely on the perception of extracellular signaling molecules via PM-localized cell surface receptors. The genome of *Arabidopsis thaliana* encodes more than 400 membrane-spanning RLKs with intracellular kinase domains (KDs) and versatile types of extracellular domains that perceive e.g. phytohormones, pathogen-associated compounds, or small peptides (Shiu and Bleecker, 2003).

Among this heterogenic group of receptors, CLV1 is one of the best-characterized RLKs with key functions in stem cell regulation in the shoot apical meristem (SAM), inflorescence meristems (IMs), floral meristems (FMs), and the (distal) root meristem (RM) (Stahl and Simon, 2012). Together with its close relatives BAM1, BAM2, and BAM3, CLV1 forms the core family of CLV (CLVf) receptors, which perceive CLE peptides at the PM through their leucine-rich repeat (LRR) receptor domains (Shinohara and Matsubayashi, 2015; Hazak et al., 2017). Beyond meristem homeostasis, CLVf receptors and their associated CLE ligands function in various contexts of plant life, e.g. differentiation of xylem and phloem (Fukuda and Hardtke, 2020), response to bacterial infections (Hanemian et al., 2016), cyst nematode parasitism (Guo et al., 2017), and intercellular spreading of small RNAs or virus particles through plasmodesmata (Rosas-Diaz et al., 2018). Functional diversity of CLE perception via CLVf receptors is also reflected by context-specific interaction and cross-regulation with other RLKs or receptor-like proteins (RLPs).

In the shoot meristems the stem cell derived peptide CLV3, founding member of the CLE family, binds to CLV1 to downregulate the stem cell fate repressing transcription factor WUSCHEL (WUS) as part of a negative feedback loop that dynamically regulates the size of the stem cell domain (Mayer et al., 1998; Schoof et al., 2000; Brand et al., 2000). Besides CLV1, the receptor network that contributes to CLV3 perception in the shoot meristems comprises BAM1 – 3 (DeYoung et al., 2006; Deyoung and Clark, 2008), the heteromeric CLV2/CORYNE (CRN) complex (Jeong et al., 1999; Müller et al., 2008; Bleckmann et al., 2010), and the LRR-RLK RECEPTOR PROTEIN KINASE2 (RPK2) (Kinoshita et al., 2010). BAM1 and BAM2, which were also shown to directly bind CLV3 peptide, can functionally replace CLV1 in the SAM and FM. However, in wild type plants their expression is suppressed in the stem cell domain in a CLV3/CLV1-dependent fashion (Shinohara and Matsubayashi, 2015; Nimchuk et al., 2015). The shoot meristem phenotypes of *clv1* and *clv2*/*crn* mutants are additive, suggesting synergistic effects in sensing CLV3 (Kayes and Clark, 1998; Müller et al., 2008). Although the CLV2/CRN heteromer resembles the structure of a typical LRR-RLK, the

heteromer cannot by itself perceive and transmit CLV3 signals (Nimchuk et al., 2011a; Shinohara and Matsubayashi, 2015).
CLVf receptors are also crucial for CLE perception in the RM. Here, CLV1 is restricted to areas distal to the stem cell organizing quiescent center (QC), where it interacts with the non-LRR-RLK ARABIDOPSIS CRINKLY4 (ACR4) to repress columella stem cell (CSC) fate via a CLE40-dependent pathway (Stahl et al., 2009, 2013). *BAM3* is specifically expressed within the proximal RM in the developing phloem cell files. Here, BAM3 functions as the receptor for CLE45 to regulate sieve element (SE) differentiation together with other phloem-specific factors and the CLV2/CRN heteromer (Anne and Hardtke, 2018; Breda et al., 2019). *BAM1* is broadly expressed in the RM and perceives CLE9/10 peptides to regulate early cell fate decisions during xylem differentiation (Qian et al., 2018).

Co-receptors additionally contribute to the signaling versatility of many LRR-receptor kinase signaling pathways. They are typically characterized by a short extracellular domain with low numbers of LRRs to complete the binding pocket of the corresponding main receptor (recent overview and classification by (Xi et al., 2019)). Mutant analyses and interaction studies revealed that the CLAVATA3 INSENSITIVE RECEPTOR KINASEs1 – 4 (CIK1 – 4) are redundant co-receptors of the CLVf receptors as well as of RPK2 (Hu et al., 2018; Cui et al., 2018; Anne et al., 2018).

The variability of CLVf receptors to function in diverse informational networks with distinct signaling outputs requires mechanisms that add specificity to each pathway. One potential layer of specificity can arise from downstream signaling. However, the immediate early events after recognition of CLE peptides by CLVf receptors are not clear. Studies in maize and Arabidopsis suggest the involvement of heterotrimeric GTP binding protein (G-protein) complexes to integrate CLE peptide responses (Bommert et al., 2013; Ishida et al., 2014; Wu et al., 2020). Mitogen-activated protein kinase (MAPK) cascades, which display a classical mode of intracellular signal transduction in RLK pathways (reviewed in (He et al., 2018)), have been proposed to mediate downstream CLE signaling (Betsuyaku et al., 2011; Lee et al., 2019). However, no physical interaction between CLVf receptors and MAPK signaling elements have yet been shown.

Many cell surface receptor-based signaling pathways rely on RLCKs as key mediators of information transduction, integration, and attenuation (reviewed in (Liang and Zhou, 2018)). RLCKs form a heterogenous group of signaling kinases that are characterized by the absence of extracellular receptor domains and lack a TMD in most cases, however, they can be PM-

associated (Bi et al., 2018). The Arabidopsis genome contains 402 potential *RLCK*-encoding genes that cluster into 15 phylogenic sub-groups (Shiu et al., 2004; Fan et al., 2018). These comprise proteins like the RLCK class VII member BOTRYTIS-INDUCED KINASE1 (BIK1), which acts as an important signaling hub downstream of various LRR-RLKs to control immune responses, e.g. via FLAGELLIN SENSING2 (FLS2), but also mediates processes of developmental regulation through BRASSINOSTEROID INSENSITIVE1 (BRI1) or the ERECTA-family (ERf) (Lu et al., 2010; Lin et al., 2013; Chen et al., 2019). Moreover, non-LRR-RLKs also depend on RLCKs. For example. FERONIA (FER), ANXUR1 (ANX1), or ANX2 from the *Catharanthus roseus* RLK1-like (*Cr*RLK1L) family regulate cell wall (CW) integrity through MARIS (MRI) (Boisson-Dernier et al., 2015). MRI belongs to the RLCK VIII subgroup, which contains 11 Arabidopsis genes that share high sequence similarity with *Pti1* from *Solanum lycopersicum* (tomato), a target of the Pto kinase conferring resistance against the bacterial speck disease (Zhou et al., 1995; Sessa et al., 2000). Furthermore, members of the Pti1-like proteins in Arabidopsis (Pti1-1, Pti1-2, Pti1-3, Pti1-4) were shown to interact with OXIDATIVE STRESS INDUCIBLE1 (OXI1), which mediates the cellular response to stress signals like ROS and fungal elicitors. Pti1-4 was also associated with MAPK signaling downstream of OXI1 (Anthony et al., 2006; Forzani et al., 2011). Additionally, the Pti1-like family members CYTOSOLIC ABA RECEPTOR KINASE1 (CARK1) and CARK6 were found to be interactors of the REGULATORY COMPONENTS OF ABA RECEPTORS (RCARs) that function in perceiving the phytohormone abscisic acid (ABA), a general trigger of abiotic stress responses (Zhang et al., 2018; Wang et al., 2019).

Although some members from the RLCK VIII family in Arabidopsis have emerged as crucial signaling intermediates of several pathways, most Pti1-like homologs are not characterized in detail, or not at all. We here report the identification of MAZZA (MAZ, Pti1-3), a member of the RLCK subgroup VIII, as an interactor of the CLVf receptors, thereby expanding the potential range of the RLCK VIII / Pti1-like family to LRR-RLK pathways. We further expand the spectrum of developmental processes regulated by CLV1 and show that MAZ acts with CLV1 in stomatal patterning.

Results

MAZ interacts with CLV1 *in vivo*

CLVf receptors are critical for meristem homeostasis but also play pivotal roles during other developmental and physiological signaling events. This is, for example, reflected in the expression of *CLV1* in various tissues besides the shoot meristems, like companion cells (CCs) of the phloem in aerial organs and the root, and in the distal RM. Furthermore, we found that *CLV1* is expressed in the epidermis of cotyledons and true leaves, particularly in developing cells of the stomata lineage (Fig. 1, Suppl. Fig. 1 A). However, direct downstream targets of CLVf receptors are not known in any of those tissues. To identify CLV1 interactors we applied an untargeted, non-organ-biased co-immunoprecipitation (CoIP) approach with magnetic anti-GFP beads (ChromoTek) against CLV1-2xGFP from whole Arabidopsis seedlings expressing the receptor-fluorophore fusion under the control of the endogenous *CLV1* promotor. This transgene is fully functional and was previously shown to complement the known phenotypes of *clv1* mutants (Nimchuk et al., 2011b). Via subsequent mass spectroscopy analyses of the Co-IP fractions we detected Pti1-like proteins among the peptide sequences specifically pulled down with CLV1 and not found in GFP controls (Suppl. Tab. 1). Most of those hits were unique for Pti1-3, while some identified peptide sequences also aligned to other Pti1-like members. Among the candidates for CLV1 interaction we identified Pti1-3 as most promising due to its predicted PM-localization and kinase function. The *Pti1-3* gene (At3g59350) encodes a protein with a predicted KD and an undefined N-terminal region. Due to its capability to interact with CLV1 *in vivo* we dubbed the protein MAZZA (MAZ, Italian for “club”, in analogy to the Latin “clavata”, and Greek “coryne”).

MAZ is also found in complex with CLV1 when following a targeted CoIP strategy with leaf material from *Nicotiana benthamiana* plants, transiently expressing the respective interaction partners fused either to GFP or mCherry (mCh) to allow subsequent immunodetection (Fig 2 A). Supplying CLV3 peptide prior to protein extraction did not influence complex formation with CLV1, pointing towards a constitutive, ligand independent interaction. To analyze the complex at subcellular level, we applied Förster resonance energy transfer (FRET)-based fluorescence-lifetime imaging microscopy (FLIM) and demonstrated direct interaction between MAZ and CLV1 at the PM (Fig. 2 B). In these FLIM experiments within transiently transformed *N. benthamiana* leaf epidermis cells, the donor-lifetime of CLV1-GFP decreases significantly in the presence of MAZ-mCh (mean FRET efficiency of 5.9 %, Supp. Tab. 2), while a PM-located negative control tagged to mCh affects donor lifetime only at a mean FRET

efficiency of 2.0 %, which we defined as the background level for randomly distributed acceptor fluorophores in all following FLIM assays. Infiltration of 5 µM CLV3 peptide into the leaves before FLIM measurements did not affect lifetime. This suggests that CLV3 ligand binding to CLV1 neither enhances the interaction with MAZ, nor induces a rapid dissociation of the two proteins within this experimental setup.

MAZ and Pti1-like homologs interact with CLVf receptors and related pathway elements

Next, we extended the FRET-FLIM interaction studies in the *N. benthamiana* expression system to test if MAZ can interact with other proteins that contribute to CLE peptide perception. We detected interactions at the PM between MAZ and the CLVf receptors BAM1 and BAM3 with mean FRET efficiencies of 6.5 % and 4.0 %, respectively (Fig 3 A, B, Suppl. Tab. 2). Furthermore, MAZ interacts with the co-receptor CIK2 (5.7 %, Fig 3 A), and with CRN in the presence of CLV2 (3.0 %, Fig. 3 B). These data indicate that MAZ could integrate different CLE peptide triggered RLK pathways.

Additionally, lifetime of MAZ-eGFP decreases in the presence of MAZ-mCh with a mean FRET efficiency of 5.3 % (Fig.3 A). Thus, MAZ can form dimers or higher ordered homomers, which might reflect auto-regulative mechanisms.

Since all 11 members of the Pti1-like family in Arabidopsis are highly conserved at amino acid (aa) sequence level (Appendix), they might be functionally redundant. Indeed, from four Pti1-like homologs that we tested additionally to MAZ, three, namely CARK1, CARK6, and Pti1-11 were able to interact with CLV1 at the PM of *N. benthamiana* leaf epidermis cells with mean FRET efficiencies ranging from 4.2 to 5.4 %. Only Pti1-2 showed no interaction with CLV1 (Fig. 3 C). This observation is not reflected in the phylogeny of the Pti1-like family, because, for example, CARK1 is more distantly related to MAZ than Pti1-2 (Fig. 3 D). However, differences in the phylogeny do not necessarily concern the sequences that are crucial for protein complex formation. *Vice versa*, detecting no change of donor lifetime in the presence of a certain acceptor does not generally exclude physical interaction, e.g. if the fluorophore fusion sterically hinders energy transfer.

Subcellular localization of MAZ at the PM depends on palmitoylation

MAZ interacts with RLKs and other signaling proteins at the PM. Accordingly, all analyzed MAZ fusion proteins with different fluorophores are PM-localized after transgene expression in *N. benthamiana* (Suppl. Fig. 3, 4) as well as in *A. thaliana* (Fig. 4, 5 Suppl. Fig. 1, 6, 7). MAZ co-localization with CLV1 at the PM is not extended to CLV1-GFP vesicles in *N. benthamiana* cells, which indicate receptor sequestration (Suppl. Fig. 3). This suggests that

MAZ is not sequestered together with CLV1 but might instead follow distinct signaling routes after RLK activation and turnover.

The MAZ protein sequence does not harbor any TMD, but the N-terminal region possesses predicted palmitoylation sites (C48, C49, Suppl. Tab. 3). S-acylation, i.e. covalent binding of palmitic acid or other fatty acids to the thiol group of cysteine residues, is reversible and thus can represent a mechanism of specific regulation (Hurst and Hemsley, 2015). We found that the predicted MAZ palmitoylation sites are responsible for its PM-localization. Exchanging the corresponding cysteines in the fusion construct *MAZ*^{PalMut}*-eGFP* results in high amounts of cytoplasmic fluorescence signals instead of PM-localization of the fusion protein after expression in *N. benthamiana* or Arabidopsis (Fig 4, Suppl. Fig. 4). This strongly indicates that subcellular PM localization of MAZ relies on post-translational modification via S-acylation.

MAZ shares expression domains with the CLVf receptors in *A. thaliana*

MAZ is expressed in various tissues and organs of Arabidopsis including the distinct expression domains of the CLVf receptors. Analyzing several independent fluorescent *MAZ* reporter lines, we observed differences between translational and transcriptional reporters suggesting that the *MAZ* coding sequence may affect protein expression (Suppl. Fig. 5). Thus, in the following experiments we used translational lines comprising the *MAZ* promotor sequence and the *MAZ* coding sequence including introns to study *MAZ* expression.

In the shoot, *MAZ* is expressed in cells of the leaf epidermis, including stomata precursor cells and guard cells (GCs), the vasculature, and the hypocotyl epidermis (Fig 5 D, Suppl. Fig. 1, 6 C). Furthermore, within the inflorescence we detected *MAZ* expression in the IM, primordia and FMs. Signal intensity is elevated in the outermost cell layer (L1) with expression peaks at the boundary regions to emerging primordia. Expression appears to be highest in newly formed primordia and slightly attenuates during further development. (Fig. 5 A, Suppl. Fig. 7). Within the root, *MAZ* is expressed in the epidermis, particularly in root hair cells, in the vasculature, and in the RM. *MAZ* is also expressed in emerging lateral roots from early stage onwards. In mature lateral roots expression resembles the pattern in the main root (Fig 5 B, C, Suppl. Fig. 6). *MAZ* expression in the RM is characterized by elevated signal intensities in the QC and the surrounding stem cells. Expression decreases from the initials gradually towards the elongation zone. However, in developing phloem cell files fluorescence signals are not attenuated but continue upstream in the vasculature cylinder (Fig. 5 B, Suppl. Fig. 6). Marking the position of mature SEs by aniline blue staining revealed that *MAZ* expression in the

differentiated vasculature is concentrated in CCs and procambial tissue, but barely in the SEs (Suppl. Fig. 1 B, C).

We detected *MAZ* signals in all *CLV1* expression domains (compare Fig. 1). Double reporter lines show co-localization of CLV1-GFP and MAZ-mCh, for example, at the border region to emerging primordia in the IM and in the distal RM (Suppl. Fig. 8). Furthermore, *MAZ* expression comprises previously reported expression domains of *BAM1* and *BAM3* (Depuydt et al., 2013; Shimizu et al., 2015). Thus, local distribution of MAZ allows its participation in different CLVf receptor pathways in Arabidopsis.

MAZ mediates CLE peptide signaling in root development

We characterized the functional impact of MAZ within CLVf pathways by analyzing mutants harboring the T-DNA *maz* allele GABI-Kat 485F03, hereafter referred to as *maz-1*. The insertion event disrupts the KD of MAZ before the predicted active site and m*az-1* plants show substantial decrease of full-length *MAZ* transcripts (~30-fold in comparison to wild type samples, Suppl. Fig. 9).

Elevated organ number typically associated with *clv*-like phenotypes reflects enhanced stem cell activity in meristems, concomitant with an increase in the sizes of shoot and floral meristems. While *clv3-9*, *clv1-20*, and *crn-10* show increased carpel numbers per silique, *maz-1* plants resemble the wild type. The double mutants *clv1-20;maz-1* and *crn-10;maz-1* resemble the single mutants *clv1-20* and *crn-10*, respectively, indicating that a loss of MAZ is insufficient to disrupt CLV3 signaling (Fig. 6 A, Suppl. Fig. 10).

To test MAZ function within CLE40-mediated stem cell differentiation in the distal RM, we quantified CSC layers in *maz-1* roots. Both, *cle40* and *clv1* mutants show increased CSC number due to reduced CLE40 signaling (Stahl et al., 2009, 2013). While increased CLE40 peptide in the growth medium reduces CSC layers in the wild type, *clv1-20* mutants are desensitized and maintain more CSC layers. *Maz-1* mutants resemble the wild type on standard growth medium but are partially resistant against external CLE40 peptide treatment that causes drastic reduction of CSC layers in Col-0 (Fig. 6 B, Suppl. Fig. 11). Notably, we found that the double mutant *clv1-20;maz-1* is fully sensitive to CLE40 peptide. This could point to an additional, parallel CLE40 perception pathway during CSC specification, for example via BAM1, which is activated in the absence of both CLV1 and MAZ.

CLE peptide treatment not only affects CSC fate but also root growth due to premature differentiation of the proximal RM. Disruption of CLE perception, for example, in *clv2, crn*, or *rpk2* mutants confers resistance against CLE-induced root shortening (Fiers et al., 2005;

Shimizu et al., 2015; Müller et al., 2008). Here, we accessed root lengths of plants grown on CLV3 peptide, which is not produced in roots but can generally substitute all root-active CLE peptides in terms of root shortening, and CLE45 peptide, which is expressed in developing phloem files and perceived via BAM3 and CRN/CLV2 (Hazak et al., 2017). Our root growth assays revealed that *maz-1* single mutants are less sensitive than Col-0 seedlings to physiological concentrations of either CLV3 or CLE45 peptide. However, *maz-1* plants grown in the presence of 100 nM CLE peptides display root reductions comparable to wild type samples (Fig. 6 C). We also observed that the *maz-1* allele partially antagonizes *crn-10* mediated resistance to CLV3 peptide in *crn-10;maz-1* double mutants at 10 nM peptide concentration. Similar to the proposed role in CSC fate control, this could again indicate a dual function of MAZ to mediate CLE responses and simultaneously repressing parallel acting CLE perception pathways.
Together, our data suggest that MAZ is involved in several CLE signaling pathways, involving CLV1 and CLV2/CRN.

We also accessed morphology and physiological constraints of *maz-1* plants regarding previously described phenotypes of other *pti1-like* mutants, i.e. impaired root hair development of *mri* mutants (Boisson-Dernier et al., 2015), and hypersensitivity to drought stress like *cark1* and *cark6* mutants (Zhang et al., 2018; Wang et al., 2019). However, in contrast to *mri-2* and *fer-4* mutants, *maz-1* seedlings display mean root hair length at wild type-level (Suppl. Fig. 12). Furthermore, within two different experimental setups, neither *maz-1* mutants nor *MAZ* overexpression lines show altered drought stress responses, which have been associated with disturbed ABA signaling of mutants or overexpressors of *CARK1* and *CARK6*, respectively (Suppl. Fig. 13, 14).

A novel role for CLV1 with MAZ in stomatal spacing

Regular patterning of stomata at the leaf epidermis is the result of finely controlled series of cell divisions of the stomata cell lineage. In this process meristemoid mother cells (MMCs) divide asymmetrically to form a meristemoid and a larger sister cell. While meristemoids are precursors of guard mother cells (GMCs) that differentiate into the two GCs of a stoma, the sister cell may become a pavement cell or undergoes a spacing division before generating a new meristemoid (reviewed in (Bergmann and Sack, 2007)). Mutants lacking this regular spacing between two stomata, for example, due to disruption of the receptor complex that senses positional cues in the leaf epidermis, include, among others, *er;erl1;erl2* triple mutants of the *ERf* receptor genes and mutants of the LRR-RLP encoding *TOO MANY MOUTHS* (*TMM*) gene.

These mutants accumulate two or more stomata directly adjacent to each other, i.e. display stomatal clustering (reviewed in (Zoulias et al., 2018)).

We observed that *clv1* mutants are also associated with defects in regular patterning in the leaf epidermis (Suppl. Fig. 15). Initial data revealed an increased number of stomata in true leaves, but not in cotyledons, of *clv1-20* plants in comparison to wild type Col-0, uncovering a novel role for CLV1 in stomatal patterning. Furthermore, CLE peptide treatment antagonized this effect in *clv1-20* mutants (Suppl. Fig. 15). We extended these analyses to include *maz-1* and the double mutant *clv1-20;maz-1*. Quantification of stomatal clusters in seedlings 14 DAG grown on ½ MS agar plates, not only confirmed defects in patterning of *clv1-20* true leaves, but also showed that the double mutant *clv1-20;maz-1* enhances this phenotype (Fig. 7). In comparison to the wild type control (Col-0) the mean stomata cluster rate of *clv1-20* is elevated (~ 2 % stomata in cluster). However, in *clv1-20;maz-1* cluster rate is significantly increased to ~ 10 %, while the single *maz-1* mutant displays no clusters. Stomata density was not significantly different between genotypes. This points towards a specific function of CLV1 and MAZ in spacing divisions, but not stomata specification. Since both, *MAZ* and *CLV1*, are expressed in cells of the stomatal lineage (Fig. 1 E, 5 D), we propose that the CLV1/MAZ signaling module serves to establish stomata spacing.

Discussion

CLVf RLKs participate in various signaling systems, thereby controlling meristem homeostasis but also processes like vascular formation or plant immunity. Here, we add stomata development to the scope of CLV1 functions. Considering the diversity of CLVf pathways, mechanisms to mediate specific downstream responses are required. With the identification of MAZ and several of its homologs as novel interactors of CLVf receptors we provide evidence that the RLCK VIII family contributes to downstream signaling after CLE perception. Furthermore, the expression pattern of *MAZ* overlaps with the places of action of the CLVf receptors in Arabidopsis. Therefore, MAZ might integrate and cross-regulate signaling cues from different CLVf receptors.

Functional redundancy of Pti1-like homologs could mask mutant phenotypes

We found that *maz-1* plants are resistant to exogenous CLE treatment in the context of CSC specification (Fig. 6 B). However, in comparison to *clv1-20* mutants, the resistance of *maz-1* is less pronounced. Also, the CLE peptide resistance of *maz-1* seedlings regarding proximal RM development is less penetrating than in mutants of the involved receptors. At higher CLE peptide concentrations root shortening of *maz-1* seedlings resembles the level of wild type-samples (Fig. 6 C). Furthermore, the *maz-1* allele confers no *clv1*-like increased carpel number (Fig. 6 A). These observations suggest that other Pti1-like homologs compensate MAZ function in *maz-1* mutants. In line, several Pti1-like proteins interact with CLV1, reflecting a conserved binding capacity of Pti1-like homologs to the CLVf receptors (Fig. 3 C).

Functional redundancy is a common feature within the Pti1-like family. For example, Pti1-1, Pti1-2, and Pti1-3 (=MAZ), respectively, interact with the stress-related kinase OXI1 (shown by yeast-two-hybrid and Co-IP). However, only the interaction of OXI1 with Pti1-2 was validated by stimulus triggered phosphorylation *in vivo* (Anthony et al., 2006). This indicates a high general potential of functional redundancy but at the same time demonstrates the presence of mechanisms that add specificity to the respective Pti1-like homologs within their physiological context.

The N-terminus of Pti1-like proteins could determine functional specification

The 11 Pti1-like homologs in Arabidopsis are especially conserved within the KDs, while their more variable N-termini allow specification (Appendix). As we demonstrated in here, the MAZ N-terminus determines its subcellular localization via palmitoylation (Fig. 4). In contrast to other mechanisms that mediate PM-localization, the attachment of a palmityl group via S-

acylation is reversible. As such, palmitoylation can dynamically regulate the subcellular localization of proteins (reviewed in (Hurst and Hemsley, 2015)). All Pti1-like family members in Arabidopsis, except Pti1-6, harbor conserved cysteines, which are predicted palmitoylation sites (Suppl. Tab. 3). In general, S-acylation is often coincidently found with protein myristoylation. However, within the Arabidopsis Pti1-like family only CARK1 is additionally equipped with a myristoylation site, suggesting it is obligatorily PM-localized. The subcellular localization of the other nine Pti1 homologs in Arabidopsis might be dynamically controlled by counteracting protein S-acyl transferases (PATs) and acyl protein thioesterases. Although the underlying mechanisms in plants are not well understood (reviewed in (Li and Qi, 2017)), palmitoylation allows stimulus-triggered subcellular re-localization and display a powerful tool for signal transduction. S-acylation of Pti1-like proteins is evolutionary conserved among various species, including monocots, as shown e.g. for ZmPti1a from maize and OsPti1a from rice (Herrmann et al., 2006; Matsui et al., 2014).

Notably, the MAZ N-terminus is longer than in most of its Arabidopsis homologs, potentially offering additional target sites for specific control, such as differential phosphorylation or protein turnover via ubiquitination. It comprises two Phospho-Serines (detected in the PhosphAt Database (Heazlewood et al., 2008)) and according to different prediction tools 3 – 7 lysine residues as potential targets for ubiquitination.

CLV1/MAZ contributes to spacing divisions in stomata development

Feedback-regulated signaling systems are crucial to integrate positional information from neighboring cells or tissues into developmental processes and to ensure dynamic but controlled growth. Such feedback loops determine, for instance, the stem cell domain in the SAM, IMs, and FMs (Fletcher et al., 1999; Brand et al., 2000), and cell fate in the leaf epidermis during stomatal patterning (reviewed in (Tameshige et al., 2017)). While the CLV pathway is the major regulative element in the shoot meristems, the ERf receptors are essential for cell fate decisions during leaf epidermis differentiation. However, the ERf also impacts stem cell homeostasis in the shoot meristems (Uchida et al., 2013; Mandel et al., 2014; Zhang et al., 2020). In turn, CLV-related pathways are involved in stomatal development, e.g. by perceiving CLE9/10 peptides (Qian et al., 2018). In here we provide first evidences that *clv1-20* mutants are defective in regular patterning of GCs and that *maz-1* enhances this phenotype as a second site mutation (Fig. 7).

In the epidermis of cotyledons and true leaves the *CLV1* promotor is predominantly active in meristemoids and stomatal lineage ground cells, while *CLV1* expression is barely detectable in

differentiated epidermis cells, neither in pavement cells nor in GCs (Fig. 1). This hints toward a specific function of the CLV1 receptor within the precise signaling events of leaf epidermis differentiation. The notion that *clv1* mutants, in contrast to, for example, *tmm* mutants (Geisler et al., 2000), show rather mild stomatal patterning defects suggests the presence of redundantly acting genes. Recently, the LRR-RLK HAESA-LIKE 1 (HSL1) was shown to regulate GC number by sensing CLE9/10 peptides, which are expressed in stomatal lineage cells of the leaf epidermis (Qian et al., 2018). Likewise, the close CLV1-homolog BAM1 is capable of binding CLE9 (Shinohara et al., 2012). However, *hsl1* mutants are resistant to CLE9/10 treatment that leads to decreased GC number of wild type cotyledons, while *bam1*, *bam2*, *bam3*, and *clv1* single mutants, as well as all tested double mutant combinations of those four, are sensitive toward peptide treatment (Qian et al., 2018). In line with this, stomata density was not affected in our experiments with *clv1-20* either. This suggests that HSL1 operates at a different stage of stomatal development than CLV1 and its homologs. The perception of CLE9/10 by HSL1 in the leaf epidermis destabilizes SPEECHLESS (SPCH), one of the central transcription factors promoting MMC fate. Negative regulation of SPCH by the CLE9/10-HSL1 module is additive to signaling via EPF2-ER, with both pathways reducing the number of cells acquiring MMC identity (Qian et al., 2018). Since the total number of stomata in *clv1* mutants is comparable to the wild type (Fig. 7), CLV1 does not determine MMC fate, but acts later in the stomatal lineage to establish the one-cell-spacing rule between two stomata. This stomatal spacing is mainly regulated by EPF1 and its primary receptor ERL1, which form a negative feedback loop with the SPCH-homolog MUTE (Hara et al., 2007; Lee et al., 2012; Qi et al., 2017). CLV1-based signaling could interfere with this feedback regulation or act in parallel to finetune spacing divisions.

Our observation that the double mutant *clv1-20;maz-1* displays increased stomata cluster rate in comparison to *clv1-20* single mutants (Fig. 7) suggests that MAZ is not only involved in stomatal pattering as a potential downstream target of CLV1, but also affects spacing divisions through CLV1-independent signaling. Therefore, MAZ is possibly a shared downstream target of CLV1 and other RLKs, e.g. ERL1. Since *maz-1* single mutants are wild type-like regarding stomata clusters, redundancy mediated by other Pti1-like homologs can be assumed. However, in combination with the *clv1-20* mutation this redundancy is partly overcome. This might be explained by the quantitative character of CLV1/MAZ signaling during stomatal development comprising additional, yet unknown components.

Conclusions

We here report on the identification of MAZ and other RLCKs of the Pti1-like family as intermediators of CLVf receptor responses. Within the versatile functional contexts of CLVf pathways, MAZ and redundantly acting homologs could contribute to differential signaling outputs. After CLE perception by CLVf receptors, signal transduction may involve transphosphorylation between the CLVf RLKs and Pti1-like RLCKs and subsequent detachment of MAZ or its homologs from the membrane to reach intracellular targets (compare Fig. 8). Deciphering how MAZ and the CLVf are functionally connected will be critical for further characterization of the Pti1-like family as downstream elements of CLVf receptor pathways.

Material and Methods

Detailed information on chemicals used for the described experiments are available in Suppl. Tab. 4.

Plant material and growth conditions

All *Arabidopsis thaliana* (L.) Heynh. plants in this study are ecotype Columbia-0 (Col-0). Origin and details on utilized mutants harboring the alleles *maz-1*, *clv1-20*, *crn-10*, *clv3-9*, *cark1-2*, *cark6-1*, *mri-2*, and *fer-4*, respectively, can be found in Suppl. Tab. 5. The presence of the respective alleles was controlled following genotyping strategies as listed in Suppl. Tab. 6. Before sowing, *A. thaliana* seeds were sterilized in ethanol solution (10 min in 80 % v/v ethanol, 1.3 % w/v sodium hypochlorite, 0.02 % w/v SDS), or in a chloric gas atmosphere (1 h in a desiccator after mixing 50 ml of 13 % w/v sodium hypochlorite with 1 ml 37 % HCl,). If not indicated differently, plants were cultivated in phytochambers under long day (LD) conditions (16 h light / 8 h dark) at 21 °C on soil. Alternatively, seedlings were cultivated for up to 14 days on ½ MS agar plates (1 % w/v sucrose, 0.22 % w/v MS salts + B5 vitamins, 0.05 % w/v MES, 12 g/l plant agar, adjusted to pH 5.7 with KOH) in phytocabinets (continuous light, 60 % humidity, and 21 °C).

N. benthamiana plants were grown 4 – 5 weeks in the greenhouse and subsequently used for transient leaf epidermis cell transformation. After infiltration, *N. benthamiana* plants were kept under high humidity in continuous light.

Cloning

Information on the entry plasmids, subsequently used for the assembly of plant expression vectors can be found in Suppl. Tab. 7. New entry plasmids generated in this study contain DNA sequences that were PCR-amplified (with Phusion High-Fidelity PCR polymerase) from genomic DNA prepared of Col-0 rosette leaves. PCR fragments were introduced via customized oligonucleotide overhangs to either pENTR® (Gateway® system, (Katzen, 2007)) or pGGA000 and pGGC000 (GreenGate system, (Lampropoulos et al., 2013)). Coding sequences of genes of interest (GOIs) were amplified without the STOP codon to allow C-terminal fusions with fluorophores. Single positions within gene sequences were modified by site-directed mutagenesis applying the QuikChange II kit according to manufacturer's protocol (Agilent Technologies).

Destination plasmids utilized for transient expression in *N. benthamiana* and for generation of stable *A. thaliana* lines are listed in Suppl. Tab. 8 and 9, respectively. Inducible vectors were

created by a Gateway® LR reaction (according to manufacturer's instructions, Thermo Fisher Scientific), combining an entry vector harboring the GOI with either pABindGFP or pABindmCherry (Bleckmann et al., 2010). Transgenes for constitutive *N. benthamiana* and stable Arabidopsis expression were constructed with the GreenGate system, assembling desired DNA sequences and the backbone pGGZ001 following a golden gate principle (compare Suppl. Tab. 8 and 9).

To amplify plasmid DNA, competent *Escherichia coli* DH5α cells were heat-shock transformed and cultivated on selective LB medium (1 % w/v tryptone, 0.5 % w/v yeast extract, 0.5 % w/v NaCl). After plasmid DNA purification via commercial kits, the plasmids were validated by restriction digest and Sanger sequencing.

Transient gene expression in *N. benthamiana*

Agrobacterium-mediated transformation of leaf epidermis cells of *N. benthamiana* was applied to monitor transient expression of transgenes. The *Agrobacterium tumefaciens* strain GV3101 pMP90 (rifampicin and gentamycin resistant) was used. Bacteria were transformed with the required plasmid vectors via the heat-shock method (aliquots of competent cells mixed with 1 µl 100 nM plasmid DNA were incubated for 5 min in liquid N_2 followed by 5 min at 37 °C and subsequent regeneration). All Gateway®-based destination plasmids were introduced to GV3101 pMP90 additionally equipped with an expression cassette for the p19 suppressor of gene silencing from the tomato bushy stunt virus to enhance efficiency of transgene expression (Voinnet et al., 2003). Plasmids constructed via the GreenGate system were introduced to *A. tumefaciens* GV3101 pMP90 pSoup. The helper plasmid pSoup confers resistance against tetracycline and contains the *RepA* gene, which encodes a trans-activating replicase for the pSA origin of replication that is mandatory for propagation of GreenGate-based destination plasmids in *A. tumefaciens* (Hellens et al., 2000).

For infiltration of *N. benthamiana* leaves, agrobacteria containing the respective expression cassettes were cultivated overnight with shaking at 28 °C in 5 ml dYT (double Yeast Tryptone, 1.6 % w/v tryptone, 1 % w/v yeast extract, 0.5 % w/v NaCl) with appropriate antibiotics (Gateway® plasmids in GV3101 pMP90 p19 with 50 µg mL^{-1} rifampicin, 50 µg mL^{-1} gentamycin, 50 µg kanamycin, and 100 µg mL^{-1} spectinomycin; GreenGate plasmids in GV3101 pMP90 pSoup with 50 µg mL^{-1} rifampicin, 50 µg mL^{-1} gentamycin, 2.5 µg tetracycline, and 100 µg mL^{-1} spectinomycin). Cell cultures were adjusted to an optical density (OD_{600nm}) of 0.3 and centrifuged (10 min, 4000 x g, 4 °C). The pellet was resuspended in infiltration medium (5 % w/v sucrose, 150 µM acetosyringone, 0.01 % v/v Silwet) and

incubated at 4 °C for 2 – 3 h. For co-expression of two or more transgenes, the corresponding transformed *A. tumefaciens* strains were mixed equally (final OD_{600nm} = 0.3 per strain). Subsequently, the bacterial resuspensions were infiltrated with a syringe into the abaxial site of the *N. benthamiana* leaves.

Plants transformed with constructs under the control of an estradiol-inducible promotor system (Zuo et al., 2000) were sprayed 2 – 4 days after infiltration and 6 – 16 h prior to sample preparation for imaging or CoIP with an estradiol solution (10 µM ß-estradiol, 0.1 % v/v Tween-20). Constitutive expressing transgenes (under the control of the *UBQ10* promotor) were used for analyses 3 days after infiltration.

Stable transformation of *A. thaliana*

To generate stable expression lines, parental *A. thaliana* plants were transformed 4 – 6 weeks after germination via the floral dip method using *A. tumefaciens* GV3101 pMP90 pSoup previously transformed with desired binary vectors (Suppl. Tab. 9, (Clough and Bent, 1998)). Agrobacteria were cultivated overnight (28°C, shaking) in selective dYT medium (supplied with 50 µg mL^{-1} rifampicin, 50 µg mL^{-1} gentamycin, 2.5 µg tetracycline, and 100 µg mL^{-1} spectinomycin). 50 ml main cultures of the transgene-harboring Agrobacterium strains were inoculated with 1 ml of an overnight preculture and centrifuged the next day (10 min, 4000 x g, 4 °C). The pellet was resuspended in transformation medium (5 % w/v sucrose, 10 nM $MgCl_2$, 0.01 % Silwet). Plants were prepared by removing already developed siliques and were then subjected to floral dip. Whole shoots with special attention to the flowers were immersed into the *A. tumefaciens* resuspension for 30 sec up to 5 min to guarantee the entry of bacteria into the floral tissue, more precisely the female gametophyte. Afterwards, the plants were kept under high humidity overnight at room temperature. Subsequently, the plants were cultivated in standard phytochamber conditions until harvest. The t1 seeds were screened for positive transformants by selection either for resistance against DL-phosphinothricin (PPT, alternatively used in form of the herbicide BASTA®), or against hygromycin. Seeds of the transformed t0 plants were screened for positive transformants by selection either for resistance against DL-phosphinothricin (PPT, alternatively used in form of the herbicide BASTA®), or against hygromycin. T1 plants harboring transgenes with the BASTA® resistance cassette were selected by spraying seedlings on soil (10 DAG) with a 120 mg/ml solution of BASTA®, or by sowing the t1 seeds on ½ MS agar plates supplied with 10 µg/ml PPT. Transgenic plants with hygromycin resistance were screened on ½ MS agar plates supplied with 15 µg/ml hygromycin.

Positive plants were further amplified for t2 selection and identification of homozygous lines. All stable *A. thaliana* lines used and generated in this work are listed in Suppl. Tab. 10.

Confocal microscopy and tissue staining

In vivo fluorescence microscopy was performed at the CLSM systems Zeiss LSM 780 and Zeiss LSM 880, respectively, employing C-Apochromat 40x/1.20 water objectives. For whole leaf imaging and quantifying stomata (Fig. 7, Suppl. Fig. 16) a Plan-Apochromat 10x/0.45 M27 air objective was used. Samples containing GFP derivates were excited with an argon laser at 488 nm and emission was detected at 490 – 530 nm by a 32-channel GaAsP detector or the Airyscan detector system with a BP 495-550 / BP 570-620 filter set. The argon laser was also used for excitation of mVenus at 514 nm, followed by measuring the emission at 520 – 550 nm with a GaAsP detector. Diode-pumped solid state (DPSS) lasers were employed to excite mCh at 561 nm. Emission was detected by photomultiplier tubes (PMTs) in the range of 570 – 650 nm. Propidium iodide (PI) was utilized to stain cell walls in roots (25 µM), shoot meristems (5 mM), and leaf epidermis (50 µM). To quantify CSC layers, roots were subjected to mPS-PI staining according to (Truernit et al., 2008), thereby marking cell walls and starch granules in differentiated columella cells. PI was excited at 561 nm by DPSS lasers and detected by PMTs at 590 – 650 nm. Alternatively, cell walls were counterstained with DAPI, which was excited at 405 nm with a laser diode and emission was recorded at 410 – 480 nm by PMTs. To visualize sieve plates of SEs, roots of Arabidopsis seedlings were incubated for 5 min in 0.01 % w/v aniline blue, subsequently rinsed in a washing solution (10 mM KCl, 10 mM $CaCl_2$, 5 mM NaCl), and imaged (excitation with a 405 nm diode, emission detected at 470 – 530 nm with PMTs).

FRET-FLIM interaction analysis

FRET-FLIM experiments were conducted at a Zeiss LSM 780 (C-Apochromat 40x/1.20 water objective) equipped with a single-photon counting device (PicoQuant Hydra Harp 400) and a linear polarized diode laser (LDH-D-C-485). GFP or mNeonGreen donor fluorophores were excited at 485 nm with a pulsed laser at a frequency of 32 MHz. Excitation power was adjusted to 1 µW. Emission was detected in perpendicular and parallel polarization by Tau-SPADs (PicoQuant) with a band-pass filter (520/35 AHF). Images were acquired with a frame size of 256 x 256, zoom 8, and a pixel dwell time of 12.6 µs. For each measurement 60 frames were taken and the intensity-weighted mean lifetimes τ [ns] were calculated using PicoQuant SymPhoTime64 software applying a biexponential fit. The displayed data were obtained from at least 3 independent experiments.

Protein extraction and CoIP

Plant material was collected and immediately frozen in liquid N_2. All following steps were performed at 4 °C. To identify novel CLV1 interactors via CoIP, whole Arabidopsis seedlings were used (grown in liquid ½ MS, continuous light, gently shaking). Medium was removed 7 DAG and plants were grinded in liquid N_2 with mortar and pestle to obtain fine powder. Per sample 500 mg material was mixed with 750 µl extraction buffer (EB: 50 mM Tris/HCl pH 7.5, 150 mM NaCl, 1 mM EDTA, 10 % v/v glycerol, 0.1 % v/v Nonident P40 substitute, 5 µM dithiothreitol (DTT), 1 tablet of cOmplete™ proteinase inhibitor cocktail dissolved in 50 ml EB). For interaction assays, 6 leaf discs (6 mm diameter, ~ 300 mg fresh weight) from transiently transformed *N. benthamiana* leaves were grinded in a tube with two glass beads (3 mm) with a TissueLyser II (Qiagen) and directly after supplied with 600 µl EB. Samples dissolved in EB were incubated on a rotator for 1.5 h and subsequently centrifuged (20 min, 17 x g). The supernatant was collected for immunodetection via sodium dodecyl sulfate polyacrylamide gel electrophoresis (SDS-PAGE, standard protocol of NEXT-GEL® with 10 % acrylamide, samples were mixed with loading buffer (5 x: 200 mM Tris/HCl pH 6.8, 8 % w/v SDS, 40 % v/v glycerol, 0.05 % w/v bromophenol blue, 50 mM DTT), and boiled 5 min at 95 °C prior to loading) and Western Blot (WB, wet electroblotting system, 80 min / 100 V) analysis or used as input material for CoIP.

For CoIP experiments 500 µl protein extract was mixed with 25 µl calibrated anti-GFP magnetic beads (ChromoTek GFP-Trap®) and incubated on a rotator for 2 h. After, supernatant was discarded and beads were washed 4 times with washing buffer (10 mM Tris/HCl pH 7.5, 150 mM NaCl, 0.5 mM EDTA). Loaded beads were subjected to mass spectrometry or proteins were eluted from beads by mixing with double concentrated loading buffer and boiling (95 °C / 5 min) for analysis via SDS-PAGE, WB, and alkaline phosphatase (AP)-based immunostaining. To detect GFP-fusion proteins, primary GFP antibodies (IgG, rat monoclonal, diluted 1:1500 in blocking solution, incubation overnight at 4°C) and secondary anti-rat-AP antibodies (1:5000, 2.5 h, room temperature) were applied. To detect RFP derivates, primary RFP antibodies (IgG, mouse monoclonal, 1:1500, overnight, 4 °C) and secondary goat anti-mouse IgG AP antibodies (1:5000, 2.5 h, room temperature) were used.

Mass spectrometric analysis

Mass spectrometry was performed at the Molecular Proteomics Laboratory (MPL, BMFZ, HHU Düsseldorf). After immunoprecipitation of samples with anti-GFP beads (free GFP n=5, CLV1-2xGFP n=5, CLV1-2xGFP + 5µM CLV3 peptide n=4), precipitated proteins were eluted

with 25 µl sample buffer (7.5% v/v glycerine, 3% w/v SDS and 37.5 mM 2-Amino-2-(hydroxymethyl)-1,3-propanediol in water, pH 7) for 10 minutes at 90°C. Samples were further processed by in-gel digestion with trypsin including reduction with dithiothreitol and alkylation with iodoacetamide as described (Grube et al., 2018). Resulting peptides were resuspended in 0.1% trifluoroacetic acid and about half of the sample from each immunoprecipitation analyzed by liquid chromatography coupled mass spectrometry as previously described (Ingold et al., 2018). Briefly, peptides were separated on C18 material on an Ultimate 3000 rapid separation liquid chromatography system (Thermo Fisher Scientific) using a one-hour gradient and injected into a QExactive plus mass spectrometer (Thermo Fisher Scientific) via a nano electrospray source interface. The mass spectrometer was operated in data dependent, positive mode. First, survey scans were recorded (resolution 70000, scan range 200 – 2000 m/z) and subsequently, up to twenty > 1 charged precursors ions were selected by the build-in quadrupole, fragmented by higher-energy collisional dissociation and MS/MS spectra recorded at a resolution of 17500.

Data analysis was carried out with MaxQuant (version 1.6.0.16, Max Planck Institute for Biochemistry, Planegg, Germany) with standard parameters if not stated otherwise and using the *A. thaliana* reference proteome sequences (UP000006548, downloaded on 2nd February 2017 from UniProt) supplemented with two entries for CLV1-2xGFP and free GFP. The "match between runs" function and label-free quantification was enabled. Peptides and proteins were accepted for identification with a false discovery rate of 1%. Only proteins identified with at least two different peptides were considered as identified. Precursor intensity-based quantification data was further analyzed using the Perseus framework (version 1.6.0.7, Max Planck Institute for Biochemistry, Planegg, Germany).

Reverse transcriptase quantitative real-time PCR (RT-qPCR)

To evaluate the amount of residual *MAZ* transcripts in *maz-1* plants, RNA from seedlings 7 DAG was extracted with the Qiagen RNeasy Plant mini kit and 2 µg RNA per reaction was used for first strand cDNA synthesis via SuperScript™ III reverse transcriptase (according manufacture's protocol with oligo(dT)$_{18}$). The qPCR reactions were performed with SsoAdvanced™ Universal SYBR® Green Supermix in a Stratagene Mx3005P qPCR System (Agilent Technologies) with an optimized dilution of cDNA (accessed via dilution series for each oligo pair). Applied oligonucleotides are listed in Suppl. Tab. 11. Data were normalized to the housekeeping genes AT2G28390, AT4G34270, and At4g26410. Technical triplicates of 3 biological replicates were considered for each condition.

Evaluation of mutant morphology

Carpel number per silique of different *A. thaliana* mutants grown on soil under LD and continuous light conditions, respectively, were quantified from 10 – 15 plants per genotype and 15 – 30 siliques per plant. Root length of seedlings 10 DAG was accessed after cultivation of the examined genotypes on ½ MS plates supplied with synthetic CLV3 peptide in the indicated concentrations. Measurements were done with ImageJ after scanning the plates. For each condition at least 67 (and up to 113) single roots were measured and normalized to the mean of the Col-0 samples of the same peptide concentration.

Root hair length and density of seedlings 5 DAG were quantified after cultivation on ½ MS and image acquisition with a Nikon SMZ25 stereomicroscope. Per genotype 20 – 25 roots were analyzed, in total with 3542 (Col-0), 975 (*fer-4*), 2433 (*mri-2*), 4360 (*maz-1*), and 3555 (*maz-1;cark1-2*) single measurements. For each seedling, the length of all root hairs in focus on one side of the root were determined.

Stomata cluster in cotyledons and leaves of seedlings 14 DAG grown on ½ MS were analyzed after PI staining and imaging by counting total number of stomata and abundance of directly adjacent stomata. For each genotype 5 – 10 cotyledons and 6 – 10 true leaves were examined by counting all stomata in 4 distinct regions (400 x 400 µm) of each sample.

Evaluation of mutant physiologic responses

Drought stress experiments to access potential involvement of the *maz-1* allele in ABA responses were performed with plants of different genetic background grown on soil under standard conditions. Two weeks after germination seedlings were subjected to water deficiency for either 10 days or 20 days and were subsequently re-watered to monitor recovery. Both, the 10 days and 20 days drought period approaches, included 3 pots of plants for each genotype, which were randomly distributed on the tray.

Water-loss assays were conducted to estimate the degree of evaporation via open stomata after dissection of 6 rosette leaves per sample (1 sample = 1 individual plant). For each genotype 8 samples (per repeat) were weighted at indicated time points. The reduction of weight was taken as an approximation for water-loss. The assay was performed in three independent repeats.

Software

Statistical analyses and data plotting were realized with GraphPad Prism v 8. For visualization and quantification of microscopic data ZEN (Zeiss, Black Version) and ImageJ v 1.51 (Schneider et al., 2012) was employed. The following prediction tools were used: CSS-Palm

4.0 (Ren et al., 2008), PredGPI (Pierleoni et al., 2008), Myristoylator by ExPASy (Bologna et al., 2004), UbPred (Radivojac et al., 2010), UbiSite (Huang et al., 2016), BDM-PUB v 1.0. Cloning was organized via Vector NTI® software. Protein alignments were done with ClustalΩ (Sievers et al., 2011), phylogenetic analyses with MEGA X (Kumar et al., 2018), and tree visualization with iTOL v 4 (Letunic and Bork, 2019).

Acknowledgements

P.B. was supported by the IMPRS *Understanding complex plant traits using computational and evolutionary approaches*, work in R.S. lab is supported by the DFG through CRC1208 and CEPLAS (EXC 2048). We thank Cornelia Gieseler, Silke Winters, and Carin Theres for technical support, Aurélien Boisson-Dernier and Zachary Nimchuk for sharing Arabidopsis seeds, Grégoire Denay, Rebecca Burkart, Marc Somssich, Frederic Boyer, and Pauline Anne for sharing plasmids, Dolf Weijers and Mark Roosjen for the "sticky list" of typical GFP control pull-downs, Vicky Howe for critical reading of the manuscript, the Center for Advanced imaging (CAi) at HHU for microscopy support, and Gereon Poschmann from the Molecular Proteomics Laboratory (MPL) at HHU for mass spec analyses.

Authors contributions

R.S. and P.B. conceived and planed the project. P.B. conducted experiments and data analyses, besides the following: J.S. performed shoot meristem imaging and image processing, S.B. did FLIM interaction studies of CLV1-mNeonG vs. Pti1-like homologs (Fig. 3 C), K.P. acquired initial stomatal cluster rate data (Suppl. Fig. 15). P.B. and R.S. wrote the manuscript.

Main figures

Supplementary material

Supplemental Figure 14 Drought stress assay revealed no clear differences between the analyzed genotypes to cope with water deficiency.

Supplemental Figure 15 Impact of the *clv1-20* allele and CLE40 peptide treatment on stomata development and clustering in Arabidopsis seedlings.

Supplemental Figure 16 Cotyledons of *clv1-20*, *maz-1*, and the double mutant *clv1-20;maz-1* display no significant changes of stomata density and cluster rate.

Supplemental Table 1 Via mass spectroscopy identified proteins in CoIP fraction against CLV1-2xGFP, which are not found in GFP-only control samples.

Supplemental Table 2 Mean FRET efficiencies of tested donor-acceptor combinations at the PM of transiently transformed *N. benthamiana* epidermis cells.

Supplemental Table 3 Pti1-like family in *Arabidopsis thaliana* and predicted PM-localization mechanisms.

Supplemental Table 4 Chemicals.

Supplemental Table 5 Analyzed *A. thaliana* mutants (Col-0 background).

Supplemental Table 6 Genotyping strategies to verify listed mutant alleles.

Supplemental Table 7 Entry plasmids.

Supplemental Table 8 Plasmids used for transient gene expression in *N. benthamiana*.

Supplemental Table 9 Plasmids used for stabile transformation of *A. thaliana*.

Supplemental Table 9 Transgenic *A. thaliana* lines applied and generated in this study.

Supplemental Table 11 Oligonucleotides for RT-qPCR.

Appendix Sequence alignment with ClustalΩ of Arabidopsis Pti1-like family and SlPti1.

References

Anne, P., Amiguet-Vercher, A., Brandt, B., Kalmbach, L., Geldner, N., Hothorn, M., and Hardtke, C.S. (2018). CLERK is a novel receptor kinase required for sensing of root-active CLE peptides in Arabidopsis. Development **145**: dev162354.

Anne, P. and Hardtke, C.S. (2018). Phloem function and development — biophysics meets genetics. Current Opinion in Plant Biology **43**: 22–28.

Anthony, R.G., Khan, S., Costa, J., Pais, M.S., and Bögre, L. (2006). The Arabidopsis protein kinase PTI1-2 is activated by convergent phosphatidic acid and oxidative stress signaling pathways downstream of PDK1 and OXI1. Journal of Biological Chemistry **281**: 37536–37546.

Bergmann, D.C. and Sack, F.D. (2007). Stomatal Development. Annual Review of Plant Biology **58**: 163–181.

Betsuyaku, S., Takahashi, F., Kinoshita, A., Miwa, H., Shinozaki, K., Fukuda, H., and Sawa, S. (2011). Mitogen-activated protein kinase regulated by the CLAVATA receptors contributes to shoot apical meristem homeostasis. Plant and Cell Physiology **52**: 14–29.

Bi, G., Zhou, Z., Wang, W., Li, L., Rao, S., Wu, Y., Zhang, X., Menke, F.L.H., Chen, S., and Zhou, J.M. (2018). Receptor-like cytoplasmic kinases directly link diverse pattern recognition receptors to the activation of mitogen-activated protein kinase cascades in Arabidopsis. Plant Cell **30**: 1543–1561.

Bleckmann, A., Weidtkamp-Peters, S., Seidel, C.A.M., and Simon, R. (2010). Stem cell signaling in Arabidopsis requires CRN to localize CLV2 to the plasma membrane. Plant Physiology **152**: 166–176.

Boisson-Dernier, A., Franck, C.M., Lituiev, D.S., and Grossniklaus, U. (2015). Receptor-like cytoplasmic kinase MARIS functions downstream of CrRLK1L-dependent signaling during tip growth. PNAS **112**: 12211–12216.

Bologna, G., Yvon, C., Duvaud, S., and Veuthey, A.-L. (2004). N-Terminal myristoylation predictions by ensembles of neural networks. Proteomics **4**: 1626–1632.

Bommert, P., Je, B. il, Goldshmidt, A., and Jackson, D. (2013). The maize Gα gene COMPACT PLANT2 functions in CLAVATA signalling to control shoot meristem size. Nature **502**: 555–558.

Brand, U., Fletcher, J.C., Hobe, M., Meyerowitz, E.M., and Simon, R. (2000). Dependence of stem cell fate in Arabidopsis on a feedback loop regulated by CLV3 activity. Science **289**: 617–9.

Breda, A.S., Hazak, O., Schultz, P., Anne, P., Graeff, M., Simon, R., and Hardtke, C.S. (2019). A Cellular Insulator against CLE45 Peptide Signaling. Current Biology **29**: 2051–2508.

Chen, S., Liu, J., Liu, Y., Chen, L., Sun, T., Yao, N., Wang, H.-B., and Liu, B. (2019). BIK1 and ERECTA Play Opposing Roles in Both Leaf and Inflorescence Development in Arabidopsis. Frontiers in Plant Science **10**: 1480.

Clough, S.J. and Bent, A.F. (1998). Floral dip: A simplified method for Agrobacterium-mediated transformation of Arabidopsis thaliana. Plant Journal **16**: 735–743.

Cui, Y., Hu, C., Zhu, Y., Cheng, K., Li, X., Wei, Z., Xue L., Lin, F., Shi, H., Yi, J., Hou, S, He, K., Li, J., and Gou, X. (2018). CIK receptor kinases determine cell fate specification during early anther development in Arabidopsis. Plant Cell **30**: 2383–2401.

Depuydt, S., Rodriguez-Villalon, A., Santuari, L., Wyser-Rmili, C., Ragni, L., and Hardtke, C.S. (2013). Suppression of Arabidopsis protophloem differentiation and root meristem growth by CLE45 requires the receptor-like kinase BAM3. PNAS **110**: 7074–9.

DeYoung, B.J., Bickle, K.L., Schrage, K.J., Muskett, P., Patel, K., and Clark, S.E. (2006). The CLAVATA1-related BAM1, BAM2 and BAM3 receptor kinase-like proteins are required for meristem function in Arabidopsis. Plant Journal **45**: 1–16.

Deyoung, B.J. and Clark, S.E. (2008). BAM receptors regulate stem cell specification and organ development through complex interactions with CLAVATA signaling. Genetics **180**: 895–904.

Fan, M., Ma, W., Liu, C., Zhang, C., Wu, S., Chen, M., Liu, K., Cai, F., and Lin, F. (2018). Evolution and expression characteristics of receptor-like cytoplasmic protein kinases in maize, rice and Arabidopsis. International Journal of Molecular Sciences **19**(11): 3680.

Fiers, M., Golemiec, E., Xu, J., van der Geest, L., Heidstra, R., Stiekema, W., and Liu, C.M. (2005). The 14-amino acid CLV3, CLE19, and CLE40 peptides trigger consumption of the root meristem in Arabidopsis through a CLAVATA2-dependent pathway. Plant Cell **17**: 2542–2553.

Fletcher, J.C., Brand, U., Running, M.P., Simon, R., and Meyerowitz, E.M. (1999). Signaling of cell fate decisions by CLAVATA3 in Arabidopsis shoot meristems. Science **283**: 1911–4.

Forzani, C., Carreri, A., de La Fuente Van Bentem, S., Lecourieux, D., Lecourieux, F., and Hirt, H. (2011). The Arabidopsis protein kinase Pto-interacting 1-4 is a common target of the oxidative signal-inducible 1 and mitogen-activated protein kinases. FEBS Journal **278**: 1126–1136.

Fukuda, H. and Hardtke, C.S. (2020). Peptide signaling pathways in vascular differentiation. Plant Physiology **182**: 1636–1644.

Gagne, J.M. and Clark, S.E. (2010). The Arabidopsis stem cell factor POLTERGEIST is membrane localized and phospholipid stimulated. Plant Cell **22**: 729–43.

Geisler, M., Nadeau, J., and Sack, F.D. (2000). Oriented asymmetric divisions that generate the stomatal spacing pattern in Arabidopsis are disrupted by the too many mouths mutation. Plant Cell **12**: 2075–2086.

Grube, L., Dellen, R., Kruse, F., Schwender, H., Stühler, K., and Poschmann, G. (2018). Mining the Secretome of C2C12 Muscle Cells: Data Dependent Experimental Approach to Analyze Protein Secretion Using Label-Free Quantification and Peptide Based Analysis. Journal of Proteome Research **17**: 879–890.

Guo, X., Wang, J., Gardner, M., Fukuda, H., Kondo, Y., Etchells, J.P., Wang, X., and Mitchum, M.G. (2017). Identification of cyst nematode B-type CLE peptides and modulation of the vascular stem cell pathway for feeding cell formation. PLOS Pathogens **13**: e1006142.

Hanemian, M.,Barlet, X., Sorin, C., Yadeta, K., Keller, H., Favery, B., Simon, R., Thomma, B., Hartmann, C., Crespi, M., Marco, Y., Tremousaygue, D., and Deslandes, L. (2016). Arabidopsis CLAVATA 1 and CLAVATA2 receptors contribute to Ralstonia solanacearum pathogenicity through a miR169-dependent pathway. New Phytologist **211**: 502–515.

Hara, K., Kajita, R., Torii, K.U., Bergmann, D.C., and Kakimoto, T. (2007). The secretory peptide gene EPF1 enforces the stomatal one-cell-spacing rule. Genes and Development **21**: 1720–1725.

Hazak, O., Brandt, B., Cattaneo, P., Santiago, J., Rodriguez-Villalon, A., Hothorn, M., and Hardtke, C.S. (2017). Perception of root-active CLE peptides requires CORYNE function in the phloem vasculature. EMBO reports **18**: 1367–1381.

He, Y., Zhou, J., Shan, L., and Meng, X. (2018). Plant cell surface receptor-mediated signaling - A common theme amid diversity. Journal of Cell Science **131**: jcs209353.

Heazlewood, J.L., Durek, P., Hummel, J., Selbig, J., Weckwerth, W., Walther, D., and Schulze, W.X. (2008). PhosPhAt: a database of phosphorylation sites in Arabidopsis thaliana and a plant-specific phosphorylation site predictor. Nucleic Acids Research **36**: 1015–1021.

Hellens, R.P., Anne Edwards, E., Leyland, N.R., Bean, S., and Mullineaux, P.M. (2000). pGreen: A versatile and flexible binary Ti vector for Agrobacterium-mediated plant transformation. Plant Molecular Biology **42**: 819–832.

Herrmann, M.M., Pinto, S., Kluth, J., Wienand, U., and Lorbiecke, R. (2006). The PTI1-like kinase ZmPti1a from maize (Zea mays L.) co-localizes with callose at the plasma membrane of pollen and facilitates a competitive advantage to the male gametophyte. BMC Plant Biology **6**: 22.

Hu, C., Zhu, Y., Cui, Y., Cheng, K., Liang, W., Wei, Z., Zhu, M., Yin, H., Zeng, L., Xiao, Y., Lv, M., Yi, J., Hou, S., He, K., Li, J., and Gou, X. (2018). A group of receptor kinases are essential for CLAVATA signalling to maintain stem cell homeostasis. Nature Plants **4**: 205–211.

Huang, C.H., Su, M.G., Kao, H.J., Jhong, J.H., Weng, S.L., and Lee, T.Y. (2016). UbiSite: Incorporating two-layered machine learning method with substrate motifs to predict ubiquitin-conjugation site on lysines. BMC Systems Biology **10**: S6.

Hurst, C.H. and Hemsley, P.A. (2015). Current perspective on protein S-acylation in plants: More than just a fatty anchor? Journal of Experimental Botany **66**(6): 1599–1606.

Ingold, I., Berndt, C., Schmitt, S., Doll, S., Poschmann, G., Buday, K., Roveri, A., Peng, X., Porto Freitas, F., Seibt, T., Mehr, L., Aichler, M., Walch, A., Lamp, D., Jastroch, M., Miyamoto, S., Wurst, W., Ursini, F., Arnér, E.S.J., Fradejas-Villar, N., Schweizer, U., Zischka, H., Angeli, J.P.F., and Conrad, M. (2018). Selenium Utilization by GPX4 Is Required to Prevent Hydroperoxide-Induced Ferroptosis. Cell **172**: 409-422.e21.

Ishida, T., Tabata R., Yamada, M., Aida, M., Mitsumasu, K., Fujiwara, M., Yamaguchi, K., Shigenobu, S., Higuchi, M., Tsuji, H., Shimamoto, K., Hasebe, M., Fukuda, H., and Sawa, S. (2014). Heterotrimeric G proteins control stem cell proliferation through CLAVATA signaling in Arabidopsis. EMBO reports **15**: 1202–1209.

Jeong, S., Trotochaud, A.E., and Clark, S.E. (1999). The Arabidopsis CLAVATA2 gene encodes a receptor-like protein required for the stability of the CLAVATA1 receptor-like kinase. Plant Cell **11**: 1925–1933.

Katzen, F. (2007). Gateway® recombinational cloning: A biological operating system. Expert Opinion on Drug Discovery **2**: 571–589.

Kayes, J.M. and Clark, S.E. (1998). CLAVATA2, a regulator of meristem and organ development in Arabidopsis. Development **125**: 3843–3851.

Kinoshita, A., Betsuyaku, S., Osakabe, Y., Mizuno, S., Nagawa, S., Stahl, Y., Simon, R., Yamaguchi-Shinozaki, K., Fukuda, H., and Sawa, S. (2010). RPK2 is an essential receptor-like kinase that transmits the CLV3 signal in Arabidopsis. Development **137**: 3911–3920.

Kumar, S., Stecher, G., Li, M., Knyaz, C., and Tamura, K. (2018). MEGA X: Molecular Evolutionary Genetics Analysis across Computing Platforms. Molecular Biology and Evolution **35**: 1547–1549.

Lampropoulos, A., Sutikovic, Z., Wenzl, C., Maegele, I., Lohmann, J.U., and Forner, J. (2013). GreenGate - a novel, versatile, and efficient cloning system for plant transgenesis. PloS one **8**: e83043.

Lee, H., Jun, Y.S., Cha, O.K., and Sheen, J. (2019). Mitogen-activated protein kinases MPK3 and MPK6 are required for stem cell maintenance in the Arabidopsis shoot apical meristem. Plant Cell Reports **38**: 311–319.

Lee, J.S., Kuroha, T., Hnilova, M., Khatayevich, D., Kanaoka, M.M., Mcabee, J.M., Sarikaya, M., Tamerler, C., and Torii, K.U. (2012). Direct interaction of ligand-receptor pairs specifying stomatal patterning. Genes and Development **26**: 126–136.

Letunic, I. and Bork, P. (2019). Interactive Tree Of Life (iTOL) v4: recent updates and new developments. Nucleic Acids Research **47**: W256–W259.

Li, Y. and Qi, B. (2017). Progress toward understanding protein S-acylation: Prospective in plants. Frontiers in Plant Science **8**: 346.

Liang, X. and Zhou, J.-M. (2018). Receptor-Like Cytoplasmic Kinases: Central Players in Plant Receptor Kinase–Mediated Signaling. Annual Review of Plant Biology **69**: 267–299.

Lin, W., Lu, D., Gao, X., Jiang, S., Ma, X., Wang, Z., Mengiste, T., He, P., and Shan, L. (2013). Inverse modulation of plant immune and brassinosteroid signaling pathways by the receptor-like cytoplasmic kinase BIK1. PNAS **110**: 12114–12119.

Lu, D., Wu, S., Gao, X., Zhang, Y., Shan, L., and He, P. (2010). A receptor-like cytoplasmic kinase, BIK1, associates with a flagellin receptor complex to initiate plant innate immunity. PNAS **107**: 496–501.

Mandel, T., Moreau, F., Kutsher, Y., Fletcher, J.C., Carles, C.C., and Williams, L.E. (2014). The ERECTA receptor kinase regulates Arabidopsis shoot apical meristem size, phyllotaxy and floral meristem identity. Development **141**: 830–841.

Matsui, H., Matsui, H., Fujiwara, M., Hamada, S., Shimamoto, K., Nomura, Y., Nakagami, H., Takahashi, A., and Hirochika, H. (2014). Plasma membrane localization is essential for oryza sativa pto-interacting protein 1a-mediated negative regulation of immune signaling in rice. Plant Physiology **166**: 327–336.

Mayer, K.F.X., Schoof, H., Haecker, A., Lenhard, M., Jürgens, G., and Laux, T. (1998). Role of WUSCHEL in regulating stem cell fate in the Arabidopsis shoot meristem. Cell **95**: 805–815.

Müller, R., Bleckmann, A., and Simon, R. (2008). The receptor kinase CORYNE of Arabidopsis transmits the stem cell-limiting signal CLAVATA3 independently of CLAVATA1. Plant Cell **20**: 934–946.

Nimchuk, Z.L., Tarr, P.T., and Meyerowitz, E.M. (2011a). An evolutionarily conserved pseudokinase mediates stem cell production in plants. Plant Cell **23**: 851–854.

Nimchuk, Z.L., Tarr, P.T., Ohno, C., Qu, X., and Meyerowitz, E.M. (2011b). Plant stem cell signaling involves ligand-dependent trafficking of the CLAVATA1 receptor kinase. Current Biology **21**: 345–352.

Nimchuk, Z.L., Zhou, Y., Tarr, P.T., Peterson, B.A., and Meyerowitz, E.M. (2015). Plant stem cell maintenance by transcriptional cross-regulation of related receptor kinases. Development **142**: 1043–1049.

Pierleoni, A., Martelli, P., and Casadio, R. (2008). PredGPI: A GPI-anchor predictor. BMC Bioinformatics **9**: 392.

Qi, X., Han, S.K., Dang, J.H., Garrick, J.M., Ito, M., Hofstetter, A.K., and Torii, K.U. (2017). Autocrine regulation of stomatal differentiation potential by EPF1 and ERECTA-LIKE1 ligand-receptor signaling. eLife **6**: e24102.

Qian, P., Song, W., Yokoo, T., Minobe, A., Wang, G., Ishida, T., Sawa, S., Chai, J., and Kakimoto, T. (2018). The CLE9/10 secretory peptide regulates stomatal and vascular development through distinct receptors. Nature Plants **4**: 1071–1081.

Radivojac, P., Vacic, V., Haynes, C., Cocklin, R.R., Mohan, A., Heyen, J.W., Goebl, M.G., and Iakoucheva, L.M. (2010). Identification, analysis, and prediction of protein ubiquitination sites. Proteins: Structure, Function and Bioinformatics **78**: 365–380.

Ren, J., Wen, L., Gao, X., Jin, C., Xue, Y., and Yao, X. (2008). CSS-Palm 2.0: an updated software for palmitoylation sites prediction. Protein Engineering, Design and Selection **21**: 639–644.

Rosas-Diaz, T., Zhang, D., Fan, P., Wang, L., Ding, X., Jiang, Y., Jimenez-Gongora, T., Medina-Puche, L., Zhao, X., Feng, Z., Zhang, G., Liu, X., Bejarano, E.R., Tan, L., Zhang, H., Zhu, J.-K., Xing, W., Faulkner, C., Nagawa, S., and Lozano-Duran, R. (2018). A virus-targeted plant receptor-like kinase promotes cell-to-cell spread of RNAi. PNAS **115**: 1388–1393.

Schneider, C.A., Rasband, W.S., and Eliceiri, K.W. (2012). NIH Image to ImageJ: 25 years of image analysis. Nature Methods **9**: 671–675.

Schoof, H., Lenhard, M., Haecker, A., Mayer, K.F.X., Jürgens, G., and Laux, T. (2000). The stem cell population of Arabidopsis shoot meristems is maintained by a regulatory loop between the CLAVATA and WUSCHEL genes. Cell **100**: 635–644.

Sessa, G., D'Ascenzo, M., and Martin, G.B. (2000). The major site of the Pti1 kinase phosphorylated by the Pto kinase is located in the activation domain and is required for Pto-Pti1 physical interaction. European Journal of Biochemistry **267**: 171–178.

Shimizu, N., Ishida, T., Yamada, M., Shigenobu, S., Tabata, R., Kinoshita, A., Yamaguchi, K., Hasebe, M., Mitsumasu, K., and Sawa, S. (2015). BAM 1 and RECEPTOR-LIKE PROTEIN KINASE 2 constitute a signaling pathway and modulate CLE peptide-triggered growth inhibition in Arabidopsis root. New Phytologist **208**: 1104–1113.

Shinohara, H. and Matsubayashi, Y. (2015). Reevaluation of the CLV3-receptor interaction in the shoot apical meristem: dissection of the CLV3 signaling pathway from a direct ligand-binding point of view. Plant Journal **82**: 328–36.

Shinohara, H., Moriyama, Y., Ohyama, K., and Matsubayashi, Y. (2012). Biochemical mapping of a ligand-binding domain within Arabidopsis BAM1 reveals diversified ligand recognition mechanisms of plant LRR-RKs. Plant Journal **70**: 845–854.

Shiu, S.H. and Bleecker, A.B. (2003). Expansion of the receptor-like kinase/Pelle gene family and receptor-like proteins in Arabidopsis. Plant Physiology **132**: 530–543.

Shiu, S.H., Karlowski, W.M., Pan, R., Tzeng, Y.H., Mayer, K.F.X., and Li, W.H. (2004). Comparative analysis of the receptor-like kinase family in Arabidopsis and rice. Plant Cell **16**: 1220–1234.

Sievers, F., Wilm, A., Dineen, D., Gibson, T.J., Karplus, K., Li, W., Lopez, R., McWilliam, H., Remmert, M., Söding, J., Thompson, J.D., and Higgins, D.G. (2011). Fast, scalable generation of high-quality protein multiple sequence alignments using Clustal Omega. Molecular Systems Biology **7**: 539.

Stahl, Y., Grabowski, S., Bleckmann, A., Kühnemuth, R., Weidtkamp-Peters, S., Pinto, K.G., Kirschner, G.K., Schmid, J.B., Wink, R.H., Hülsewede, A., Felekyan, S., Seidel, C.A.M., Simon, R. (2013). Moderation of Arabidopsis root stemness by CLAVATA1 and ARABIDOPSIS CRINKLY4 receptor kinase complexes. Current Biology **23**: 362–71.

Stahl, Y. and Simon, R. (2012). Receptor Kinases in Plant Meristem Development. In Signaling and Communication in Plants, F. Tax and B. Kemmerling, eds (Springer: Berlin, Heidelberg), pp. 23–39.

Stahl, Y., Wink, R.H., Ingram, G.C., and Simon, R. (2009). A Signaling Module Controlling the Stem Cell Niche in Arabidopsis Root Meristems. Current Biology **19**(11): 909–914.

Tameshige, T., Ikematsu, S., Torii, K.U., and Uchida, N. (2017). Stem development through vascular tissues: EPFL-ERECTA family signaling that bounces in and out of phloem. J Exp Bot **68**: 45–53.

Truernit, E., Lè Ne Bauby, H., Dubreucq, B., Grandjean, O., Runions, J., Barthé Lé, J., and Palauqui, J.-C. (2008) High-Resolution Whole-Mount Imaging of Three-Dimensional Tissue Organization and Gene Expression Enables the Study of Phloem Development and Structure in Arabidopsis. Plant Cell **20**: 1494–1503.

Uchida, N., Shimada, M., and Tasaka, M. (2013). ERECTA-Family Receptor Kinases Regulate Stem Cell Homeostasis via Buffering its Cytokinin Responsiveness in the Shoot Apical Meristem. Plant and Cell Physiology **54**: 343–351.

Voinnet, O., Rivas, S., Mestre, P., and Baulcombe, D. (2003). An enhanced transient expression system in plants based on suppression of gene silencing by the p19 protein of tomato bushy stunt virus. Plant Journal **33**(5): 949–956.

Wang, J., Zhang, Q., Yu, Q., Peng, L., Wang, J., Dai, Q., Yang, Y., and Li, X. (2019). CARK6 is involved in abscisic acid to regulate stress responses in Arabidopsis thaliana. Biochemical and Biophysical Research Communications **513**(2): 460–464.

Wu, Q., Xu, F., Liu, L., Char, S.N., Ding, Y., Je, B. il, Schmelz, E., Yang, B., and Jackson, D. (2020). The maize heterotrimeric G protein β subunit controls shoot meristem development and immune responses. PNAS **117**: 1799–1805.

Xi, L., Wu, X.N., Gilbert, M., and Schulze, W.X. (2019). Classification and interactions of LRR receptors and co-receptors within the arabidopsis plasma membrane – An overview. Frontiers in Plant Science **10**: 472.

Zhang, L., DeGennaro, D., Lin, G., Chai, J., and Shpak, E.D. (2020). ERECTA family signaling constrains CLAVATA3 and WUSCHEL to the center of the shoot apical meristem. bioRxiv Developmental Biology: 2020.02.24.962787.

Zhang, L., Li, X., Li, D., Sun, Y., Li, Y., Luo, Q., Liu, Z., Wang, J., Li, X., Zhang, H., Lou, Z., and Yang, Y. (2018). CARK1 mediates ABA signaling by phosphorylation of ABA receptors. Cell Discovery **4**: 1–10.

Zhou, J., Loh, Y.T., Bressan, R.A., and Martin, G.B. (1995). The tomato gene Pti1 encodes a serine/threonine kinase that is phosphorylated by Pto and is involved in the hypersensitive response. Cell **83**: 925–935.

Zoulias, N., Harrison, E.L., Casson, S.A., and Gray, J.E. (2018). Molecular control of stomatal development. Biochemical Journal **475**: 441–454.

Zuo, J., Niu, Q.W., and Chua, N.H. (2000). An estrogen receptor-based transactivator XVE mediates highly inducible gene expression in transgenic plants. Plant Journal **24**: 265–273.

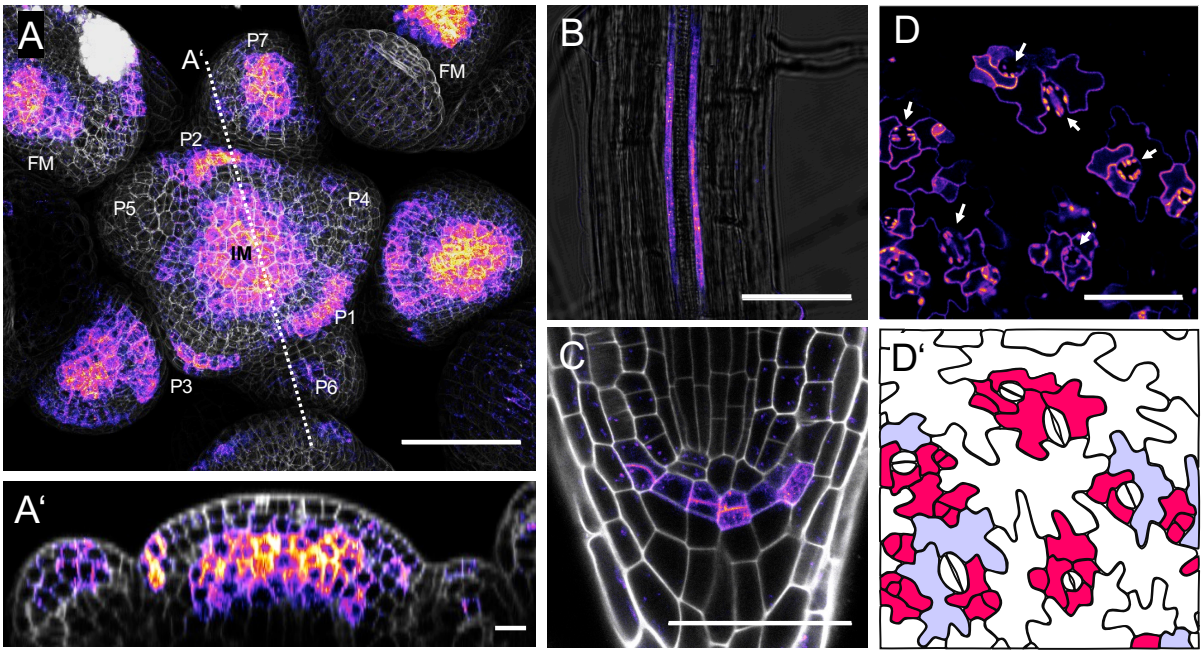

Figure 1 Expression patterns of *CLV1:CLV1-2xGFP* in different tissues of Arabidopsis.

A, A' Inflorescence with inflorescence meristem (IM), floral primordia, and floral meristems (FM) of 5 weeks old *CLV1*:*CLV1-2xGFP//clv1-11* plants depicted as maximum intensity projection of a z-stack (A) and XZ section (A') at indicated position. *CLV1* is expressed in the central zone of the meristems and in border cells toward newly arising primordia. **B** Root section within the differentiation zone of a seedling 5 DAG shows presence of the fusion protein CLV1-2xGFP in companion cell files (compare Suppl. Fig. 1 A). **C** Within the root meristem *CLV1* expression is restricted to columella stem cells and epidermis/lateral root cap initials (seedling 5 DAG). **D** In the epidermis of first true leaves (14 DAG) *CLV1-2xGFP* expression is predominantly found in cells of the stomata lineage. Guard cells (white arrows in D) show no expression at the PM (note autofluorescence of chloroplasts). **D'** The schematic representation of D illustrates outlines of all cells (based on bright field channel). Cells with clear GFP fluorescence signals at the PM are colored in pink, with weak signals in light blue. A, A', C: merge of GFP channel (LUT: fire) and PI (grey). B: merge of GFP (fire) with bright field (grey). Scale bares: 50 µm (A, B, C, D) and 10 µm (A').

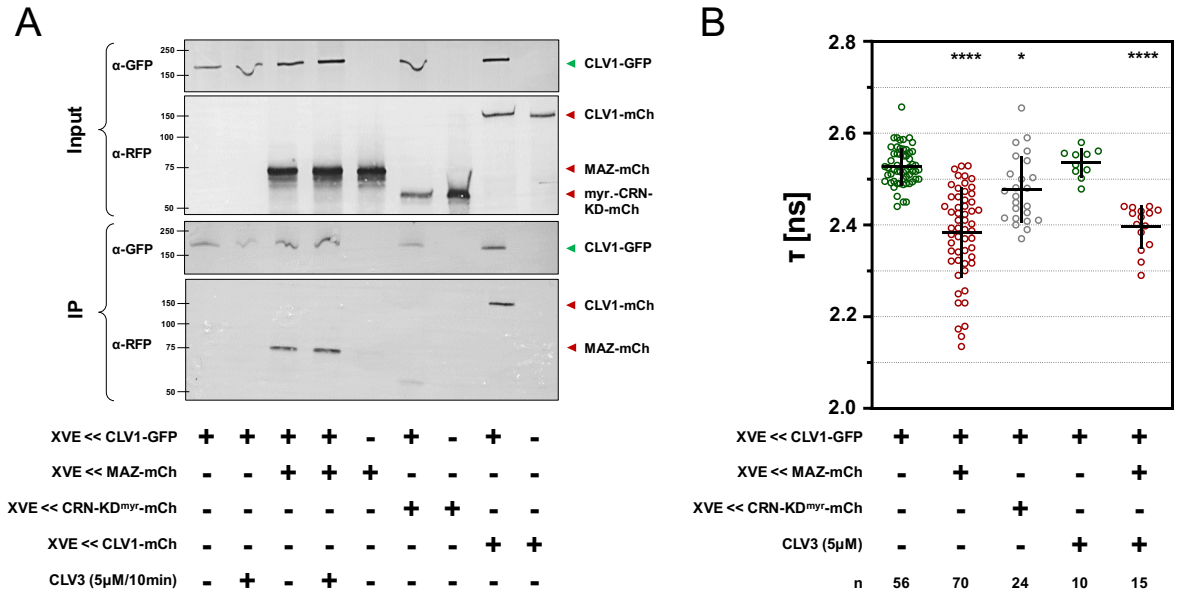

Figure 2 *In vivo* interaction analysis of MAZ and CLV1 via CoIP and FLIM.

CoIP and FLIM was performed with *N. benthamiana* leaf epidermis material transiently expressing combinations of indicated fluorophore fusions under the control of the *XVE<<oLexA-35S* estradiol inducible system. **A** MAZ-mCherry (mCh) is co-immunoprecipitated with CLV1-GFP using anti-GFP magnetic beads and subsequent immunodetection with antibodies against GFP and RFP, respectively. The negative control, myristoylated CRN-KD-mCh, is not pulled down together with CLV1-GFP, while the detection of CLV1-mCh reflects the previously reported homomerization of CLV1 (Bleckmann et al., 2010). Treatment of CLV3 peptide (5µM, 10 min prior to sample preparation) does not affect the interaction in this setup. **B** The fluorescence lifetime τ [ns] of CLV1-GFP is reduced in the presence of MAZ-mCh, while the PM control (CRN-KD^{myr}-mCh) reduces the τ of CLV1-GFP with low efficiency. Infiltration of a 5 µM CLV3 peptide solution into the leaves 5 – 15 min prior to measurements does not alter the τ values of donor-only nor FRET samples. Number of repetitions are indicated, p-values were calculated by ANOVA and Dunnett´s post hoc test, with * for $p \leq 0.05$, and **** for $p \leq 0.0001$. Error bars display SD.

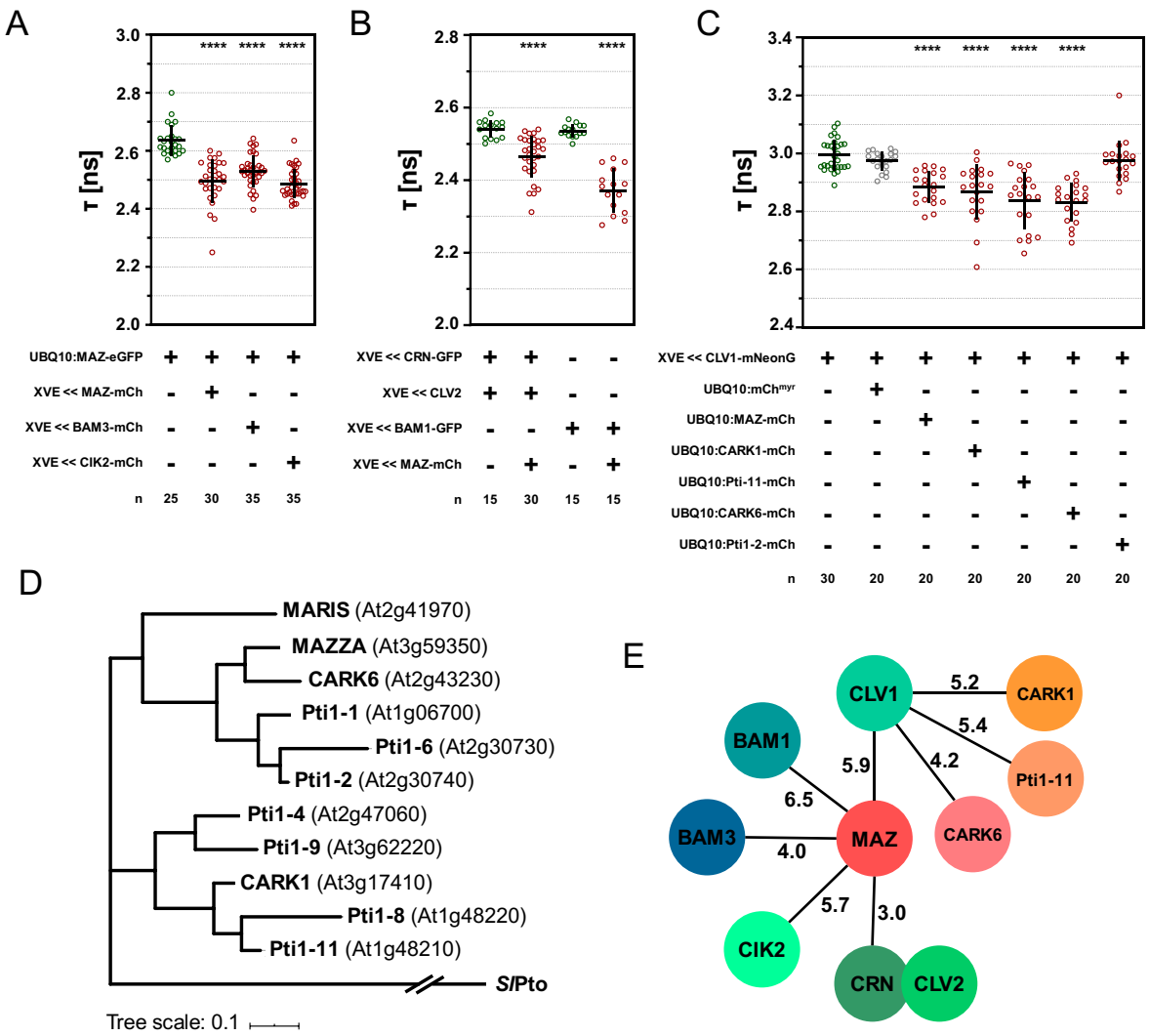

Figure 3 FLIM interactome of CLVf receptors and related signaling elements with the Pti1-like family.

A – C Fluorescence lifetime τ [ns] was determined in the *N. benthamiana* system, expressing the indicated constructs via the constitutive *UBQ10* promoter or under the control of the *XVE<<oLexA-35S* estradiol inducible module. **A** Donor τ of MAZ-eGFP is reduced in the presence of MAZ-mCh, BAM3-mCh, and CIK2-mCh, respectively. Note that the enhanced GFP variant (eGFP) was used here, explaining the slight differences compared to donor-only τ values in Fig 2 B and 3 B with constructs harboring the regular (F64) GFP. **B** The τ of CRN-GFP is decreased significantly but with a comparable low mean FRET efficiency of 3 % in the presence of MAZ-mCh and CLV2, while τ of BAM1-GFP is reduced with a FRET efficiency of 6.5 % by MAZ-mCh. **C** The τ of CLV1-mNeonGreen is significantly reduced in the presence of MAZ-mCh, CARK1-mCh, Pti1-11-mCh, CARK6-mCh, but not in combination with Pti1-2-mCh (nor by the negative control myristoylated mCh). Number of repetitions for FLIM experiments are indicated, p-values were calculated by ANOVA and Dunnett´s post hoc test, with **** for $p \leq 0.0001$. Error bars display SD. **D** Phylogram of the Pti1-homologs of *A. thaliana* and the *Solanum lycopersicum* SlPto as outgroup. The tree was generated after initial multiple sequence alignment (ClustalΩ) and subsequently applying a Maximum Likelihood strategy in MEGAX (via the JTT-matrix based model and 1000 repetitions). Final tree visualization was realized with iTOL software. Branch length is in scale as indicated displaying the calculated substitutions/site rate. **E** Graphical summary of the FLIM interactions identified here, mean FRET efficiency values are indicated for each pair (compare Suppl. Tab. 2).

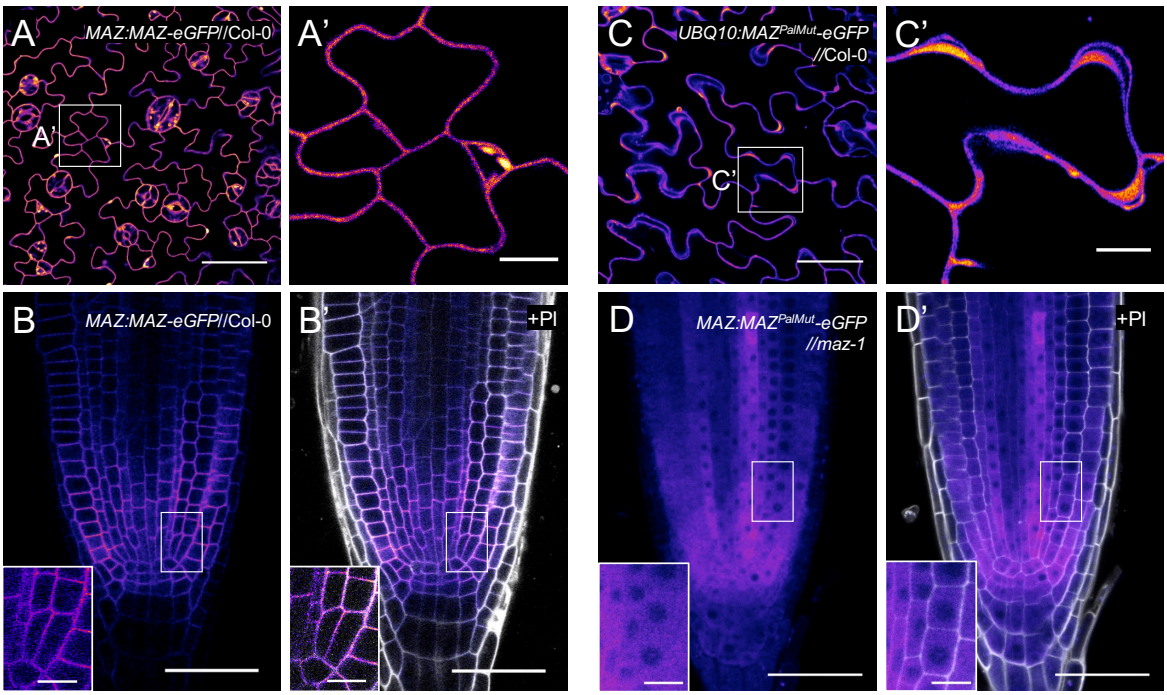

Figure 4 Subcellular localization of MAZ at the PM depends on conserved palmitoylation sites.

Stable expression of different MAZ variants demonstrate the impact of the predicted palmitoylation sites C48, C49 (and the adjacent C51) on subcellular localization of MAZ-eGFP. **A – B'** The wild typic MAZ protein (fused to eGFP) is located at the PM after expression under the native *MAZ* promotor, as shown here in rosette leaves (A, A') and in the root meristem (RM, B, B'). **C – D'** Site directed mutagenesis of the palmitoylation sites causes a shift of localization of the mutant MAZ^{PalMut}-eGFP fusion protein from the PM to the cytoplasm, both, when expressed under the *UBQ10* promotor, e.g. in leaf epidermis cells (C, C''), or under the control of the native *MAZ* promotor, shown here in the RM region. Sale bars: 50 µm (A, B, B', C, D, D'), 10 µm (A', C', detail views of B, B', D, D'). All images are displayed in the LUT fire, in B' and D' the merge with PI (grey) is shown.

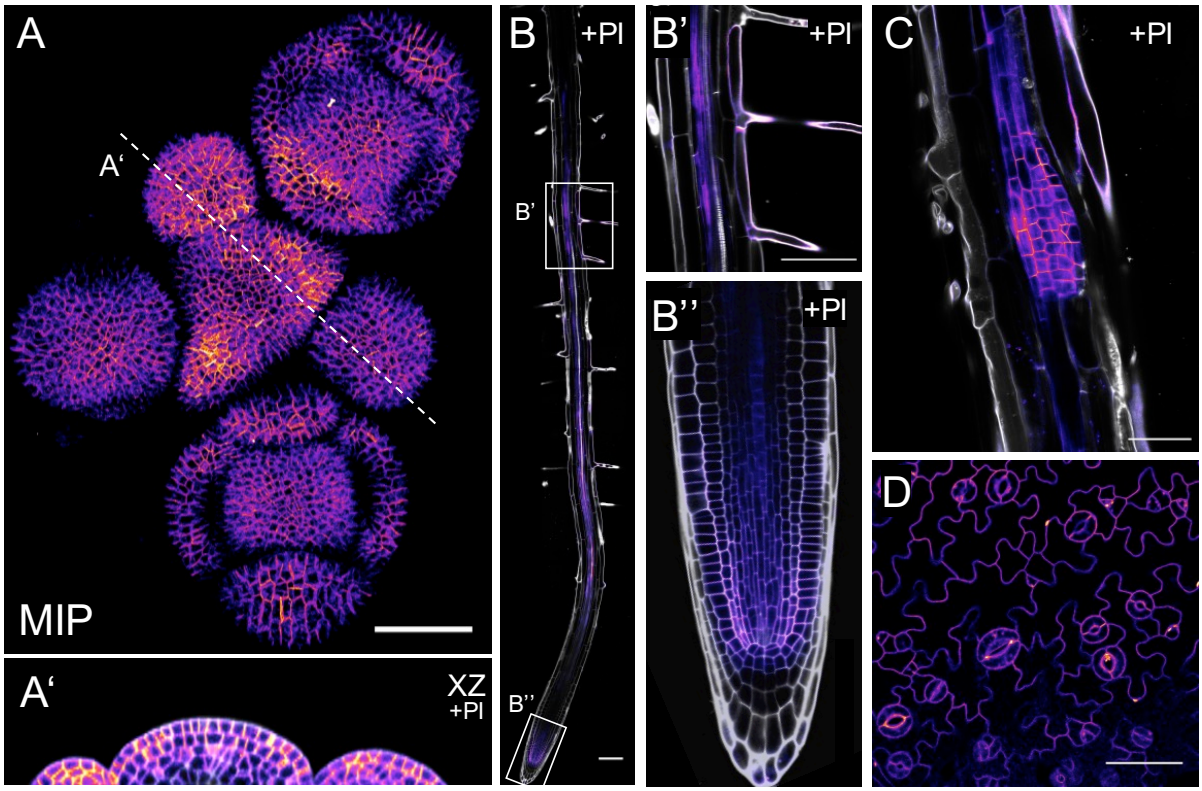

Figure 5 Expression analysis of *MAZ:MAZ-eGFP*//Col-0.

A, A’ Within the inflorescence, MAZ-eGFP is found in all cell layers. Z-stack acquired from a sample of a 5 weeks old plant, presented here as maximum intensity projection **(**MIP, A) and XZ section at indicated position (A’). *MAZ* expression is elevated at boundary regions towards newly formed primordia and towards organs in later stages of development. **B, B’, B’’** *MAZ* expression in the root (imaged 5 DAG) comprises the vasculature, root hairs (B’), and the root meristem (B’’). **C** Emerging lateral roots show distinct fluorescence signals of the MAZ-eGFP fusion (10 DAG, compare Suppl. Fig. 6). **D** In the epidermis of cotyledons (14 DAG), MAZ-eGFP is present in pavement cells, in the stomata lineage, and in mature guard cells. Scale bars: 50 µm (A, B’ – D), 10 µm (A’), 100 µm (B). GFP-signals visualized by the LUT fire, in A’ – C merge with PI (grey).

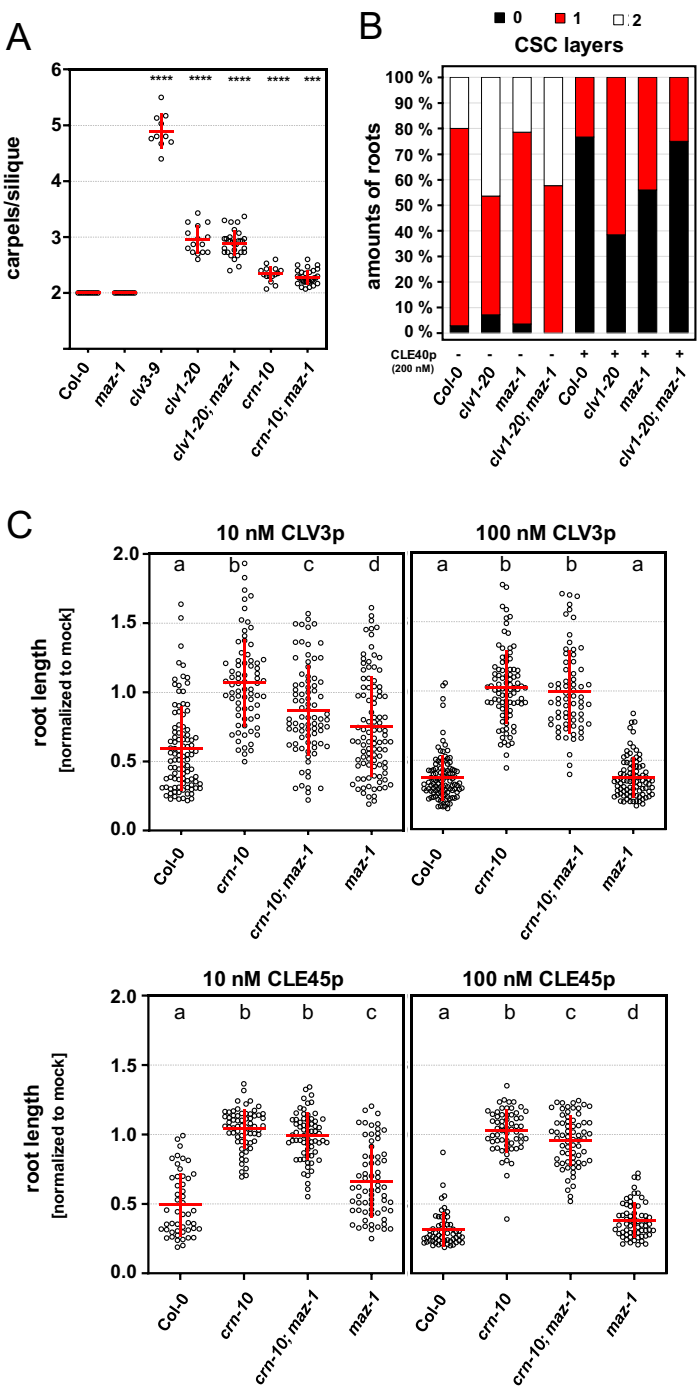

Figure 6 *Maz-1* mutants show no increased carpel number but are partially resistant against CLE peptide treatment.

A Mean carpel number per silique of indicated genotypes monitored in 6 – 8 weeks old plants grown under long day conditions. For each genotype 10 – 30 plants were analyzed by counting the carpels of 15 – 30 siliques per plant. The average carpel numbers for each plant are plotted. P-values calculated by ANOVA and Dunnett´s post hoc test with *** for $p \leq 0.001$, and **** for $p \leq 0.0001$. Sample mean and SD displayed in red. **B** CSC layers of indicated mutants quantified after mPS-PI staining of seedlings 5 DAG grown on ½ MS agar plates with and without 200 nM CLE40 peptide. **C** Root length of different genotypes 10 DAG grown on ½ MS agar plates supplemented with CLV3p or CLE45p at 10 nM and 100 nM, respectively. Data are normalized to the mean of the corresponding genotype grown without peptide. Statistical groups were assigned after calculating p-values by ANOVA and Dunnett´s post hoc test (differential grouping from $p \leq 0.05$). Sample mean and SD displayed.

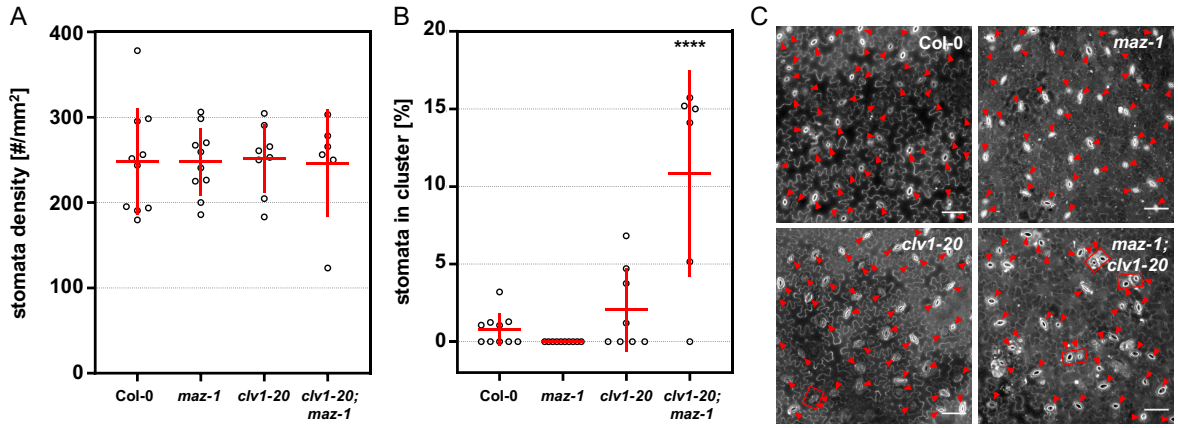

Figure 7 *Clv1-20;maz-1* double mutants display significantly increased stomata cluster rates.

A Stomatal density and **B** cluster rate were accessed from true leaves of indicated genotypes. Each plotted data point represents the mean value of 4 areas within one leaf of individual plants. Seedlings were grown on ½ MS agar plates. 14 DAG leaves were stained with PI to image abaxial epidermis cells. Significant differences in comparison to the Col-0 sample are indicated with **** for $p \leq 0.0001$, calculated by ANOVA and Dunnett´s post hoc test. Sample mean and SD displayed with red lines. **C** Representative images of the analyzed leaf epidermis areas counterstained with PI. Arrow heads mark stomata and boxes indicate clusters. Scale bars: 50 µm.

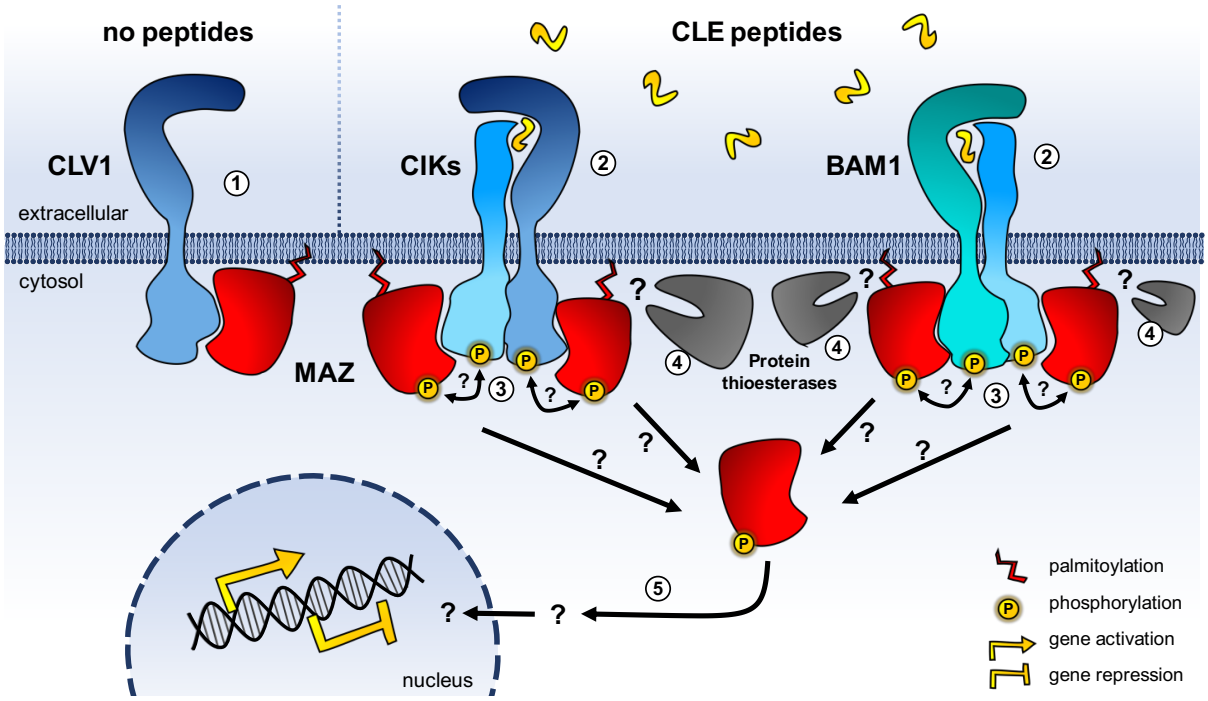

Figure 8 Model of MAZ as a signaling hub downstream of CLVf receptors.

In the absence of CLE peptides CLVf receptors and MAZ probably build preformed complexes (**1**). The CLE peptide perception by cognate CLVf receptors is aided by CIK co-receptors (**2**). Transphosphorylation between (co-)receptors and MAZ could transmit signal downstream (**3**). Protein thioesterases could catalyze release of activated MAZ from the PM by removing palmitoylation (**4**). Activated MAZ in the cytosol could mediate signal transduction to the nucleus (**5**).

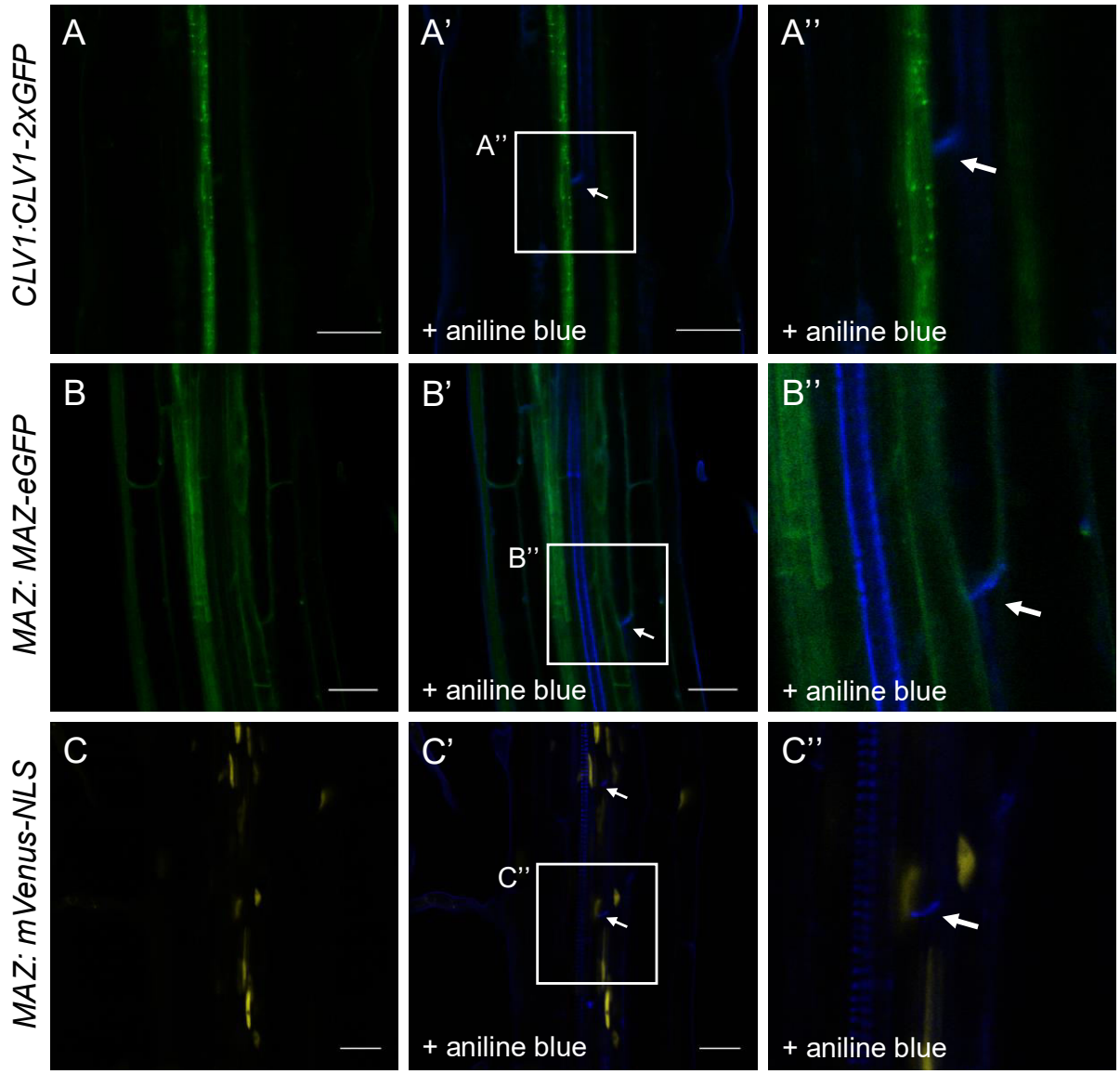

Supplemental Figure 1 Expression domains of *CLV1* and *MAZ* in the vasculature of Arabidopsis roots.

Different reporter lines 3 DAG grown on ½ MS were counterstained with aniline blue to visualize callose at the sieve plates (white arrows) and thereby marking the position of sieve elements (SE) within the vasculature cylinder. **A – A'' '** The *CLV1-2xGFP* fusion under the control of the endogenous *CLV1* promotor is expressed in companion cells (CC), directly adjacent to the SEs, which show no fluorescence signal. **B – B'' '** The *MAZ:MAZ-eGFP* reporter also mediates strong expression in the CCs. However, the expression domain is extended to other cell files in the vasculature, including the procambial tissue. In contrast, signals from the SEs are barely detectable. **C – C'' '** Expression pattern of the transcriptional *MAZ:mVenus-NLS* reporter in the vasculature cylinder are in line with the translational reporter in B – B''. Scale bars: 25 µm.

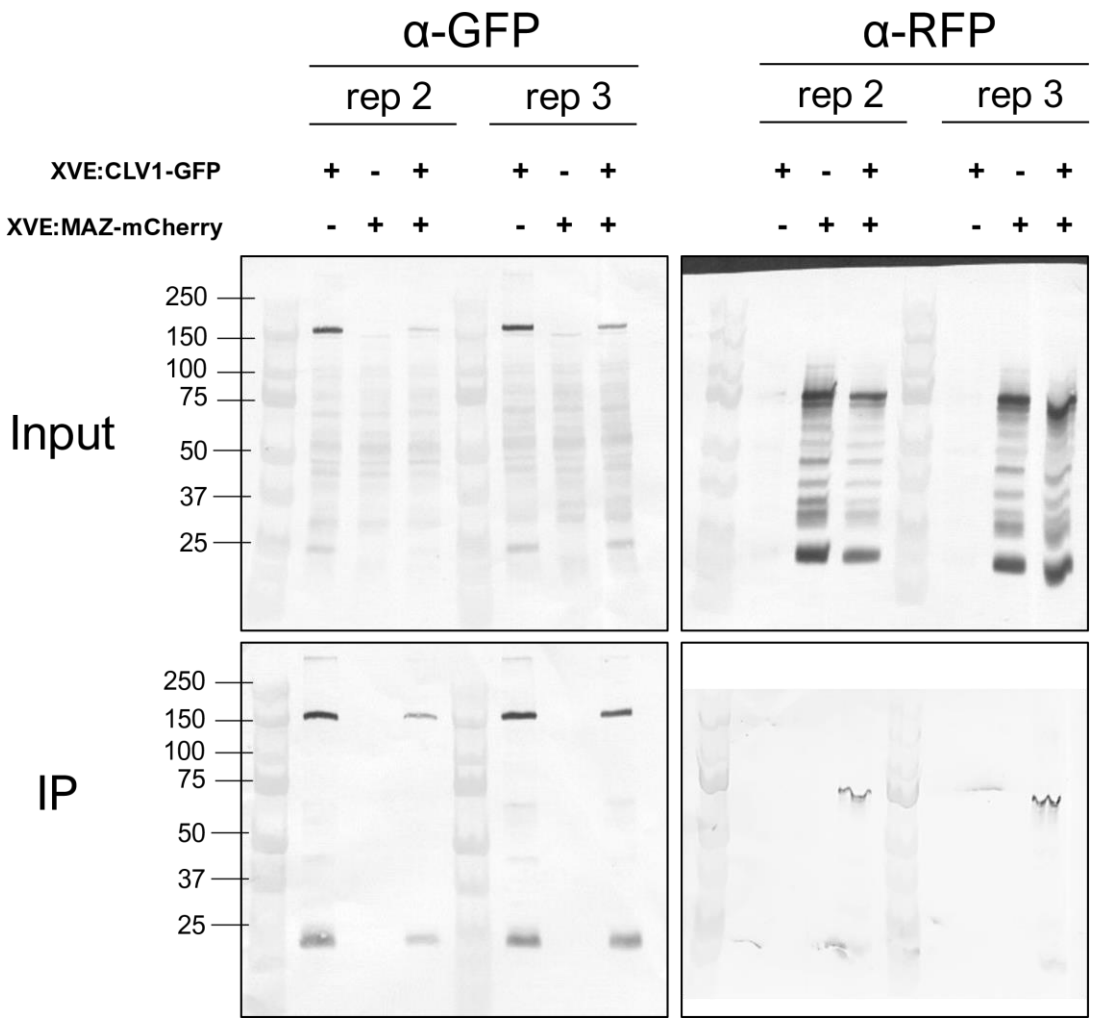

Supplemental Figure 2 Two independent CoIP repetitions of CLV1-GFP with MAZ-mCherry.

Following the same protocol as described above and shown in Figure 2 A, transiently transformed *N. benthamiana* leaf material (two independent Agrobacterium cultures, different plants, and separate CoIP reactions) harboring the indicated combinations of *XVE*-driven inducible transgenes was deployed to show the capacity of CLV1-GFP to pull down MAZ-mCh. MAZ-mCh alone is not immuno-precipitated via anti-GFP beads (ChromoTek). The Precision Plus Protein™ Dual Color Standard (Bio-Rad) was used for SDS-PAGE (band sizes indicated left).

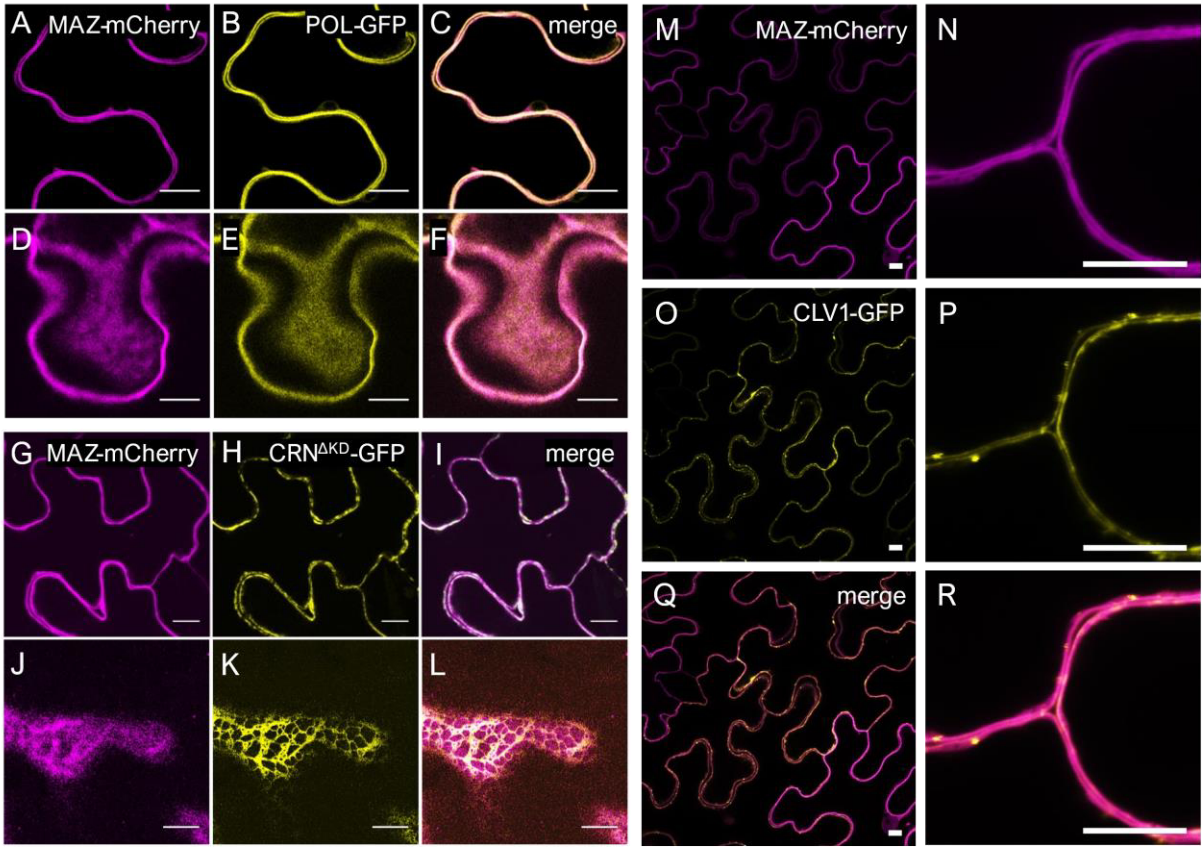

Supplemental Figure 3 Subcellular localization of MAZ in *N. benthamiana* leaf epidermis cells.

A – F Co-expression of *MAZ-mCherry (mCh)* and *POLTERGEIST(POL)-GFP* results in a high degree of local overlap between the two fluorescence signals. POL is known to be localized at the PM (Gagne and Clark, 2010). **G – F** MAZ-mCh does not display notable co-localization with $CRN^{\Delta KD}$-GFP (that is ER-localized in the absence of CLV2). In D – F, and J – L the cell surface is in focus to visualize homogenous distribution of PM-located proteins and network-like structure of ER-associated signals, respectively. **H – R** CLV1-GFP and MAZ-mCh co-localize at the PM, but MAZ is not present in CLV1-GFP vesicles, which probably indicate receptor internalization. All constructs were expressed under the control of the *XVE* promotor system for estradiol induced expression. Scale bars: 10 µm.

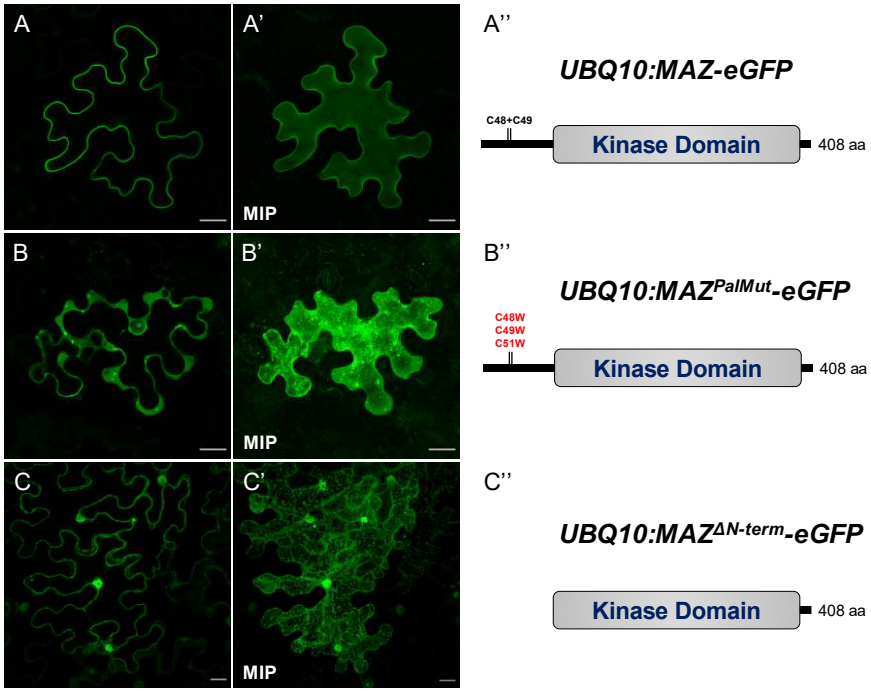

Supplemental Figure 4 Predicted palmitoylation sites at the N-terminus of MAZ are mandatory for PM-localization.

Transient expression of different *MAZ* variants demonstrate the impact of the N-terminus and the predicted palmitoylation sites C48, C49 (and the adjacent C51) on subcellular localization of MAZ-eGFP. Representative images of *N. benthamiana* leaf epidermis cells expressing the transgenes under the control of the *UBQ10* promotor (**A, B, C**), the corresponding maximum intensity projections (MIP) of z-stacks through the epidermal layer (**A', B', C'**) and schematic representations of the MAZ protein structure in the indicated constructs (**A'', B'', C''**). **A – A''** The full-length MAZ protein (fused to eGFP) is located at the PM. **B – B''** Site directed mutagenesis of the palmitoylation sites causes a shift of protein localization from the PM to the cytoplasm. **C – C''** Deletion of the entire N-terminus (the deletion variant starts directly with the kinase domain) results in protein localization within the cytoplasm, around the ER, and in the nucleus. Sale bars: 25 µm.

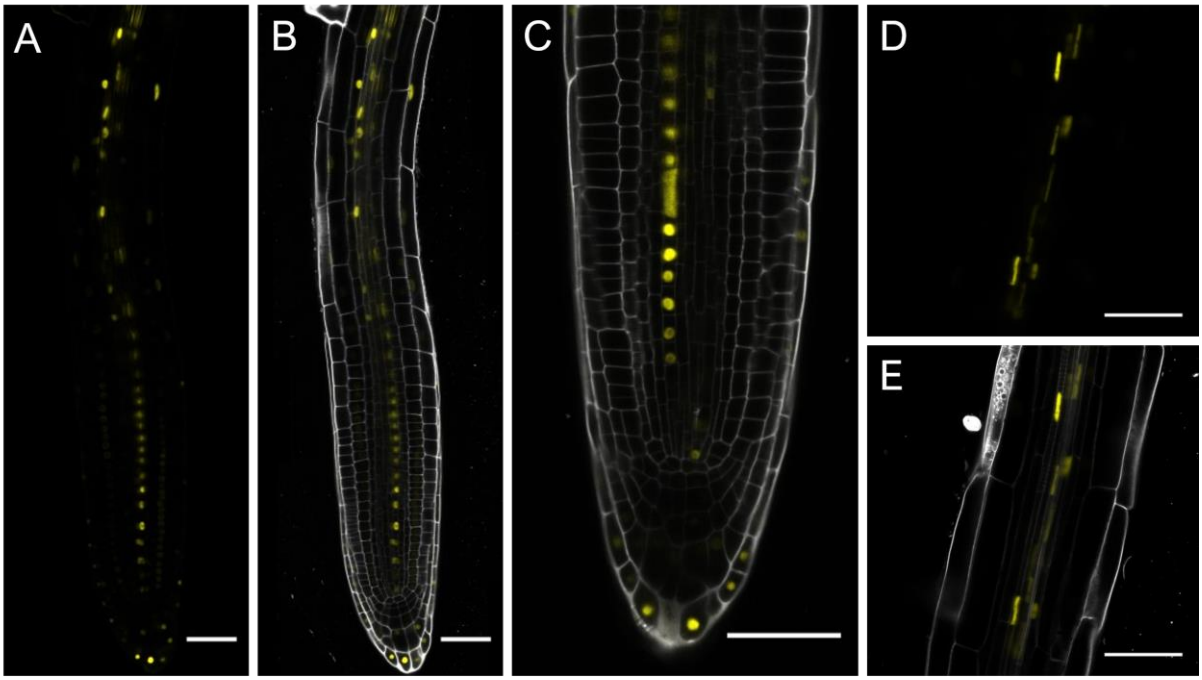

Supplemental Figure 5 Expression pattern of the transcriptional reporter *MAZ:mVenus-NLS*//Col-0 in the root (3 DAG).

A, B The *MAZ* promotor mediates expression predominantly in the vasculature and less pronounced also in other cell files within the meristematic zone of the root. **C** Occasionally observed dispersal of the *per se* nucleus-located fluorescence reporter suggests organelle degradation typical for phloem cells. **D, E** Within the differentiation zone most of the signal is found in the dispersed non-nucleic form, indicating expression within sieve elements. All shown samples are counterstained with PI, merge of mVenus and PI channels in B, C, E. Scalebars: 50 µm.

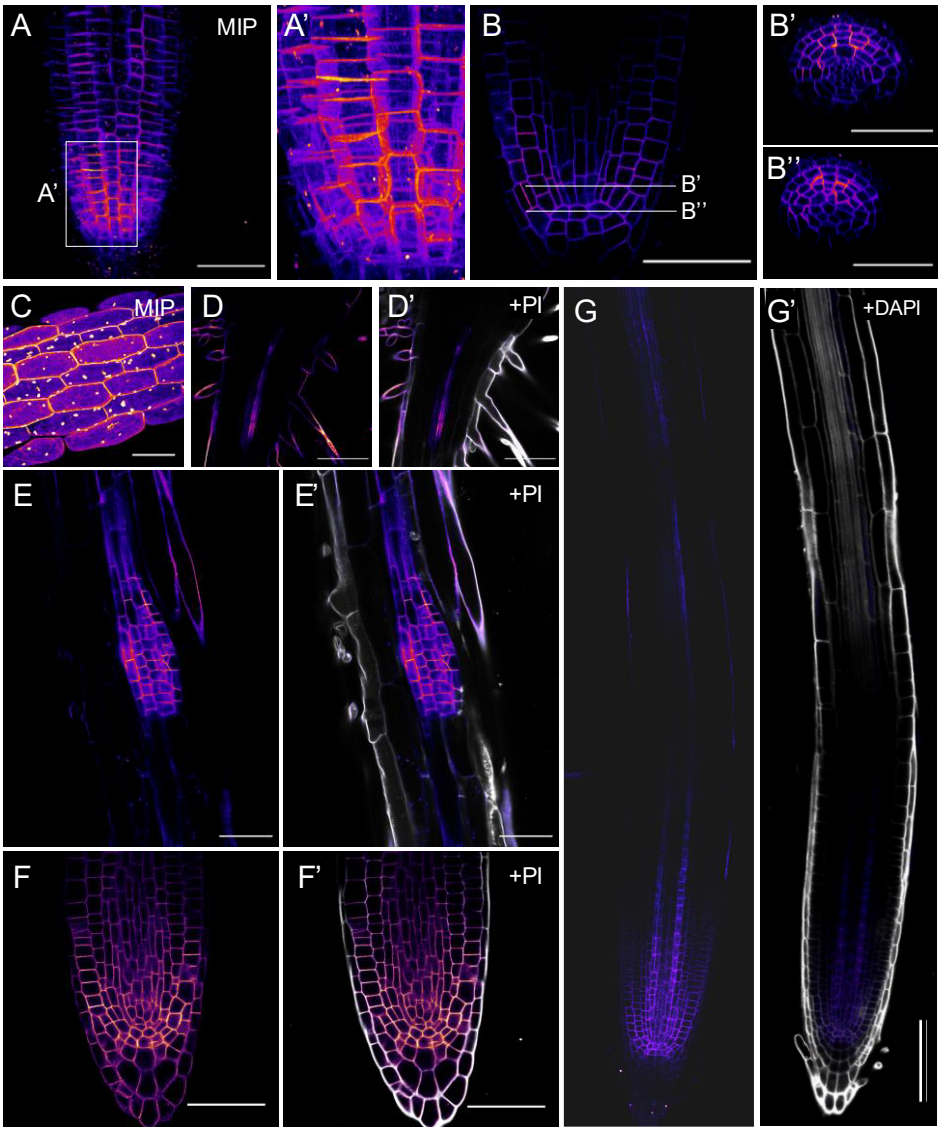

Supplemental Figure 6 *MAZ* expression by *MAZ* promotor in different translational reporters.

A – B'' ***MAZ-eGFP* expression in the root meristem. The fusion protein is PM-located and found in the QC, initials, and the adjacent cells as different projections of a z-stack through the root tip show, i.e. maximum intensity projection (MIP, A, A'') and YZ cross sections (B', B'') as indicated in B (5 DAG). **C** MIP of a z-stack through the epidermal layer of the hypocotyl of a *MAZ-eGFP* expressing seedling (5 DAG). **D, D'** In the transition region between root and hypocotyl MAZ-eGFP is found in the vasculature and in root hair cells (5 DAG). **E, E'** MAZ-eGFP is present in emerging lateral roots (10 DAG). **F, F'** *MAZ-eGFP* in mature lateral roots resembles its expression in the main root meristem (10 DAG). **G, G'** *MAZ* expression in the root is not dependent on the fluorophore fusion, since MAZ-mCh is found, like MAZ-eGFP, in the vasculature, root hair cells, and the RM (3 DAG). Scalebars: 50 µm (A, D–G), 100 µm (D, D'). Fluorophore signals are visualized with the LUT fire, in D', E', F' merge with PI (grey), in G' merge with DAPI (grey).

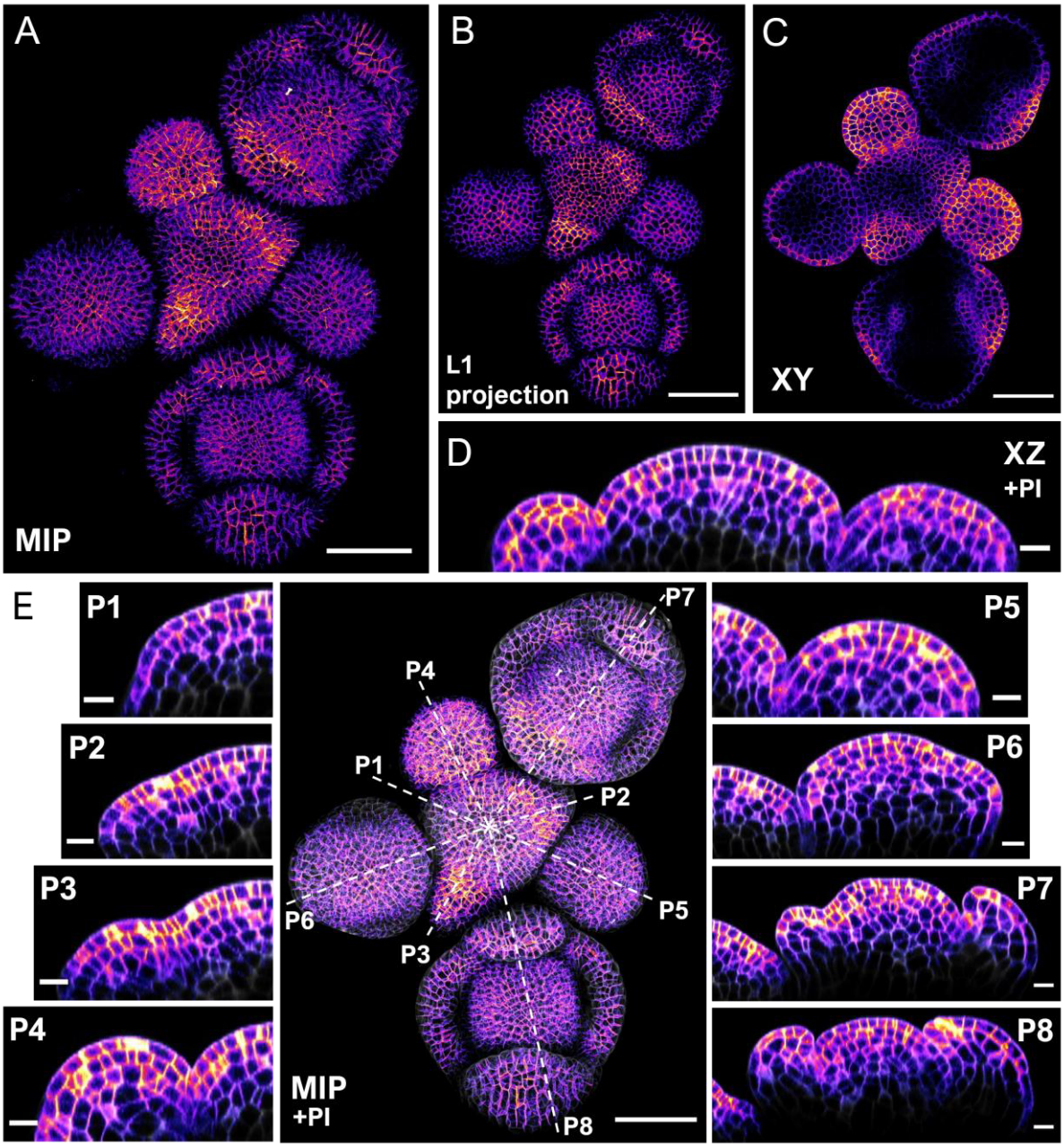

Supplemental Figure 7 Expression of *MAZ:MAZ-eGFP* in the SAM of 5 weeks old *A. thaliana*.

Various representations of a z-stack through the inflorescence with flower primordia (P) expressing *MAZ-eGFP* driven by the *MAZ* promotor and counterstained with PI (GFP-channel only visualized by LUT fire in A - C; merge with PI in grey displayed in D, E, P1 – P8). **A** The maximum intensity projection (MIP), **B** the L1 projection, **C** a transversal (XY) view, and **D** an orthogonal section through the central region (and P4 + P5), respectively, all indicate a broad *MAZ* expression with areas of higher signal intensity. Those include the boundary regions towards newly formed primordia and towards organs in later stages of development. In general, L1 expression appears elevated with a decreasing intensity gradient towards the L3 layers. **E** MIP as in A but merged with PI channel and cross sections through all primordia (indicated by dotted lines). Scalebars: 50 µm (A, B, C, E), 10 µm (D and primordia (P1 – P8) transversals).

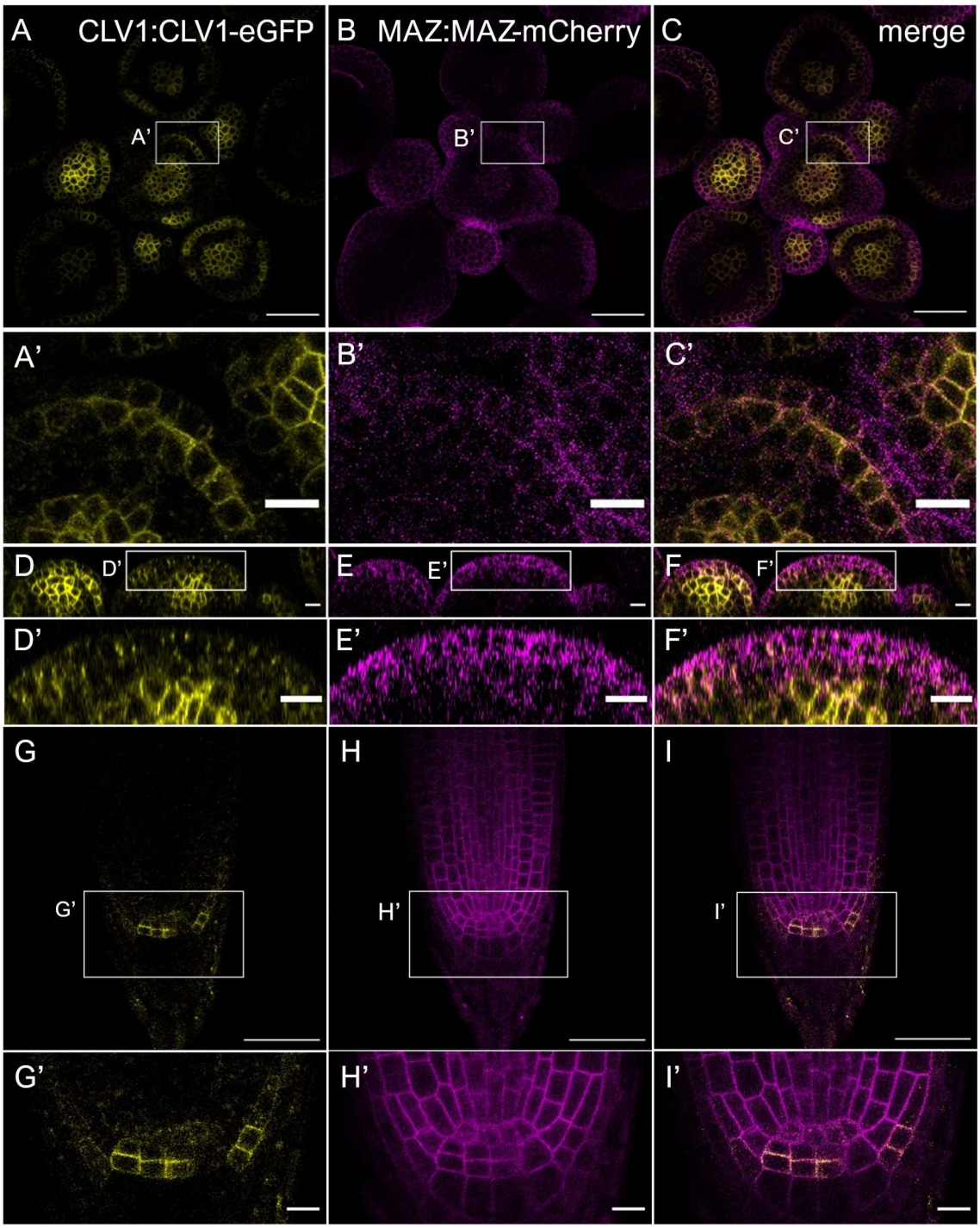

Supplemental Figure 8 Co-localization of CLV1-eGFP and MAZ-mCherry in shoot and root.

A – F Expression pattern of *CLV1* and *MAZ* under the control of the respective endogenous promotors in SAM and flower primordia of 5 weeks old plants. Both, the transversal (XY) cut through the meristem (A – C) and the orthogonal view (XZ, D – F), display CLV1-eGFP in the central zone and in specific areas of the L1, while *MAZ-mCh* is expressed in the entire L1 and only slightly in the central zone. Note the general weak expression of this mCh fusion in the shoot. Nevertheless, the expression pattern is comparable with *MAZ-eGFP* lines (compare Fig. 5). **G – I** In the distal root meristem *CLV1* expression is limited to few cells, like the columella stem cells (5 DAG). Here, CLV1 co-localize with MAZ. However, in the root meristem the *MAZ* expression domain is extended to the complete meristematic zone. A' – I' display the indicated areas in A – I. Scale bars: 50 µm (A – C, G – I), 20 µm (D – F), 10 µm (A' – I').

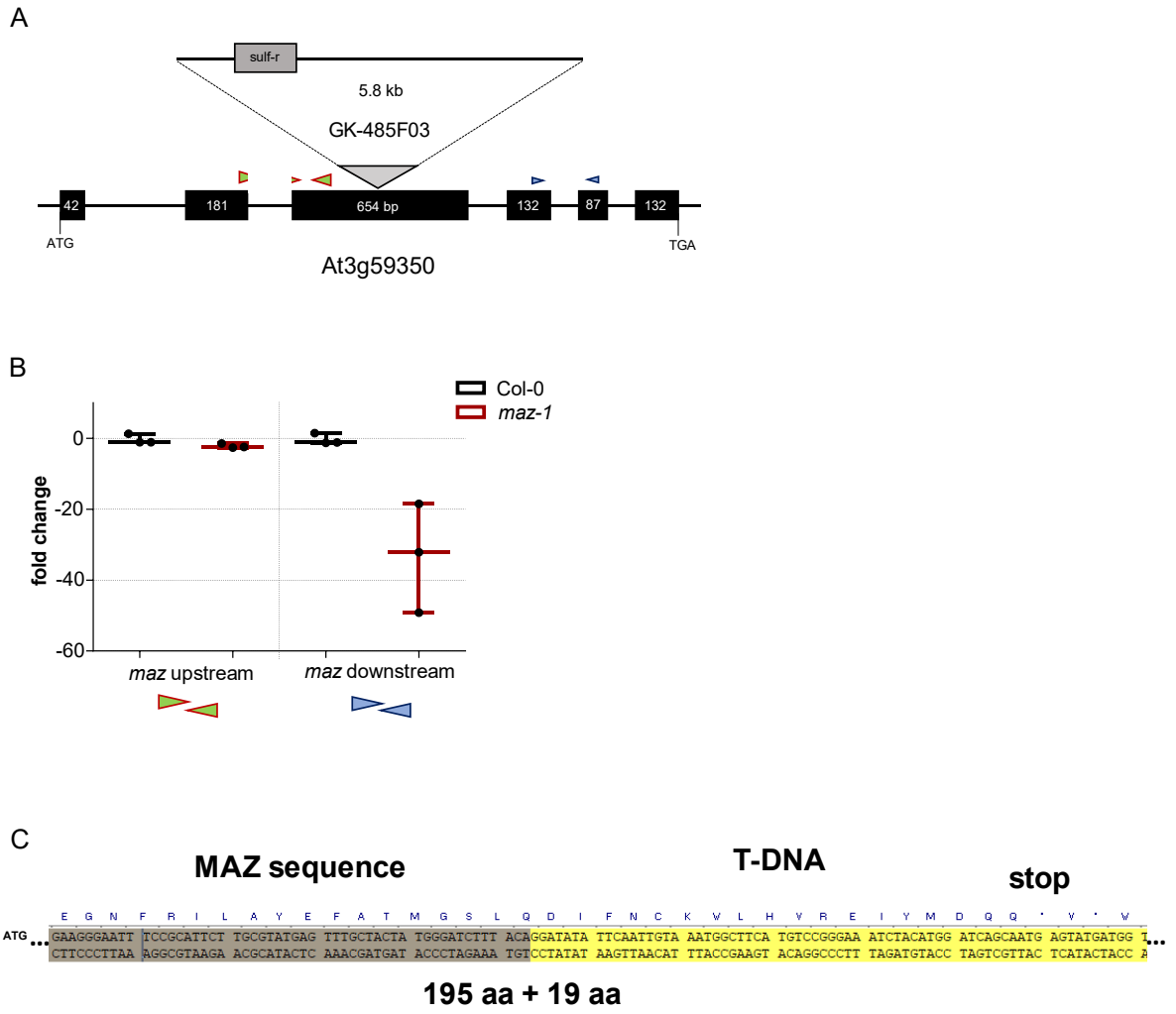

Supplemental Figure 9 Characterization of the *maz-1* allele GABI-Kat 485F03.

A The schematic representation of the genomic region of the *MAZ* gene At3g59350 displays the exon-intron structure as found in the TAIR database and verified by sequencing of cDNA clones (data not shown). Further, the predicted position of the GABI-Kat T-DNA insertion and the binding sites of the two oligo pairs used for quantitative expression analysis are shown. **B** RT-qPCR results from material of Col-0 and *maz-1* (whole seedlings 7 DAG) show a massive decrease of transcripts (up to 50-fold) in the mutant compared to the WT if the oligos bind downstream of the T-DNA insertion. This indicates that the mutant does not express full length MAZ protein anymore. However, there is also a decrease of transcript levels in *maz-1* compared to Col-0 when using an oligo pair upstream of the T-DNA, suggesting instability of the residual mutant *MAZ* mRNA. **C** Transition region from the *MAZ* sequence to the T-DNA insertion start in *maz-1* verified by Sanger sequencing. The insertion event leads to a disruption of the amino acid (aa) sequence of the MAZ protein after 195 aa. The reading frame continuous for 19 triplets of the T-DNA until the first in-frame STOP codon.

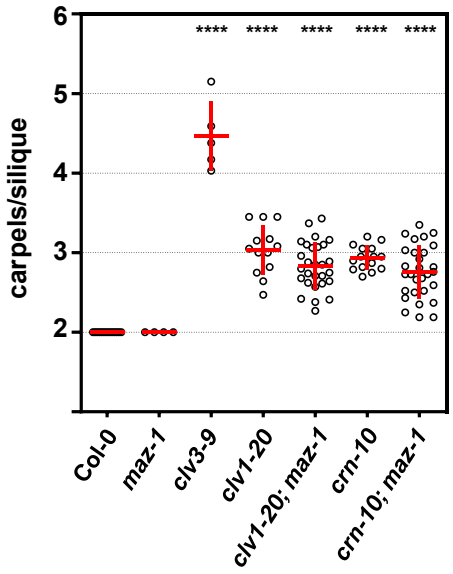

Supplemental Figure 10 Carpel number of m*az-1* mutants is wild typic in continuous light (CL).

Mean carpel number per silique of indicated genotypes monitored in 6–8 weeks old plants grown under CL. For each genotype 5–30 plants were analyzed by counting the carpels of 15–30 siliques per plant. The average carpel numbers for each plant are plotted. P-values calculated by ANOVA and Dunnett´s post hoc test with **** $p \leq 0.0001$. Sample mean and SD displayed in red.

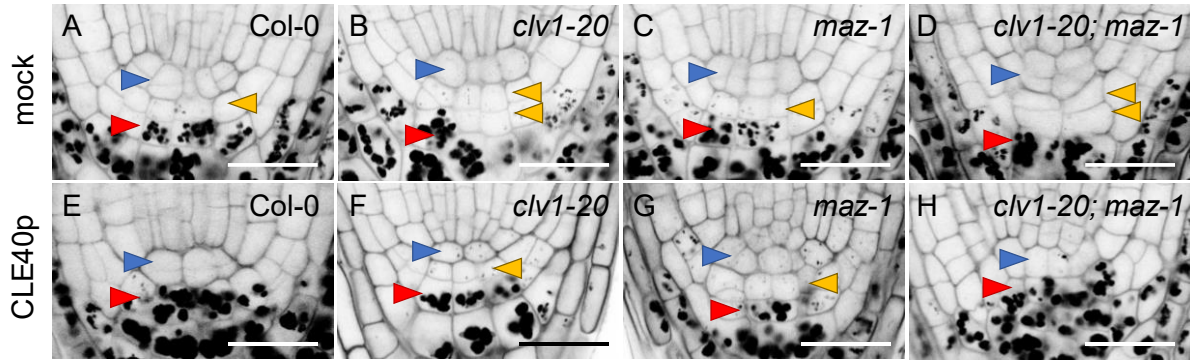

Supplemental Figure 11 *Maz-1* mutants are partially resistant to CLE40p treatment in terms of columella stem cell (CSC) layer specification.

Representative images of root meristem of mPS-PI stained seedlings (5 DAG) of indicated genotypes, grown on ½ MS plates with mock (A – D) or with CLE40p (200 nM, E – H). Arrow heads mark the QC cells (blue), CSC layers (yellow), and differentiated columella cells (red) with starch granules. Compare Fig. 6 B for quantification.

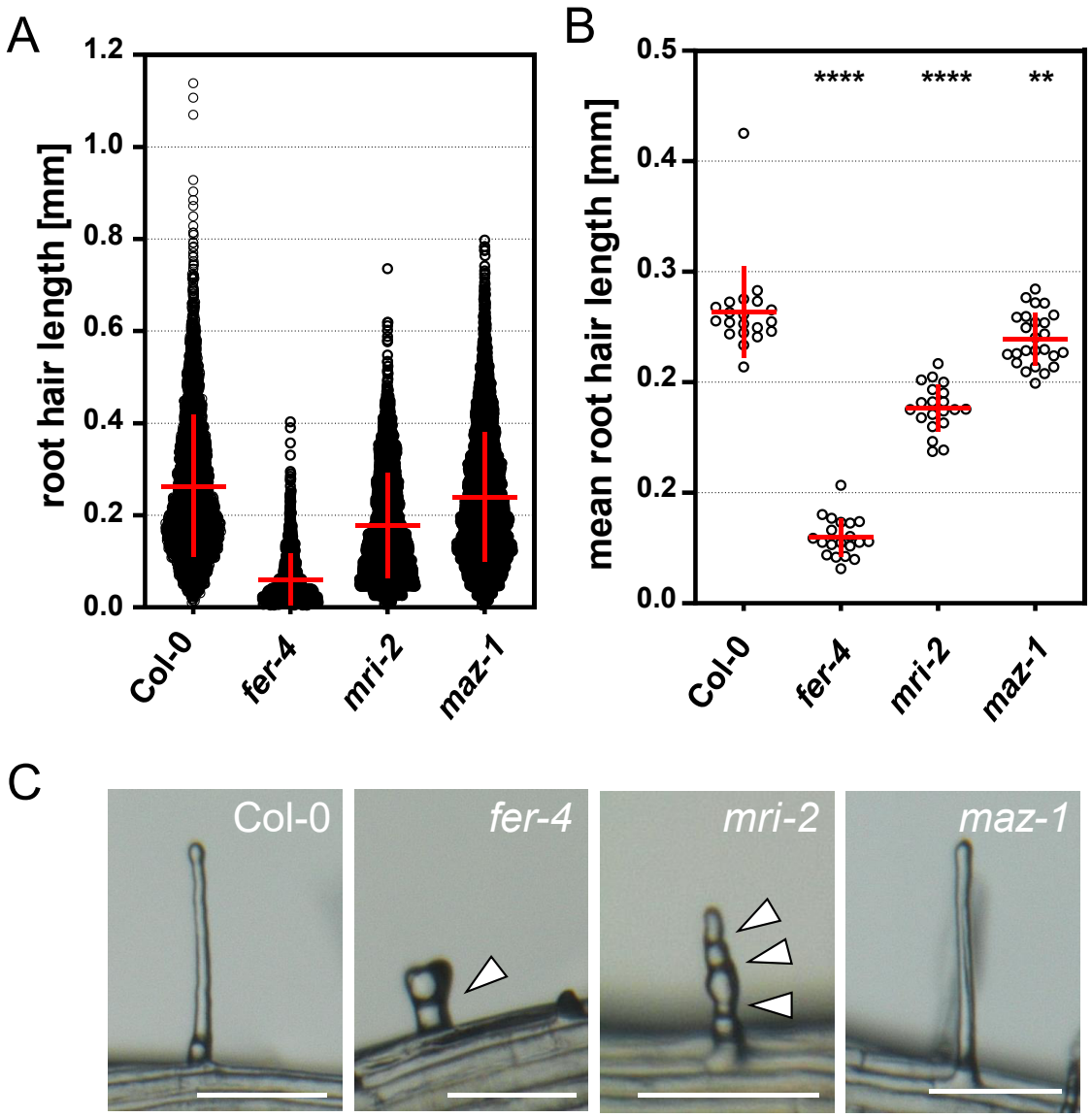

Supplemental Figure 12 The *maz-1* mutant does not display defects in root hair development.

Seedlings of indicated genotypes were grown on ½ MS agar plates and analyzed regarding root hair development. Root hair length was measured from 20 – 25 roots per genotype (all root hairs in focus on one side of the root) with total n = 3542 (Col-0), 975 (*fer-4*), 2433 (*mri-2*), and 4360 (*maz-1*). Plotting all single measurements (**A**) and the mean values per plant (**B**) revealed that *fer-4* and *mri-2* mutants show reduction of root hair length, while *maz-1* root hair length is comparable to Col-0 samples. P-values in B were calculated by ANOVA and Dunnett´s post hoc test, with ** for $p \leq 0.01$, and **** for $p \leq 0.0001$. **C** Exemplarily selected stereomicroscopy images of root hairs of the analyzed genotypes. Arrow heads show constrictions in the root hairs, probably caused by defective tip growth. This morphology was not observed in *maz-1* mutants. Scale bars: 100 µm.

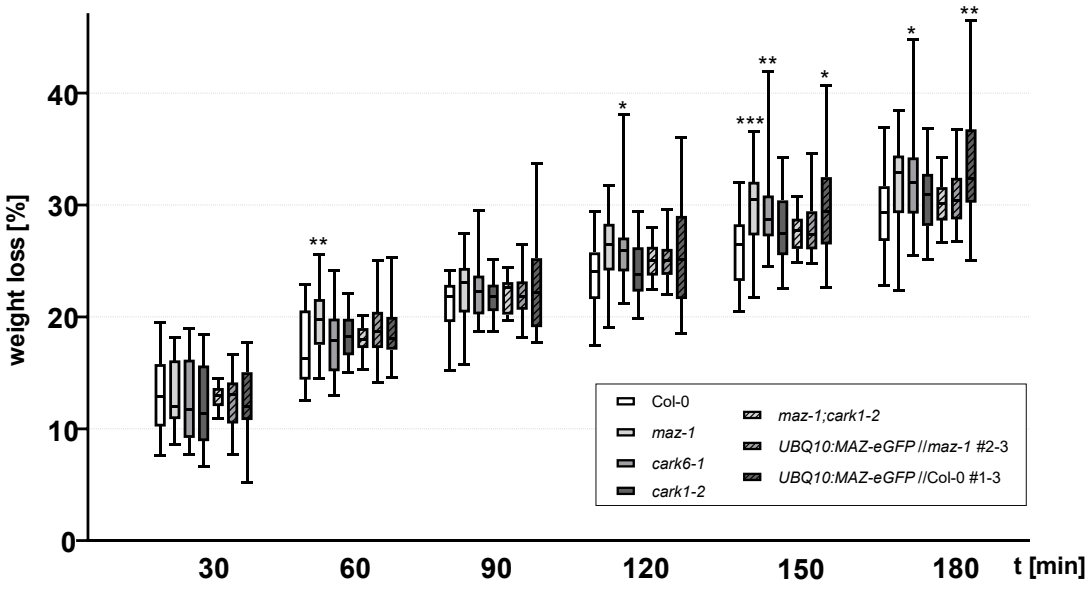

Supplemental Figure 13 Water loss assay of Arabidopsis leaves to monitor potential differential stomata closure as an indication for a role of Pti1-homologs in ABA signaling.

To estimate water loss through wilting, the reduction of leave fresh weight over time was accessed. The weight of 6 rosette leaves per sample/plant was determined directly after clipping off the leaves at the petioles and again at the indicated time points. The boxplots indicate the distribution of relative weight loss in comparison to the initial measurement for each time point. Alleles of different *pti1-like* mutants, (*maz-1*, *cark6-1*, *cark1-2*, and the double mutant *maz-1;cark1-2*) were included in the assay, as well as a *maz-1* complementing line, and a *MAZ* OE line. For each genotype 24 individual plants were analyzed in 3 independent experiments (in the case of *maz-1;cark1-2* only 16 plants in 2 independent experiments). Plants were cultivated for 4 – 5 weeks under standard LD conditions. The p-values were calculated by ANOVA and Dunnett´s post hoc test in comparison to the Col-0 WT sample for each time point, with * for $p \leq 0.05$, ** for $p \leq 0.01$, and *** for $p \leq 0.001$.

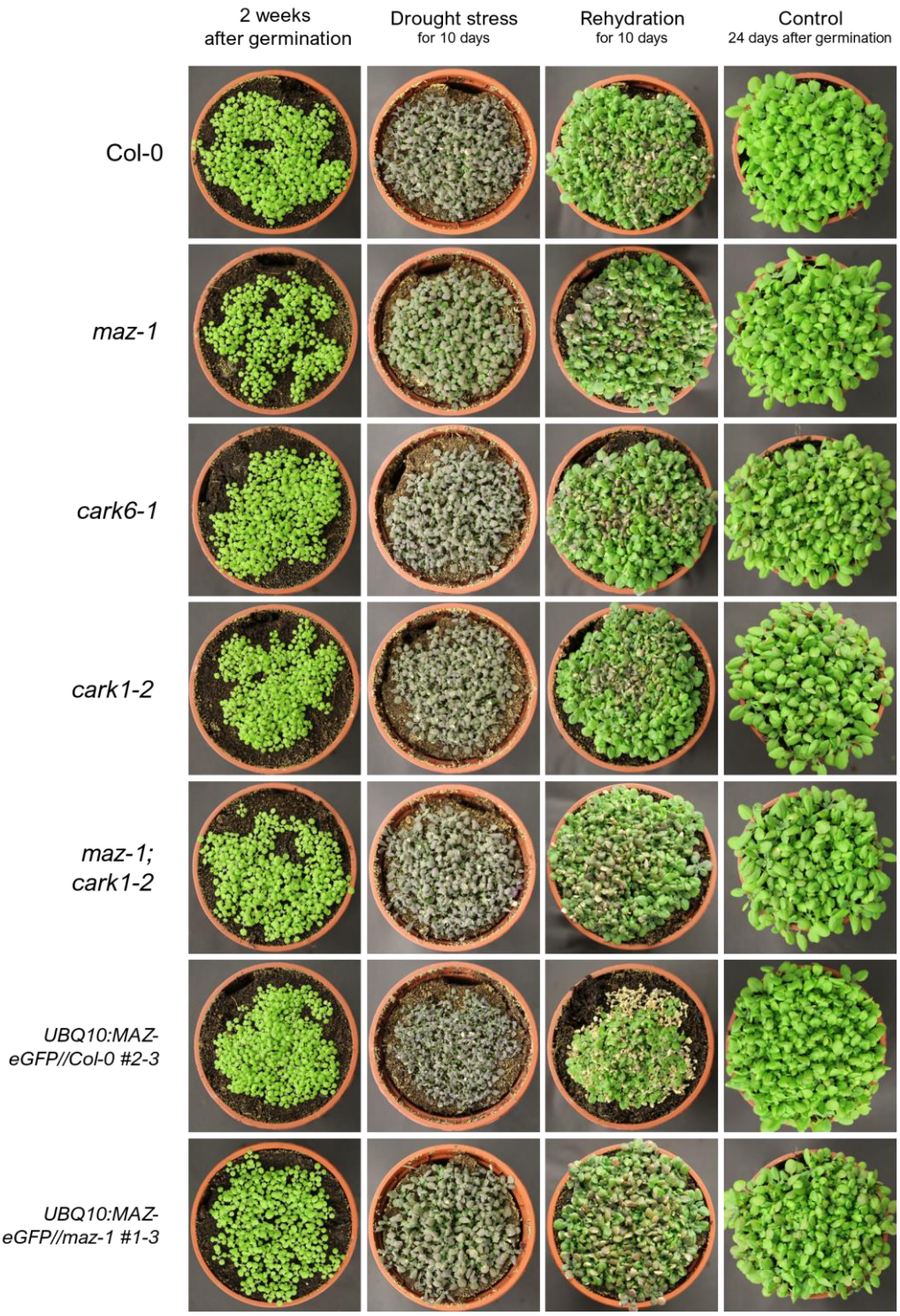

Supplemental Figure 14 Drought stress assay revealed no clear differences between the analyzed genotypes to cope with water deficiency.

Plants were cultivated under standard LD conditions for 2 weeks (images in column 1). During the following 10 days plants were kept in drought (column 2) und subsequently supplied with water again. Recovery was monitored after 10 days (column 3). The control plants were watered regularly (column 4, 24 days after germination). Representative images from 3 repetitions, all genotypes were randomly distributed over the tray to minimize local effects.

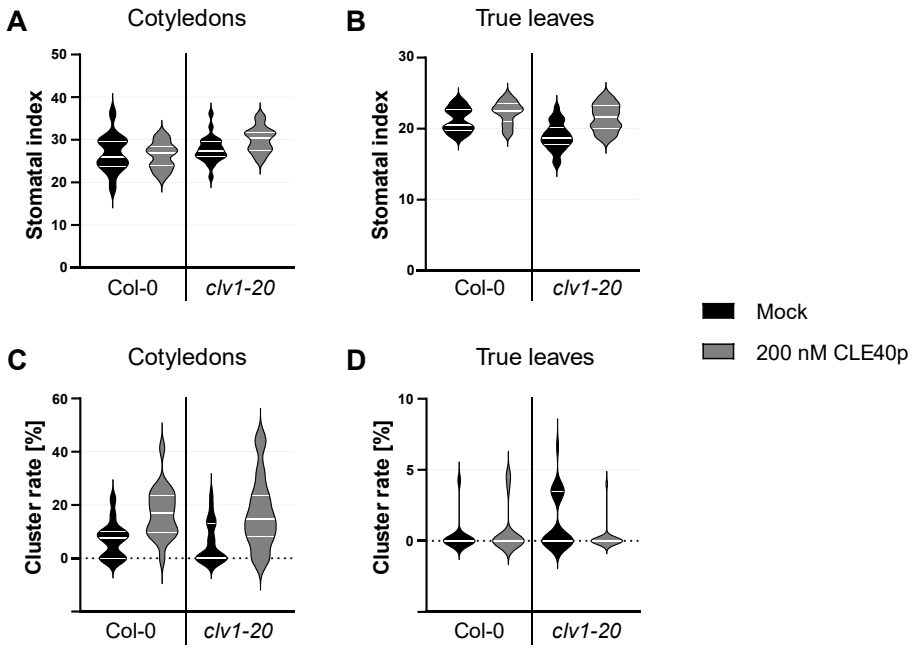

Supplemental Figure 15 Impact of the *clv1-20* allele and CLE40 peptide treatment on stomata development and clustering in Arabidopsis seedlings.

A, B The stomatal index is constant between Col-0 WT and *clv1-20* mutants in cotyledons (A), as well as in true leaves (B). Suppling 200 nM CLE40p to the growth medium (½ MS) does not affect the stomatal index. **C, D** The cluster rate of Col-0 and *clv1-20* is not altered in cotyledons, but CLE40p treatment increases clustering (C). In true leaves *clv1-20* mutants display increased clustering of stomata, which is counteracted by treatment of CLE40p (D). All plants were analysed 14 DAG.

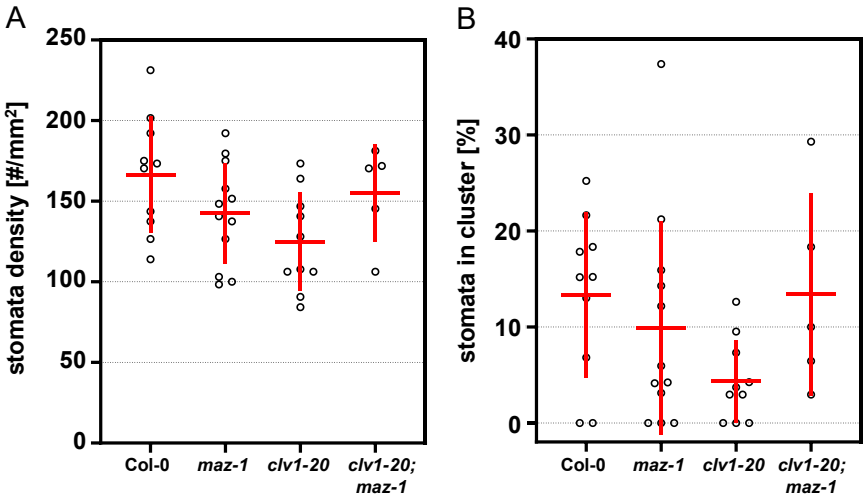

Supplemental Figure 16 Cotyledons of *clv1-20*, *maz-1*, and the double mutant *clv1-20; maz-1* display no significant changes of stomata density and cluster rate.

A Stomatal density and **B** cluster rate were accessed from cotyledons of indicated genotypes. Each plotted data point represents the mean value of 4 areas within one cotyledon of individual plants. Seedlings were grown on ½ MS agar plates. 14 DAG cotyledons were stained with PI to image abaxial epidermis cells. No significant differences in comparison to the Col-0 sample were identified by ANOVA and Dunnett´s post hoc test. Sample mean and SD displayed with red lines.

Supplemental Table 1 Via mass spectroscopy identified proteins in CoIP fraction against CLV1-2xGFP, which are not found in GFP-only control samples.

Gene ID	Protein name	Subcellular localization	MS/MS hits
At1g75820	CLAVATA1 (CLV1)	PM	23
At5g38530	Tryptophan synthase beta chain (TSBtpye2)	chloroplast, cytosol	20
At3g56650	PsbP domain-containing protein 6 (PPD6)	chloroplast	20
At4g24510	Protein ECERIFERUM 2 (CER2)	nucleus, ER	19
At3g10060	Peptidyl-prolyl cis-trans isomerase (FKBP16-4)	chloroplast	16
At3g01420	Alpha-dioxygenase 1 (DOX1)	n/a	16
At1g16080	uncharacterized protein	apoplast, ER	16
At4g11290	Peroxidase 39 (PER39)	extracellular	15
At3g06350	Bifunctional 3-dehydroquinate dehydratase/shikimate dehydrogenase (EMB3004)	chloroplast	15
At2g46520	Exportin-2 (CAS)	nucleus	12
At1g72160	Patellin-3 (PATL3)	PM, cytoplasm	11
At2g26250	3-ketoacyl-CoA synthase 10 (FDH)	ER	11
At5g47840	Adenylate kinase 2	chloroplast stoma	10
At5g55730	Fasciclin-like arabinogalactan protein 1 (FLA1)	PM, apoplast	10
At4g28440	uncharacterized protein	cytosol	10
At4g12470	pEARLI1-like lipid transfer protein 1 (AZI1)	CW, plasmodesmata, ER	10
At5g18660	Divinyl chlorophyllide a 8-vinyl-reductase (DVR)	chloroplast	9
At5g05730	Anthranilate synthase alpha subunit 1 (ASA1)	chloroplast	9
At3g16520	UDP-glycosyltransferase 88A1 (UGT88A1)	cytosol	9
At3g59350	PTI1-like tyrosine-proteine kinase 3 (Pti1-3)	PM-associated	8
At1g69530	Expansin-A1 (EXPA1)	CW, extracellular, mitochondria	7
At3g14100	Oligouridylate-binding protein 1C (UBP1C)	nucleus	6
At2g37760	Aldo-keto reductase family 4 member C8 (AKR4C8)	cytosol	5

Supplemental Table 2 Mean FRET efficiencies of tested donor-acceptor combinations at the PM of transiently transformed *N. benthamiana* epidermis cells.

Donor	Acceptor	FRET efficiency [%] ± SD
CLV1-GFP	MAZ-linker-mCherry	5.9 ±3.7
CLV1-GFP + 5 µM CLV3	MAZ-linker-mCherry	5.5 ±1.8
CLV1-GFP	CRN-KD^{myr}-mCherry	2.0 ±2.8
BAM1-GFP	MAZ-linker-mCherry	6.5 ±2.3
MAZ-eGFP	MAZ-linker-mCherry	5.3 ±2.8
MAZ-eGFP	BAM3-mCherry	4.0 ±2.0
MAZ-eGFP	CIK2-mCherry	5.7 ±1.9
CRN-GFP (+CLV2)	MAZ-linker-mCherry	3.0 ±2.3
CLV1-mNeonGreen	MAZ-mCherry	3.7 ±1.8
CLV1-mNeonGreen	mCherry^{myr}	0.7 ±1.1
CLV1-mNeonGreen	CARK1-mCherry	5.2 ±3.2
CLV1-mNeonGreen	Pti1-11-mCherry	5.4 ±2.2
CLV1-mNeonGreen	CARK6-mCherry	4.2 ±3.2
CLV1-mNeonGreen	Pti1-2-mCherry	0.6 ±2.3

Supplemental Table 3 Pti1-like family in *Arabidopsis thaliana* and predicted PM-localization mechanisms.

Name	TAIR locus	Length [aa]	Myristoylation[1]	Palmitoylation[2]	GPI-anchor[3]
Pti1-1	At1g06700	361	no	C6, C7, C9	no
Pti1-2	At2g30740	366	no	C6, C7	no
MAZZA	At3g59350	408	no	C48, C49	no
Pti1-4	At2g47060	365	no	C3, C6, C7	no
MARIS	At2g41970	365	no	C3, C4	no
Pti1-6	At2g30730	338	no	no	no
CARK6	At2g43230	440	no	C79, C80, C82	no
Pti1-8	At1g48220	364	no	C3, C7	no
Pti1-9	At3g62220	361	no	C3, C6, C7	no
CARK1	At3g17410	364	score = 0.6*	C3, C6, C7	no
Pti1-11	At1g48210	363	no	C3, C7	no

[1] predicted by CSS-Palm 4.1
[2] predicted by Myristoylator (ExPASy)
[3] predicted by PredGPI

* indicating medium confidence

Supplemental Table 4 Chemicals.

Name	Producer/Source	Product no.	CAS no.
Acetosyringone (3',5'-Dimethoxy-4'-hydroxy-acetophenone)	Sigma-Aldrich (Merck)	D134406	2478-38-8
Aniline blue (water soluble)	Thermo Fisher Scientific	B8563	28631-66-5
BASTA® non-selective herbicide	Bayer CropScience	84442615	N/A
β-estradiole	Sigma-Aldrich (Merck)	E8875	50-28-2
Carbenicillin disodium salt	Carl Roth	6344.2	4800-94-6
cOmplete™ Protease Inhibitor Cocktail	Roche	11697498001	N/A
DAPI (4',6-diamidino-2-phenylindole)	N/A	N/A	28718-90-3
DL-phosphinothricin (PPT)	Duchefa Biochemie bv	P0159	77182-82-2
Gentamicin sulfate	Sigma-Aldrich (Merck)	G1264	1405-41-0
GFP antibody [3H9] (IgG, rat monoclonal)	ChromoTek	3h9-20	N/A
GFP-Trap® magnetic agarose	ChromoTek	gmt-20	N/A
Goat anti-mouse IgG Alkaline Phosphatase (AP)	Sigma-Aldrich (Merck)	AP124A	N/A
Goat anti-rat IgG Alkaline Phospatase (AP)	Sigma-Aldrich (Merck)	A8438	N/A
Hygromycin B	Duchefa Biochemie bv	H0192	31282-04-9
Kanamycin monosulfate	Duchefa Biochemie bv	K0126.0005	25389-94-0
MES hydrate	Sigma-Aldrich (Merck)	10240885	1266615-59-1
Murashige & Skoog Medium (+Gamborg B5 vitamins)	Duchefa Biochemie bv	M0231.0050	N/A
NEXT GEL® 10 % acrylamide	VWR Life Science	M256	N/A
Nonident™ P40 substitute	Sigma-Aldrich (Merck)	100980769	9016-45-9
Phusion High-Fidelity PCR polymerase	Thermo Fisher Scientific	F530S	N/A
Propidium iodide	Thermo Fisher Scientific	P1304MP	25535-16-4
RFP antibody [6G6] (IgG, mouse monoclonal)	ChromoTek	6g6-20	N/A
Rifampicin	TCI	R0079	13292-46-1
Spectinomycin HCl pentahydrate	Duchefa Biochemie bv	S0188	22189-32-8
SsoAdvanced Univerasal SYBR® Green Supermix	Bio-Rad	1725271	N/A
SuperScript™ reverse transcriptase	Thermo Fisher Scientific	18080-093	N/A
Synthetic CLV3 (RCV[Hyp]SG[Hyp]DPLHHH)	Peptides & Elephants	costumized	N/A
Synthetic CLE40 (RQV[Hyp]TGSDPLHHK)	Peptides & Elephants	costumized	N/A
Synthetic CLE45 (RRVRRGSDPIHN)	Peptides & Elephants	costumized	N/A
Tetracycline	Sigma-Aldrich (Merck)	87128	60-54-8

Supplemental Table 5 Analyzed *A. thaliana* mutants (Col-0 background).

Allele	Type	Gene	Reference
maz-1	T-DNA	At3g59350	GABI-Kat 485F03
clv1-20	T-DNA	At1g75820	Durbak and Tax, 2011; SALK 008670
clv3-9	EMS	At2g27250	Rüdiger Simon, 2003; W62Stop
crn-10	CRISPR/Cas9	At5g13290	Nimchuk, 2017
cark1-2	T-DNA	At3g17410	SALK 094451
cark6-1	T-DNA	At2g43230	Wang et al. 2019; SALK 203094
mri-2	T-DNA	At2g41970	Boisson-Dernier et al. 2015; GABI-Kat 820D05
fer-4	T-DNA	At3g51550	Haruta et al. 2014; GABI-Kat 106A06

Supplemental Table 6 Genotyping strategies to verify listed mutant alleles.

Allele	Method	Details
maz-1	PCR	Fwd 5'-CAGCTCAGTTTGTTAGGCTGGATA-3' Rev (WT) 5'-CAGTATTTTATGGTTAGCGTTTTG-3' Rev (T-DNA) 5'-ATAATAACGCTGCGGACATCTACATTTT-3' (GABI o8474) WT amplicon = 1403 bp; mutant amplicon = 750 bp
clv1-20	PCR	Fwd 5'-TTTGAATAGTGTGTGACCAAATTTGA-3' Rev (WT) 5'-TCCAATGGTAATTCACCGGTG-3' Rev (T-DNA) 5'-TGGTTCACGTAGTGGGCCATCG-3' (SALK LBa1) WT amplicon = 860 bp; mutant amplicon = 1200 bp
crn-10	dCAPS	Fwd 5'-GTAGAAGCAGCAATGAAGCAAAGAAGAAGGTG-3' Rev 5'-GTGTAGATGATGTTGAAGTTGTGGATAAGTG-3' subsequent HphI digestion, WT = 128 + 41 bp, mutant = 169 bp
cark1-2	PCR	Fwd (WT) 5'-TCAACACACTGCTTCACCTTG-3' Fwd (T-DNA) 5'-ATTTTGCCGATTTCGGAAC-3' (SALK LBa1.3) Rev 5'-GAAAAGGTGTTAAAGGGGCAC-3' WT amplicon = 1066 bp; mutant amplicon = 700 bp
cark1-6	PCR	Fwd (WT) 5'-TGTTCGATTGGATAAACCGAG-3' Fwd (T-DNA) 5'-ATTTTGCCGATTTCGGAAC-3' (SALK LBa1.3) Rev 5'-CCCGGTAAGAAGTTCCAAAAG-3' WT amplicon = 1169 bp; mutant amplicon = 725 bp
mri-2	PCR	Fwd 5'-GTTCTATTCTTCGACCAAATGG-3' Rev (WT) 5'-CTGCATACTGGTTTGCGGG-3' Rev (T-DNA) 5'-GGGCTACACTGAATTGGTAGCTC-3' (GABI o8760) WT amplicon = 935 bp; mutant amplicon = 880 bp (see Boisson-Dernier et al. 2016)
fer-4	PCR	Fwd (WT) 5'-GATTACTCTCCAACAGAGAAAATCCT-3' Rev (WT) 5'-CGTATTGCTTTTCGATTTCCTA-3' Fwd (T-DNA) 5'-ACGGTCTCAACGCTACCAAC-3' Rev (T-DNA) 5'-TTTCCCGCCTTCGGTTTA-3' WT amplicon = 1254 bp; mutant amplicon = 570 bp (see Haruta et al. 2014)

Supplemental Table 7 Entry plasmids.

Name	Description (insert)	Gene	Backbone	Bacterial resistance	Oligos for insert amplification, mutagenesis (or reference)
MAZ/pENTR	genomic region of MAZ (START to one codon before STOP, including Introns)	At3g59350	*pENTR/D-TOPO®*	Kanamycin	5'-CACCATGTATCCGATGGATTCTGATTAC-3' 5'-GGCTTCCTGGACTGGTACAG-3'
pMAZ/pGGA	promotor region of MAZ (1.8 kb)	At3g59350	*pGGA000*	Ampicillin	5'-TTTGGTCTCAACCTCTATAAATTACAGACATTCAAATAC-3' 5'-TTTGGTCTCATGTTAGTGAAAGACGGATCG-3'
MAZ/pGGC	genomic region of MAZ (START to one codon before STOP, including Introns)	At3g59350	*pGGC000*	Ampicillin	5'-TTTGGTCTCAGGCTTAATGTATCCGATGGATTC-3' 5'-TTTGGTCTCACTGAGGCTTCCTGGACTG-3'
MAZ^{PalMut}/pGGC	C48W, C49W, C51W in MAZ (site-directed mutagenesis of MAZ/pGGC)	At3g59350	*pGGC000*	Ampicillin	5'-GATGCGTAGGTGGTTGTGGTGGGCTTGGCACGTTGAAGAAC-3' 5'-GTTCTTCAACGTGCCAAGCCCACCACAACCACCTACGCATC-3'
MAZ$^{\Delta N\text{-term}}$/pGGC	genomic region of MAZ (from F113, w/o STOP, including Introns)	At3g59350	*pGGC000*	Ampicillin	5'-TTTGGTCTCAGGCTCAATGTTTGGATCAAAGTCATTG-3' 5'-TTTGGTCTCACTGAGGCTTCCTGGACTG-3'
Pti1-2/pGGC	genomic region of Pti1-2 (START to one codon before STOP, including Introns)	At2g30740	*pGGC000*	Ampicillin	5'-TTTGGTCTCAGGCTTAATGCGTAGGTGGATCTGTTGT-3' 5'-TTTGGTCTCACTGAGGATTCCGGTACTGGGGCTGG-3'
CARK1/pGGC	genomic region of CARK1 (START to one codon before STOP, including Introns)	At3g17410	*pGGC000*	Ampicillin	5'-AAACGTCTCAGGCTTGATGGGCTGCTTTGGTT-3' 5'-AAACGTCTCACTGAATACGGGTTCCTGTGTGG-3'
CARK6/pGGC	genomic region of CARK6 (START to one codon before STOP, including Introns)	At2g43230	*pGGC000*	Ampicillin	5'-TTTGGTCTCAGGCTATGGATCGTGATTTTCATCG-3' 5'-TTTGGTCTCACTGAAGGTTGAGGTGTTGG-3'
Pti1-6/pGGC	genomic region of Pti1-6 (START to one codon before STOP, including Introns)	At1g48210	*pGGC000*	Ampicillin	5'-TTTGGTCTCAGGCTTAATGTTTTTTTTTTCTTGTCATCACAT-3' 5'-TTTGGTCTCACTGAGAATTGCGGTATTGAGCCTGT-3'
BAM3/pENTR	BAM3 coding region (with introns)	At4g20270	*pENTR/D-TOPO®*	Kanamycin	5'-CACCATGGCAGACAAGATCTTCAC-3' 5'-GAAAGTATTAGGCTGTTTAGCC-3'
CIK2/pENTR	CIK2 coding region	At2g23950	*pENTR/D-TOPO®*	Kanamycin	Pauline Anne (Christian Hardtke Lab)
POL/pENTR	POLTERGEIST coding region	At2g46920	*pENTR/D-TOPO®*	Kanamycin	Frederic Boyer
BAM1/pENTR	BAM1 coding region	At5g65700	*pENTR/D-TOPO®*	Kanamycin	Marc Somssich
myr-CRN-KD/pENTR	KD of CRN with myristoylation motif	At5g13290	*pENTR/D-TOPO®*	Kanamycin	Marc Somssich
linker-eGFP/pGGD	11 aa linker fused upstream to eGFP	-	*pGGD000*	Ampicillin	Grégoire Denay (pGD165)
mVenus/pGGC	mVenus w/o STOP codon	-	*pGGC00*	Ampicillin	Rebecca Burkart (pRD43)
mCherry/pGGD	mCherry with STOP codon	-	*pGGD000*	Ampicillin	Rebecca Burkart (pRD53)

Supplemental Table 8 Plasmids used for transient gene expression in *N. benthamiana*.

Name	Expression cassette	Cloning strategy	Details	Bacterial resistance
BAM1/pAB118	XVE<<LexA-min35S:BAM1-mCherry	LR reaction	*BAM1/pENTR + pAB118*	Spectinomycin
BAM3/pAB118	XVE<<LexA-min35S:BAM3-mCherry	LR reaction	*BAM3/pENTR + pAB118*	Spectinomycin
CIK2/pAB118	XVE<<LexA-min35S:CIK2-mCherry	LR reaction	*CIK2/pENTR + pAB118*	Spectinomycin
CLV1/pAB117	XVE<<LexA-min35S:CLV1-GFP	LR reaction	*Bleckmann et al. 2010*	Spectinomycin
CLV1/pAB118	XVE<<LexA-min35S:CLV1-mCherry	LR reaction	*Bleckmann et al. 2010*	Spectinomycin
CLV2 (untagged)	XVE<<LexA-min35S:CLV2	LR reaction	*Bleckmann et al. 2010*	Spectinomycin
CRN/pAB117	XVE<<LexA-min35S:CRN-GFP	LR reaction	*Bleckmann et al. 2010*	Spectinomycin
CRN$^{\Delta KD}$/pAB117	XVE<<LexA-min35S:CRN$^{\Delta KD}$-GFP	LR reaction	*Bleckmann et al. 2010*	Spectinomycin
MAZ/pAB118	XVE<<LexA-min35S:MAZ-mCherry	LR reaction	*MAZ/pENTR + pAB118*	Spectinomycin
myr-CRN-KD/pAB118	XVE<<LexA-min35S:myr-CRN-KD-mCherry	LR reaction	*myr-CRN-KD/pENTR + pAB118*	Spectinomycin
POL/pAB117	XVE<<LexA-min35S:POL-GFP	LR reaction	*POL/pENTR + pAB117*	Spectinomycin
UBQ10:MAZ-eGFP/pGGZ001	pUBQ10:Ω-MAZ-eGFP:tUBQ10<<HygR	GreenGate reaction	*pGGA006, pGGB002, MAZ/pGGC, linker-eGFP/pGGD, pGGE009, pGGF005 + pGGZ001*	Spectinomycin
UBQ10:MAZ-mCherry/pGGZ001	pUBQ10:Ω-MAZ-mCherry:tUBQ10<<HygR	GreenGate reaction	*pGGA006, pGGB002, MAZ/pGGC, mCherry/pGGD, pGGE009, pGGF005 + pGGZ001*	Spectinomycin
UBQ10:Pti1-2-mCherry/pGGZ001	pUBQ10:Ω-Pti1-2-mCherry:tUBQ10	GreenGate reaction	*pGGA006, pGGB002, Pti1-2/pGGC, mCherry/pGGD, pGGE009, dummy/pGGF + pGGZ001*	Spectinomycin
UBQ10:CARK1-mCherry/pGGZ001	pUBQ10:Ω-CARK1-mCherry:tUBQ10	GreenGate reaction	*pGGA006, pGGB002, CARK1/pGGC, mCherry/pGGD, pGGE009, dummy/pGGF + pGGZ001*	Spectinomycin
UBQ10:CARK6-mCherry/pGGZ001	pUBQ10:Ω-CARK6-eGFP:tUBQ10	GreenGate reaction	*pGGA006, pGGB002, CARK6/pGGC, mCherry/pGGD, pGGE009, dummy/pGGF + pGGZ001*	Spectinomycin
UBQ10:Pti1-6-mCherry/pGGZ001	pUBQ10:Ω-Pti1-6-mCherry:tUBQ10	GreenGate reaction	*pGGA006, pGGB002, Pti1-6/pGGC, mCherry/pGGD, pGGE009, dummy/pGGF + pGGZ001*	Spectinomycin
UBQ10:CLV1-mNeonGreen/pGGZ001	pUBQ10:Ω-CLV1-mNeonGreen:tUBQ10<<HygR	GreenGate reaction	*Grégoire Denay (pGD354)*	Spectinomycin
UBQ10:myr-mCherry/pGGZ001	pUBQ10:Ω-myr-mCherry:tUBQ10<<HygR	GreenGate reaction	*Grégoire Denay (pGD321)*	Spectinomycin

Supplemental Table 9 Plasmids used for stabile transformation of *A. thaliana*.

Name	Promotor	N-tag	CDS	C-tag	Terminator	Plant Resistance	Backbone
MAZ:MAZ-eGFP+BastaR/pGGZ001	pMAZ/pGGA	pGGB002	*MAZ/pGGC*	linker-eGFP/pGGD	pGGE009	pGGF008	pGGZ001
MAZ:MAZ-mCherry+HygR/pGGZ001	pMAZ/pGGA	pGGB002	*MAZ/pGGC*	mCherry/pGGD	pGGE009	pGGF005	pGGZ001
UBQ10:MAZ-eGFP+BastaR/pGGZ001	pGGA006	pGGB002	*MAZ/pGGC*	linker-eGFP/pGGD	pGGE009	pGGF008	pGGZ001
MAZ:MAZ^{PalMut}-eGFP+BastaR/pGGZ001	pMAZ/pGGA	pGGB002	*MAZ*^{PalMut}/pGGC	linker-eGFP/pGGD	pGGE009	pGGF008	pGGZ001
UBQ10:MAZ^{PalMut}-eGFP+BastaR/pGGZ001	pGGA006	pGGB002	*MAZ*^{PalMut}/pGGC	linker-eGFP/pGGD	pGGE009	pGGF008	pGGZ001
MAZ:mVenus-NLS+BastaR/pGGZ001	pMAZ/pGGA	pGGB002	mVenus/pGGC	pGGD007	pGGE009	pGGF008	pGGZ001

Supplemental Table 9 Transgenic *A. thaliana* lines applied and generated in this study.

Name	Transgene description	Reference
CLV1:CLV1-2xGFP//clv1-11	pCLV1:CLV1-2xmGFP/pBJ36 (HygR)	Nimchuk *et al.* 2011
*MAZ:MAZ-eGFP+BastaR//*Col-0	pMAZ:Ω-MAZ-eGFP:tUBQ10<<pNOS:BastaR:tNOS	this study
*MAZ:MAZ-mCh+HygR//*Col-0	pMAZ:Ω-MAZ-mCherry:tUBQ10<<pUBQ10:HygR:tOCS	this study
MAZ:MAZ^{PalMut}-eGFP+BastaR//maz-1	pMAZ:Ω-MAZ^{PalMut}*-eGFP:tUBQ10<<pNOS:BastaR:tNOS*	this study
*MAZ:mVenus-NLS+BastaR//*Col-0	pMAZ:Ω-mVenus-NLS:tUBQ10<<pNOS:BastaR:tNOS	this study
*UBQ10:MAZ-eGFP+BastaR//*Col-0	pUBQ10:Ω-MAZ-eGFP:tUBQ10<<pNOS:BastaR:tNOS	this study
UBQ10:MAZ-eGFP+BastaR//maz-1	pUBQ10:Ω-MAZ-eGFP:tUBQ10<<pNOS:BastaR:tNOS	this study
*UBQ10:MAZ^{PalMut}-eGFP+BastaR//*Col-0	pUBQ10:Ω-MAZ^{PalMut}*-eGFP:tUBQ10<<pNOS:BastaR:tNOS*	this study

Supplemental Table 11 Oligonucleotides for RT-qPCR.

Gene	Forward	Revers
MAZ (upstream)	CACAATGATTTTGGGGCATCAC	GCGACAGCCTTTCCATCTTTC
MAZ (downstream)	TGGTAGGAAACCCGTCGAT	TGGATCAACACATTGCTTCAC
AT2G28390	GGATTTTCAGCTACTCTTCAAGCTA	TCCTGCCTTGACTAAGTTGACA
AT4G34270	GCTCATGGTTCCTCCTCTTG	TCTTCGCCAAACCTATAATGC
AT4G26410	CGTCCACAAAGCTGAATGTG	CGAAGTCATGGAAGCCACTT

Appendix Sequence alignment with ClustalΩ of Arabidopsis Pti1-like family and SlPti1.

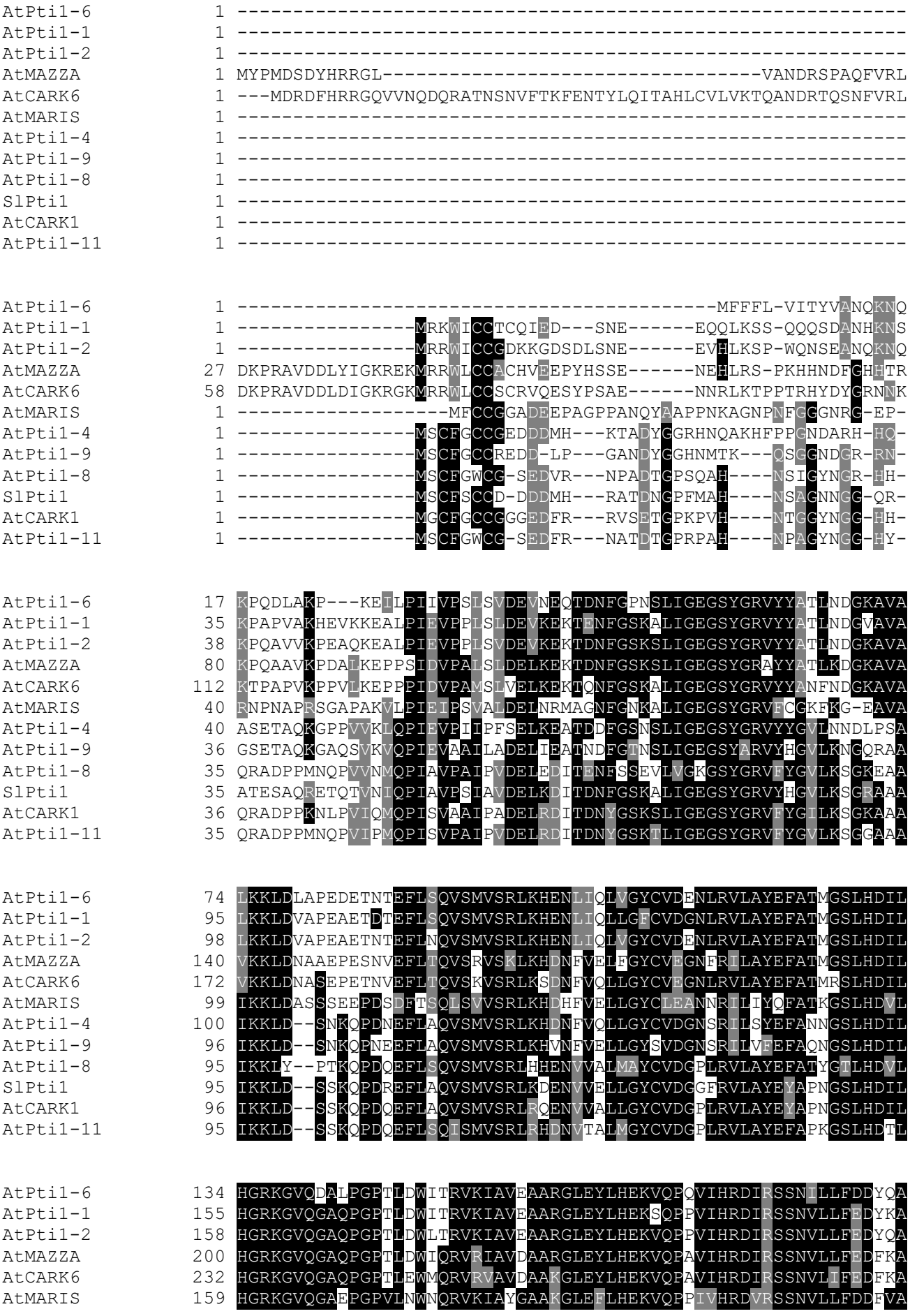

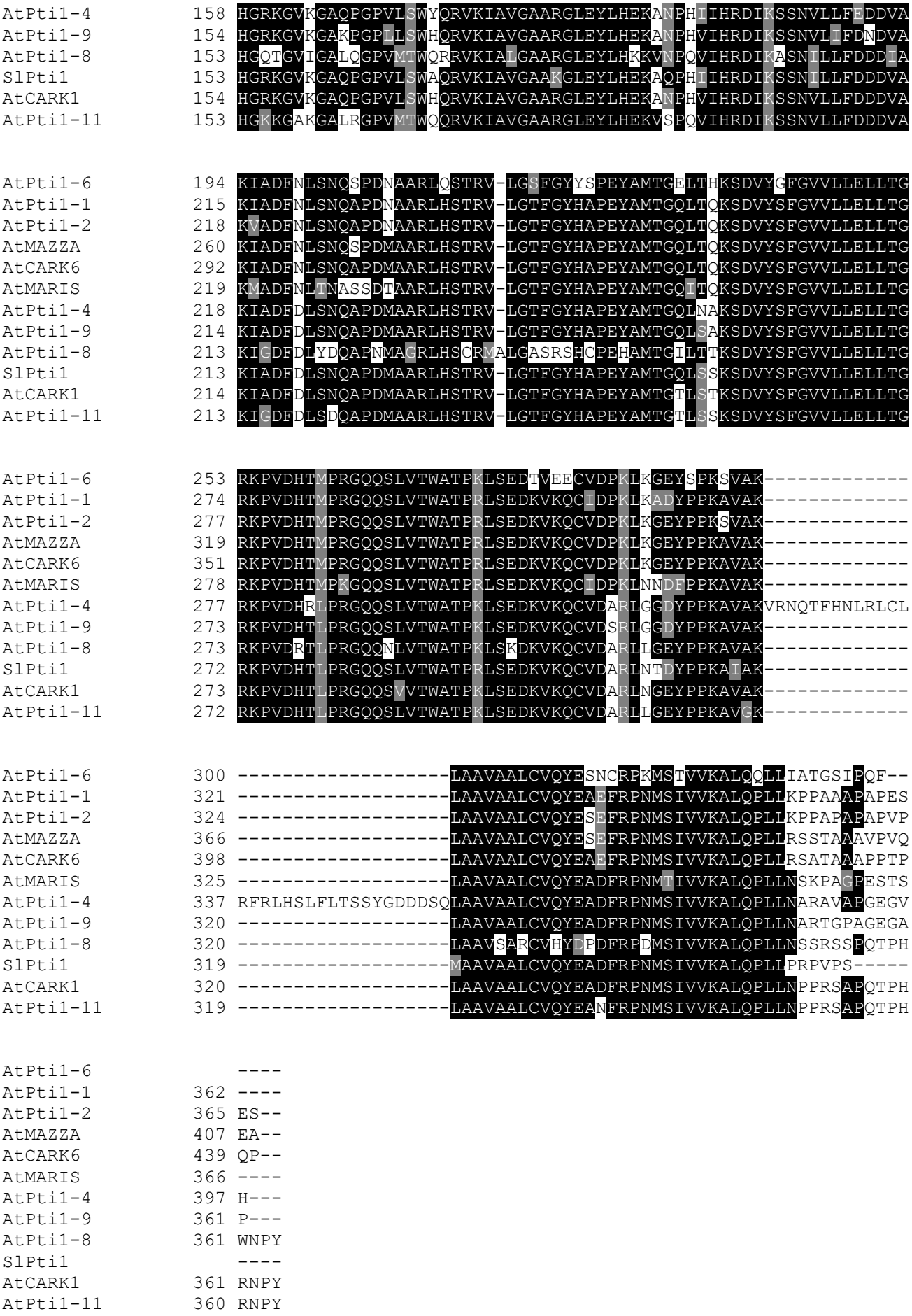
AtPti1-4 158 HGRKGVKGAQPGPVLSWYQRVKIAVGAARGLEYLHEKANPHIIHRDIKSSNVLLFEDDVA
AtPti1-9 154 HGRKGVKGAKPGPLLSWHQRVKIAVGAARGLEYLHEKANPHVIHRDIKSSNVLIFDNDVA
AtPti1-8 153 HGQTGVIGALQGPVMTWQRRVKIALGAARGLEYLHKKVNPQVIHRDIKASNILLFDDDIA
SlPti1 153 HGRKGVKGAQPGPVLSWAQRVKIAVGAAKGLEYLHEKAQPHIIHRDIKSSNILLFDDDVA
AtCARK1 154 HGRKGVKGAQPGPVLSWHQRVKIAVGAARGLEYLHEKANPHVIHRDIKSSNVLLFDDDVA
AtPti1-11 153 HGKKGAKGALRGPVMTWQQRVKIAVGAARGLEYLHEKVSPQVIHRDIKSSNVLLFDDDVA
AtPti1-6 194 KIADFNLSNQSPDNAARLQSTRV-LGSFGYYSPEYAMTGELTHKSDVYGFGVVLLELLTG
AtPti1-1 215 KIADFNLSNQAPDNAARLHSTRV-LGTFGYHAPEYAMTGQLTQKSDVYSFGVVLLELLTG
AtPti1-2 218 KVADFNLSNQAPDNAARLHSTRV-LGTFGYHAPEYAMTGQLTQKSDVYSFGVVLLELLTG
AtMAZZA 260 KIADFNLSNQSPDMAARLHSTRV-LGTFGYHAPEYAMTGQLTQKSDVYSFGVVLLELLTG
AtCARK6 292 KIADFNLSNQAPDMAARLHSTRV-LGTFGYHAPEYAMTGQLTQKSDVYSFGVVLLELLTG
AtMARIS 219 KMADFNLTNASSDTAARLHSTRV-LGTFGYHAPEYAMTGQITQKSDVYSFGVVLLELLTG
AtPti1-4 218 KIADFDLSNQAPDMAARLHSTRV-LGTFGYHAPEYAMTGQLNAKSDVYSFGVVLLELLTG
AtPti1-9 214 KIADFDLSNQAPDMAARLHSTRV-LGTFGYHAPEYAMTGQLSAKSDVYSFGVVLLELLTG
AtPti1-8 213 KIGDFDLYDQAPNMAGRLHSCRMALGASRSHCPEHAMTGILTTKSDVYSFGVVLLELLTG
SlPti1 213 KIADFDLSNQAPDMAARLHSTRV-LGTFGYHAPEYAMTGQLSSKSDVYSFGVVLLELLTG
AtCARK1 214 KIADFDLSNQAPDMAARLHSTRV-LGTFGYHAPEYAMTGTLSTKSDVYSFGVVLLELLTG
AtPti1-11 213 KIGDFDLSDQAPDMAARLHSTRV-LGTFGYHAPEYAMTGTLSSKSDVYSFGVVLLELLTG
AtPti1-6 253 RKPVDHTMPRGQQSLVTWATPKLSEDTVEECVDPKLKGEYSPKSVAK----------
AtPti1-1 274 RKPVDHTMPRGQQSLVTWATPRLSEDKVKQCIDPKLKADYPPKAVAK----------
AtPti1-2 277 RKPVDHTMPRGQQSLVTWATPRLSEDKVKQCVDPKLKGEYPPKSVAK----------
AtMAZZA 319 RKPVDHTMPRGQQSLVTWATPRLSEDKVKQCVDPKLKGEYPPKAVAK----------
AtCARK6 351 RKPVDHTMPRGQQSLVTWATPRLSEDKVKQCVDPKLKGEYPPKAVAK----------
AtMARIS 278 RKPVDHTMPKGQQSLVTWATPRLSEDKVKQCIDPKLNNDFPPKAVAK----------
AtPti1-4 277 RKPVDHRLPRGQQSLVTWATPKLSEDKVKQCVDARLGGDYPPKAVAKVRNQTFHNLRLCL
AtPti1-9 273 RKPVDHTLPRGQQSLVTWATPKLSEDKVKQCVDSRLGGDYPPKAVAK----------
AtPti1-8 273 RKPVDRTLPRGQQNLVTWATPKLSKDKVKQCVDARLLGEYPPKAVAK----------
SlPti1 272 RKPVDHTLPRGQQSLVTWATPRLSEDKVKQCVDARLNTDYPPKAIAK----------
AtCARK1 273 RKPVDHTLPRGQQSVVTWATPKLSEDKVKQCVDARLNGEYPPKAVAK----------
AtPti1-11 272 RKPVDHTLPRGQQSLVTWATPKLSEDKVKQCVDARLLGEYPPKAVGK----------
AtPti1-6 300 ----------LAAVAALCVQYESNCRPKMSTVVKALQQLLIATGSIPQF--
AtPti1-1 321 ----------LAAVAALCVQYEAEFRPNMSIVVKALQPLLKPPAAAPAPES
AtPti1-2 324 ----------LAAVAALCVQYESEFRPNMSIVVKALQPLLKPPAPAPAPVP
AtMAZZA 366 ----------LAAVAALCVQYESEFRPNMSIVVKALQPLLRSSTAAAVPVQ
AtCARK6 398 ----------LAAVAALCVQYEAEFRPNMSIVVKALQPLLRSATAAAPPTP
AtMARIS 325 ----------LAAVAALCVQYEADFRPNMTIVVKALQPLLNSKPAGPESTS
AtPti1-4 337 RFRLHSLFLTSSYGDDDSQLAAVAALCVQYEADFRPNMSIVVKALQPLLNARAVAPGEGV
AtPti1-9 320 ----------LAAVAALCVQYEADFRPNMSIVVKALQPLLNARTGPAGEGA
AtPti1-8 320 ----------LAAVSARCVHYDPDFRPDMSIVVKALQPLLNSSRSSPQTPH
SlPti1 319 ----------MAAVAALCVQYEADFRPNMSIVVKALQPLLPRPVPS-----
AtCARK1 320 ----------LAAVAALCVQYEADFRPNMSIVVKALQPLLNPPRSAPQTPH
AtPti1-11 319 ----------LAAVAALCVQYEANFRPNMSIVVKALQPLLNPPRSAPQTPH
AtPti1-6 ----
AtPti1-1 362 ----
AtPti1-2 365 ES--
AtMAZZA 407 EA--
AtCARK6 439 QP--
AtMARIS 366 ----
AtPti1-4 397 H---
AtPti1-9 361 P---
AtPti1-8 361 WNPY
SlPti1 ----
AtCARK1 361 RNPY
AtPti1-11 360 RNPY

Chapter III

CORYNE-dependent CLE peptide signaling controls root meristem homeostasis non-cell-autonomously

This chapter is a manuscript in preparation for submission.

Authors:

Patrick Blümke and Rüdiger Simon

Affiliations:

Institute for Developmental Genetics, Heinrich Heine University,
Universitätsstraße 1, 40225 Düsseldorf, Germany

Author contributions:

R.S. and P.B. conceived and planed the project. P.B. conducted experiments and data analyses. P.B. and R.S. wrote the manuscript.

CORYNE-dependent CLE peptide signaling controls root meristem homeostasis non-cell-autonomously

Patrick Blümke and Rüdiger Simon

Institute for Developmental Genetics, Heinrich Heine University, Universitätsstraße 1, 40225 Düsseldorf, Germany

Abstract

Root development is governed by small stem cell populations, which give rise to an organized system of cell files with distinct functions. Within the meristematic zone at the root tip stem cell descendants divide frequently and eventually differentiate. The transition from proliferation to differentiation is influenced by small secreted peptides of the CLAVATA3 (CLV3)/ EMBRYO SURROUNDING REGION (ESR)-related (CLE) family. Increased CLE concentrations cause premature root meristem (RM) differentiation, which leads to drastic reduction of root length. CLE peptides are perceived by leucine-rich repeat (LRR) receptor-like kinases (RLKs), e.g. by CLAVATA1 (CLV1) and the related BARELY ANY MERISTEM1 – 3 (BAM1 – 3) receptors. CLE perception in the root additionally relies on a heteromeric complex of CLAVATA2 (CLV2) and CORYNE (CRN). Previously, CRN was reported to act in the developing phloem to mediate systemic CLE responses by controlling BAM3 availability at the PM. However, the expression domain of *CRN* in the RM includes not only the phloem but is extended to various cell files of the RM. Here, we found that *CRN* expression in tissues beyond the context of phloem development is also sufficient for CLE-triggered RM differentiation. Furthermore, our data suggest that CRN-dependent CLE signaling pathways can non-cell-autonomously control RM differentiation in the transition zone. Our results hint to a complex situation of CLE signaling in the RM, where CRN together with CLV2 could act as a global regulator of CLE peptide perception.

Introduction

Postembryonic development in plants depends on meristems, which provide undifferentiated stem cells for the generation of new tissues and organs. Meristem homeostasis, i.e. the balance between proliferation to enlarge the pool of stem cells and differentiation to exit from the stem cell domain, is crucial to guarantee coordinated growth. Therefore, mechanisms evolved to dynamically define stem cell domains. In the dome-shaped shoot apical meristem (SAM) of *Arabidopsis thaliana*, which gives rise to most aerial parts of the plant, stem cell fate is regulated via a negative feedback loop between stem cells of the central zone (CZ) and quiescent cells in a region underneath, called the organizing center (OC) (Stahl and Simon, 2005). WUSCHEL (WUS), a mobile, stem cell promoting homeodomain transcription factor, moves through plasmodesmata (PD) from the OC to the CZ to establish the stem cell niche (Laux et al., 1996; Mayer et al., 1998; Yadav et al., 2011; Daum et al., 2014). Stem cells express *CLAVATA 3* (*CLV3*), a member of the *CLE* gene family (Fletcher et al., 1999; Cock and McCormick, 2001). The CLV3 precursor protein is cleaved, post-translationally modified, and secreted to the apoplast (Rojo et al., 2002; Ohyama et al., 2009; Shinohara and Matsubayashi, 2013). CLV3 peptide (CLV3p) diffuses towards the OC and binds to the extracellular LRR domain of the cell surface located RLK CLV1 to stimulate an intracellular signaling cascade that causes the repression of *WUS* expression. Hence, the stem cell derived CLV3p transmits a stem cell fate repressive signal, establishing a feedback regulated non-cell autonomous communication system (Fletcher et al., 1999; Schoof et al., 2000; Brand et al., 2000).

At receptor level, several proteins besides CLV1 participate in stem cell maintenance in the shoot, like the close CLV1 homologs BAM1 – 3, the LRR-RLK RECEPTOR-LIKE PROTEIN KINASE2 (RPK2), and the receptor-like protein (RLP) CLV2 together with CRN (Somssich et al., 2016b). Genetical and physical interactions of those proteins contribute to the formation of intertwined CLE perception complexes at the plasma membrane (PM) (Nimchuk et al., 2015; Somssich et al., 2015). Yet, the spatio-temporal dynamics underlying are not fully understood, partially owing to the morphological complexity of the SAM.

The meristematic zone at the root tip orchestrates subterrestrial development. Its stem cell niche comprises few organizing cells of the quiescent center (QC) surrounded by stem cells, also called initials. While the stem cells distal to the QC contribute to the reservoir of columella cells, lateral and proximal initials give rise to distinct files of epidermis, cortex, endodermis, pericycle, and the vascular tissues phloem, xylem, and procambium in the stele. Along the root axis initial daughter cells proliferate within the meristematic zone, substantially increase their cell length in the elongation zone, and finally enter the differentiation zone (Petricka et al.,

2012). The RM structurally differs from the SAM, yet many signaling elements that regulate the stem cell domains are conserved or functionally related (Sarkar et al., 2007). For instance, QC cells express *WUSCHEL RELATED HOMEOBOX5* (*WOX5*) encoding a close WUS homolog that moves through PD towards neighboring cells and promotes columella stem cell (CSC) fate. Furthermore, WOX5 counteracts differentiation in the proximal stem cell domain, but depends there on other transcription factors like the SCARECROW (SCR) / SHORTROOT (SHR) module or the PLETHORA proteins (Sarkar et al., 2007). However, a recent study revealed that mobility of WOX5 is not mandatory for CSC maintenance, thus, WOX5 could mediate stem cell fate only indirectly (Berckmans et al., 2020).

CLV3 expression is restricted to shoot meristems, but several other CLE peptides are involved in stem cell regulation in the root. Among 26 CLE peptides in Arabidopsis, which are encoded by 32 *CLE* genes, at least 19 trigger severe root length reduction when supplied to the growth media (Ito et al., 2006; Kondo et al., 2011; Goad et al., 2017). However, this list of root-active CLE peptides reflects high functional redundancy within the CLE family rather than specific action of all single *CLE* genes in RM control, because it includes non-root expressed *CLEs* like *CLV3*, *CLE8*, or *CLE21* (Hobe et al., 2003; Jun et al., 2010). Overexpression of *CLE* genes or exogenous CLE peptide application promote premature differentiation of proximal stem cell daughters in the RM due to reduced cell division rates, which gradually leads to the consumption of the meristematic zone. Yet, the identity of the QC and initials are not primarily affected by these processes (Casamitjana-Martínez et al., 2003; Fiers et al., 2004, 2005; Meng and Feldman, 2010). CLE peptide signaling in the context of RM differentiation depends on CRN and CLV2, since *crn* and *clv2* mutants are resistant to CLE-induced root shortening (Fiers et al., 2005; Müller et al., 2008; Miwa et al., 2008). How CRN and CLV2 contribute to CLE perception is not clear. The two proteins form heteromers, which is obligatory for their proper PM-localization, and together they resemble the structure of an LRR-RLK. However, it is unlikely that CRN/CLV2 alone can perceive and transmit CLE signals, since CLV2 failed to bind CLE peptides *in vitro* and CRN lacks kinase activity under standard conditions (Bleckmann et al., 2010; Nimchuk et al., 2011; Shinohara and Matsubayashi, 2015).

Among the few *CLE* genes with known functions in RM development, the peptide product of *CLE40* has the highest sequence similarity to CLV3p. *CLE40* is expressed in columella cells and in the stele starting from the late meristematic zone (Hobe et al., 2003; Stahl et al., 2009). Thus, unlike *CLV3*, *CLE40* is expressed in differentiated cells and not stem cells. When expressed from the *CLV3* promotor, *CLE40* can rescue the shoot defects of *clv3* mutants, indicating that both peptides can likely interact with the same repertoire of receptors (Hobe et

al., 2003). In the distal RM CLE40 promotes differentiation of CSCs via CLV1 and the non-LRR-RLK ARABIDOPSIS CRINKLY4 (ACR4), as excess of CLE40p causes loss of the CSC layer, while disturbed CLE40 signaling results in additional layers of CSCs (Stahl et al., 2009, 2013). Notably, *cle40* mutants are characterized by reduced root length, thus, display a similar phenotype as CLE40p-treated plants (Hobe et al., 2003). This observation indicates that a CLE40-specific signaling pathway represses differentiation, in parallel to a CLE dependent pathway, activated by a range of different CLE peptides, that promotes differentiation (Pallakies and Simon, 2014).

Apart from *CLE40*, *CLE* genes that are assigned to specific functions in the RM include *CLE9/10* and *CLE45*, which both control vascular differentiation. The two genes *CLE9* and *CLE10* encode the identical mature CLE peptide and negatively regulate periclinal cell divisions in xylem precursor cell files (Kondo et al., 2011; Qian et al., 2018). CLE9/10p bind the extracellular receptor domain of BAM1 and this perception is critical for proper xylem development, since CLE9/10p treatment does not cause severe reduction of the xylem file number in *bam1* mutants but in wild type samples. However, *bam1* mutants are not resistant to exogenous application of CLE9/10p regarding premature differentiation of the proximal RM (Shinohara et al., 2012; Shimizu et al., 2015; Qian et al., 2018).

CLE45 has a key role in early phloem development. *CLE45* is expressed in the sieve element (SE) precursor cells and their descendants in the protophloem SE (PPSE) file, where CLE45p mediates signaling that inhibits PPSE differentiation (Depuydt et al., 2013; Rodriguez-Villalon et al., 2014). Genetic and biochemical data place BAM3 as the main CLE45p receptor (Hazak et al., 2017). Proper localization of BAM3 at the PM of developing PPSEs depends on the presence of CRN/CLV2, which interact with BAM3. The PM-associated protein OCTOPUS (OPS) displays subcellular polarity within the PPSE files and disturbs interaction between BAM3 and CRN, thereby counteracting CLE45-BAM3 signaling and adding an additional level of phloem-specific CLE45 signaling (Depuydt et al., 2013; Rodriguez-Villalon et al., 2014; Breda et al., 2017, 2019). A recent study found that also RPK2 specifically contributes to the precise cell fate decisions within phloem differentiation by perceiving CLE45p in the PPSE-surrounding cell files to repress PPSE identity there (Gujas et al., 2020).

Impaired phloem differentiation systemically affects RM development by restricting access of nutrients as well as signaling molecules. Thus, premature RM differentiation of CLE peptide treated plants could be an indirect consequence of CLE responses in developing PPSEs via BAM3 and CRN/CLV2. In line, re-introducing *CRN* solely in the developing PPSEs, is sufficient to fully restore the sensitivity of *crn* mutants for CLE-induced premature RM

differentiation (Hazak et al., 2017). This suggests that, within RM homeostasis, CRN mainly functions to regulate CLE45 signaling by controlling the amount of available BAM3 at the PM of developing PPSEs. However, *crn* mutants are resistant to a range of CLE peptides concerning premature RM differentiation, which are not known to bind to the receptor domain of BAM3, while *bam3* mutants are specifically resistant to CLE45p (Depuydt et al., 2013). Furthermore, native expression of both, *CRN* and *CLV2*, within the RM is not restricted to the *BAM3* expression domain (Somssich et al., 2016a).

To extend the understanding of CLE peptide signaling in the context of RM differentiation, we analyzed the impact of CRN/CLV2 on CLE perception in other tissues than developing PPSEs. Our data reveal that CRN functions in different cell types of the RM, and even CRN activity in few cells of the QC is apparently sufficient to induce the typical CLE signaling outcomes.

Results

CLE signaling impacts root development by dynamically controlling differentiation of RM cells. Root shortening of Arabidopsis wild type plants caused by premature RM differentiation at elevated CLE peptide concentrations in the growth media is macroscopically observable (Fig. 1 A). Thus, it can serve as an easily to monitor indicator for functional CLE signaling. The null allele *crn-10* confers resistance to the application of exogenous CLE peptides regarding root shortening (Fig. 1 B), and *CRN* expression in the *BAM3* domain is sufficient to rescue *crn-10* mutants (Hazak et al., 2017). However, native *CRN* expression in the RM is not limited to the *BAM3* domain, i.e. developing PPSEs, but comprises in the entire RM including the QC and the stem cell niche (Fig. 2, (Müller et al., 2008; Somssich et al., 2016a)).

To decipher CRN function within different subdomains of its endogenous expression domain we constructed several promotor lines mediating the tissue specific expression of a *CRN-mVenus* fusion in the *crn-10* background. The obtained stable Arabidopsis lines were subjected to peptide assays to elucidate their capability for CLE signaling. Peptide effects on plant development were accessed over time by monitoring root length from 5 days after germination (DAG) until 14 DAG. In general, growth defects of CLE-sensitive plants accumulated during this period, i.e. consequences of constitutive high CLE signaling became most obvious the longer the seedlings were cultivated. In contrast, resistance of *crn-10* mutants was not dampened even after 2 weeks of CLE treatment (Fig. 1 B). To evaluate potential differential perception of distinct CLEs peptides, our assays included CLV3p, CLE40p, and CLE45p, which all cause root shortening of Col-0 seedlings when externally applied (Fig. 1 A) and, thus, can be considered as root-active.

CRN expression in the *BAM3* domain restores CLE sensitivity

First, we aimed to confirm the developing PPSEs as one of the mayor sites of CRN function in CLE sensing. Therefore, independent transgenics expressing *CRN-mVenus* under the control of the *BAM3* promotor in *crn-10* mutants were generated. In line with Hazak *et al.* 2017, our reporter fully rescued *crn-10* in terms of premature RM differentiation after CLE peptide treatment. The reduction of root length of *BAM3:CRN-mVenus//crn-10* lines was as strong as in Col-0 plants and comparable to lines with the endogenous *CRN* promotor (*CRN:CRN-mVenus//crn-10*, Fig. 2 A – B'', Suppl. Fig. 1 A, B). Furthermore, *crn-10* mutants expressing the *CRN-mVenus* fusion under the control of the *BAM3* promotor are sensitive against all three tested CLE peptides, which is in line with the previous report of Hazak *et al.* 2017. The subcellular localization of CRN-mVenus within the *BAM3* expression domain is not restricted

to the PM, but fluorescence signals are detectable in the entire cell besides of the nucleus (Fig 3 B). Since the *BAM3* promotor mediates higher expression than the native *CRN* promotor, the ratio of CRN and CLV2, which is mandatory for CRN transport to the PM, might be unbalanced. Notably, the PM distribution of CRN-mVenus within the developing SEs shows polarity with higher signal intensity at the apical and basal ends of each cell, potentially reflecting CRN interaction with the phloem file-specific, polar-localized protein OPS (Breda et al., 2019).

CRN expression in the *SCR* expression domain restores CLE sensitivity

Crn-10 mutants harboring the expression cassette *SCR:CRN-mVenus* are also sensitive against CLE peptide treatment (Fig 2 C – C'', Suppl. Fig 1 C). CRN presence in the *SCR* domain, i.e. the endodermis and QC, is sufficient to re-establish active CLE peptide perception in the RM. This observation reveals that CRN can mediate CLE-induced premature RM differentiation independent of BAM3, which is not present in the *SCR* domain. Root shortening of *SCR:CRN-mVenus* lines is at a comparable level after treatment with CLV3p, CLE40p, and CLE45p, respectively. Thus, CLE45p can be perceived by other receptors than BAM3. One candidate for alternative CLE45p perception is RPK2 that was already reported to participate in phloem-specific CLE45 signaling and that is also expressed within the *SCR* domain (Racolta et al., 2018; Gujas et al., 2020).

Root shortening of *SCR:CRN-mVenus//crn-10* lines is substantially, but appears to be slightly delayed in comparison to Col-0 with less pronounced root length reduction between 5 and 7 DAG. This could suggest different timing of CRN signaling in endodermis and the QC in comparison to developing SEs, with faster CLE responses in the phloem tissue. Alternatively, the effect might be due to the experimental setup. Since peptides are supplied externally, the CLEs may be transported within the vascular bundles and therefore, concentrations could rise faster in those tissues. The subcellular localization of CRN in the *SCR* domain is only partially at the PM, while fluorescence signals derived from intracellular structures, like vesicles or the ER, are predominantly present (Fig. 3 C). This can be explained with insufficient amounts of CLV2 partner proteins for efficient CRN transport to the PM. However, the amount of CRN at the PM in the *SCR:CRN-mVenus* lines allows functional CLE perception.

CRN expression in the *WOX5* domain restores CLE sensitivity

To further narrow down the place of action of CRN we constructed transgenic lines expressing *CRN-mVenus* under the control of the *WOX5* promotor that mediates expression predominantly in the QC, but also in the initials of the proximal RM (Fig. 2 D, 3 D). Although covering only

a comparably small part of the native *CRN* expression domain, *WOX5:CRN-mVenus* lines can restore CLE peptide sensitivity. However, the effect is only observable from 10 DAG and the three tested CLE peptides cause different signaling outputs (Fig. 2 D' – D''). While CLE40p treatment triggers root length reduction already at concentrations of 10 nM, CLV3p affects root length at concentrations of 100 nM or higher. Notably, application of CLE45p does not induce root shortening of the tested *WOX5:CRN-mVenus* lines at all, suggesting that the *WOX5* expression domain lacks a signaling component, which is mandatory for CLE45p perception, but not for sensing of other CLE peptides like CLV3p or CLE40p. Furthermore, we noticed that a second independent *WOX5:CRN-mVenus* line was less sensitive to CLE peptide treatment in general, indicating that CRN-dependent CLE responses in the *WOX5* domain could rely on precise CRN expression levels (Suppl. Fig. 1 D).

The observation that CRN-dependent CLE signaling in the QC and first proximal initials can affect processes in other tissues, i.e. RM differentiation in the transition zone, suggest a non-cell-autonomous regulation, potentially by controlling the distribution or production of a phytohormone.

Discussion

CLE signaling pathways affect overall root development. Yet, it is an open question whether the massive reduction of proximal meristem size and root length after non-specifically increasing CLE concentrations is due to local, tissue-specific developmental changes, or caused by a general mechanism that alters the ratio of division and differentiation in all cell files of the meristematic zone.

CRN-dependent CLE signaling limited to developing PPSEs is sufficient to restore CLE sensitivity of *crn-10* mutants regarding premature RM differentiation (Hazak et al., 2017). This observation could reflect that responses of exogenous CLE treatment are primarily integrated in the *BAM3* domain, causing disruptions in phloem development, which then determine overall RM differentiation. Indeed, by suppling photoassimilates and transporting signaling molecules like the phytohormone cytokinin or small RNAs to the RM, the phloem has an important impact on root architecture (Lucas et al., 2001; Bishopp et al., 2011). Furthermore, cells of the phloem strand differentiate earlier than all surrounding cells (Blob et al., 2018). The CLE45-BAM3 module, which depends on the presence of CRN/CLV2, might even function cell-autonomously, which is a rather untypical mode of action for CLE peptides (Breda et al., 2019).

However, our data now provide evidence that CLE signaling pathways that trigger premature RM differentiation and root shortening, not necessarily depend on phloem-specific CLE perception. Instead, *CRN* expression, for example, in the *SCR* domain is also sufficient to re-establish CRN-dependent CLE responses in *crn-10* mutants. Still, the *SCR* expression domain includes all developmental stages along the root axis, i.e. organizer (QC), stem cells (cortex/endodermis initials), endodermis precursor cells in the meristematic zone, cells in the transition to differentiation, and differentiated endodermis cells. To further dissect these areas, we used the *WOX5* promotor for the *crn-10* rescue experiments. Interestingly, *CRN* expression in the small *WOX5* domain restores CLE responses in the *crn-10* mutant background, at least partially. Since the *WOX5* promotor additionally drives expression at low levels in the proximal initials, we cannot exclude that the observed partial rescue is mediated there rather than in the QC. Furthermore, CLE40p treatment leads to an expansion of the *WOX5* expression domain towards the vasculature initials. Because this upregulation was strongly reduced in a *clv2* mutant background, it is assumable that the control of *WOX5* expression is dependent on CLV2, and most likely on CRN (Stahl et al., 2009; Berckmans et al., 2020). Expressing *CRN* under the *WOX5* promotor could therefore establish a positive feedforward regulation. Continuous CLE treatment may increase the area of *CRN* expressing cells, making those susceptible for CLE-

mediated *WOX5* upregulation. These processes could explain the delayed response of *WOX5:CRN-mVenus//crn-10* seedlings to CLE treatment, which show significant root length reduction only 10 DAG (Fig 2 D''). However, even if the *WOX5* expression domain is extended at elevated CLE concentrations, it is spatially separated from the transition zone. Thus, the CRN-dependent CLE perception in the *WOX5* expression domain non-cell-autonomously triggers premature RM differentiation in the transition zone.

Gradual RM consumption after enhanced CLE signaling is a consequence of premature transition from division to differentiation. The transition zone is positioned by an auxin minimum that correlates with a cytokinin maximum (dello Ioio et al., 2007; di Mambro et al., 2017). Thus, it is likely that phytohormone signaling and CLE pathways are interconnected to determine the developmental status within the RM. In the SAM cytokinin promotes *WUS* expression and WUS represses negative regulators of cytokinin responsive gene expression (Leibfried et al., 2005; Gordon et al., 2009). In contrast, in the root cytokinin represses *WOX5* expression (Pernisova et al., 2018). Another indication for a role of cytokinin within CLE signaling in the root is that double mutants of class-B *ARABIDOPSIS RESPONSE REGULATOR 10* (*ARR10*) and *ARR12*, encoding cytokinin inducible transcription factors, are resistant to CLE-mediated repression of protoxylem differentiation (Kondo et al., 2011). However, *arr10 arr12* plants are not resistant to CLE-induced root shortening, suggesting that the premature differentiation of the proximal RM and cell division in the protoxylem are differentially regulated.
Thus, it remains unresolved, how a putative integration of CLE signaling into auxin/cytokinin interactions is realized. CLE responses may interfere with key mediators of the auxin/cytokinin antagonism, like SHORT HYPOCOTYL 2 (SHY2) (dello Ioio et al., 2008). Furthermore, CLE signaling could impact polar auxin transport (PAT), e.g. by regulating expression of *PIN-FORMED* (*PIN*) genes, that encode polar auxin efflux carriers (Blilou et al., 2005).

Crosstalk with phytohormone pathways in general could explain how independent loci of CRN mediated CLE perception, like PPSEs and the endodermis, can systemically influence RM maintenance. Still, a major open question is, if different *CRN* expression domains share the same mode of CLE perception, e.g. CLV2/CRN via broadly expressed receptors like BAM1 or RPK2. Alternatively, cell file specific CLE perception could activate distinct signaling cascades that individually rely on CRN/CLV2 presence, and which cause the same output, i.e. root shortening, when overcharged. Additionally, cell-file specific CLE pathways, e.g. via CLE45 or CLE9/10, which not necessarily need to be involved in the signaling cascades that cause

premature differentiation of the proximal RM, contribute to the complexity of CLE signaling in the RM.

Therefore, deciphering the molecular mode of action of the CLV2/CRN module will be of high interest. Since the heteromer is probably not capable to perceive and transmit CLE signals intrinsically, its function is likely characterized by regulating other receptors. For instance, CRN/CLV2 could stabilize receptor complexes at the PM (Somssich et al., 2015). Possibly, CRN may function in mediating the transport of RLKs to the PM, which is indicated by the observation that the subcellular localization of BAM3 at the PM is less pronounced in *crn-10* mutant background than in the wild type (Hazak et al., 2017). Future work needs to clarify these mechanisms, as well as the involved receptors.

Our study underlines that the CRN/CLV2 module has a major, but multifaceted role in CLE signaling and RM development.

Material and Methods

Information on chemicals used in the described experiments are accessible in Suppl. Tab. 1.

Plant material and growth conditions

The *Arabidopsis thaliana* (L.) Heynh. ecotype Columbia-0 (Col-0) is the genetic background of all deployed plants in this study. The *crn-10* mutant was described earlier (Nimchuk, 2017). To verify the presence of the allele a dCAPS strategy was applied with the oligomers 5'-GTAG AAGCAGCAATGAAGCAAAGAAGAAGGTG-3' and 5'-GTGTAGATGATGTTGAAGTT GTGGATAAGTG-3' and subsequent HphI digestion. Arabidopsis seeds were sterilized in a chloric gas atmosphere (1 h in a desiccator after mixing 50 ml of 13 % w/v sodium hypochlorite with 1 ml 37 % HCl) and sowed on ½ MS agar plates (1 % w/v sucrose, 0.22 % w/v MS salts + B5 vitamins, 0.05 % w/v MES, 12 g/l plant agar, adjusted to pH 5.7 with KOH) in phytocabinets (continuous light, 60 % humidity, and 21 °C). For cultivation on soil seeds were sterilized in ethanol solution (10 min in 80 % v/v ethanol, 1.3 % w/v sodium hypochlorite, 0.02 % w/v SDS) and kept in phytochambers under long day (LD) conditions (16 h light / 8 h dark) at 21 °C.

Cloning

The expression cassettes combining different promotors with the *CRN-mVenus* sequence were assembled following the GreenGate strategy (Lampropoulos et al., 2013). The *CRN* coding sequence, the *CRN* promotor (1.7 kb), the *BAM*3 promotor (2 kb), the *SCR* promotor (2.5 kb), and the *WOX5* (4.6 kb) promotor were PCR-amplified (with Phusion High-Fidelity PCR polymerase) from genomic DNA prepared of Col-0 rosette leaves with oligos listed in Suppl. Tab. 2 and introduced to entry vectors. To eliminate internal BsaI recognition sites, site-directed mutagenesis with the QuikChange II kit according to manufacturer's protocol (Agilent Technologies) was applied. Final binary expression plasmids were combined of the desired promotor entry plasmid, pGGB002, CRN/pGGC, mVenus/pGGD, pGGE009, pGGF008, and pGGZ001 (Lampropoulos et al., 2013).

To amplify plasmid DNA, competent *Escherichia coli* DH5α cells were heat-shock transformed and cultivated on selective LB medium (1 % w/v tryptone, 0.5 % w/v yeast extract, 0.5 % w/v NaCl). After plasmid DNA purification via commercial kits, the plasmids were validated by restriction digest and Sanger sequencing.

Stable transformation of *A. thaliana*

All transgenic *A. thaliana* lines in this study are in the *crn-10* mutant background. Parental *crn-10* plants were transformed 4 – 6 weeks after germination via the floral dip method using *A. tumefaciens* GV3101 pMP90 pSoup previously transformed with desired binary vectors (Clough and Bent, 1998). Subsequently, plants were kept under high humidity overnight at room temperature and cultivated in long day phytochamber conditions until harvest. The t1 generation was screened for positive transformants by spraying 120 mg/ml BASTA® solution, containing DL-phosphinothricin (PPT). T2 plants were selected by sowing seeds of resistant t1 plants on ½ MS agar plates supplied with 10 µg/ml PPT. Positive plants were further amplified for identification of homozygous lines. The transgenic lines generated in this study are listed in Suppl. Tab. 3.

Confocal microscopy and tissue staining

In vivo fluorescence microscopy was performed at the Zeiss LSM 780 equipped with a C-Apochromat 40x/1.20 water objective. To image mVenus fluorescence samples were excited with an argon laser at 514 nm and emission was detected at 520 – 550 nm by with a GaAsP detector. Cell walls of the analyzed root samples with PI at a final concentration of 25 µM was visualized by excited the samples with a Diode-pumped solid state (DPSS) laser at 561 nm and detecting emission via a photomultiplier tube (PMT) at 590 – 650 nm. Images were acquired with ZEN (Zeiss, Black Version) and processed with ImageJ v 1.51 (Schneider et al., 2012).

Root length assays

The effects of CLE peptide treatment on root growth were analyzed by cultivating seedlings on ½ MS agar plates (squared) supplied with CLV3p, CLE40p, or CLE45p at indicated concentrations. The respective transgenic lines were co-cultivated with wild type (Col-0), and *crn-10* mutants on the same plate. The plates were kept upright in continuous light, 21°C, and 60 % humidity (phytocabinet). Root growth was accessed 5, 7, 10, and 14 DAG by scanning the plates and using ImageJ to measure the root lengths. For each condition 11 – 42 single roots were measured. The plotted data are normalized to the mean of the analyzed genotype under mock conditions at the respective timepoint. Graphs and statistical analyses were done with Prism v.8.

Acknowledgements

P.B. was supported by the IMPRS *Understanding complex plant traits using computational and evolutionary approaches*, work in R.S. lab is supported by the DFG through CRC1208 and CEPLAS (EXC 2048). We thank Cornelia Gieseler, Silke Winters, and Carin Theres for technical support, Rebecca Burkart for sharing plasmids, and the Center for Advanced imaging (CAi) at HHU for microscopy support.

Main figures

Figure 1 CLE peptides impact root development via CRN-dependent signaling.

Figure 2 Tissue specific expression of *CRN-mVenus* restores CLE peptide sensitivity of *crn-10* mutants.

Figure 3 Subcellular localization of CRN-mVenus fusions in *crn-10* mutants after expression under different promotors.

Supplemental materials

Supplemental Figure 1 Tissue specific expression of *CRN-mVenus* restores CLE peptide sensitivity of *crn-10* mutants

Supplemental Figure 2 Shoot phenotype of *crn-10* mutants harboring different tissue specific *CRN-mVenus* expression constructs.

Supplemental Table 1 Chemicals utilized for the described experiments.

Supplemental Table 2 Oligonucleotides for amplification of insert sequences for entry plasmid construction.

Supplemental Table 3 Stable transgenic *A. thaliana* lines generated in this study.

References

Berckmans, B., Kirschner, G., Gerlitz, N., Stadler, R., and Simon, R. (2020). CLE40 Signaling Regulates Root Stem Cell Fate. Plant physiology **182**: 1776–1792.

Bishopp, A., Lehesranta, S., Vatén, A., Help, H., El-Showk, S., Scheres, B., Helariutta, K., Mähönen, A.P., Sakakibara, H., and Helariutta, Y. (2011). Phloem-transported cytokinin regulates polar auxin transport and maintains vascular pattern in the root meristem. Current Biology **21**: 927–932.

Bleckmann, A., Weidtkamp-Peters, S., Seidel, C.A.M., and Simon, R. (2010). Stem cell signaling in Arabidopsis requires CRN to localize CLV2 to the plasma membrane. Plant Physiology **152**: 166–176.

Blilou, I., Xu, J., Wildwater, M., Willemsen, V., Paponov, I., Frimi, J., Heldstra, R., Aida, M., Palme, K., and Scheres, B. (2005). The PIN auxin efflux facilitator network controls growth and patterning in Arabidopsis roots. Nature **433**: 39–44.

Blob, B., Heo, J. ok, and Helariutta, Y. (2018). Phloem differentiation: an integrative model for cell specification. Journal of Plant Research **131**: 31–36.

Brand, U., Fletcher, J.C., Hobe, M., Meyerowitz, E.M., and Simon, R. (2000). Dependence of stem cell fate in Arabidopsis on a feedback loop regulated by CLV3 activity. Science **289**: 617–9.

Breda, A.S., Hazak, O., and Hardtke, C.S. (2017). Phosphosite charge rather than shootward localization determines OCTOPUS activity in root protophloem. PNAS **114**: E5721–E5730.

Breda, A.S., Hazak, O., Schultz, P., Anne, P., Graeff, M., Simon, R., and Hardtke, C.S. (2019). A Cellular Insulator against CLE45 Peptide Signaling. Current Biology **29**: 2051–2508.

Casamitjana-Martínez, E., Hofhuis, H.F., Xu, J., Liu, C.-M., Heidstra, R., and Scheres, B. (2003). Root-Specific CLE19 Overexpression and the sol1/2 Suppressors Implicate a CLV-like Pathway in the Control of Arabidopsis Root Meristem Maintenance. Current Biology **13**(16): 1453–1451.

Clough, S.J. and Bent, A.F. (1998). Floral dip: a simplified method for Agrobacterium-mediated transformation of Arabidopsis thaliana. The Plant Journal **16**: 735–743.

Cock, J.M. and McCormick, S. (2001). A large family of genes that share homology with Clavata3. Plant Physiology **126**: 939–942.

Daum, G., Medzihradszky, A., Suzaki, T., and Lohmann, J.U. (2014). A mechanistic framework for noncell autonomous stem cell induction in Arabidopsis. PNAS **111**: 14619–14624.

Depuydt, S., Rodriguez-Villalon, A., Santuari, L., Wyser-Rmili, C., Ragni, L., and Hardtke, C.S. (2013). Suppression of Arabidopsis protophloem differentiation and root meristem growth by CLE45 requires the receptor-like kinase BAM3. PNAS **110**: 7074–9.

Fiers, M., Golemiec, E., Xu, J., van der Geest, L., Heidstra, R., Stiekema, W., and Liu, C.M. (2005). The 14-amino acid CLV3, CLE19, and CLE40 peptides trigger consumption of the root meristem in Arabidopsis through a CLAVATA2-dependent pathway. Plant Cell **17**: 2542–2553.

Fiers, M., Hause, G., Boutilier, K., Casamitjana-Martinez, E., Weijers, D., Offringa, R., van der Geest, L., van Lookeren Campagne, M., and Liu, C.M. (2004). Mis-expression of the CLV3/ESR-like gene CLE19 in Arabidopsis leads to a consumption of root meristem. Gene **327**: 37–49.

Fletcher, J.C., Brand, U., Running, M.P., Simon, R., and Meyerowitz, E.M. (1999). Signaling of cell fate decisions by CLAVATA3 in Arabidopsis shoot meristems. Science **283**: 1911–4.

Goad, D.M., Zhu, C., and Kellogg, E.A. (2017). Comprehensive identification and clustering of CLV3/ESR-related (CLE) genes in plants finds groups with potentially shared function. New Phytologist **216**: 605–616.

Gordon, S.P., Chickarmane, V.S., Ohno, C., and Meyerowitz, E.M. (2009). Multiple feedback loops through cytokinin signaling control stem cell number within the Arabidopsis shoot meristem. PNAS **106**: 16529–16534.

Gujas, B., Kastanaki, E., Sturchler, A., Cruz, T.M.D., Ruiz-Sola, M.A., Dreos, R., Eicke, S., Truernit, E., and Rodriguez-Villalon, A. (2020). A Reservoir of Pluripotent Phloem Cells Safeguards the Linear Developmental Trajectory of Protophloem Sieve Elements. Current Biology **30**: 755-766.

Hazak, O., Brandt, B., Cattaneo, P., Santiago, J., Rodriguez-Villalon, A., Hothorn, M., and Hardtke, C.S. (2017). Perception of root-active CLE peptides requires CORYNE function in the phloem vasculature. EMBO reports **18**: 1367–1381.

Hobe, M., Müller, R., Grünewald, M., Brand, U., and Simon, R. (2003). Loss of CLE40, a protein functionally equivalent to the stem cell restricting signal CLV3, enhances root waving in Arabidopsis. Development genes and evolution **213**: 371–81.

dello Ioio, R., Linhares, F.S., Scacchi, E., Casamitjana-Martinez, E., Heidstra, R., Costantino, P., and Sabatini, S. (2007). Cytokinins Determine Arabidopsis Root-Meristem Size by Controlling Cell Differentiation. Current Biology **17**(8): 678–682.

dello Ioio, R., Nakamura, K., Moubayidin, L., Perilli, S., Taniguchi, M., Morita, M.T., Aoyama, T., Costantino, P., and Sabatini, S. (2008). A genetic framework for the control of cell division and differentiation in the root meristem. Science **322**: 1380–1384.

Ito, Y., Nakanomyo, I., Motose, H., Iwamoto, K., Sawa, S., Dohmae, N., and Fukuda, H. (2006). Dodeca-CLE as peptides as suppressors of plant stem cell differentiation. Science **313**: 842–845.

Jun, J., Fiume, E., Roeder, A.H.K., Meng, L., Sharma, V.K., Osmont, K.S., Baker, C., Ha, C.M., Meyerowitz, E.M., Feldman, L.J., and Fletcher, J.C. (2010). Comprehensive analysis of CLE polypeptide signaling gene expression and overexpression activity in arabidopsis. Plant Physiology **154**: 1721–1736.

Kondo, Y., Hirakawa, Y., Kieber, J.J., and Fukuda, H. (2011). CLE peptides can negatively regulate protoxylem vessel formation via cytokinin signaling. Plant and Cell Physiology **52**: 37–48.

Lampropoulos, A., Sutikovic, Z., Wenzl, C., Maegele, I., Lohmann, J.U., and Forner, J. (2013). GreenGate - a novel, versatile, and efficient cloning system for plant transgenesis. PloS one **8**: e83043.

Laux, T., Mayer, K.F.X., Berger, J., and Jürgens, G. (1996). The WUSCHEL gene is required for shoot and floral meristem integrity in Arabidopsis. Development **122**: 87–96.

Leibfried, A., To, J.P.C., Busch, W., Stehling, S., Kehle, A., Demar, M., Kieber, J.J., and Lohmann, J.U. (2005). WUSCHEL controls meristem function by direct regulation of cytokinin-inducible response regulators. Nature **438**: 1172–1175.

Lucas, W.J., Yoo, B., and Kragler, F. (2001). RNA as a long-distance information macromolecule in plants. Nature Reviews **2**: 849–857.

Di Mambro, R., De Ruvo, M., Pacifici, E., Salvi, E., Sozzani, R., Benfey, P.N., Busch, W., Novak, O., Ljung, K., Di Paola, L., Marée, A.F.M., Costantino, P., Grieneisen, V.A., and Sabatini, S. (2017). Auxin minimum triggers the developmental switch from cell division to cell differentiation in the Arabidopsis root. PNAS **114**: E7641–E7649.

Mayer, K.F.X., Schoof, H., Haecker, A., Lenhard, M., Jürgens, G., and Laux, T. (1998). Role of WUSCHEL in regulating stem cell fate in the Arabidopsis shoot meristem. Cell **95**: 805–815.

Meng, L. and Feldman, L.J. (2010). CLE14/CLE20 peptides may interact with CLAVATA2/CORYNE receptor-like kinases to irreversibly inhibit cell division in the root meristem of Arabidopsis. Planta **232**: 1061–74.

Miwa, H., Betsuyaku, S., Iwamoto, K., Kinoshita, A., Fukuda, H., and Sawa, S. (2008). The receptor-like kinase SOL2 mediates CLE signaling in Arabidopsis. Plant & Cell Physiology **49**: 1752–7.

Müller, R., Bleckmann, A., and Simon, R. (2008). The receptor kinase CORYNE of Arabidopsis transmits the stem cell-limiting signal CLAVATA3 independently of CLAVATA1. Plant Cell **20**: 934–946.

Nimchuk, Z.L. (2017). CLAVATA1 controls distinct signaling outputs that buffer shoot stem cell proliferation through a two-step transcriptional compensation loop. PLOS Genetics **13**: e1006681.

Nimchuk, Z.L., Tarr, P.T., and Meyerowitz, E.M. (2011). An evolutionarily conserved pseudokinase mediates stem cell production in plants. Plant Cell **23**: 851–854.

Nimchuk, Z.L., Zhou, Y., Tarr, P.T., Peterson, B.A., and Meyerowitz, E.M. (2015). Plant stem cell maintenance by transcriptional cross-regulation of related receptor kinases. Development **142**: 1043–1049.

Ohyama, K., Shinohara, H., Ogawa-Ohnishi, M., and Matsubayashi, Y. (2009). A glycopeptide regulating stem cell fate in Arabidopsis thaliana. Nature Chemical Biology **5**: 578–580.

Pallakies, H. and Simon, R. (2014). The CLE40 and CRN/CLV2 signaling pathways antagonistically control root meristem growth in Arabidopsis. Molecular Plant **7**: 1619–1636.

Pernisova, M., Grochova, M., Konecny, T., Plackova, L., Harustiakova, D., Kakimoto, T., Heisler, M.G., Novak, O., and Hejatko, J. (2018). Cytokinin signalling regulates organ identity via the AHK4 receptor in Arabidopsis. Development **145**: v163907.

Petricka, J.J., Winter, C.M., and Benfey, P.N. (2012). Control of Arabidopsis Root Development. Annual Review of Plant Biology **63**: 563–590.

Qian, P., Song, W., Yokoo, T., Minobe, A., Wang, G., Ishida, T., Sawa, S., Chai, J., and Kakimoto, T. (2018). The CLE9/10 secretory peptide regulates stomatal and vascular development through distinct receptors. Nature Plants **4**: 1071–1081.

Racolta, A., Nodine, M.D., Davies, K., Lee, C., Rowe, S., Velazco, Y., Wellington, R., and Tax, F.E. (2018). A common pathway of root growth control and response to CLE peptides through two receptor kinases in arabidopsis. Genetics **208**: 687–704.

Rodriguez-Villalon, A., Gujas, B., Kang, Y.H., Breda, A.S., Cattaneo, P., Depuydt, S., and Hardtke, C.S. (2014). Molecular genetic framework for protophloem formation. PNSA **111**: 11551–11556.

Rojo, E., Sharma, V.K., Kovaleva, V., Raikhel, N. v., and Fletcher, J.C. (2002). CLV3 is localized to the extracellular space, where it activates the Arabidopsis CLAVATA stem cell signaling pathway. Plant Cell **14**: 969–977.

Sarkar, A.K., Luijten, M., Miyashima, S., Lenhard, M., Hashimoto, T., Nakajima, K., Scheres, B., Heidstra, R., and Laux, T. (2007). Conserved factors regulate signalling in Arabidopsis thaliana shoot and root stem cell organizers. Nature **446**: 811–814.

Schneider, C.A., Rasband, W.S., and Eliceiri, K.W. (2012). NIH Image to ImageJ: 25 years of image analysis. Nature Methods **9**: 671–675.

Schoof, H., Lenhard, M., Haecker, A., Mayer, K.F.X., Jürgens, G., and Laux, T. (2000). The stem cell population of Arabidopsis shoot meristems is maintained by a regulatory loop between the CLAVATA and WUSCHEL genes. Cell **100**: 635–644.

Shimizu, N., Ishida, T., Yamada, M., Shigenobu, S., Tabata, R., Kinoshita, A., Yamaguchi, K., Hasebe, M., Mitsumasu, K., and Sawa, S. (2015). BAM 1 and RECEPTOR-LIKE PROTEIN KINASE 2 constitute a signaling pathway and modulate CLE peptide-triggered growth inhibition in Arabidopsis root. New Phytologist **208**: 1104–1113.

Shinohara, H. and Matsubayashi, Y. (2013). Chemical Synthesis of Arabidopsis CLV3 Glycopeptide Reveals the Impact of Hydroxyproline Arabinosylation on Peptide Conformation and Activity. Plant and Cell Physiology **54**: 369.

Shinohara, H. and Matsubayashi, Y. (2015). Reevaluation of the CLV3-receptor interaction in the shoot apical meristem: dissection of the CLV3 signaling pathway from a direct ligand-binding point of view. The Plant Journal **82**: 328–36.

Shinohara, H., Moriyama, Y., Ohyama, K., and Matsubayashi, Y. (2012). Biochemical mapping of a ligand-binding domain within Arabidopsis BAM1 reveals diversified ligand recognition mechanisms of plant LRR-RKs. The Plant Journal **70**: 845–854.

Somssich, M., Bleckmann, A., and Simon, R. (2016a). Shared and distinct functions of the pseudokinase CORYNE (CRN) in shoot and root stem cell maintenance of Arabidopsis. Journal of Experimental Botany **67**: 4901–4915.

Somssich, M., Je, B. il, Simon, R., and Jackson, D. (2016b). CLAVATA-WUSCHEL signaling in the shoot meristem. Development **143**: 3238–3248.

Somssich, M., Ma, Q., Weidtkamp-Peters, S., Stahl, Y., Felekyan, S., Bleckmann, A., Seidel, C.A.M., and Simon, R. (2015). Real-time dynamics of peptide ligand-dependent receptor complex formation in planta. Science signaling **8**: ra76.

Stahl, Y., Grabowski, S., Bleckmann, A., Kühnemuth, R., Weidtkamp-Peters, S., Pinto, K.G., Kirschner, G.K., Schmid, J.B., Wink, R.H., Hülsewede, A., Felekyan, S., Seidel, C.A.M., Simon, R. (2013). Moderation of Arabidopsis root stemness by CLAVATA1 and ARABIDOPSIS CRINKLY4 receptor kinase complexes. Current Biology **23**: 362–71.

Stahl, Y. and Simon, R. (2005). Plant stem cell niches. International Journal of Developmental Biology **49**: 479–489.

Stahl, Y., Wink, R.H., Ingram, G.C., and Simon, R. (2009). A Signaling Module Controlling the Stem Cell Niche in Arabidopsis Root Meristems. Current Biology **19**(11): 909–914.

Yadav, R.K., Perales, M., Gruel, J., Girke, T., Jönsson, H., and Venugopala Reddy, G. (2011). WUSCHEL protein movement mediates stem cell homeostasis in the Arabidopsis shoot apex. Genes and Development **25**: 2025–2030.

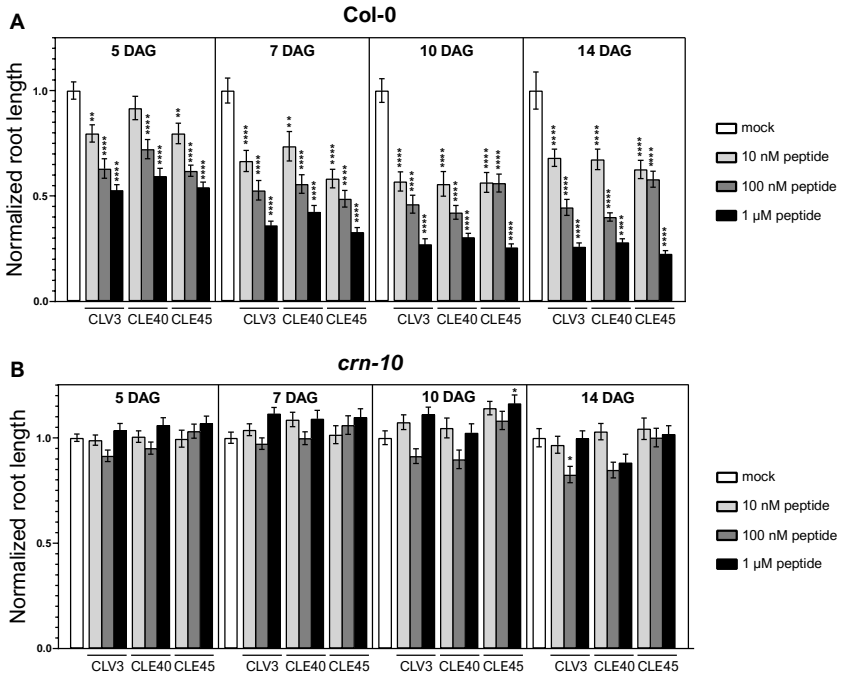

Figure 1 CLE peptides impact root development via CRN-dependent signaling.

Effect of different CLE peptides at increasing concentrations on root growth of wild type plants (**A**, Col-0) and *crn-10* mutants (**B**). Root length was measured 5, 7, 10, and 14 DAG and data were normalized to the corresponding sample grown on ½ MS agar plates without peptide supplementation. Means (± SEM) are plotted, p-values testing differences to the corresponding mock samples were calculated by ANOVA and Dunnett´s post hoc test, with * for $p \leq 0.05$, ** for $p \leq 0.01$, *** for $p \leq 0.001$, and **** for $p \leq 0.0001$.

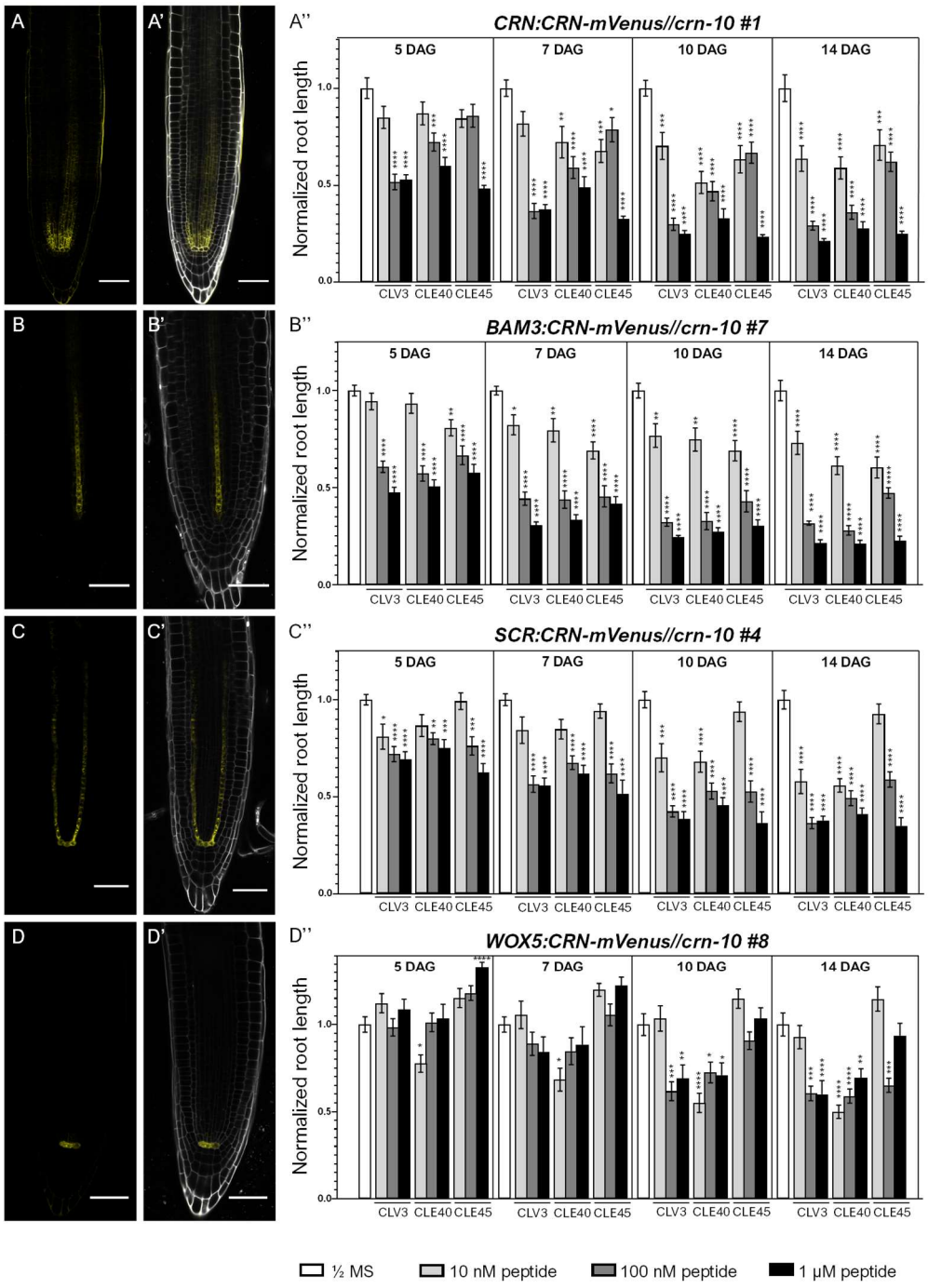

Figure 2 Tissue specific expression of *CRN-mVenus* restores CLE peptide sensitivity of *crn-10* mutants.

Transgenic lines were constructed identically, besides of the utilized promotor sequences, which are the native *CRN* promotor (**A – A''**), the *BAM3* promotor (**B – B''**), the *SCR* promotor (**C – C''**), and the *WOX5* promotor (**D – D''**), respectively. Expression patterns observed via CLSM match the previously described promotor activities. A, B, C, D show mVenus signals only and A', B', C', D' display merges of mVenus and PI channels (seedlings 5 DAG, grown on ½ MS). Scale bars: 50 µm. In A'', B'', C'', D'' means (± SEM) of normalized root length of the corresponding reporter lines are plotted at indicated peptide concentrations and time points (DAG). P-values testing differences to the corresponding mock samples were calculated by ANOVA and Dunnett´s post hoc test, with * for $p \leq 0.05$, ** for $p \leq 0.01$, *** for $p \leq 0.001$, and **** for $p \leq 0.0001$.

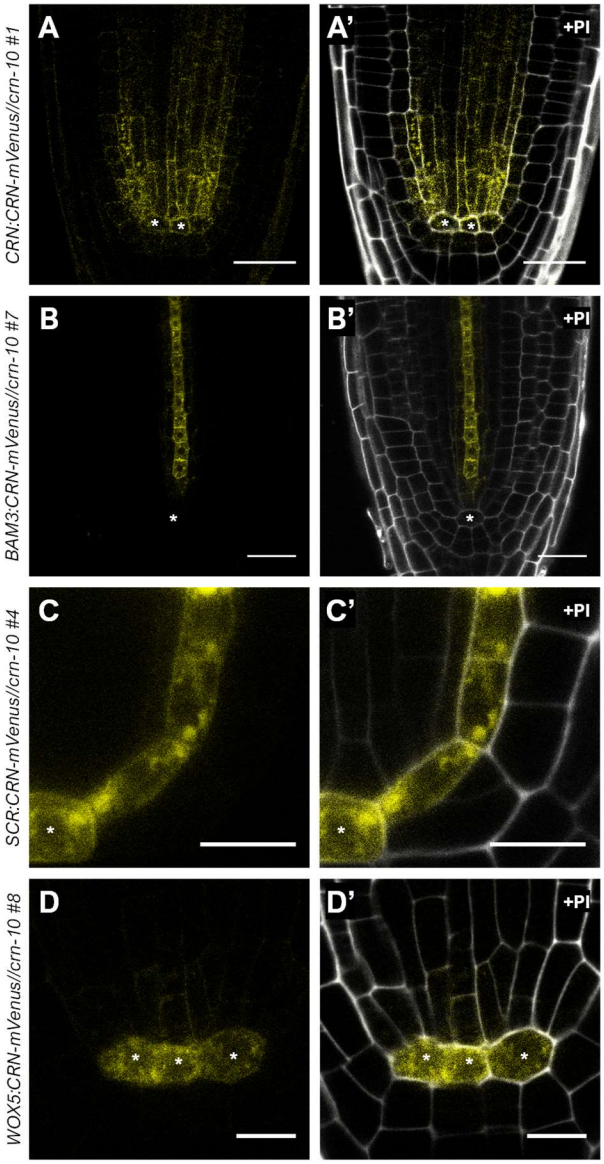

Figure 3 Subcellular localization of CRN-mVenus fusions in *crn-10* mutants after expression under different promotors.

A, A' The native *CRN* promotor mediates expression in the proximal RM including the QC. The fluorescent protein product is predominantly found at the PM. **B, B'** Expressed under the *BAM3* promotor, CRN-mVenus is present in the developing phloem files and located at the PM with higher signal intensity at the basal and apical sides of each cell. Additionally, fluorescence is detectable in the entire cell besides the nucleus. **C, C'** The *SCR* promotor restricts expression to the endodermis file including the QC. CRN-mVenus is detectable at the PM, but mainly within intracellular structures. **D, D'** Expression under the control of the *WOX5* promotor is found in the QC. Faint signals are detectable in the proximal initials. Fluorescence signals can be detected at the PM, but mainly intracellularly. A', B', C' display merges of mVenus signals with propidium iodide (PI) cell wall staining. Asterisks mark the position of the QC. Scalebars: 25 µm (A – B'), 10 µm (C – D').

Supplemental material

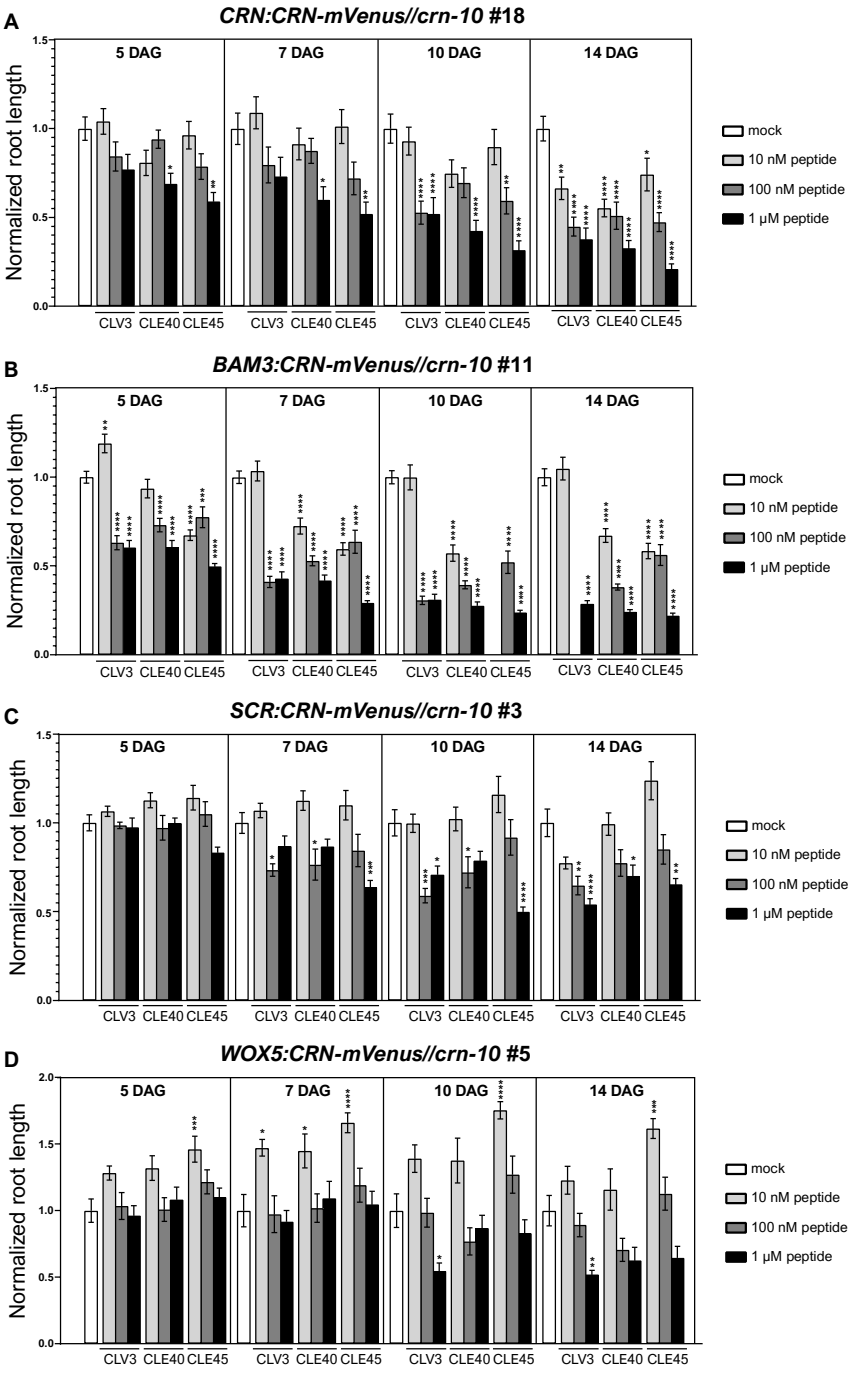

Supplemental Figure 1 Tissue specific expression of *CRN-mVenus* restores CLE peptide sensitivity of *crn-10* mutants.

Normalized root length data as shown and described in Fig. 2 for a second independent transgenic line of each analyzed promotor construct. For details see Fig. 2.

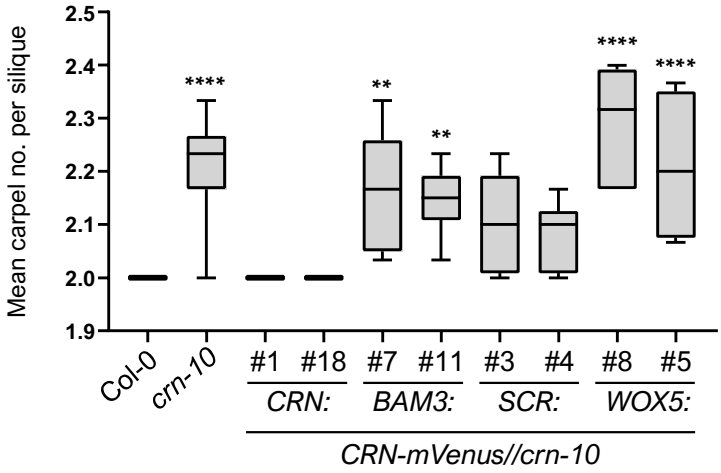

Supplemental Figure 2 Shoot phenotype of *crn-10* mutants harboring different tissue specific *CRN-mVenus* expression constructs.

Mean carpel number per silique was determined from 6 – 8-weeks-old plants grown in long day conditions to evaluate the capability of the generated promotor constructs to rescue the typical increased organ phenotype of *crn-10* mutants. While the native CRN promotor fully rescues the *crn-10* carpel number phenotype, all other promotor lines displayed higher mean carpel numbers per silique than the Col-0 wild type. P-values testing differences to the Col-0 sample were calculated by ANOVA and Dunnett´s post hoc test, with ** for $p \leq 0.01$, and **** for $p \leq 0.0001$.

Supplemental Table 1 Chemicals utilized for the described experiments.

Name	Producer/Source	Product no.	CAS no.
BASTA® non-selective herbicide	Bayer CropScience	84442615	N/A
Carbenicillin disodium salt	Carl Roth	6344.2	4800-94-6
DL-phosphinothricin (PPT)	Duchefa Biochemie bv	P0159	77182-82-2
Gentamicin sulfate	Sigma-Aldrich (Merck)	G1264	1405-41-0
MES hydrate	Sigma-Aldrich (Merck)	10240885	1266615-59-1
Murashige & Skoog Medium (+Gamborg B5 vitamins)	Duchefa Biochemie bv	M0231.0050	N/A
Phusion High-Fidelity PCR polymerase	Thermo Fisher Scientific	F530S	N/A
Propidium iodide (PI)	Thermo Fisher Scientific	P1304MP	25535-16-4
Rifampicin	TCI	R0079	13292-46-1
Spectinomycin HCl pentahydrate	Duchefa Biochemie bv	S0188	22189-32-8
Synthetic CLV3 (RCV[Hyp]SG[Hyp]DPLHHH)	Peptides & Elephants	costumized	N/A
Synthetic CLE40 (RQV[Hyp]TGSDPLHHK)	Peptides & Elephants	costumized	N/A
Synthetic CLE45 (RRVRRGSDPIHN)	Peptides & Elephants	costumized	N/A
Tetracycline	Sigma-Aldrich (Merck)	87128	60-54-8

Supplemental Table 2 Oligonucleotides for amplification of insert sequences for entry plasmid construction.

Sequence	Forward	Revers
CRN coding sequence (w/ introns, w/o STOP)	AAAGGTCTCAGGCTTAATGAAGCAAAGAAGAAG	TTTGGTCTCACTGAAAAAGCTGTGCAGTT
CRN promotor (1.7 kb)	AAAGGTCTCAACCTTAAAGATGCATAGGCT	TTTGGTCTCATGTTCATTGCTGCTTCTAC
BAM3 promotor (2 kb)	AAAGGTCTCAACCTGATCACATACCACATTGATCTGC	AAAGGTCTCATGTTGGCTCACTATGTTCTGGAGTTG
SCR promotor (2.5 kb)	AAAGGTCTCAACCTCCACCACCGTCAAC	AAAGGTCTCATGTTGGAGATTGAAGGGTTGTTGG
WOX5 promotor (4.7 kb)	AAAGGTCTCAACCTAAAGACTTTTATCTACCAACTTC	ATAGGTCTCATGTTCGTTCAGATGTAAAGTCC

Supplemental Table 3 Stable transgenic *A. thaliana* lines generated in this study.

Name	Transgene description	Plant resistance
CRN:CRN-mVenus//crn-10	*pCRN:Ω-CRN-mVenus:tUBQ10<<pNOS:BastaR:pNOS*	Phosphinothricin/BASTA®
BAM3:CRN-mVenus//crn-10	*pBAM3:Ω-CRN-mVenus:tUBQ10<<pNOS:BastaR:pNOS*	Phosphinothricin/BASTA®
SCR:CRN-mVenus//crn-10	*pSCR:Ω-CRN-mVenus:tUBQ10<<pNOS:BastaR:pNOS*	Phosphinothricin/BASTA®
WOX5:CRN-mVenus//crn-10	*pWOX5:Ω-CRN-mVenus:tUBQ10<<pNOS:BastaR:pNOS*	Phosphinothricin/BASTA®

Chapter IV

A Cellular Insulator against CLE45 Peptide Signaling

This manuscript was published in Current Biology in August 2019.

https://doi.org/10.1016/j.cub.2019.06.037

Authors:

Alice S. Breda[1*], Ora Hazak[1*], Patrick Schultz[2*°], Pauline Anne[1], Moritz Graeff[1], Rüdiger Simon[2], and Christian S. Hardtke[1]

Affiliations:

[1] Department of Plant Molecular Biology, University of Lausanne, Biophore Building, 1015 Lausanne, Switzerland

[2] Institute for Developmental Genetics, Heinrich Heine University, 40225 Düsseldorf, Germany

* These authors contributed equally

° present name: Patrick Blümke

Author contributions:

A.S.B., P.A., and C.S.H. conceived and designed this project. A.S.B., O.H., P.S., P.A., and M.G. designed and performed the experiments. O.H. and C.S.H. drafted the manuscript. All authors analyzed data and contributed to the writing of the final manuscript.

Report

Current Biology

A Cellular Insulator against CLE45 Peptide Signaling

Highlights

- OPS activity antagonizes CLE45 signaling in developing protophloem sieve elements
- Enhanced CLE45 signaling can be overcome by increased OPS dosage
- OPS dampens CLE45 sensing by direct interference with CLE45 signaling components
- OPS hyperactivity confers resistance to various root-active CLE peptides

Authors

Alice S. Breda, Ora Hazak, Patrick Schultz, Pauline Anne, Moritz Graeff, Rüdiger Simon, Christian S. Hardtke

Correspondence

christian.hardtke@unil.ch

In Brief

This study by Breda et al. reveals a novel mechanism in the quantitative modulation of CLE peptide signaling. The authors demonstrate that the *Arabidopsis* protein OPS promotes root protophloem differentiation by antagonizing autocrine CLE45 peptide signaling, through direct interference with the CLE45 signaling components BAM3 and CLV2|CRN.

Breda et al., 2019, Current Biology *29*, 2501–2508
August 5, 2019
https://doi.org/10.1016/j.cub.2019.06.037

CellPress

Current Biology
Report

A Cellular Insulator against CLE45 Peptide Signaling

Alice S. Breda,[1,3] Ora Hazak,[1,3] Patrick Schultz,[2,3] Pauline Anne,[1] Moritz Graeff,[1] Rüdiger Simon,[2] and Christian S. Hardtke[1,4,*]
[1]Department of Plant Molecular Biology, University of Lausanne, Biophore Building, 1015 Lausanne, Switzerland
[2]Institute for Developmental Genetics and Cluster of Excellence on Plant Sciences, Heinrich Heine University, 40225 Düsseldorf, Germany
[3]These authors contributed equally
[4]Lead Contact
*Correspondence: christian.hardtke@unil.ch
https://doi.org/10.1016/j.cub.2019.06.037

SUMMARY

Plants continuously elaborate their bodies through post-embryonic, reiterative organ formation by apical meristems [1]. Meristems harbor stem cells, which produce daughter cells that divide repeatedly before they differentiate. How transitions between stemness, proliferation, and differentiation are precisely coordinated is not well understood, but it is known that phytohormones as well as peptide signals play important roles [2–7]. For example, in *Arabidopsis thaliana* root meristems, developing protophloem sieve elements (PPSEs) express the secreted CLAVATA3/EMBRYO SURROUNDING REGION-RELATED 45 (CLE45) peptide and its cognate receptor, the leucine-rich repeat receptor kinase (LRR-RK) BARELY ANY MERISTEM 3 (BAM3). Exogenous CLE45 application or transgenically increased CLE45 dosage impairs protophloem formation, suggesting autocrine inhibition of PPSE differentiation by CLE45 signaling. Since CLE45 and BAM3 are expressed throughout PPSE development, it remains unclear how this inhibition is eventually overcome. The *OCTOPUS* (*OPS*) gene is required for proper PPSE differentiation and therefore the formation of continuous protophloem strands. OPS dosage increase can mend the phenotype of other mutants that display protophloem development defects in association with CLE45-BAM3 hyperactivity [8, 9]. Here, we provide evidence that OPS protein promotes differentiation of developing PPSEs by dampening CLE45 perception. This markedly quantitative antagonism is likely mediated through direct physical interference of OPS with CLE45 signaling component interactions. Moreover, hyperactive OPS confers resistance to other CLE peptides, and ectopic OPS overexpression triggers premature differentiation throughout the root. Our results thus reveal a novel mechanism in PPSE transition toward differentiation, wherein OPS acts as an ''insulator'' to antagonize CLE45 signaling.

RESULTS AND DISCUSSION

A. thaliana root meristems display a stereotypical morphology [10, 11]. Stem cells at the root tip produce daughter cells that divide repeatedly to generate cell files, which acquire distinct tissue identities depending on their position. The balance between cell production and timing of differentiation determines root meristem size and growth rate and is coordinated by intersecting hormone and peptide signals [3, 6, 12–17]. Exogenous application of many CLE peptides suppresses root growth [13, 18–20]. Sensing of these so-called root-active CLE peptides requires the receptor-like protein CLAVATA2 (CLV2) and the CORYNE (CRN) pseudokinase in the protophloem [21]. CLV2 and CRN function as a heteromer (CLV2|CRN) and are interdependent for their efficient plasma membrane recruitment [22, 23].

Protophloem is critical for meristem maintenance [8, 24, 25]. Differentiating protophloem sieve elements (PPSEs) undergo major cellular rearrangements, such as cell-wall buildup and nucleus degradation [8, 26]. In *brevis radix* (*brx*) and *ops* mutants, PPSEs frequently fail to differentiate. Such cells appear as ''gaps'' that interrupt protophloem strand continuity and thereby obstruct efficient phloem sap delivery to the meristem [8, 9]. *brx* or *ops* defects can be rescued by *bam3* second site mutations [8, 18, 21]. Conversely, CLE45 peptide application or dosage increase suppresses PPSE differentiation, suggesting a role for autocrine peptide signaling in protophloem formation [8, 18, 27, 28]. Moreover, CLE45 signaling through BAM3 is quantitatively limited by the CLV2|CRN heteromer [21], which is why *crn* mutants are resistant to CLE45.

BRX and OPS are plant-specific plasma membrane-associated, polar proteins [8, 9]. BRX localizes rootward, where it modulates auxin flux [29], whereas OPS localizes shootward. The molecular mode of OPS action remains largely obscure. Ectopic overexpression of OPS triggers severe developmental phenotypes [30, 31], which could be explained by OPS interference with brassinosteroid signaling in the case of hypocotyl elongation [30]. However, a pertinent OPS deletion variant can still complement the *ops* root protophloem phenotype [31, 32]. The most remarkable feature of OPS is its strongly quantitative action [31]. For example, OPS gain-of-function mutations as well as increased OPS dosage can rescue *brx* protophloem (and thus root growth) defects [8, 28, 31].

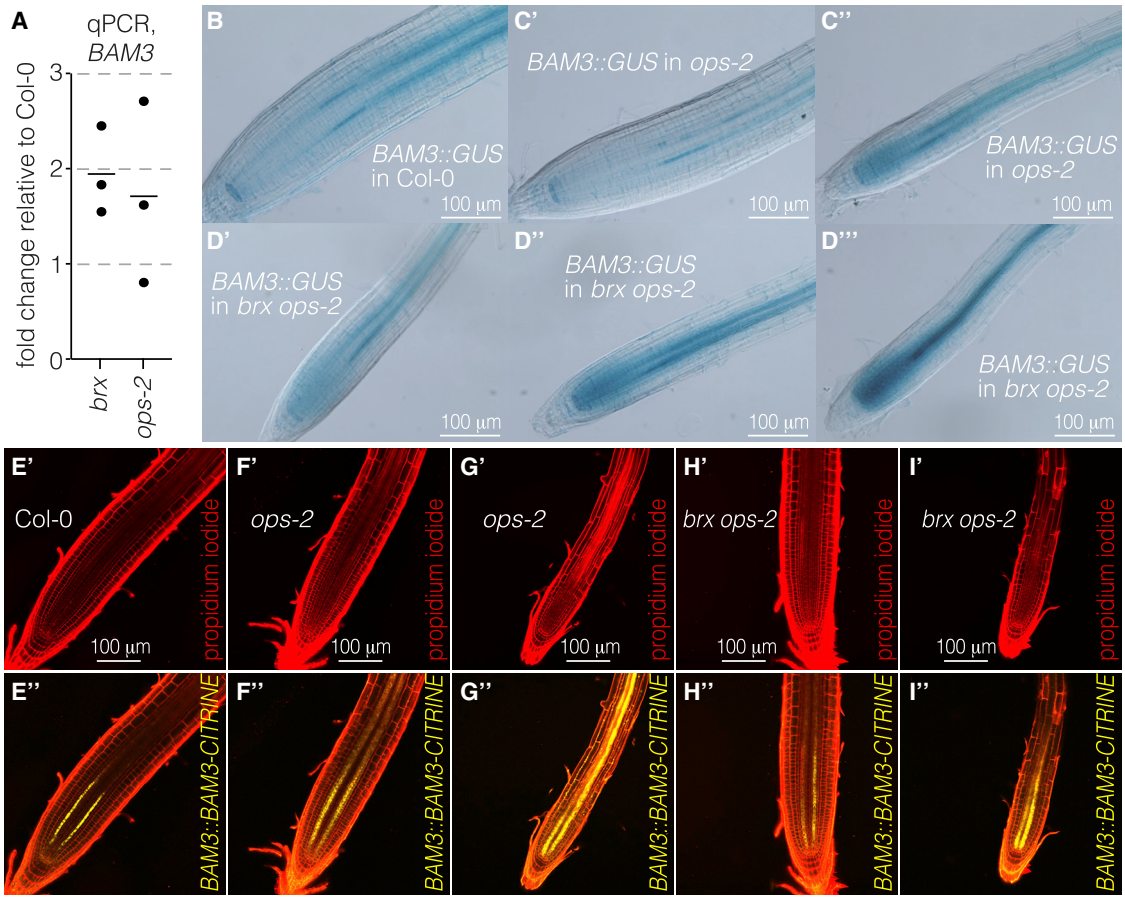

Figure 1. *BAM3* Expression in *ops* Loss-of-Function Mutants

(A) Expression level of *BAM3* mRNA in primary root tips of *Arabidopsis brx* or *ops* loss-of-function mutants, determined by quantitative real-time PCR as compared to Col-0 wild type (3 technical replicates each for 3 biological replicates; bar, mean).

(B–D) Detection of beta-glucuronidase (GUS) reporter activity expressed under control of *BAM3* promoter in root tips of indicated genotypes. Representative roots for Col-0 (B) and mutant individuals of different phenotypic severity (C and D) are shown.

(E–I) Detection of BAM3-CITRINE fusion protein expressed under control of *BAM3* promoter in root tips of indicated genotypes. Representative roots for Col-0 (E) and mutant individuals of different phenotypic severity (F–I) are shown. Top panels: cell outlines revealed by propidium iodide (PI) cell-wall staining, red fluorescence. Bottom panels: the BAM3-CITRINE fluorescence signal (yellow) merged with the PI signal in 7-day-old seedlings.

Quantitative Antagonism between CLE45 Signaling and OPS Determines Protophloem Differentiation

BAM3 transcription is elevated in *brx* root tips [18], which we confirmed by qPCR and also observed in *ops* loss-of-function mutants (Figure 1A). Interestingly, however, GUS reporter expression under control of the *BAM3* promoter (*BAM3::GUS*) varied in *ops* mutants and correlated with the stochastic range of phenotypic severity (Figures 1B and 1C). Similar variation was observed in *brx ops* double mutants, although they generally expressed *BAM3::GUS* at higher level (Figure 1D). These observations were confirmed with BAM3-CITRINE fusion protein (*BAM3::BAM3-CITRINE*) (Figures 1E–1I). Thus, *BAM3* expression varied across mutant individuals and higher levels correlated with a stronger phenotype. Moreover, expression was overall higher in *brx ops* double mutants, consistent with reported additive effects of *brx* and *ops* loss of function [31].

A semi-dominant *ops* second site mutation, ops^{E319K}, renders OPS hyperactive and can partially rescue *brx* mutants [8, 31]. Even more intriguing, *brx* mutants are frequently fully rescued by introduction of an *OPS::OPS-GFP* transgene ($brx^{OPS::OPS\text{-}GFP}$) [8]. Since ops^{E319K} roots also display resistance to CLE45 application [8], we explored whether *brx* rescue by *OPS* gain of function or dosage increase could reflect a role of *OPS* in antagonizing CLE45 perception. Indeed, *brx* ops^{E319K} double mutants were slightly CLE45-resistant, although less so than ops^{E319K} single mutants (Figure 2A), with the caveat that these genotypes are difficult to compare because protophloem defects are only partially restored in *brx* ops^{E319K} double mutants. In contrast, both protophloem development and root growth were normal in most $brx^{OPS::OPS\text{-}GFP}$ seedlings. Yet while roots of the transgenic Col-$0^{OPS::OPS\text{-}GFP}$ wild type were strongly CLE45-resistant, this was barely the case for $brx^{OPS::OPS\text{-}GFP}$ seedlings (Figure 2B). Moreover, CITRINE fusions of differentially active OPS variants [31] conferred varying degrees of CLE45 resistance in Col-0 as well as *ops* backgrounds, but less so, if at all, in *brx ops* double mutants (Figure 2C). Thus, overall the extent of CLE45 resistance was a function of the overlay between *OPS* gene dosage and/or protein activity and the

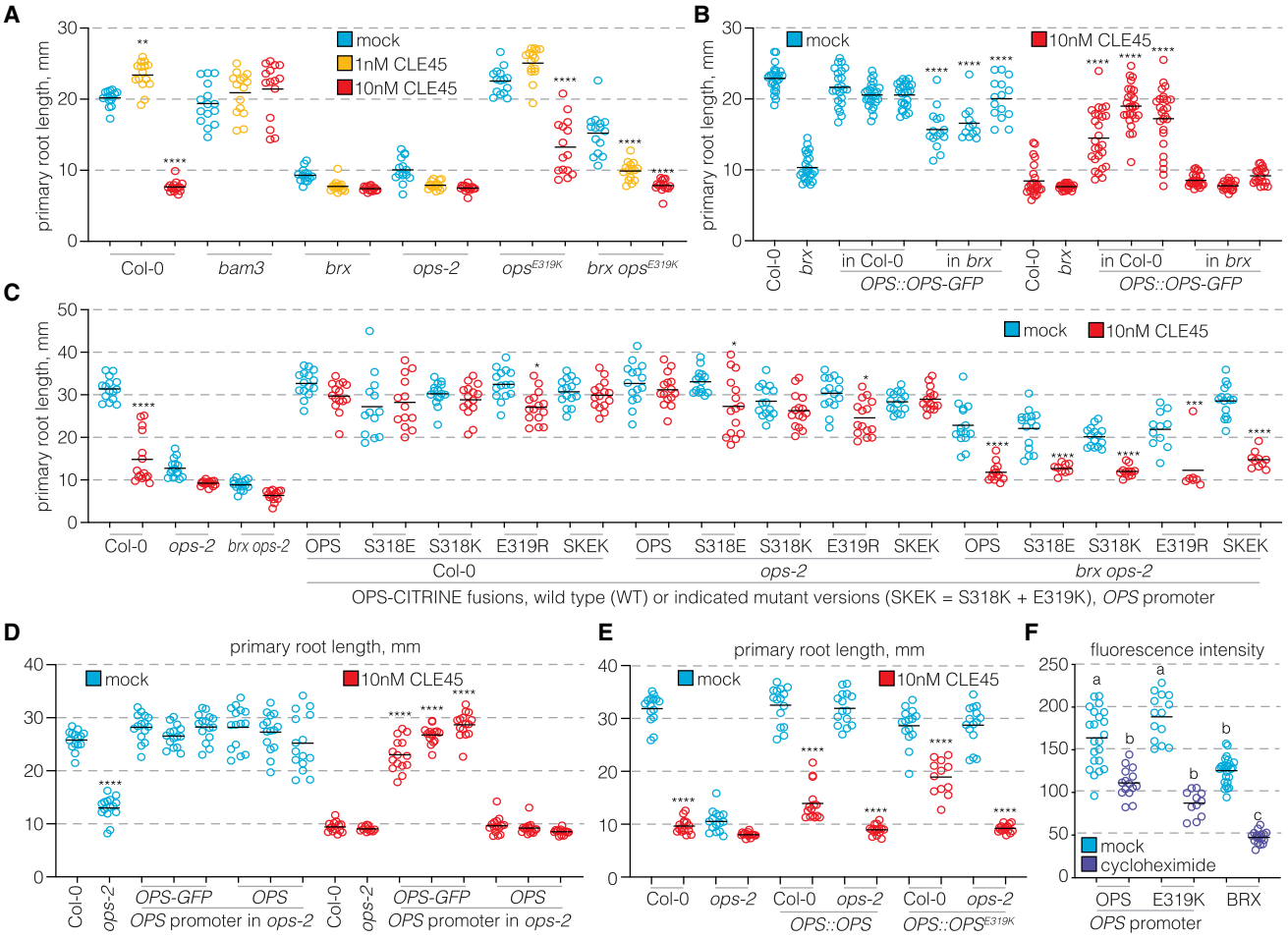

Figure 2. Quantitative, Background-Dependent CLE45 Resistance Conferred by OPS Gain of Function

(A) Root length of indicated genotypes on media supplemented with CLE45 peptide. Note that *ops-2* is a loss-of-function allele, while *ops*^{E319K} is a gain-of-function allele. The statistically significant difference compared to mock is indicated.

(B) CLE45 response of seedlings that carry an *OPS::OPS-GFP* transgene in Col-0 or *brx* background (three independent lines per transgene, comparable expression levels). The statistically significant difference compared to background is indicated.

(C) CLE45 response of transgenic seedlings that express indicated OPS variants in different backgrounds (representative lines). The statistically significant difference compared to mock is indicated.

(D) CLE45 response of transgenic seedlings that express indicated transgenes in *ops* background (three independent lines per transgene). The statistically significant difference compared to Col-0 is indicated.

(E) CLE45 response of seedlings that carry indicated transgenes in Col-0 or *ops* loss-of-function background (representative lines). The statistically significant difference compared to mock is indicated.

(F) Quantification of fluorescence in roots upon 1 h mock or 50 μM cycloheximide treatment, for OPS-GFP fusion proteins and BRX-CITRINE fusion protein (averages of 11–22 roots, 10–20 cells per root).

Seven-day-old seedlings. Plots display individual values (dots) and the mean (bar). *p < 0.05; ***p < 0.001; ****p < 0.0001; see also Figures S1 and S2 and Data S1 for statistical test details.

presence or absence of *BRX*. Our observations therefore suggest that antagonism between CLE45 signaling and OPS action is sensitive to quantitative variation and plays an important role in PPSE differentiation.

C-Terminal Fusions Impact OPS Activity

We previously observed that fluorescent tags impact OPS activity [31]. To determine whether tags also affect the ability of *OPS* to antagonize CLE45 signaling, we tested Col-0$^{OPS::OPS}$ and Col-0$^{OPS::OPS\text{-}GFP}$ lines. Indeed, compared to the GFP-tagged version, untagged OPS conferred less CLE45 resistance (Figure 2D). Yet again, untagged OPS^{E319K} conferred stronger resistance than untagged OPS (Figure 2E). Moreover, although both untagged transgenes complemented *ops* mutants, they conferred hardly any resistance in this background (Figures 2D and 2E), reiterating the importance of total OPS dosage in antagonizing CLE45 signaling. Interestingly, the impact of the fluorescent tags was not related to their size, since HA- or FLAG-epitope-tagged OPS versions were also relatively stronger agents than untagged OPS (Figure S1B). Thus, in general, C-terminal extensions amplified OPS activity. In summary, we can conclude that a combination of expression

level and protein activity determines overall OPS capacity to antagonize CLE45 signaling, reiterating the highly quantitative action of OPS [31].

Previous analyses suggested that OPS protein is turned over rapidly [31]. In cycloheximide-treated *OPS::OPS-GFP* seedlings, the OPS-GFP signal disappeared indeed swiftly (Figure 2F). This could neither be counteracted by protease inhibitor nor by proteasome inhibitor treatment (Figure S1C). Although it remains unclear whether our assays reflect realistic turnover because of the influence of the GFP tag, we could confirm the notion that OPS is rather unstable [31]. The mutated site in OPS^{E319K} apparently influences the phosphorylation state of a neighboring phosphoserine (S318) [31]. S318 seems to play a role in OPS turnover, because an OPS^{S318A} variant is much less abundant than wild-type OPS [31]. However, corroborating that gain-of-function alleles in this phosphosite do not notably affect OPS protein levels [31], no significant difference in relative turnover was observed for OPS^{E319K} (Figure 2F). Thus, OPS^{E319K} is apparently not hyperactive because of increased protein stability.

Alleviation of CLE45 Signaling Partially Rescues *ops* Phenotypes

Consistent with the observed antagonism between OPS and CLE45-BAM3, the *ops* phenotype can be fully rescued by *bam3* second site mutation [8, 18]. However, *BAM3::NLS-3XVENUS* transgene expression was not altered in ops^{E319K} roots (Figure S2A), suggesting that ops^{E319K} mutants are not CLE45-resistant due to reduced *BAM3* levels. Therefore, increased OPS activity might confer CLE45 resistance through post-transcriptional mechanisms. Because the CLV2|CRN heteromer is necessary for full CLE45 sensing in the protophloem [21], second-site *crn* mutation partially rescues *brx* root meristem size and growth [21]. We observed the same for *crn ops* double mutants (Figures S2B and S2C). However, although *brx crn* and *crn ops* phenotypes were on average less severe and meristems without defects in tendency more frequent, in aggregate protophloem gap frequencies were not significantly reduced (Figures S2D and S2E). In part, this could be explained by the larger meristems of the double mutants, which renders gaps more easily recognizable. Yet in summary, reduction of CLE45 signaling through *CRN* knockout could not compensate for reduced *OPS* activity to the same extent as *BAM3* mutation, suggesting quantitatively different roles of CRN and BAM3 in CLE45 response.

OPS Can Interact with CLE45 Signaling Components

To explore whether OPS might directly interfere with CLE45 perception, we sought to determine whether OPS can interact with CLE45 signaling components. Because our proteins of interest are either mainly plasma membrane-integral or -associated, we chose *in vivo* FRET-FLIM to investigate this question. Efficient CRN plasma membrane localization requires its heteromerization with CLV2 [22, 23]; thus, we first tested whether the presence of OPS changes the interaction dynamics between CRN and CLV2. To this end, *Nicotiana benthamiana* leaves were transiently transformed with fluorescent fusion proteins expressed under a constitutive promoter. In these assays, CRN-CFP fluorescence lifetime in presence of CLV2-CITRINE was further reduced by OPS-CITRINE co-expression (Figure S3A), indicating that OPS could interact with the CLV2|CRN complex. To confirm this notion, we switched to an inducible system that permits controlled expression timing and levels. In presence of untagged CLV2, we observed reduced fluorescence lifetime of CRN-GFP upon OPS-mCHERRY co-expression (Figure 3A), again indicative of interaction. Moreover, CRN-GFP fluorescence lifetime was significantly reduced upon BAM3-mCHERRY co-expression, but not upon co-expression of another plasma membrane-integral LRR-RK fusion, FLAGELLIN-SENSITIVE 2 (FLS2)-mCHERRY (Figure 3A). These results were confirmed in a reverse setup that monitored BAM3-GFP fluorescence lifetime (Figure S3B). Further, interaction of CRN with BAM3 and OPS was also observed in yeast split ubiquitin assays (Figure S3C). In summary, our results suggest that known CLE45 signaling components can interact with each other as well as with OPS *in vivo*.

OPS Can Interfere with CLE45 Signaling Component Interactions

Engineering increasingly positive charge into the OPS phosphosite creates progressively more active OPS variants [31], as exemplified by ops^{E319K}. To check whether this could alter interaction strength with CLV2|CRN, we included the strongest OPS variant, S318K E319K (OPS^{SKEK}), in our *N. benthamiana* FRET-FLIM assays. Compared to wild-type OPS, interaction between CRN and OPS^{SKEK} appeared to be more robust and somewhat stronger, but not in all replicate experiments, and not at statistically significant levels (Figure 3A). Thus, OPS^{SKEK} hyperactivity can likely not be explained by an increased propensity to interact with CLV2|CRN. We also determined whether the presence of CLE45 changes the quality or strength of any of the observed interactions, which was, however, not the case (Figure 3B).

Finally, we sought to monitor the dynamics of all four proteins upon simultaneous expression. Fluorescence lifetime reduction of constitutively expressed CRN-GFP in presence of untagged CLV2 and constitutively expressed BAM3-mCHERRY confirmed the proposed interaction between CRN and BAM3 (Figure 3C). However, this reduction was prevented by simultaneously induced co-expression of an OPS-CERULEAN fusion protein. These observations were confirmed in an alternative setup, where fluorescence lifetime of constitutively expressed CRN-GFP (in presence of untagged CLV2) could be reduced by induced BAM3-mCHERRY co-expression, but the effect could be reversed by simultaneous OPS-CERULEAN induction (Figures 3C and S3D). In summary, these results suggest that OPS can interfere with interactions between CLE45 signaling components. Because of the comparable abundance of the different proteins in the protophloem (Figures S3E–S3H), such interference likely affects CLE45 perception. To further characterize the interference, we conducted additional assays with a BAM3 deletion variant that lacked the intracellular kinase domain (but not the entire intracellular domain). This $BAM3^{\Delta KD}$-mCHERRY fusion protein still interacted with CRN-GFP, as well as with a CRN deletion variant that lacked the intracellular pseudokinase domain ($CRN^{\Delta PKD}$-GFP) (Figure 3D). Therefore, interaction between BAM3 and CLV2|CRN appears to be mediated by the extracellular and/or transmembrane domains. The $BAM3^{\Delta KD}$-mCHERRY interaction with CRN-GFP could still be disturbed by simultaneous OPS-CERULEAN expression. However, this

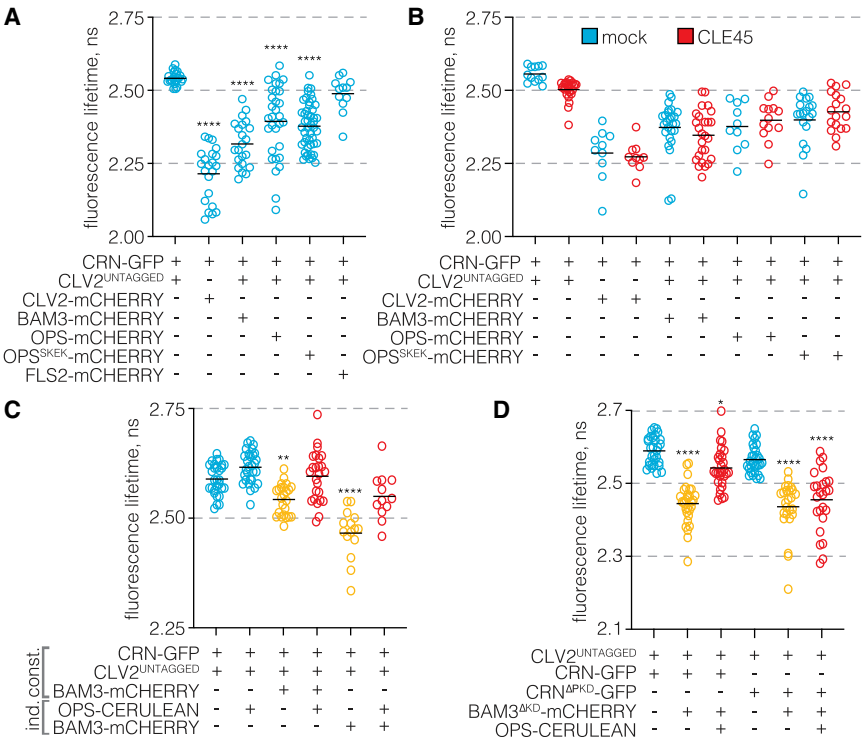

Figure 3. Protein-Protein Interactions between CLE45 Signaling Components and OPS

(A) FRET-FLIM measurements of CRN-GFP in combination with indicated fusion proteins expressed in transiently transformed *N. benthamiana* cells, under inducible promoter. The statistically significant difference compared to CRN-GFP + untagged CLV2 control is indicated.

(B) *N. benthamiana* FRET-FLIM measurements as in (A) after mock or CLE45 infiltration (no significant differences between treatments).

(C) *N. benthamiana* FRET-FLIM measurements of constitutively expressed CRN-GFP in presence of untagged CLV2, in combination with constitutive or induced BAM3-mCHERRY, and induced OPS-CERULEAN expression. The statistically significant difference compared to CRN-GFP + untagged CLV2 control is indicated.

(D) *N. benthamiana* FRET-FLIM measurements of induced CRN-GFP or a deletion variant that lacks the intracellular pseudokinase domain ($CRN^{\Delta PKD}$-GFP) in presence of untagged CLV2, in combination with induced BAM3-mCHERRY in presence or absence of induced OPS-CERULEAN expression. The statistically significant difference compared to CRN-GFP or $CRN^{\Delta PKD}$-GFP + untagged CLV2 controls is indicated.

Plots display individual values (dots) and the mean (bar). $^{**}p < 0.01$; $^{****}p < 0.0001$; see also Figure S3 and Data S1 for statistical test details.

was no longer the case when CRN-GFP was replaced by $CRN^{\Delta PKD}$-GFP (Figure 3D). These results suggest that OPS interferes with the interaction between BAM3 and CRN through binding to their intracellular domains, thereby quantitatively dampening CLE45 perception in a likely non-linear manner.

OPS Gain of Function Confers Resistance to Various Root-Active CLE Peptides

The results from the interaction assays were in line with the genetic hierarchy and suggest that OPS limits CLV2|CRN activity, which in turn quantitatively promotes BAM3 activity. Moreover, while BAM3 is specific for CLE45 in the root [18, 33], CLV2|CRN is required to sense various root-active CLE peptides [14, 21, 34, 35]. Therefore, if OPS can interfere with receptor interactions of CLV2|CRN, our results predicted that OPS gain of function might to some degree also interfere with sensing of other root-active CLE peptides. Indeed, ops^{E319K} mutants exhibited some resistance to application of a range of CLE peptides (Figures 4A and 4B). The extent of resistance was, however, variable and, unlike resistance of *crn* mutants monitored in parallel, not observed for all CLE peptides tested (8 out of 13). Moreover, CLE resistance of ops^{E319K} mutants was always weaker than CLE resistance of *crn* mutants (Figures 4A and 4B). These data are consistent with the idea that OPS can quantitatively interfere with CLV2|CRN activity and thereby modulate signaling strength of various CLE pathways.

Ectopic OPS Overexpression Promotes Early Differentiation

OPS is specifically expressed in the root protophloem [8, 9]. However, redundant, conserved OPS homologs exist [9, 31, 36], and in pertinent loss-of-function double mutants the *ops* phenotype is aggravated [36]. Consistent with suppression of protophloem differentiation by CLE peptides [21, 27, 28] and a role for OPS in antagonizing CLE signaling, these double mutants display substantial delays and frequent failures in protophloem differentiation [36]. Although the strong systemic impact of discontinuous protophloem strands on overall root meristem activity [24, 28] renders interpretation of these phenotypes difficult, the observed differentiation delays could be viewed as reduced capacity of developing PPSEs to escape the meristematic stage.

Whether conversely a strong increase in OPS activity can render plants even more resistant to CLE peptides remains unclear, because ectopic overexpression of OPS has severe consequences on root as well as shoot development [30, 31]. For instance, plants that express OPS-CITRINE fusions proteins under control of *UBIQUITIN 10* (*UBQ10*) promoter exhibit a variable growth phenotype, *in extremis* resulting in severely dwarfed plants that cannot complete their life cycle. Reemphasizing the highly quantitative nature of OPS action, phenotypic severity is also a function of transgene overexpression level [31]. This could be observed in the progeny of hemizygous *UBQ10::OPS-CITRINE* plants with moderate expression level, which segregated various root meristem phenotypes, ranging from nearly wild type to severely impaired growth (Figures 4C–4F), whereby phenotypic severity correlated with increased OPS-CITRINE level (Figures S4A and S4B). Yet, phenotypic severity was *a priori* not associated with apparent patterning defects. Rather, increased OPS-CITRINE correlated with earlier, sometimes nearly immediate PPSE elongation and differentiation (Figure 4G). Moreover, reduction of the meristematic state was essentially observed across all cell layers. For instance, cortex

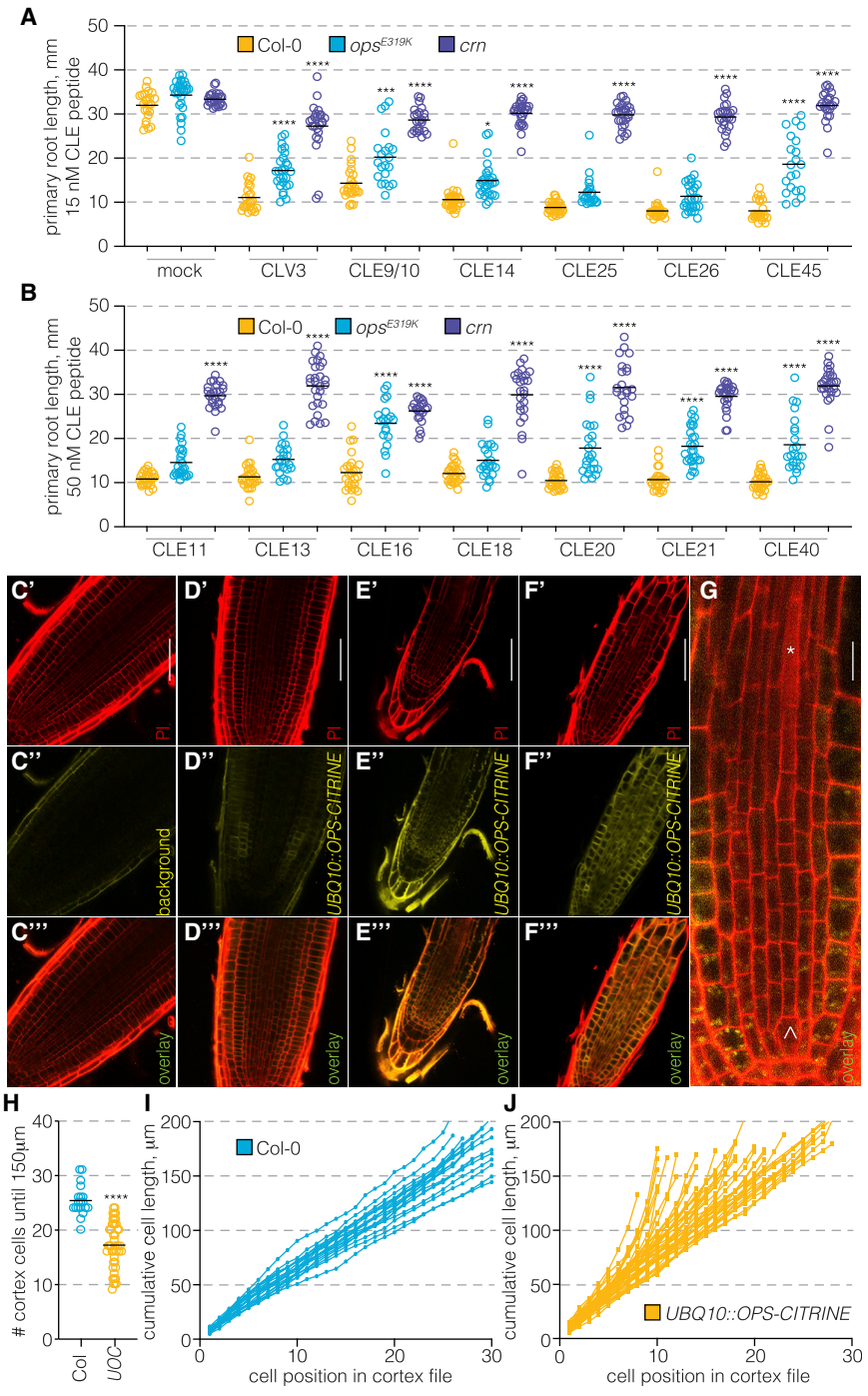

Figure 4. Developmental Consequences of OPS Hyperactivity

(A and B) Response of Col-0, *ops*^{E319K} and *crn* seedlings to efficient concentrations (15 nM in A; 50 nM in B) of various root active CLE peptides. The statistically significant difference compared to Col-0 is indicated.

(C–F) Phenotypic variation in the progeny of a hemizygous transgenic line as a function of the constitutive expression level of OPS-CITRINE fusion protein. Col-0 wild type is shown in (C). (D), (E) and (F) show different seedlings segregating from a hemizygous *UBQ10::OPS-CITRINE* mother plant. Note that confocal settings in (C′′)–(F′′) were not the same, due to the very strong CITRINE signals in (E′′) and (F′′).

(G) Accelerated protophloem differentiation from stem cell (arrowhead) to mature PPSE (asterisk) upon OPS-CITRINE overexpression.

(H) Number of cells in the first 150 µm of cortex cell files, starting from the stem cell daughter. UOC, *UBQ10::OPS-CITRINE* transgenic plants.

(I and J) Cumulative cell length in individual cortex cell files of Col-0 (I) or *UBQ10::OPS-CITRINE* (J) plants. Note frequently early cell elongation in *UBQ10::OPS-CITRINE* transgenic plants.

Seven-day-old seedlings. Plots display individual values (dots) and the mean (bar). ***p < 0.001; ****p < 0.0001; see also Figure S4 and Data S1 for statistical test details.

cells entered differentiation-elongation markedly earlier than in wild type (Figures 4H–4J), in extreme cases as early as one or two divisions after the initial stem cell division. One tangible interpretation of our results is that OPS ectopic overexpression accelerates the transition from proliferation to differentiation in protophloem as well as other root tissues.

Conclusion

Collectively, our findings support a scenario where OPS antagonizes CLE45 perception by direct interference with CLE45 signaling. This process is highly sensitive to quantitative perturbations on both sides. How this antagonism plays out along the protophloem to guide developing PPSEs from proliferation to differentiation remains unclear at this point. All the components identified in this network so far are expressed from the beginning to the end of PPSE development; thus, post-translational modifications might play an important role. For instance, OPS activity could be modulated by differential phosphorylation during PPSE ontogeny. Novel biochemical and cell biological tools will be necessary to comprehensively address this question in future studies. Yet from the genetic and cell biological data at hand, we can conclude that OPS is a key antagonist of BAM3 and CLV2|CRN, thereby acting as a "cellular insulator" against CLE45 signaling.

STAR★METHODS

Detailed methods are provided in the online version of this paper and include the following:

- KEY RESOURCES TABLE
- LEAD CONTACT AND MATERIALS AVAILABILITY

SUPPLEMENTAL INFORMATION

Supplemental Information can be found online at https://doi.org/10.1016/j.cub.2019.06.037.

ACKNOWLEDGMENTS

This work was supported by SNSF grant 31003A_166394 (awarded to C.S.H.), a DFG post-doctoral fellowship (awarded to M.G.), EMBO long-term post-doctoral fellowship ALTF 480-2016 (awarded to P.A.), and by the DFG through SFB1208 (awarded to R.S.). We would like to thank Dr. P. Cattaneo for the *BAM3::NLS-3XVENUS* construct, as well as Dr. J.-C. Palauqui and Prof. E. Farmer for sharing materials to perform yeast split ubiquitin assays.

AUTHOR CONTRIBUTIONS

A.S.B., P.A., and C.S.H. conceived and designed this project. A.S.B., O.H., P.S., P.A., and M.G. designed and performed the experiments. O.H. and C.S.H. drafted the manuscript. All authors analyzed data and contributed to the writing of the final manuscript.

DECLARATION OF INTERESTS

The authors declare no competing interests.

Received: October 16, 2018
Revised: April 22, 2019
Accepted: June 12, 2019
Published: July 18, 2019

REFERENCES

1. Somssich, M., Je, B.I., Simon, R., and Jackson, D. (2016). CLAVATA-WUSCHEL signaling in the shoot meristem. Development *143*, 3238–3248.
2. Caggiano, M.P., Yu, X., Bhatia, N., Larsson, A., Ram, H., Ohno, C.K., Sappl, P., Meyerowitz, E.M., Jönsson, H., and Heisler, M.G. (2017). Cell type boundaries organize plant development. eLife *6*, e27421.
3. Dello Ioio, R., Nakamura, K., Moubayidin, L., Perilli, S., Taniguchi, M., Morita, M.T., Aoyama, T., Costantino, P., and Sabatini, S. (2008). A genetic framework for the control of cell division and differentiation in the root meristem. Science *322*, 1380–1384.
4. Gaillochet, C., Stiehl, T., Wenzl, C., Ripoll, J.J., Bailey-Steinitz, L.J., Li, L., Pfeiffer, A., Miotk, A., Hakenjos, J.P., Forner, J., et al. (2017). Control of plant cell fate transitions by transcriptional and hormonal signals. eLife *6*, e30135.
5. Leibfried, A., To, J.P., Busch, W., Stehling, S., Kehle, A., Demar, M., Kieber, J.J., and Lohmann, J.U. (2005). WUSCHEL controls meristem function by direct regulation of cytokinin-inducible response regulators. Nature *438*, 1172–1175.
6. Matsuzaki, Y., Ogawa-Ohnishi, M., Mori, A., and Matsubayashi, Y. (2010). Secreted peptide signals required for maintenance of root stem cell niche in Arabidopsis. Science *329*, 1065–1067.
7. Shi, B., Guo, X., Wang, Y., Xiong, Y., Wang, J., Hayashi, K.I., Lei, J., Zhang, L., and Jiao, Y. (2018). Feedback from lateral organs controls shoot apical meristem growth by modulating auxin transport. Dev. Cell. *44*, 204–216.
8. Rodriguez-Villalon, A., Gujas, B., Kang, Y.H., Breda, A.S., Cattaneo, P., Depuydt, S., and Hardtke, C.S. (2014). Molecular genetic framework for protophloem formation. Proc. Natl. Acad. Sci. USA *111*, 11551–11556.
9. Truernit, E., Bauby, H., Belcram, K., Barthélémy, J., and Palauqui, J.C. (2012). OCTOPUS, a polarly localised membrane-associated protein, regulates phloem differentiation entry in Arabidopsis thaliana. Development *139*, 1306–1315.
10. Dolan, L., Janmaat, K., Willemsen, V., Linstead, P., Poethig, S., Roberts, K., and Scheres, B. (1993). Cellular organisation of the Arabidopsis thaliana root. Development *119*, 71–84.
11. Scheres, B., Benfey, P., and Dolan, L. (2002). Root development. Arabidopsis Book *1*, e0101.
12. Blilou, I., Xu, J., Wildwater, M., Willemsen, V., Paponov, I., Friml, J., Heidstra, R., Aida, M., Palme, K., and Scheres, B. (2005). The PIN auxin efflux facilitator network controls growth and patterning in Arabidopsis roots. Nature *433*, 39–44.
13. Hobe, M., Müller, R., Grünewald, M., Brand, U., and Simon, R. (2003). Loss of CLE40, a protein functionally equivalent to the stem cell restricting signal CLV3, enhances root waving in Arabidopsis. Dev. Genes Evol. *213*, 371–381.
14. Meng, L., Buchanan, B.B., Feldman, L.J., and Luan, S. (2012). CLE-like (CLEL) peptides control the pattern of root growth and lateral root development in Arabidopsis. Proc. Natl. Acad. Sci. USA *109*, 1760–1765.
15. Stahl, Y., Grabowski, S., Bleckmann, A., Kühnemuth, R., Weidtkamp-Peters, S., Pinto, K.G., Kirschner, G.K., Schmid, J.B., Wink, R.H., Hülsewede, A., et al. (2013). Moderation of Arabidopsis root stemness by CLAVATA1 and ARABIDOPSIS CRINKLY4 receptor kinase complexes. Curr. Biol. *23*, 362–371.
16. Stahl, Y., Wink, R.H., Ingram, G.C., and Simon, R. (2009). A signaling module controlling the stem cell niche in Arabidopsis root meristems. Curr. Biol. *19*, 909–914.
17. Whitford, R., Fernandez, A., Tejos, R., Pérez, A.C., Kleine-Vehn, J., Vanneste, S., Drozdzecki, A., Leitner, J., Abas, L., Aerts, M., et al. (2012). GOLVEN secretory peptides regulate auxin carrier turnover during plant gravitropic responses. Dev. Cell *22*, 678–685.
18. Depuydt, S., Rodriguez-Villalon, A., Santuari, L., Wyser-Rmili, C., Ragni, L., and Hardtke, C.S. (2013). Suppression of Arabidopsis protophloem differentiation and root meristem growth by CLE45 requires the receptor-like kinase BAM3. Proc. Natl. Acad. Sci. USA *110*, 7074–7079.
19. Ito, Y., Nakanomyo, I., Motose, H., Iwamoto, K., Sawa, S., Dohmae, N., and Fukuda, H. (2006). Dodeca-CLE peptides as suppressors of plant stem cell differentiation. Science *313*, 842–845.
20. Kinoshita, A., Nakamura, Y., Sasaki, E., Kyozuka, J., Fukuda, H., and Sawa, S. (2007). Gain-of-function phenotypes of chemically synthetic CLAVATA3/ESR-related (CLE) peptides in Arabidopsis thaliana and Oryza sativa. Plant Cell Physiol. *48*, 1821–1825.
21. Hazak, O., Brandt, B., Cattaneo, P., Santiago, J., Rodriguez-Villalon, A., Hothorn, M., and Hardtke, C.S. (2017). Perception of root-active CLE peptides requires CORYNE function in the phloem vasculature. EMBO Rep. *18*, 1367–1381.
22. Bleckmann, A., Weidtkamp-Peters, S., Seidel, C.A., and Simon, R. (2010). Stem cell signaling in Arabidopsis requires CRN to localize CLV2 to the plasma membrane. Plant Physiol. *152*, 166–176.
23. Somssich, M., Ma, Q., Weidtkamp-Peters, S., Stahl, Y., Felekyan, S., Bleckmann, A., Seidel, C.A., and Simon, R. (2015). Real-time dynamics of peptide ligand-dependent receptor complex formation in planta. Sci. Signal. *8*, ra76.
24. Anne, P., and Hardtke, C.S. (2018). Phloem function and development-biophysics meets genetics. Curr. Opin. Plant Biol. *43*, 22–28.
25. Lavrekha, V.V., Pasternak, T., Ivanov, V.B., Palme, K., and Mironova, V.V. (2017). 3D analysis of mitosis distribution highlights the longitudinal

zonation and diarch symmetry in proliferation activity of the Arabidopsis thaliana root meristem. Plant J. *92*, 834–845.

26. Furuta, K.M., Yadav, S.R., Lehesranta, S., Belevich, I., Miyashima, S., Heo, J.O., Vatén, A., Lindgren, O., De Rybel, B., Van Isterdael, G., et al. (2014). Plant development. Arabidopsis NAC45/86 direct sieve element morphogenesis culminating in enucleation. Science *345*, 933–937.
27. Czyzewicz, N., Wildhagen, M., Cattaneo, P., Stahl, Y., Pinto, K.G., Aalen, R.B., Butenko, M.A., Simon, R., Hardtke, C.S., and De Smet, I. (2015). Antagonistic peptide technology for functional dissection of CLE peptides revisited. J. Exp. Bot. *66*, 5367–5374.
28. Rodriguez-Villalon, A., Gujas, B., van Wijk, R., Munnik, T., and Hardtke, C.S. (2015). Primary root protophloem differentiation requires balanced phosphatidylinositol-4,5-biphosphate levels and systemically affects root branching. Development *142*, 1437–1446.
29. Marhava, P., Bassukas, A.E.L., Zourelidou, M., Kolb, M., Moret, B., Fastner, A., Schulze, W.X., Cattaneo, P., Hammes, U.Z., Schwechheimer, C., and Hardtke, C.S. (2018). A molecular rheostat adjusts auxin flux to promote root protophloem differentiation. Nature *558*, 297–300.
30. Anne, P., Azzopardi, M., Gissot, L., Beaubiat, S., Hématy, K., and Palauqui, J.C. (2015). OCTOPUS negatively regulates BIN2 to control phloem differentiation in Arabidopsis thaliana. Curr. Biol. *25*, 2584–2590.
31. Breda, A.S., Hazak, O., and Hardtke, C.S. (2017). Phosphosite charge rather than shootward localization determines OCTOPUS activity in root protophloem. Proc. Natl. Acad. Sci. USA *114*, E5721–E5730.
32. Kang, Y.H., Breda, A., and Hardtke, C.S. (2017). Brassinosteroid signaling directs formative cell divisions and protophloem differentiation in Arabidopsis root meristems. Development *144*, 272–280.
33. Kang, Y.H., and Hardtke, C.S. (2016). Arabidopsis MAKR5 is a positive effector of BAM3-dependent CLE45 signaling. EMBO Rep. *17*, 1145–1154.
34. Fiers, M., Golemiec, E., Xu, J., van der Geest, L., Heidstra, R., Stiekema, W., and Liu, C.M. (2005). The 14-amino acid CLV3, CLE19, and CLE40 peptides trigger consumption of the root meristem in Arabidopsis through a CLAVATA2-dependent pathway. Plant Cell *17*, 2542–2553.
35. Müller, R., Bleckmann, A., and Simon, R. (2008). The receptor kinase CORYNE of Arabidopsis transmits the stem cell-limiting signal CLAVATA3 independently of CLAVATA1. Plant Cell *20*, 934–946.
36. Ruiz Sola, M.A., Coiro, M., Crivelli, S., Zeeman, S.C., Schmidt Kjølner Hansen, S., and Truernit, E. (2017). OCTOPUS-LIKE 2, a novel player in Arabidopsis root and vascular development, reveals a key role for OCTOPUS family genes in root metaphloem sieve tube differentiation. New Phytol. *216*, 1191–1204.
37. Rodrigues, A., Santiago, J., Rubio, S., Saez, A., Osmont, K.S., Gadea, J., Hardtke, C.S., and Rodriguez, P.L. (2009). The short-rooted phenotype of the brevis radix mutant partly reflects root abscisic acid hypersensitivity. Plant Physiol. *149*, 1917–1928.
38. Kurihara, D., Mizuta, Y., Sato, Y., and Higashiyama, T. (2015). ClearSee: a rapid optical clearing reagent for whole-plant fluorescence imaging. Development *142*, 4168–4179.
39. Wahl, M., Koberling, F., Patting, M., Rahn, H., and Erdmann, R. (2004). Time-resolved confocal fluorescence imaging and spectrocopy system with single molecule sensitivity and sub-micrometer resolution. Curr. Pharm. Biotechnol. *5*, 299–308.
40. Voinnet, O., Rivas, S., Mestre, P., and Baulcombe, D. (2003). An enhanced transient expression system in plants based on suppression of gene silencing by the p19 protein of tomato bushy stunt virus. Plant J. *33*, 949–956.
41. Lampropoulos, A., Sutikovic, Z., Wenzl, C., Maegele, I., Lohmann, J.U., and Forner, J. (2013). GreenGate—a novel, versatile, and efficient cloning system for plant transgenesis. PLoS ONE *8*, e83043.

STAR★METHODS

KEY RESOURCES TABLE

REAGENT or RESOURCE	SOURCE	IDENTIFIER
Bacterial and Virus Strains		
Agrobacterium tumefaciens GV3101 pMP90	widely distributed	N/A
Chemicals, Peptides, and Recombinant Proteins		
CLE45 peptide, custom synthesized	Genscript	N/A
CLE40 peptide, custom synthesized	Genscript	N/A
CLE26 peptide, custom synthesized	Genscript	N/A
CLE25 peptide, custom synthesized	Genscript	N/A
CLE21 peptide, custom synthesized	Genscript	N/A
CLE20 peptide, custom synthesized	Genscript	N/A
CLE18 peptide, custom synthesized	Genscript	N/A
CLE16 peptide, custom synthesized	Genscript	N/A
CLE14 peptide, custom synthesized	Genscript	N/A
CLE13 peptide, custom synthesized	Genscript	N/A
CLE11 peptide, custom synthesized	Genscript	N/A
CLE9/10 peptide, custom synthesized	Genscript	N/A
CLV3 peptide, custom synthesized	Genscript	N/A
Experimental Models: Organisms/Strains		
Arabidopsis thaliana Col-0 wild-type background	widely distributed	N/A
Nicotiana benthamiana	widely distributed	N/A
Saccharomyces cerevisiae NMY51	Dual System Biotech	N/A
Arabidopsis thaliana BAM3::NLS-3XVENUS transgenic line	this study	N/A
Oligonucleotides		
PP2A-A3 qPCR forward GCA ATC TCT CAT TCC GAT AGT C	Microsynth	N/A
PP2A-A3 qPCR reverse ATA CCG AAC ATC AAC ATC TGG	Microsynth	N/A
actin qPCR forward CCC TCG TAG ATT GGC ACA GT	Microsynth	N/A
actin qPCR reverse GCC ATC CAA GCT GTT CTC TC	Microsynth	N/A
BAM3 qPCR forward CGT CGT TTT AGC TGT GGT CA	Microsynth	N/A
BAM3 qPCR reverse TGC AAC TTC TTC TCC GTT TG	Microsynth	N/A
Software and Algorithms		
GraphPad Prism version 7.0e	GraphPad software	N/A

LEAD CONTACT AND MATERIALS AVAILABILITY

Further information and requests for resources and reagents should be directed to and will be fulfilled by the Lead Contact, Christian S. Hardtke (christian.hardtke@unil.ch). There are no restrictions to the availability of reagents.

EXPERIMENTAL MODEL AND SUBJECT DETAILS

Plant materials and growth conditions

Arabidopsis thaliana Columbia-0 (Col-0) was used as the wild-type for phenotypic analyses and is the background of all mutants investigated: *ops-2* [9]; *brx-2* [37]; *bam3-2* [18]; *ops*^{E319K} [8]; the *clv2* allele *rlp10-1* and *crn-10* [21]. Transgenic constructs used in this study have been described before [8, 18, 21, 28, 31], except *BAM3::NLS-3XVENUS*, which was a gift from Dr. P. Cattaneo. Seeds were surface sterilized, germinated and grown vertically under continuous light at 22°C on 0.5X Murashige and Skoog media supplemented with 0.8% or 1% agar, and 0.3% or 1.0% sucrose (media was homogeneous within a given experiment).

METHOD DETAILS

Quantitative real-time PCR

To determine *BAM3* expression levels, 5mm root tips were collected from 7-day-old seedlings for total RNA extraction (QIAGEN), and cDNAs were produced by reverse transcriptase (Invitrogen). Quantitative real-time PCR was performed in triplicate on three biological replicates (Data S1) using MESA Blue qPCR MasterMix Plus for SYBR assay Low Rox (Eurogentec). *PP2A-A3* and *ACTIN* were used as reference genes (primers 5′-GCA ATC TCT CAT TCC GAT AGT C-3′ + 5′-ATA CCG AAC ATC AAC ATC TGG-3′ and 5′-CCC TCG TAG ATT GGC ACA GT-3′ + 5′-GCC ATC CAA GCT GTT CTC TC-3′, respectively). *BAM3* transcripts were quantified using primers 5′-CGT CGT TTT AGC TGT GGT CA-3′ and 5′-TGC AAC TTC TTC TCC GTT TG-3′.

Physiological assays

All assays were performed in tissue culture under the growth conditions specified above. CLE peptides were obtained from a commercial supplier (Genscript), synthesized at > 80% purity, diluted in water and used at final concentration as indicated. For root length measurements, plates were scanned at 600 dpi resolution, and seedling root length was determined using Fiji software. To investigate OPS protein stability, 5-day-old seedlings were transferred to media containing 50 μM of the protein synthesis inhibitor cycloheximide. At the end of the treatment, the seedlings were transferred to fixation solution (4% paraformaldehyde in 1X PBS) for one hour, washed with 1X PBS and cleared with ClearSee solution [38]. One hour before imaging, samples were incubated with Calcofluor white solution (0.2% in ClearSee solution) to stain the cell walls. Fluorescence intensity of OPS-GFP or OPS^{E319K}-GFP was measured at the plasma membrane of protophloem cells using the segmented line tool of the Fiji software. The raw measurements of the assays are available in Data S1.

Reporter detection and microscopy

GUS reporter staining was performed as described previously [18, 28]. Fluorescent protein signals were acquired by confocal microscopy using Zeiss LSM 700, 710 or 880 inverted confocal scanning microscopes following standard procedures [21, 31]. Pictures were taken with 20 × or 40 × water/oil immersion objectives. For comparisons, samples were grown in parallel and analyzed on the same day, with identical microscopy settings, unless indicated otherwise.

FRET/FLIM interaction studies

For the initial FRET-FLIM studies, leaves of 4-week-old *Nicotiana benthamiana* plants were co-infiltrated with *A. tumefaciens* cultures carrying T-DNA constructs of CRN-CFP together with either CLV2-CITRINE, OPS-CITRINE, or CLV2-CITRINE and OPS-CITRINE, all expressed under the *35S* promoter. The fluorescence lifetime of CRN-CFP was measured in these leaves after 2 and 3 days at the plasma membrane of transformed epidermis cells, using a Leica SP8 with the PicoHarp 300 TCSPC Module and a pulsed 440 nm laser at 10 kHz. At last 1000 counts/pixel were acquired for 25 images for every co-infiltration. The recorded decay plots were fitted against a erythrosine B decay plot using an exponential reconvolution model (n = 2) [39] for lifetime calculations.

The subsequent lifetime analyses were performed in a transient *Nicotiana benthamiana* expression system, using plants cultivated 4 weeks under standard greenhouse conditions before infiltration of leaves with *Agrobacterium tumefaciens* strain GV3101 pMP90 harboring the silencing suppressor p19 [40] and the expression plasmids for the fluorophore-tagged proteins of interest. The Gateway compatible vectors pABindGFP and pABindmCh [22] provide an estradiol-inducible transgene activation mechanism and were completed via LR-reaction with the coding regions of *CRN* (At5G13290), *CLV2* (AT1G65380), *BAM3* (At4g20270), *OPS* (AT3G09070), and *FLS2* (AT5G46330) as a plasma membrane-localized negative control. For constitutive expression under the *UBQ10* or the *35S* promoter, additional transgenes were constructed using GreenGate cloning [41]. The BAM3 deletion construct encompassed amino acids 1 to 691. The CRN deletion construct encompassed amino acids 1 to 93. *A. tumefaciens* strains were cultivated overnight and adjusted to an OD_{600nm} of 0.3 each in 5% (w/v) sucrose, 450μM acetosyringone, and 0.01% (v/v) silwet, and incubated for 2h at 4°C prior to infiltration. After 2-3 days plants were induced by spraying 20μM estradiol + 0.1% Tween-20 and analyzed within 6 to 20 h. For CLE45 treatments, transformed plants were infiltrated with mock (5% sucrose, 0.02% Silwet) or CLE45 solution (5% sucrose, 0.02% Silwet, 10μM CLE45), and FRET/FLIM measurements were performed 5-30 min. immediately after. For FRET/FLIM measurements, a Zeiss confocal laser scanning microscope LSM 780 (40x water immersion objective, Zeiss C-PlanApo, NA 1.2) equipped with a single-photon counting device (PicoQuant Hydra Harp 400) was used. The GFP donor was excited at 485 nm by a linearly polarized diode laser (LDH-D-C-485) working at a frequency of 32 MHz. Excitation power was adjusted to 1 μW. Emission was detected in perpendicular and parallel polarization by Tau-SPADs (PicoQuant) with a band-pass filter (520/35 AHF). Image acquisition was done at zoom 8 with a frame size of 256 × 256 and a pixel dwell time of 12.6 μs, taking 60 frames for each measurement. To calculate the average lifetime of each measurement, further analysis was performed using PicoQuant SymphoTime software applying a biexponential fit. The displayed values are intensity-weighted mean lifetimes τ in ns. Data were obtained from at least 3 independent experiments. The raw measurements of the assays are available in Data S1.

Yeast split ubiquitin assays

Split ubiquitin assays were performed using the DUAL Membrane system (Dual System Biotech). The full coding sequence of OPS was inserted into the pPR3-N vector by SfiI restriction. Truncated versions of BAM3 and CRN were cloned into the pPR3-SUC and pBT3-SUC vectors by SfiI restriction, respectively, such that their target peptide sequence was replaced by the yeast target peptide.

The yeast NMY51 strain was then co-transformed with 250ng of prey and 250ng of bait vectors by thermic shock and selected on SD -LW media. Colonies were transferred onto SD – LWH (+/−3AT) to monitor interactions. Plasma membrane-localized Fur4-NubI was used as a positive control, Fur4-NubG as a negative control.

QUANTIFICATION AND STATISTICAL ANALYSIS

Statistical analyses were performed in Graphpad Prism software, version 7.0e. Details for each pertinent figure panel are available in Data S1.

DATA AND CODE AVAILABILITY

The published article includes all datasets generated or analyzed during this study.

Current Biology, Volume *29*

Supplemental Information

A Cellular Insulator

against CLE45 Peptide Signaling

Alice S. Breda, Ora Hazak, Patrick Schultz, Pauline Anne, Moritz Graeff, Rüdiger Simon, and Christian S. Hardtke

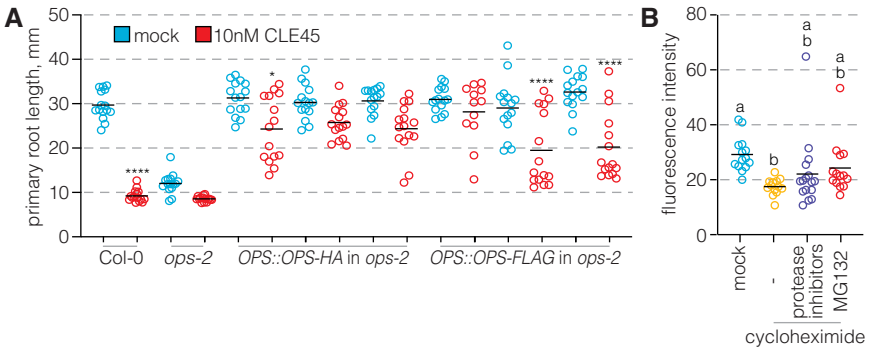

Figure S1. Various assays, related to Figure 2. (A) CLE45 response of seedlings that carry the indicated transgenes in *ops-2* background (three independent lines per transgenic genotype). Statistically significant difference compared to mock is indicated. (B) Quantification of GFP fluorescence in roots of seedlings that express an *OPS::OPS-GFP* transgene, after 1h mock or 50μM cycloheximide treatment, with or without protease inhibitor cocktail or MG132 proteasome inhibitor (averages of 7-16 roots, 7-14 cells per root). 7-day-old seedlings. Plots display individual values (dots) and the mean (bar). * = $p<0.05$; **** = $p<0.0001$; See Data S1 for statistical test details.

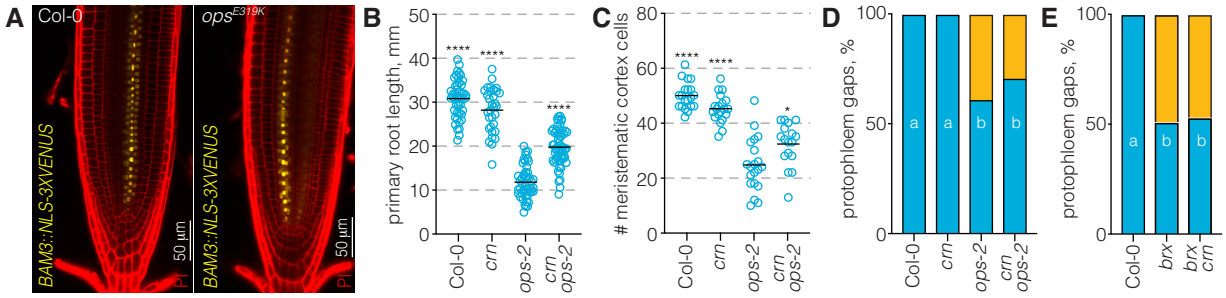

Figure S2. Partial rescue of *ops-2* phenotypes by *crn* loss-of-function, related to Figure 2. (A) Expression of an NLS-3XVENUS reporter (yellow fluorescence) under control of the *BAM3* promoter, in indicated genotypes. (B) Root length in seedlings of indicated genotypes. Statistically significant difference compared to *ops-2* is indicated. (C) Meristematic cortex cell number, indicative of root meristem size, in seedlings of indicated genotypes. Statistically significant difference compared to *ops-2* is indicated. (D-E) Frequency of protophloem strands with gap cells (yellow) in indicated genotypes. 7-day-old seedlings. Plots display individual values (dots) and the mean (bar). * = p<0.05; **** = p<0.0001; See Data S1 for statistical test details.

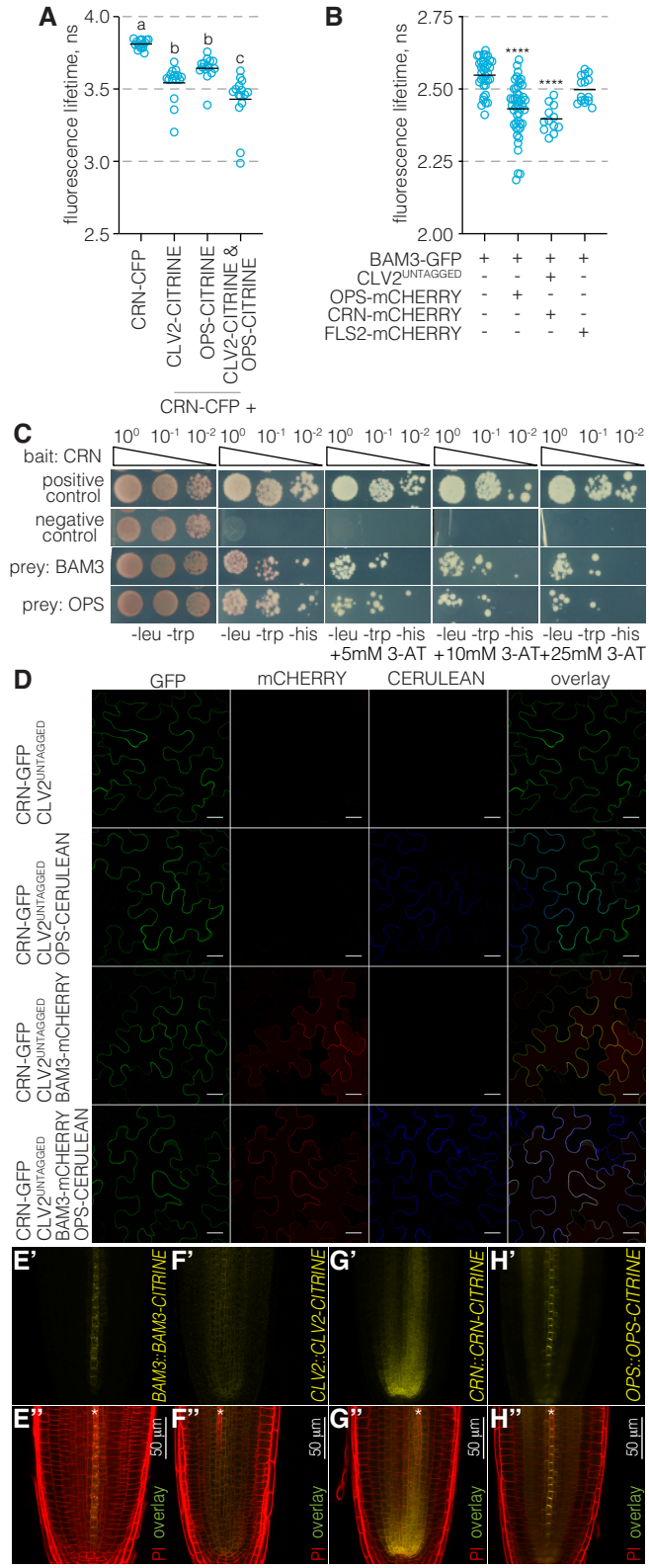

Figure S3. Protein interactions between CLE45 signaling components and OPS, related to Figure 3. (A) FRET-FLIM measurements of indicated fusion proteins expressed in transiently transformed *N. benthamiana* cells, under constitutive promoter. (B) *N. benthamiana* FRET-FLIM measurements of BAM3-GFP in combination with indicated fusion proteins, under inducible promoter. Statistically significant difference compared to BAM3-GFP control is indicated. (C) Yeast split ubiquitin protein interaction assays with CRN as bait and indicated proteins as prey. (D) Expression of FRET-FLIM fusion proteins in *N. benthamiana*, representative confocal microscopy images. Different fluorescence channels (left to right) are shown for different protein combinations (top to bottom). All proteins were expressed constitutively except OPS-CERULEAN, which was induced. Size bars are 25µm. (E-H) Confocal microscopy images demonstrating fusion protein expression levels in the wild type situation, representative lines. For comparison of approximate abundance, all samples were imaged in parallel with the same settings, except CLV2-CITRINE for which gain had to be increased to detect the protein. Plots display individual values (dots) and mean (bar). **** = p<0.0001; See Data S1 for statistical test details.

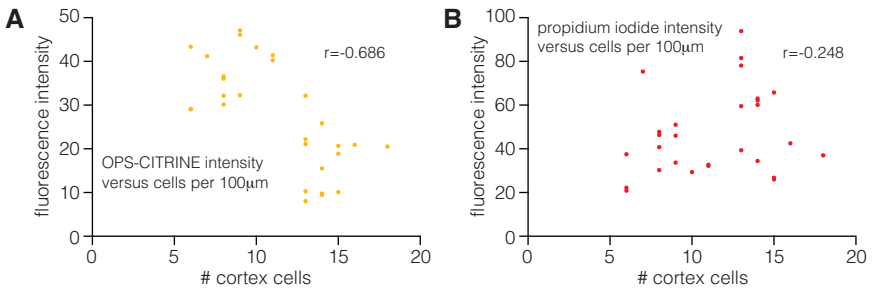

Figure S4. Correlation between OPS-CITRINE signal intensity and root meristem phenotype, related to Figure 4. (A) Mean OPS-CITRINE fluorescence intensity in *UBQ10::OPS-CITRINE* plants, measured across the center of cortex cell files, for 100µm starting from the first cortex cell, plotted against the number of cells encompassed by the trace. (B) As in A), for corresponding propidium iodide traces. Note that correlations reflect a lower and upper bound, respectively, because of the plasma membrane-association of OPS-CITRINE and the apoplastic propidium iodide staining, combined with the fact that a stronger phenotype is reflected in fewer cells.

Chapter V

Over the rainbow: A practical guide for fluorescent protein selection in plant FRET experiments

This manuscript was published in Plant Direct in November 2019.

https://doi.org/10.1002/pld3.189

Authors:

Grégoire Denay[1], Patrick Schultz[1°], Sebastian Hänsch[2], Stefanie Weidtkamp-Peters[2], Rüdiger Simon[1]

Affiliations:

[1] Institute for Developmental Genetics, Heinrich Heine University, 40225 Düsseldorf, Germany

[2] Center for Advanced Imaging, Heinrich Heine University, 40225 Düsseldorf, Germany

° present name: Patrick Blümke

Author contributions:

GD conceived the project and designed the experiments with input from all authors. GD prepared the figures and wrote the manuscript with the help of RS. GD and PS created expression vectors and performed measurements. GD, PS, and SH analyzed the data. SH and SWP provided critical help with lifetime measurement and analysis. All authors discussed the results and commented on the manuscript.

Received: 16 September 2019 | Revised: 7 November 2019 | Accepted: 8 November 2019

DOI: 10.1002/pld3.189

ORIGINAL RESEARCH

Over the rainbow: A practical guide for fluorescent protein selection in plant FRET experiments

Grégoire Denay[1] | Patrick Schultz[1] | Sebastian Hänsch[2] | Stefanie Weidtkamp-Peters[2] | Rüdiger Simon[1]

[1]Institute for Developmental Genetics, Heinrich Heine University Düsseldorf, Düsseldorf, Germany

[2]Center for Advanced Imaging, Heinrich Heine University Düsseldorf, Düsseldorf, Germany

Correspondence
Rüdiger Simon, Institute for Developmental Genetics, Heinrich Heine University Düsseldorf, Universitätsstraße 1, Düsseldorf 40225, Germany.
Email: ruediger.simon@hhu.de

Abstract

Receptor-like kinases (RLK) and receptor-like proteins (RLP) often interact in a combinatorial manner depending on tissue identity, membrane domains, or endo- and exogenous cues, and the same RLKs or RLPs can generate different signaling outputs depending on the composition of the receptor complexes they are involved in. Investigation of their interaction partners in a spatial and dynamic way is therefore of prime interest to understand their functions. This is, however, limited by the technical complexity of assessing it in endogenous conditions. A solution to close this gap is to determine protein interaction directly in the relevant tissues at endogenous expression levels using Förster resonance energy transfer (FRET). The ideal fluorophore pair for FRET must, however, fulfil specific requirements: (a) The emission and excitation spectra of the donor and acceptor, respectively, must overlap; (b) they should not interfere with proper folding, activity, or localization of the fusion proteins; (c) they should be sufficiently photostable in plant cells. Furthermore, the donor must yield sufficient photon counts at near-endogenous protein expression levels. Although many fluorescent proteins were reported to be suitable for FRET experiments, only a handful were already described for applications in plants. Herein, we compare a range of fluorophores, assess their usability to study RLK interactions by FRET-based fluorescence lifetime imaging (FLIM) and explore their differences in FRET efficiency. Our analysis will help to select the optimal fluorophore pair for diverse FRET applications.

KEYWORDS

fluorescence imaging, förster resonance energy transfer, membrane proteins, protein–protein interactions, receptor-like kinase

1 | INTRODUCTION

Receptor-like kinases (RLK) are essential components of the plant signaling machinery. They serve to coordinate developmental processes, pathogen recognition, symbiotic interaction with beneficial microorganisms, or other aspects of environmental sensing (Osakabe, Yamaguchi-Shinozaki, Shinozaki, & Tran, 2013). RLKs usually act in complexes consisting of a receptor and a co-receptor,

This manuscript was previously deposited as a preprint at https://doi.org/10.1101/734616

and can form higher-order complexes that rearrange dynamically upon ligand perception (Wan, Fröhlich, Pruitt, Nürnberger, & Zhang, 2019). The same receptors can interact with different partners and be a part of different complexes with different signaling specificity (Bücherl et al., 2017; Liebrand, Burg, & Joosten, 2014; Wan et al., 2019). Most studies of RLK interaction initially relied on in vitro experiments and could not provide insights into the spatial localization and complexity of interactions. However, advances in imaging techniques now allow to study colocalization and interactions of RLKs in living plant cells (Bücherl et al., 2017; Somssich et al., 2015). In particular, Förster Resonance Energy Transfer (FRET) is an attractive technique as it allows to resolve protein–protein interactions in live plants in a cell-specific and dynamic manner (Lampugnani, Wink, Persson, & Somssich, 2018; Long et al., 2017; Somssich et al., 2015; Weidtkamp-Peters & Stahl, 2017).

Determination of protein interaction by FRET relies on the energy transfer from a fluorescent donor to an acceptor fluorophore. This phenomenon leads to fluorescence quenching of the donor and radiation-free energy transfer to the acceptor, which becomes in an excited state. Energy can be relaxed by fluorescence emission (Förster, 1946). FRET requires that several conditions are met: (a) The emission spectrum of the donor must overlap with the excitation spectrum of the acceptor; (b) both molecules must be in close proximity (typically < 10 nm); and (c) the dipole moments of both fluorophores must be aligned (Bajar, Wang, Zhang, Lin, & Chu, 2016; Clegg, 2006; Förster, 1946). FRET can be measured in several different ways including intensity-based methods, spectral recording, photobleaching, anisotropy, or fluorescence lifetime (Bajar, Wang, Zhang, et al., 2016; Pietraszewska-Bogiel & Gadella, 2011). Each molecular complex exhibits a specific FRET efficiency, which depends in part on relative fluorophore distance and orientation. However, as FRET is measured through diffraction-limited microscopy, only the apparent FRET efficiency, which represents a mean FRET efficiency in the observation volume, is experimentally accessible (Bajar, Wang, Zhang, et al., 2016). We will refer to the apparent FRET efficiency in the following as "FRET efficiency," by extension.

Fluorophore pairs for FRET experiments should have a considerable overlap between their emission and excitation spectra, yield a sufficient brightness to fit the fluorescence decay and limit background fluorescence, allow proper folding of the fused protein, do not affect localization, and do not trigger artefactual interactions. There is now a large choice of available fluorescent proteins (Lambert, 2019); however, most of these fluorophores were characterized solely in vitro or in mammalian cell systems (Bajar, Wang, Zhang, et al., 2016; van der Krogt, Ogink, Ponsioen, & Jalink, 2008). The plant community focused mostly on the use of the GFP-RFP pair (and their derivatives eGFP and mCherry) for FRET experiments (Lampugnani et al., 2018). Additionally, CFP-YFP and other pairs based on improvements upon CFP or YFP were used in plant systems, notably for the Cameleon calcium sensors (Kanchiswamy, Malnoy, Occhipinti, & Maffei, 2014). Only one study assessed the quality of different FRET pairs in plants and focused on using SYFP2 either as an acceptor for SCFP3A or mTurquoise, or as a donor for mStrawberry, mCherry, or mRFP (Long et al., 2018). In this study, the root expressed transcription factors that were analyzed are relatively tolerant to fusions with additional protein domains. However, many membrane proteins consisting of domains with very different properties appear to be more sensitive.

In order to test the suitability of a set of genetically encoded fluorophores for FRET-FLIM applications with membrane-localized proteins in plants, we chose the CORYNEΔkinase (CRNΔKi)—a kinase-deleted version of CRN—and CLAVATA2 (CLV2), a receptor-like protein with extracellular leucine-rich-repeats (LRRs) from Arabidopsis thaliana as a test system. Both are membrane localized due to their transmembrane domains, and their interaction in vivo has been reported in a number of previous studies (Bleckmann, Weidtkamp-Peters, Seidel, & Simon, 2010; Breda et al., 2019; Kinoshita et al., 2010; Zhu et al., 2010). CRN and CLV2 are obligate heteromers, and their interaction is necessary for export form the endoplasmic reticulum (ER) to the plasma membrane (PM) (Bleckmann et al., 2010; Somssich, Bleckmann, & Simon, 2016). Fusions of fluorophores such as eGFP and mCherry to the cytoplasmic domains of CRNΔKi and CLV2, respectively, showed a very high FRET efficiency (Bleckmann et al., 2010; Somssich & Simon, 2017). For these reasons, CLV2/CRN form an attractive test system to compare the performances of different FRET pairs to study plant membrane proteins interaction: High FRET efficiency can yield a more sensitive readout for comparison, and inactive fusion proteins unable to interact with their RLK partner will remain localized in the ER. To objectively compare different fluorophore pairs for plant FRET assays of RLK, we observed parameters such as localization, photo-stability, and FRET efficiency for several different FRET pairs, including several so far untested combinations in plant systems.

2 | MATERIAL AND METHODS

2.1 | Generation of GreenGate entry plasmids

Unless otherwise stated, template, destination, and additional entry plasmids used in this work were previously described and are available from the GreenGate cloning kit (Lampropoulos et al., 2013).

The XVE coding sequence was amplified from pABindGFP (Bleckmann et al., 2010) with primers GG_XVE_F and GG_XVE_R (Table S1), internal *Bsa*I site was removed with PW_XVE_3084_AT_R and PW_XVE_3084_TA_F, and the product was cloned in pGGC000 to create pRD71. The LexA-mini35S promoter was amplified from pABindGFP (Bleckmann et al., 2010) with primers GG_EST_F and GG_EST_R and cloned in pGGA000 to create pBLAA001. The coding sequences from CLV2 and CRNΔKi were amplified from pAB125 and pAB128 (Bleckmann et al., 2010) with PS-GG-CDS-Clv2-F and PS-GG-CDS-Clv2-R, and oGD335 and oGD336, respectively, and cloned in pGGC000 to create pGD292 and pGD293. The myristoylation sequence (myr) was created by annealing oGD339 and oGD340 before cloning the resulting double-stranded oligonucleotide in pGGC000 to create pGD318. The resistance dummy cassette

contains the very short SV40 origin of replication which was amplified from pmCherry-N1 (Clontech) with PW_GG_SV40ori_F and PW_GG_SV40ori_R and cloned in pGGF000 to create pPW53.

eGFP coding sequence was amplified from pGGD001 with oGD261 and oGD262 and cloned in pGGD000 to create pGD165. Clover coding sequence was amplified from Clover-mRuby2-FRET-10 (M. Davidson, Addgene) with oGD317 and oGD318 and cloned in pGGD000 with a linker made up by annealing oGD315 and oGD316 (D-TGCA linker) to create pGD250. mCerulean3 coding sequence was amplified from pmCer3-N1 (Markwardt et al., 2011) with oGD317 and oGD318 and cloned in pGGD000 with the D-TGCA linker to create pGD251. T-Sapphire coding sequence was amplified from *Pst*I-digested p35S::T-Sapphire-mOrange-nos plasmid (Bayle, Nussaume, & Bhat, 2008) with oGD317 and oGD318 and cloned in pGGD000 with the D-TGCA linker to create pGD252. mTurquoise2 was amplified from mTurquoise2-N1 (Goedhart et al., 2012) and cloned in pGGD000 with the D-TGCA linker to create pGD425. mRuby2 coding sequence was amplified from Clover-mRuby2-FRET-10 with oGD325 and oGD326 and cloned in pGGD000 to create pGD253. mRuby3 was amplified from pNCS-mRuby3 (Bajar, Wang, Lam, et al., 2016) with oGD325 and oGD318 and cloned into pGGD000 to create pGD341. mOrange coding sequence was amplified from p35S::T-Sapphire-mOrange-nos with oGD318 and oGD331, followed by a second PCR with oGD327 and oGD318 and cloned in pGGD000 to create pGD254. Venus coding sequence was amplified from pABindVenus (Bleckmann et al., 2010) with oGD317 and oGD318 and cloned in pGGD000 with the D-TGCA linker to create pGD255. mNeonGreen coding sequence was amplified from pNCS-mNeonGreen (Allele Biotechenology) with oGD343 and oGD344 and cloned in pGGD000 with the D-TGCA linker to create pGD352. mCherry coding sequence was amplified from pGGC015 with RD_GG_mCherry_C-tag_F and RD_GG_mCherry_C-tag_R cloned in pGGD000 to create pRD53. mScarlet coding sequence was amplified from pmScarlet-C1 (Bindels et al., 2017) with RD_GG_mScarlet_C-tag_R and RD_GG_mScarlet_C-tag_F cloned in pGGD000 to create pRD134. mKate2 coding sequence was amplified from pmKate2-C1 (Shcherbo et al., 2009) with RD_mKate2_GG_C-tag_R and RD_mKate2_GG_C-tag_F cloned in pGGD000 to create pRD141.

2.2 | Generation of transient expression plasmids

The plasmid backbone containing the XVE expression cassette under the control of the 35S promoter and RBCS terminator, and the A and G GreenGate cloning sites (pGD283) was generated by combining the inserts from pGGA004 (p35S), pGGB002 (Omega element), pRD71 (XVE), pGGD002 (N-dummy), pGGE001 (tRBCS), pGGG001 (F-H adapter), and a double-stranded methylated linker containing H and G GreenGate sites (Table S1) into pGGZ001 in a single step GreenGate reaction (Lampropoulos et al., 2013).

Individual expression cassettes were prepared as intermediate plasmids. Donor constructs were prepared by combining pBLAA001 (pLexA-mini35S), pGGB002, pGD293 (CRNΔKi), fluorophore entry plasmid, pGGE009 (tUBQ10), and pGGG001 (F-H adapter) into pGGM000 in a single step GreenGate reaction. For the acceptor constructs, pGD293 was replaced by pGD292 (CLV2) or pGD318 (myr) and pGGG001 by pGGG002 (H-A adapter), pPW53 was added and pGGN000 was used as a destination plasmid. For the donor and acceptor only constructs, untagged CRNΔKi and CLV2 expression cassettes were generated using pGGD002 in place of a fluorophore entry plasmid.

Transient expression plasmids containing both donor and acceptor fusion proteins were generated by combining the donor and the acceptor intermediate plasmids in the pGD283 backbone. For the expression of a single fusion protein, either the donor or acceptor intermediate plasmids were replaced with linkers with A-H or H-G overhangs (Table S1), respectively.

2.3 | Transient expression in *Nicotiana*

Nicotiana benthamiana infiltration was carried out using standard protocol (Li, 2011). Briefly, agrobacterium strain C58:pmp90:pSOUP carrying the expression plasmid were cultivated overnight in dYt medium. Cells were then pelleted and resuspended in infiltration medium ($MgCl_2$ 10 mM; MES-K 10 mM pH5.6; 150 μM acetosyringone) to an OD_{600} of 0.4 and incubated for 2 hr at room temperature. Bacteria solutions were then mixed in equal quantities with Agrobacterium strain GV3101:p19 expressing the p19 silencing inhibitor. For the co-infiltration of CRNΔKi-eGFP and CLV2-mCherry or CLV2 untagged, bacteria were resuspended in infiltration medium to an OD_{600} of 0.6 and mixed in 1:3 ratio with GV3101:p19 cells. Bacteria mixes were then infiltrated to the abaxial side of 3- to 4-week-old *Nicotiana benthamiana*. After 2–4 days under continuous light, protein expression was induced overnight by spraying the abaxial side of infiltrated leaves with an estradiol solution (Estradiol 20 μM; Tween-20 0.1%).

2.4 | Fluorescence imaging

Fluorescence imaging was performed with a Zeiss LSM 780 confocal microscope (40× Water immersion objective, Zeiss C-PlanApo, NA 1.2). T-Sapphire was excited at 405 nm; mCerulean3 and mTurquoise2 at 458 nm; Clover, mNeonGreen, and eGFP at 488 nm; Venus at 514 nm; and mCherry, mRuby2, mRuby3, mScarlet, mKate2, and mOrange at 561 nm. Signal for each fluorophore was recorded within the maximum emission peak while avoiding auto-fluorescence above 650 nm. The fluorescent properties of the fluorophores used here are available as "protein collection" on the website fpbase.org (https://www.fpbase.org/collection/332/).

2.5 | Time-correlated single photon counting

Fluorescence lifetime was acquired with a Zeiss LSM 780 confocal microscope (40× Water immersion objective, Zeiss C-PlanApo, NA 1.2). Time-correlated single photon counting was performed with

picosecond resolution (PicoQuant Hydra Harp 400). Fluorophores were excited with either a 440 nm (LDH-D-C-440, 32 MHz) or 485 nm (LDH-D-C-485, 32 MHz) pulsed polarized diode laser with a power of 1 μW at the objective lens. Emitted light was separated by a polarizing beam splitter and parallel and perpendicular photons were selected with a fluorophore-specific band-pass filter (Table S2) and detected with Tau-SPADs (PicoQuant) simultaneously for the acceptor and donor channels. Image acquisition was done at zoom 8 with a resolution of 256x256 pixel with a pixel size of 0.1 μm a dwell time of 12.6 μs, and photons were collected over 60 frames. Special care was taken during imaging to avoid chloroplasts-containing regions and cells with very high donor expression to avoid pile-up effect.

2.6 | Fluorescence decay analysis

Fluorescence decay was analyzed in Symphotime 64 (version 2.4; PicoQuant) using the Lifetime FRET Image analysis tool. Only data from the donor parallel channel were kept for the analysis. TCSPC channels were binned by eight, count threshold was set so that the background was removed, and chloroplasts were manually removed. Additionally, in case some pixels were above the pile-up limit (10% of the laser repetition rate, *that is* 2,421 counts), they were manually removed; counts values were in most cases below 5% of the laser repetition rate. Internal response function was determined by measuring the fluorescence decay of saturated erythrosine, or Atto425 dye for blue donors, quenched in saturated KI using the same hardware settings as for the FRET pair of interest. Fluorescence decay was fitted using a multi-exponential decay, and the amplitude-weighted lifetime was considered as the sample's apparent lifetime. FRET efficiency was calculated as the lifetime of the FRET sample over the arithmetic mean of the lifetimes of the donor-only samples measured in the same experiment: $FRET_{eff} = 1 - \left(\frac{\tau_{FRET}}{\tau_{donor}}\right)$. All measurements were done in at least two independent experiments.

2.7 | Fluorescence intensity measurement

To calculate the A/D ratio, donor and acceptor were excited with a 485 nm pulsed laser (LDH-D-C-485, 32 MHz, 1 μW) and intensities were recorded with Tau-SPADs (PicoQuant) in the setup described above. Fluorescence intensity was extracted using FIJI (Rueden et al., 2017; Schindelin et al., 2012). Membrane regions were selected by thresholding the donor channel and the same ROI was applied on the acceptor channel and the signal's integrated density was measured in the ROI.

Background fluorescence was similarly measured by imaging mock-infiltrated plants and extracting the signal intensity over the whole image in the donor channel. Likewise, bleed-through measurements were performed on plants co-expressing CRNΔKi-untagged and CLV2-donor constructs. Donor intensities were calculated in the same way using donor-only samples.

For photobleaching, plants co-expressing either CRNΔKi-donor and CLV2-untagged or CRNΔKi-untagged and CLV2-donor were excited with the donor excitation laser and fluorescence was recorded as for a lifetime measurement. A ROI was set over the membrane, and fluorescence intensity was recorded in every frame.

3 | RESULTS

3.1 | Optimization of fusion protein co-expression in *Nicotiana*

A quick, easy, and reliable way to test protein–protein interaction by FRET in plants is to use transient expression systems in *Nicotiana benthamiana* (thereafter Nicotiana). For this, both fluorescently tagged proteins must be co-expressed in the same cells. A classical way of co-expressing proteins in Nicotiana is to infiltrate leaves with different plasmids, each carrying the expression cassette for a single protein (Norkunas, Harding, Dale, & Dugdale, 2018). This system, however, presents several problems: Co-expression is highly variable, ranging from only a few cells to almost all cells co-expressing both constructs (Hecker et al., 2015); in addition, the relative expression levels of both constructs are very variable from cell to cell (Figure 1d). Since FRET is measured with pixel-wise resolution and not at the single molecule level, apparent FRET will differ according to the relative concentration of donor and acceptor (Fábián, Rente, Szöllosi, Mátyus, & Jenei, 2010) (Figure 1a). It is also important to control expression levels as expression under strong promoters can trigger ER stress, protein aggregation, and artefactual interactions (Bleckmann et al., 2010; Zuo, Niu, Frugis, & Chua, 2002). To solve the latter problem, we used an estradiol-inducible expression system that was previously shown to allow controlled expression of CRN and CLV2 (Bleckmann et al., 2010).

With the aim of reducing variability in the ratio of acceptor to donor, we designed an expression vector allowing simultaneous expression of two distinct fusion proteins under the control of the estradiol-inducible system from a single T-DNA. We measured both Acceptor/Donor (A/D) fluorescence ratio and FRET efficiency of cells co-expressing CRNΔKi-eGFP and CLV2-mCherry from a single T-DNA and compared them to cells co-expressing from individual T-DNAs (Figure 1b and c). While co-expression from a single T-DNA did not significantly change the measured fluorescence intensity of GFP, it resulted in a strong reduction in the variance of the A/D ratio (*F* test, $p < .01$; Figure 1b). Surprisingly, the average A/D ratio was higher than when the fusion proteins were co-expressed from independent T-DNAs, although we cannot explain this effect. This resulted in the FRET efficiency being higher as more acceptor was available to quench the donor fluorophore (Figure 1c). Consistent with expectations, nearly all expressing cells co-expressed both constructs when carried on a single T-DNA (Figure 1d). In conclusion, co-expression of both fusion proteins from a single T-DNA proved to be a more suitable system for FRET analysis than the classical way of co-expressing proteins from distinct T-DNAs, for the following reasons: (a) It reduced the

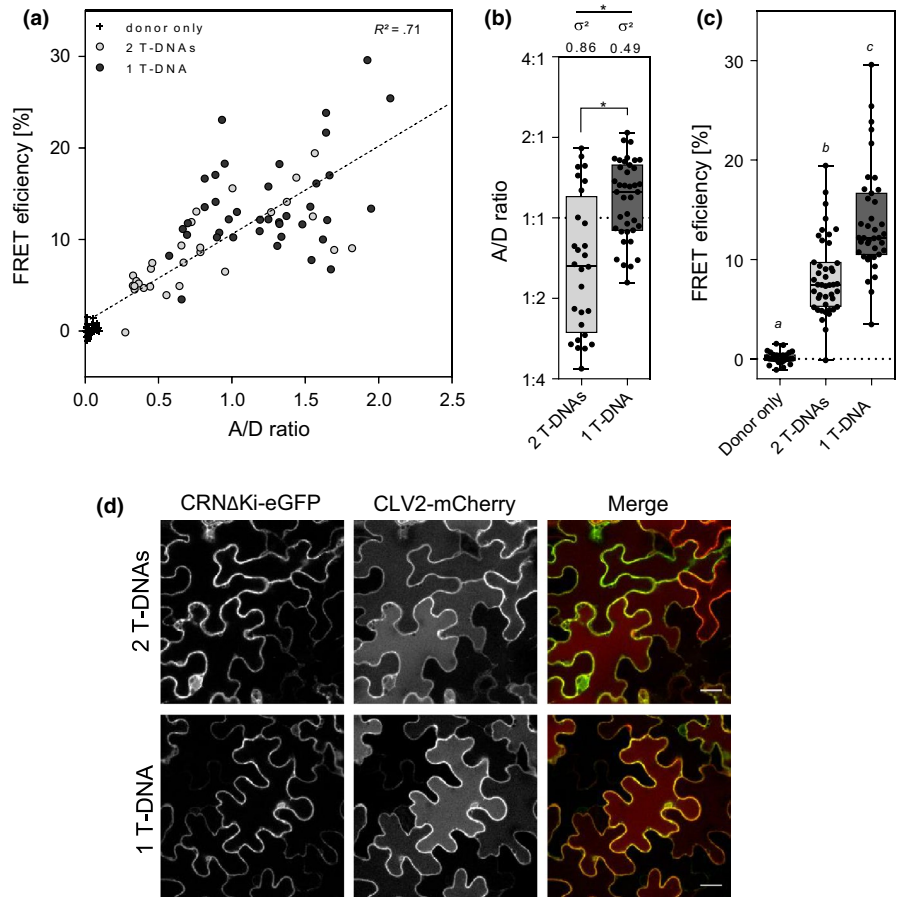

FIGURE 1 Comparison of the co-expression of fusion proteins from a single or two T-DNAs effect on FRET efficiency. (a) FRET efficiency depends on the expression ratio of acceptor to donor. A/D intensity ratio was calculated as a proxy for the relative level of each fusion protein and plotted against the FRET efficiency of the sample. Both variables are linearly correlated (R^2 = .71; dotted line). White: expression of CRNΔKi-eGFP only; dark gray: expression of both CRNΔKi-eGFP and CLV2-mCherry from a single T-DNA; light gray: expression of CRNΔKi-eGFP and CLV2-mCherry from distinct T-DNAs. (b) A/D ratio (Log2 scale) was significantly higher in samples co-expressing the two fusion proteins from a single T-DNA in comparison with those expressing from two T-DNAs (Tukey, $p < .0001$, $N \geq 28$). The variance (σ^2) of the two samples was also significantly different (F test $p < .01$). (c) FRET efficiency was significantly higher in samples co-expressing the two fusion proteins from a single T-DNA in comparison with those expressing from two T-DNAs (Tukey, $p < .0001$, $N \geq 29$). (d) Co-expression of CRNΔKi-eGFP (Green) and CLV2-mCherry (Red) from the single T-DNA (bottom row) results in a higher co-expression rate than when expressed from 2T-DNAs (top row). Yellow indicates colocalization of both eGFP and mCherry. Scale bar: 25 μm

variability in co-expression levels, thereby reducing the potential influence of relative protein concentration on apparent FRET and increasing measurement reproducibility; (b) it increased the apparent FRET due to lower mCherry expression in our hands; (c) it greatly improved the co-expression rate, reducing the amount of time spent finding suitable cells. We therefore used the co-expression system for the rest of this study.

3.2 | Selection and expression of fluorophore pairs for FRET measurements

Several fluorophore pairs were previously described to yield efficient FRET in plant or mammalian models (Table 1). We used the above described system allowing inducible transient co-expression of tagged CRNΔKi-donor and CLV2-acceptor fusion proteins from a single T-DNA to assess the quality of these different FRET pairs in Nicotiana cells.

FRET requires sufficient rotational freedom of the fluorophores, so that dipole moments can align and permit resonance energy transfer. The conformational state of the fusion proteins is, however, mostly unpredictable. Addition of linker sequences between the fusion protein and the fluorophore can increase the likelihood of FRET (Lissandron et al., 2005; Osad'ko, 2015; Stryer & Haugland, 1967), if the linker increases free rotation of the fluorophore while being short enough to keep the fluorophores in close proximity in case of complex formation. Whether a linker sequence improves FRET efficiency can be experimentally tested for individual protein combinations.

3.3 | Fluorophore effect on protein localization

CLV2 and CRN are exported from the ER to the PM only if they interact with each other via their transmembrane domains (Bleckmann et al., 2010; Somssich et al., 2016), and they therefore constitute a

TABLE 1 Overview of the FRET pairs used in this study

Donor	Acceptor	R_0 [Å]	Organism	Refs
Green-Red				
eGFP	mCherry	52.88	Human cell cultures *N. benthamiana*	(Albertazzi, Arosio, Marchetti, Ricci, & Beltram, 2009) (Bleckmann et al., 2010)
eGFP	mScarlet	56.75	Human cell cultures	(Bindels et al., 2017)
Clover	mRuby2	63.28	Human cell cultures	(Lam et al., 2012)
mNeonGreen	mRuby2	63.41	Human cell cultures	(Shaner et al., 2013)
mNeonGreen	mRuby3	64.17	Human cell cultures	(Bajar, Wang, Lam, et al., 2016)
Yellow-Red				
Venus	mKate2	54.55	*N. benthamiana*	Stahl Y. and Burkart R. (personal communication)
Venus	mRuby3	62.77	–	–
Cyan-Green				
mCerulean3	mNeonGreen	55.06	*N. benthamiana*	Somssich M. (personal communication)
mTurquoise2	mNeonGreen	61.55	Human cell cultures	(Mastop et al., 2017)
Cyan-Yellow				
mCerulean3	Venus	61.55	Mammalian cell cultures	(Markwardt et al., 2011)
mTurquoise2	Venus	57.62	Human cell cultures	(Mastop et al., 2017)
Green-Orange long-stoke shift				
T-Sapphire	mOrange	55.88	*N. benthamiana*	(Bayle et al., 2008)

Note: References for previously published FRET experiments and study organisms used are indicated.
Abbreviation: R_0, Förster radius of the FRET pair.

convenient system to investigate the correct folding and interaction of fusion proteins.

High levels of protein expression can result in overloading of the vesicular transport system and lead to protein retention in the ER and formation of organized smooth endoplasmic reticulum (OSER) through weak protein–protein interactions (Ferrero et al., 2015; Snapp et al., 2003). For these reasons we used the abovementioned estradiol-inducible system, allowing controlled expression of the transgene, so that the optimal timing for measurement can be tested for each fusion proteins. It was previously shown that a short induction time of 4h led to predominantly PM localization of CLV2 and CRN, while longer induction time of more than 12h led to the formation of protein aggregates and predominant ER localization (Bleckmann et al., 2010). However, in our hands, overnight expression of CRNΔKi-eGFP and CLV2-mCherry resulted in predominantly PM localization occasionally associated with ER localization, while aggregation was observed in only a few cells (Figure 1d). As FLIM experiments typically require extended amount of time, we used overnight induction and acquired fluorescence lifetime over the course of a full day. Expression of all gene constructs resulted in a minor amount of ER localization of the fusion proteins, in addition to their expected PM localization, but aggregation was rarely observed (Figure 2), indicating that none of the fluorophores significantly interfered with CLV2-CRN interaction.

Fusion proteins with Venus and Clover typically showed higher ER retention than other fluorophores. This may be due to the presence of an Alanine in position 206 of both proteins which is responsible for weak dimerization and the accumulation of membrane-localized fusion proteins in ER structures (Snapp et al., 2003; Zacharias, Violin, Newton, & Tsien, 2002). For this reason, the monomeric variants mClover3 and mVenus should be preferred for membrane proteins fusions. Expression of CRNΔKi-T-Sapphire and CLV2-mOrange was typically weak and showed extensive accumulation in cytoplasmic regions in zones of high membrane curvature. Like Venus and Clover, T-Sapphire contains an Alanine in position 206, enabling it to dimerize. Additionally, T-Sapphire is a fast folding mutant of GFP (Zapata-Hommer & Griesbeck, 2003). Fast folding of the fluorophore might lead to the misfolding of the RLK moiety and accumulation of aggregated, misfolded fusion proteins in specific membrane or cytoplasmic regions.

mCherry, mScarlet, mRuby2, mRuby3, mTurquoise2, and mCerulean3 fusions typically showed a weak fluorescence in the vacuole of expressing cells. This could be a sign of protein recycling or storage in the vacuole and is likely a general property of all fluorophores. As these fluorescent proteins have a low pKa (≤5.3), they are still fluorescent at the slightly acidic vacuolar pH (5.5–6), at which eGFP fluorescence at 488nm is largely quenched (Haupts, Maiti, Schwille, & Webb, 1998; Martinière et al., 2013). These less pH-sensitive fluorophores may be useful to study proteins targeted to acidic compartments such as the lytic vacuole or apoplasm.

3.4 | Fluorophore sensitivity to photobleaching

Energy transfer from the donor fluorophore to the acceptor is impaired by bleaching of the latter. While this is the leveraged

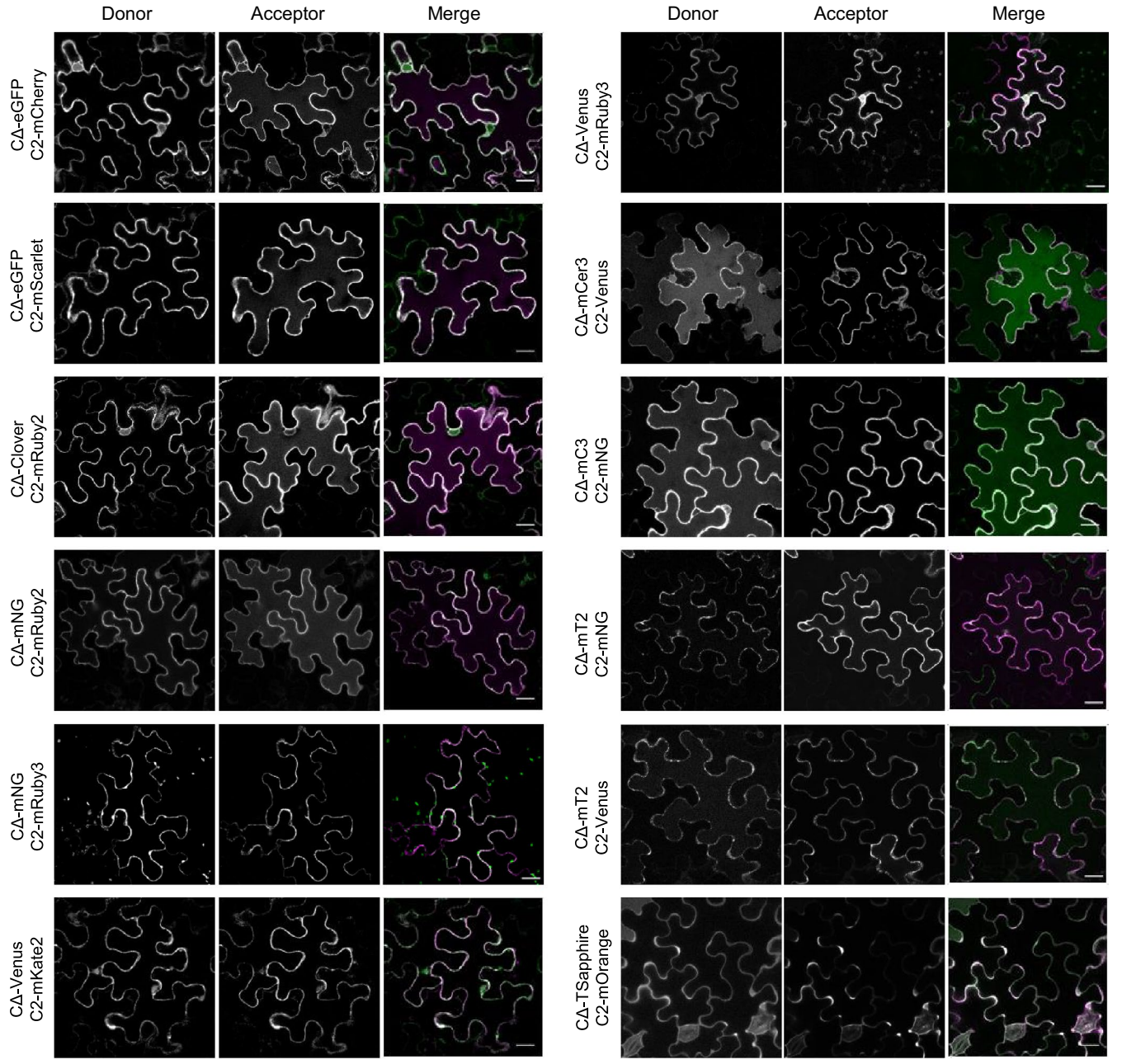

FIGURE 2 Subcellular localization of the RLK-fluorophore fusion proteins. Confocal microscopy of Benthamiana cells co-expressing CRNΔKi-donor (CΔ) and CLV2-acceptor (C2) fusion proteins. Both donor (left row) and acceptor (middle row) are shown as gray scale and in false colors in the merged images (right row; green: donor; magenta: acceptor). Scale bar: 25 µm. mNG: mNeonGreen; mCer3: mCerulean3; mT2: mTurquoise2

mechanism for FRET measurement in acceptor-photobleaching experiments, this can be a disadvantage in FLIM experiments as the measured lifetime will increase in correlation with acceptor bleaching. We therefore quantified acceptor photobleaching during a typical FLIM experiments (Figure 3a): In order to do this, we expressed only the acceptor fusion protein and recorded its fluorescence emission in a specific channel during excitation with the corresponding acceptor-excitation laser. We found mCherry to be the most stable of all red acceptors, with minimal fluorescence intensity loss by the end of the measurement. mScarlet, mRuby3, and mKate2 showed bleaching of about 20% of the initial signal, while mRuby2 and Venus were the most sensitive acceptors with about 25% of signal loss during the course of the acquisition. Surprisingly, mNeonGreen and mOrange appeared to be photoactivated by the 440 nm laser used for donor excitation, and their signal intensities increased by over 20% during the measurement. However, while this increase was steady for mNeonGreen, mOrange went through a first bleaching phase before its fluorescence sharply increased.

Donor photobleaching during lifetime acquisition decreases the signal-to-noise ratio over time, impacting the quality of the data. Additionally, as bleaching can occur before the relaxation of the

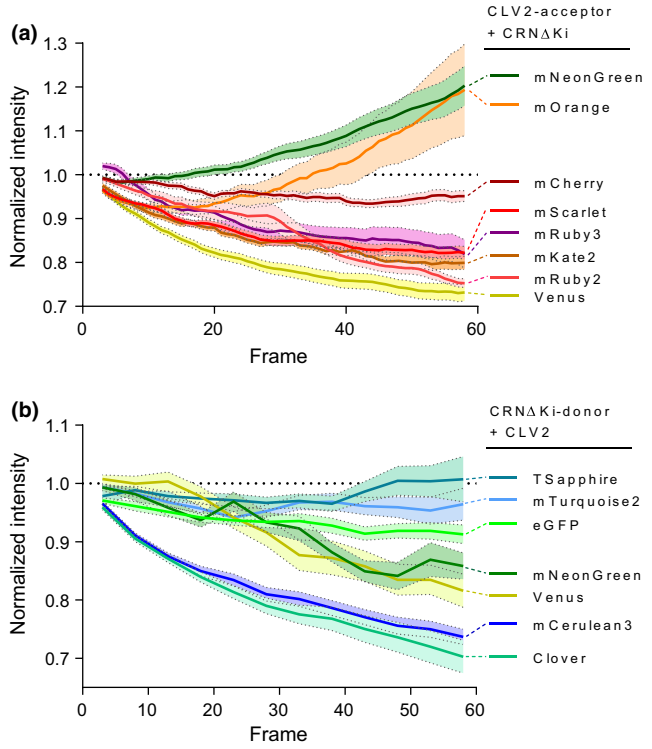

FIGURE 3 Photobleaching effect during lifetime acquisition. Acceptor (a) and donor (b) photobleaching during lifetime measurement in the absence of their FRET partner. Running average fluorescence intensity of 10 samples was calculated over 5 frames (plain lines). Running standard error of the means is represented as colored areas between dotted lines. Fluorophores are indicated on the right, connected to their final value by a dotted line. Intensity was normalized to that of the first frame

fluorophore and therefore before the emission of a photon, this can artificially decrease the apparent lifetime. We therefore examined donor bleaching over time during lifetime acquisition (Figure 3b). Among the blue-spectral range donors, mTurquoise 2 was very stable (<5% bleaching), while mCerulean3 showed continuous bleaching over the course of acquisition. For the green and yellow donors, T-Sapphire was the most stable with barely any bleaching over the course of the acquisition. eGFP was relatively stable with less than 10% bleaching, mNeonGreen, and Venus showed mild bleaching of about 15% of the initial fluorescence, while Clover bleached rapidly down to about 40% of the initial fluorescence. Because of their instability, mCerulean3 and Clover should therefore be avoided as donors for FLIM experiments.

3.5 | Auto-fluorescence background

Plant cells contain numerous compounds such as chlorophyll and phenols that give strong auto-fluorescence in the red and blue range, respectively. As these compounds' fluorescence lifetime is typically very short, these can lower the apparent lifetime of the sample when their signal is too strong in the donor channels.

We therefore measured fluorescence background of mock-infiltrated Nicotiana for all the different laser and filter combinations that we used (Figure 4). The setups used for the acquisition of green-red and yellow-red pairs yielded the least background fluorescence, typically one order of magnitude lower than a typical fluorophore measurement. Setups used for the acquisition of the blue-range donors yielded more variable fluorescence, which was in some rare cases in the order of magnitude of a typical fluorophore measurement. Auto-fluorescence originated from the cell wall in these cases and was therefore spatially confounded with the fluorophore signal. Similarly, the setup used for the acquisition of T-Sapphire yielded a relatively high background in comparison with a typical fluorophore measurement, representing around one third of the signal. Nevertheless, auto-fluorescence giving rise to very short lifetime can be filtered out using post-acquisition data filtering (Antonik, Felekyan, Gaiduk, & Seidel, 2006).

3.6 | Acceptor bleed-through effect

As the signal collected in the donor channels does not discriminate between donor- and acceptor-emitted photons, it is crucial to determine whether the acceptor-emitted light is able to reach the donor's channel detectors, albeit the presence of a wavelength-specific band-pass filter. We therefore expressed untagged CRNΔKi together with acceptor-tagged CLV2 and measured the number of photons collected in the corresponding donor channels (Figure 4). In almost all cases, the photon counts were similar to that of the background (mock-infiltrated Nicotiana). However, mOrange yielded a large photon count in the T-Sapphire channels when excited with the 440nm pulsed laser. As we used a 520/35 band-pass filter before the single photon detectors of the donor channels, mOrange signal should have been intercepted. Although a green-range fluorescence state was never described for mOrange, it is possible that when excited with indigo light, mOrange fluoresces in a green state as described for DsRed, from which mOrange derives (Baird, Zacharias, & Tsien, 2000).

3.7 | Comparison of fluorophore pairs for FRET efficiency

We next compared the FRET efficiency of the different fluorophore pairs. Therefore, fluorescence decay of the donor was quantified in Nicotiana epidermis cells transiently expressing either CRNΔKi-donor and CLV2-acceptor or CRNΔKi-donor and untagged CLV2 (donor only) with picosecond resolution. We then eliminated background and ER signals by setting a photon minimum count threshold and manually excluding ER and chloroplast-containing regions in order to enrich our samples in PM-localized fluorescence. Fluorescence decays can be well-described by multi-exponential models which allow to extract fluorescence lifetime (τ) as a model's parameter (Berezin & Achilefu, 2010). As multi-exponential models yield several lifetime components, these need to be weighted and averaged to extract a single τ per sample. For this, each decay

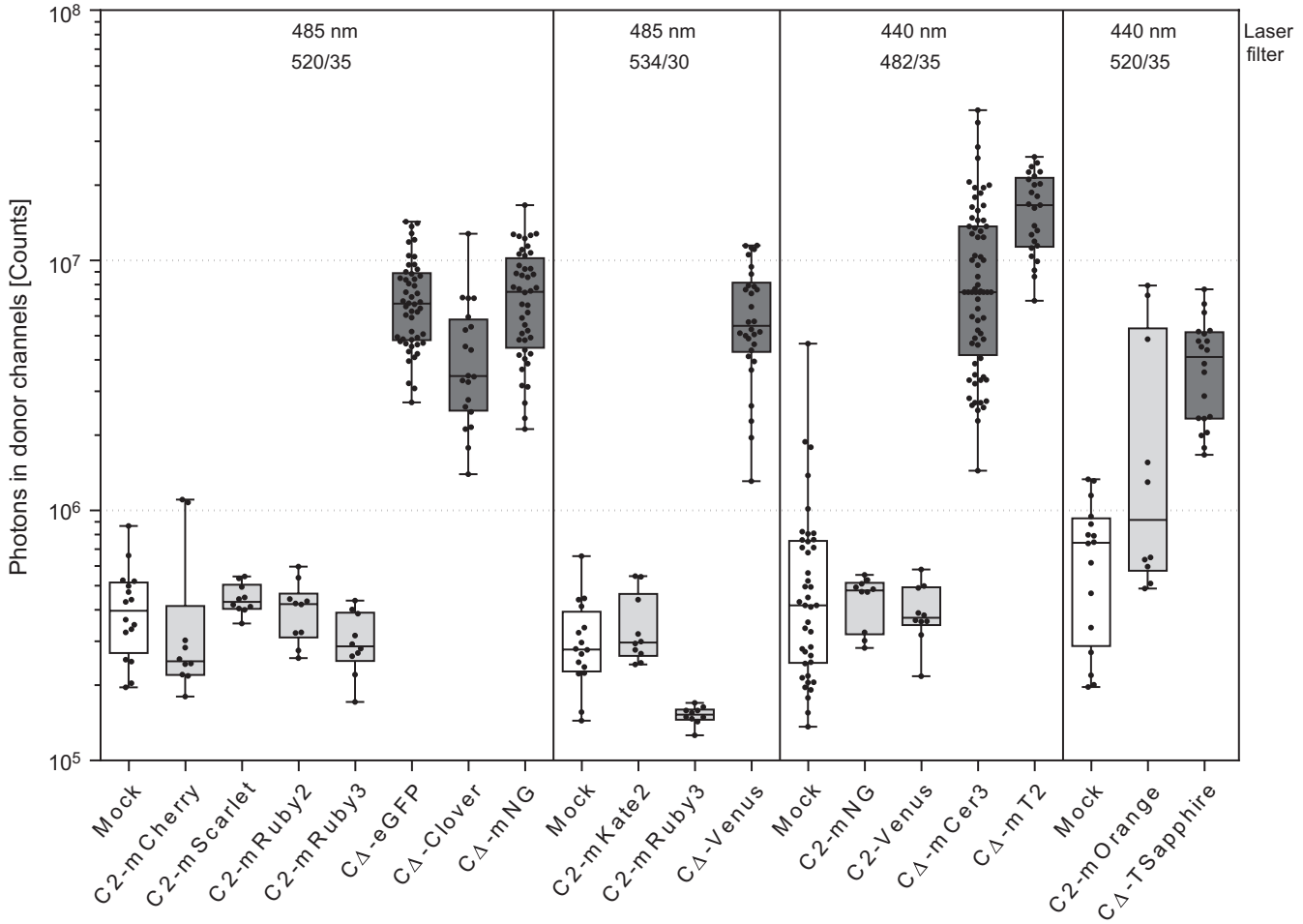

FIGURE 4 Background and bleed-through controls for the different FRET pairs tested. For each different microscope settings (Laser wavelength and band-pass filter indicated on top of each section), we measured the intensity of the fluorescent background of mock-infiltrated plants (white) and the emission of the CLV2-acceptor constructs in the acceptor channels (light gray). Data are represented in comparison with the fluorescence intensity of representative CRNΔKi-donor only constructs (dark gray). Total amount of photons collected are displayed as a log scale

component's τ is weighted by its contribution to the decay's amplitude. Most donor-only samples could be fitted with a single exponential model to the exception of mCerulean3 and T-Sapphire, which required a bi- and tri-exponential model, respectively. Apart from the T-Sapphire-mOrange FRET pair, which required a tri-exponential model, all FRET pair decays could be fitted with a bi-exponential model. FRET efficiency can then be determined as a measure of the reduction in the donor's lifetime in the presence of an acceptor in comparison with donor-only samples. FRET efficiency is typically expressed in percent, with 0% representing the absence of lifetime reduction and 100% representing total quenching of the donor's fluorescence.

In order to ensure that lifetime reduction was due to interaction between CRNΔKi and CLV2 and not a consequence of the presence of a large concentration of acceptor surrounding the donor fluorophore at the plasmamembrane, we co-expressed CRNΔKi-eGFP, CLV2-untagged, and a myristoylated version of mCherry (myr-mCherry) anchored in the PM (Turnbull & Hemsley, 2017). CRNΔKi-eGFP and myr-mCherry largely co-localized (Figure S2). Although the ratio of eGFP to mCherry signal was in the same order of magnitude for the myr-mCherry construct as for the previously described CLV2-mCherry constructs (Figure S1 and Figure 1), eGFP fluorescence lifetime was not significantly reduced (Figure 5b), indicating that the mere presence of the acceptor at the membrane is not sufficient to quench the donor. Lifetime reduction is therefore a consequence of protein–protein interaction.

We therefore proceeded to determine the FRET efficiency of our candidate FRET pairs (Figure 5). Surprisingly, we failed to detect any significant FRET between Clover and mRuby2, although this was described as an efficient pair in mammalian cells (Lam et al., 2012). For mCerulean3, we encountered difficulties to consistently fit lifetime (Figure S2; RSD of 14%), and the average lifetime value we determined (2.9 ns) is inconsistent with the theoretical value of (4.1 ns). Because of the considerable bleed-through of mOrange in the donor channel of T-Sapphire, the inconsistent localization of both fluorophores, and the high variation of T-Sapphire lifetime between experiments (Figure S2; RSD of 22%), we decided to leave the T-Sapphire-mOrange FRET pair out of our lifetime analysis. They

TABLE 2 Summary of the FRET pairs examined

FRET pair			Donor lifetime		Fitting model (*N* exponentials)		FRET efficiency (mean ± *SD*)	Bleaching (mean ± *SD*)		Acceptor bleedthrough[c] (mean ± *SD*)	Background[c] (mean ± *SD*)
Donor	Acceptor	Localization	mean ± *SD* [ns]	RSD[a]	Donor only	FRET pair		Donor	Acceptor[b]		
eGFP	mCherry	PM/ ER	2.61 ± 0.07	3%	1	2	14.1 ± 5.7%	9 ± 11%	5 ± 9%	5 ± 4%	6 ± 2%
	mScarlet	PM/ ER				2	6.1 ± 2.7%		18 ± 10%	6 ± 1%	
Clover	mRuby2	PM/ ER	2.93 ± 0.13	4%	1	2	3.2 ± 4.7%	30 ± 20%	25 ± 7%	8 ± 2%	9 ± 4%
mNeonGreen	mRuby2	PM/ ER	2.88 ± 0.07	2%	1	2	5.8 ± 3.9%	14 ± 16%	25 ± 7%	5 ± 1%	6 ± 2%
	mRuby3	PM/ ER				2	7.7 ± 3.1%		18 ± 23%	4 ± 1%	
Venus	mKate2	PM/ ER	2.86 ± 0.06	1%	1	2	10.9 ± 3%	18 ± 20%	21 ± 11%	5 ± 2%	5 ± 2%
	mRuby3	PM/ ER				2	14.4 ± 6.3%		18 ± 23%	2 ± 0%	
mCerulean3	mNeonGreen	PM/ ER	2.86 ± 0.39	14%	2	2	13.2 ± 8.8%	26 ± 9%	−20 ± 32%	4 ± 1%	6 ± 7%
	Venus	PM/ ER				2	12 ± 10.3%		27 ± 14%	3 ± 1%	
mTurquoise2	mNeonGreen	PM/ ER	3.91 ± 0.04	1%	2	2	14.1 ± 11.1%	4 ± 19%	−20 ± 32%	2 ± 1%	4 ± 5%
	Venus	PM/ ER				2	16.25 ± 8.8%		27 ± 14%	2 ± 1%	
T-Sapphire	mOrange	PM/ Cytoplasm	2.15 ± 0.47	22%	2	2	N.D.	0 ± 23%	−19 ± 74%	55 ± 64%	17 ± 10%

[a]Relative standard deviation.

[b]Negative values indicate an increase of fluorescence.

[c]Given in percent of the mean donor intensity.

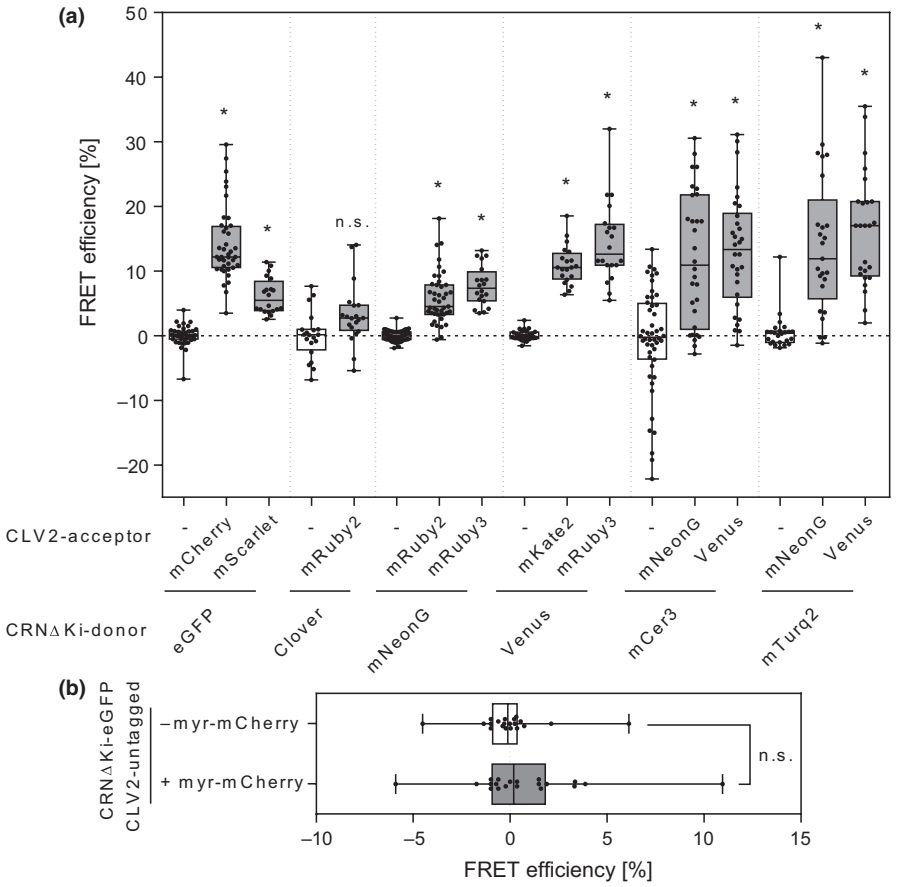

FIGURE 5 FRET efficiencies of the different FRET pairs tested. FRET efficiencies of the donor-only samples (white) and FRET pairs (gray) for CLV2 and CRNΔKi fusion proteins (a) or CRNΔKi-eGFP and plama membrane-localized myr-mCherry control (b). FRET efficiencies were calculated as a normalized measure of the donor's lifetime reduction. mNeonG: mNeonGreen; mCer3: mCerulean3; mTurq2: mTurquoise2; myr: myristoylation. Asterisks in A indicate that the sample mean is significantly different to the donor only mean (*; Holm-Sidak corrected $p < .01$; $N \geq 20$). Absence of difference between the two populations in B was determined by Student's *t* test ($p > .1$; $N = 20$)

were, however, described as a well-performing FRET pair to measure interaction between a transmembrane and a cytosolic protein in another report (Bayle et al., 2008). However, in this report, T-Sapphire was fused to a soluble protein, and it is possible that fusion of T-Sapphire to transmembrane proteins results in misfolding or mislocalization. Importantly, the previously described eGFP-mCherry combination was one of the best performing pairs, confirming its status of reference FRET pair for plant experiments. However, combination of Venus with either mKate2 or mRuby3 and using mCerulean3 or mTurquoise2 as donors for either mNeonGreen or Venus yielded comparable FRET efficiencies. The recently described mNeonGreen-mRuby2 and eGFP-mScarlet pair (Bindels et al., 2017; Shaner et al., 2013) yielded measurable FRET, although lower than the eGFP-mCherry pair. mNeonGreen performed significantly better as a donor for mRuby3.

4 | DISCUSSION

4.1 | Improved FRET measurement from T-DNA stacking

FRET measurements require the presence of both donor and acceptor in the same cell, and efficiency is partially dependent on acceptor-to-donor ratios. As both these factors are highly variable when co-infiltrating donor and acceptor constructs in Nicotiana, we used the GreenGate system (Lampropoulos et al., 2013) to conveniently create a large number of constructs allowing inducible co-expression of donors and acceptors from single T-DNAs, respectively. As previously reported for a similar Gateway-based system (Hecker et al., 2015), this resulted in a drastic increase in co-expression rate and a decrease in donor-to-acceptor ratio variability. Additionally, the use of the GreenGate system allows to easily change expression driver (inducible or constitutive, weak or strong), fluorescent tag, and fusion orientation, providing a flexibility unmatched by Gateway-based systems. The ability to freely vary these parameters can be leveraged to increase measurements robustness and sensitivity, and time-efficiency of FRET-FLIM experiments. It should be noted however, that for proteins with highly different maturation times, turnover, and/or stability, inducing protein expression at different times might be favorable over this simultaneous co-expression system.

4.2 | Comparison of fluorophore suitability in fusion to RLKs

The optimal fluorophore combination to measure FRET is dependent on the fusion proteins, and therefore, several combinations could be tried using the present study as a starting point. Fusion protein folding, stability, and activity may be improved by adding amino acid linker sequences of various lengths and composition between the protein of interest and the fluorophore moiety. It is necessary prior

for a FRET experiment to verify that the fusion proteins localize properly and are functional.

In addition to the specific protein fusion behaviors, individual fluorophores exhibit different properties, which should be carefully considered before selecting a protein fusion. One point of particular importance for membrane proteins transiting through the ER is to avoid the use of fluorescent proteins that can self-interact, forming oligomers. As membrane proteins are stacked in a single plane, they can reach high local concentration in over-expression situations. In conjunction with weakly self-interacting fluorophores, this can lead to the formation of oligomers that convert the ER tubular network into organized smooth ER (Costantini, Fossati, Francolini, & Snapp, 2012; Snapp et al., 2003). For this reason, monomeric variants such as mEGFP, mVenus, or mClover3 should be preferred. It is also important to confirm that the fusion protein correctly localizes, since some fluorophore fusions can prevent proper folding of their cargo and lead to non-functional and/or mislocalized proteins. For this reason, we decided to exclude the T-Sapphire-mOrange pair from our lifetime analysis, although they were shown to perform well for soluble proteins (Bayle et al., 2008). Another aspect to be evaluated for individual fluorophores is their signal-to-noise ratio in the cellular context. Imaging of blue-range donors typically yields high cell-wall fluorescence and very bright fluorophores have to be employed to minimize interference from auto-fluorescence. mCerulean3 and mTurquoise2 typically yielded a very bright signal, which counterbalanced the background. It is to note that mTurquoise2 was significantly brighter than mCerulean3 and can therefore be considered a more suitable donor fluorophore for plasmamembrane-localized proteins (Goedhart et al., 2012). Similarly, fluorophores emitting in the far-red spectral range should not be selected for experiments in photosynthetic tissues.

Lifetime determination from the fluorescence decay requires a high photon budget; however, as photons are accumulated over several frames weak fluorescence signal can be balanced out by longer acquisition provided that: (a) Fluorophores are photostable; (b) background fluorescence is an order of magnitude lower than the signal, or can be filtered out during downstream analysis (Antonik et al., 2006); (c) the proteins of interest are slow diffusing; and (d) the tissues of interest do not present significant growth during the measurement.

4.3 | Comparison of FRET pairs quality

In this work we compared the FRET performances of 12 different FRET pairs (Table 2). T-Sapphire and mOrange resulted in mislocalization of the fusion proteins. Additionally, mOrange emission can affect the detection of T-Sapphire emission, leading to a bias in T-Sapphire lifetime determination and should therefore be avoided. Clover and mCerulean3 photobleached significantly during lifetime acquisition; furthermore, we failed to detect FRET between Clover and mRuby2. Therefore, using mCerulean3 and Clover should also be avoided. On the other side, we measured FRET between several other pairs. mScarlet did not perform and mCherry as an acceptor for eGFP. The eGFP-mCherry pair is preferable when using eGFP as a donor, especially since there is now a considerable amount of literature using this FRET pair. Several good alternatives to this pair exist: (a) Venus can serve as an excellent donor for both mKate2 and mRuby3, where mRuby3 yields a higher FRET efficiency; (b) mTurquoise2 can be employed as an efficient donor for both mNeonGreen and Venus. mNeonGreen is less sensitive to photobleaching than Venus and will therefore be preferred, although this effect is marginal on FRET efficiency. mNeonGreen gave a reliable FRET as a donor for mRuby3, although yields a lower efficiency than the abovementioned pairs.

There are several newer and more performant versions of some of the fluorophores we tested here that could further increase FRET performances in plant systems. For example, SYFP2 was described to be a brighter variant of Venus which was successfully applied for FLIM measurement of plant transcription factors (Kremers, Goedhart, Munster, & Gadella, 2006; Long et al., 2018). Likewise, mClover3 is a more stable variant of Clover that may display better characteristics than its ancestor in plant FRET experiments (Bajar, Wang, Lam, et al., 2016).

While most FRET applications look at interactions between two partners, a few recent publications pushed this boundary to investigate interactions between three or even four partners within RLK complexes (Breda et al., 2019; Gloeckner et al., 2019). These studies rely on the measurement of competitive interactions or the direct measurement of three-fluorophore FRET-FLIM, both using combinations of three different fluorophores forming overlapping FRET pairs. In the present study, we identify two such combinations—namely mTurquoise2-mNeonGreen-mRuby3 and mTurquoise2-Venus-mRuby3—that could further improve these new applications.

ACKNOWLEDGMENTS

The work of all authors was supported by the DFG through CRC1208. We wish to thank R. Burkart and A. Bleckmann for sharing unpublished plasmids, and Y. Stahl and M. Somssich for useful discussion. Clover-mRuby2-FRET-10 was a gift from Michael Davidson (Addgene plasmid # 58169; http://n2t.net/addgene:58169; RRID: Addgene_58169).

CONFLICT OF INTEREST

The authors declare no conflict of interest associated with the work described in this manuscript.

AUTHORS CONTRIBUTIONS

GD conceived the project and designed the experiments with input from all authors. GD prepared the figures and wrote the manuscript with the help of RS. GD and PS created expression vectors and performed measurements. GD, PS, and SH analyzed the data. SH and SWP provided critical help with lifetime measurement and analysis. All authors discussed the results and commented on the manuscript.

DATA AVAILABILITY STATEMENT

Plasmids listed in Table S3 are available from Addgene (77188). All other materials are available upon request.

REFERENCES

Albertazzi, L., Arosio, D., Marchetti, L., Ricci, F., & Beltram, F. (2009). Quantitative FRET analysis with the EGFP-mCherry fluorescent protein pair. *Photochemistry and Photobiology*, *85*, 287–297.

Antonik, M., Felekyan, S., Gaiduk, A., & Seidel, C. A. M. (2006). Separating structural heterogeneities from stochastic variations in fluorescence resonance energy transfer distributions via photon distribution analysis. *The Journal of Physical Chemistry B*, *110*, 6970–6978. https://doi.org/10.1021/jp057257+

Baird, G. S., Zacharias, D. A., & Tsien, R. Y. (2000). Biochemistry, mutagenesis, and oligomerization of DsRed, a red fluorescent protein from coral. *Proceedings of the National Academy of Sciences of the United States of America*, *97*, 11984–11989. https://doi.org/10.1073/pnas.97.22.11984

Bajar, B. T., Wang, E. S., Lam, A. J., Kim, B. B., Jacobs, C. L., Howe, E. S., … Chu, J. (2016). Improving brightness and photostability of green and red fluorescent proteins for live cell imaging and FRET reporting. *Scientific Reports*, *6*, 20889. https://doi.org/10.1038/srep20889

Bajar, B. T., Wang, E. S., Zhang, S., Lin, M. Z., & Chu, J. (2016). A guide to fluorescent protein FRET pairs. *Sensors Basel Sensors*, *16*(9), e1488. https://doi.org/10.3390/s16091488

Bayle, V., Nussaume, L., & Bhat, R. A. (2008). Combination of novel green fluorescent protein mutant TSapphire and DsRed variant mOrange to set up a versatile in planta FRET-FLIM assay. *Plant Physiology*, *148*, 51–60. https://doi.org/10.1104/pp.108.117358

Berezin, M. Y., & Achilefu, S. (2010). Fluorescence lifetime measurements and biological imaging. *Chemical Reviews*, *110*, 2641–2684. https://doi.org/10.1021/cr900343z

Bindels, D. S., Haarbosch, L., van Weeren, L., Postma, M., Wiese, K. E., Mastop, M., … Gadella, T. W. J. (2017). mScarlet: A bright monomeric red fluorescent protein for cellular imaging. *Nature Methods*, *14*, 53–56. https://doi.org/10.1038/nmeth.4074

Bleckmann, A., Weidtkamp-Peters, S., Seidel, C. A. M., & Simon, R. (2010). Stem cell signaling in Arabidopsis requires CRN to localize CLV2 to the plasma membrane. *Plant Physiology*, *152*, 166–176. https://doi.org/10.1104/pp.109.149930

Breda, A. S., Hazak, O., Schultz, P., Anne, P., Graeff, M., Simon, R., & Hardtke, C. S. (2019). A cellular insulator against CLE45 peptide signaling. *Current Biology*, *29*(15), 2501–2508. https://doi.org/10.1016/j.cub.2019.06.037

Bücherl, C. A., Jarsch, I. K., Schudoma, C., Segonzac, C., Mbengue, M., Robatzek, S., … Zipfel, C. (2017). Plant immune and growth receptors share common signalling components but localise to distinct plasma membrane nanodomains. *eLife*, *6*, e25411. https://doi.org/10.7554/eLife.25114

Clegg, R. M. (2006). The history of fret. In C. D. Geddes, & J. R. Lakowicz (Eds.), *Reviews in fluorescence 2006* (pp. 1–45). Boston, MA: Springer.

Costantini, L. M., Fossati, M., Francolini, M., & Snapp, E. L. (2012). Assessing the tendency of fluorescent proteins to oligomerize under physiologic conditions. *Traffic*, *13*, 643–649. https://doi.org/10.1111/j.1600-0854.2012.01336.x

Fábián, Á. I., Rente, T., Szöllosi, J., Mátyus, L., & Jenei, A. (2010). Strength in numbers: Effects of acceptor abundance on FRET efficiency. *ChemPhysChem*, *11*, 3713–3721. https://doi.org/10.1002/cphc.201000568

Ferrero, S., Grados-Torrez, R. E., Leivar, P., Antolín-Llovera, M., López-Iglesias, C., Cortadellas, N., … Campos, N. (2015). Proliferation and morphogenesis of the endoplasmic reticulum driven by the membrane domain of 3-Hydroxy-3-Methylglutaryl Coenzyme A reductase in plant cells. *Plant Physiology*, *168*, 899–914. https://doi.org/10.1104/pp.15.00597

Förster, T. (1946). Energiewanderung und fluoreszenz. *Naturwissenschaften*, *33*, 166–175. https://doi.org/10.1007/BF00585226

Gloeckner, N., zur Oven-Krockhaus, S., Wackenhut, F., Burmeister, M., Wanke, F., Holzwart, E., … Harter, K. (2019). Three-fluorophore FRET-FLIM enables the study of trimeric protein interactions and complex formation with nanoscale resolution in living plant cells. *BioRxiv*, https://doi.org/10.1101/722124

Goedhart, J., von Stetten, D., Noirclerc-Savoye, M., Lelimousin, M., Joosen, L., Hink, M. A., … Royant, A. (2012). Structure-guided evolution of cyan fluorescent proteins towards a quantum yield of 93%. *Nature Communications*, *3*, 751. https://doi.org/10.1038/ncomms1738

Haupts, U., Maiti, S., Schwille, P., & Webb, W. W. (1998). Dynamics of fluorescence fluctuations in green fluorescent protein observed by fluorescence correlation spectroscopy. *Proceedings of the National Academy of Sciences of the United States of America*, *95*, 13573–13578. https://doi.org/10.1073/pnas.95.23.13573

Hecker, A., Wallmeroth, N., Peter, S., Blatt, M. R., Harter, K., & Grefen, C. (2015). Binary 2in1 vectors improve in planta (co)localization and dynamic protein interaction studies. *Plant Physiology*, *168*, 776–787. https://doi.org/10.1104/pp.15.00533

Kanchiswamy, C. N., Malnoy, M., Occhipinti, A., & Maffei, M. E. (2014). Calcium imaging perspectives in plants. *International Journal of Molecular Sciences*, *15*, 3842–3859. https://doi.org/10.3390/ijms15033842

Kinoshita, A., Betsuyaku, S., Osakabe, Y., Mizuno, S., Nagawa, S., Stahl, Y., … Sawa, S. (2010). RPK2 is an essential receptor-like kinase that transmits the CLV3 signal in Arabidopsis. *Development*, *137*, 3911–3920. https://doi.org/10.1242/dev.048199

Kremers, G.-J., Goedhart, J., van Munster, E. B., & Gadella, T. W. J. (2006). Cyan and yellow super fluorescent proteins with improved brightness, protein folding, and FRET Förster radius. *Biochemistry*, *45*, 6570–6580.

Lam, A. J., St-Pierre, F., Gong, Y., Marshall, J. D., Cranfill, P. J., Baird, M. A., … Lin, M. Z. (2012). Improving FRET dynamic range with bright green and red fluorescent proteins. *Nature Methods*, *9*, 1005–1012. https://doi.org/10.1038/nmeth.2171

Lambert, T. J. (2019). FPbase: A community-editable fluorescent protein database. *Nature Methods*, *16*, 277–278. https://doi.org/10.1038/s41592-019-0352-8

Lampropoulos, A., Sutikovic, Z., Wenzl, C., Maegele, I., Lohmann, J. U., & Forner, J. (2013). GreenGate––a novel, versatile, and efficient cloning system for plant transgenesis. *PLoS ONE*, *8*, e83043. https://doi.org/10.1371/journal.pone.0083043

Lampugnani, E. R., Wink, R. H., Persson, S., & Somssich, M. (2018). The toolbox to study protein–protein interactions in plants. *Critical Reviews in Plant Sciences*, *37*(4), 308–334. https://doi.org/10.1080/07352689.2018.1500136

Li, X. (2011). Infiltration of Nicotiana benthamiana protocol for transient expression via agrobacterium. *Bio-Protocol*, *1*(14), e95. https://doi.org/10.21769/BioProtoc.95

Liebrand, T. W. H., van den Burg, H. A., & Joosten, M. H. A. J. (2014). Two for all: Receptor-associated kinases SOBIR1 and BAK1. *Trends in Plant Science*, *19*, 123–132. https://doi.org/10.1016/j.tplants.2013.10.003

Lissandron, V., Terrin, A., Collini, M., D'alfonso, L., Chirico, G., Pantano, S., & Zaccolo, M. (2005). Improvement of a FRET-based indicator for cAMP by linker design and stabilization of donor-acceptor interaction. *Journal of Molecular Biology*, *354*, 546–555. https://doi.org/10.1016/j.jmb.2005.09.089

Long, Y., Stahl, Y., Weidtkamp-Peters, S., Postma, M., Zhou, W., Goedhart, J., … Blilou, I. (2017). In vivo FRET-FLIM reveals cell-type-specific protein interactions in Arabidopsis roots. *Nature*, *548*, 97–102. https://doi.org/10.1038/nature23317

Long, Y., Stahl, Y., Weidtkamp-Peters, S., Smet, W., Du, Y., Gadella, T. W. J., … Blilou, I. (2018). Optimizing FRET-FLIM labeling conditions to detect nuclear protein interactions at native expression levels in

living arabidopsis roots. *Frontiers in Plant Science*, *9*, 639. https://doi.org/10.3389/fpls.2018.00639

Markwardt, M. L., Kremers, G.-J., Kraft, C. A., Ray, K., Cranfill, P. J. C., Wilson, K. A., … Rizzo, M. A. (2011). An improved cerulean fluorescent protein with enhanced brightness and reduced reversible photoswitching. *PLoS ONE*, *6*, e17896. https://doi.org/10.1371/journal.pone.0017896

Martinière, A., Bassil, E., Jublanc, E., Alcon, C., Reguera, M., Sentenac, H., … Paris, N. (2013). In vivo intracellular pH measurements in tobacco and Arabidopsis reveal an unexpected pH gradient in the endomembrane system. *The Plant Cell*, *25*, 4028–4043.

Mastop, M., Bindels, D. S., Shaner, N. C., Postma, M., Gadella, T. W. J., & Goedhart, J. (2017). Characterization of a spectrally diverse set of fluorescent proteins as FRET acceptors for mTurquoise2. *Scientific Reports*, *7*, 11999. https://doi.org/10.1038/s41598-017-12212-x

Norkunas, K., Harding, R., Dale, J., & Dugdale, B. (2018). Improving agroinfiltration-based transient gene expression in Nicotiana benthamiana. *Plant Methods*, *14*, 71. https://doi.org/10.1186/s13007-018-0343-2

Osad'ko, I. S. (2015). Dependence of FRET efficiency on distance in single donor-acceptor pairs. *The Journal of Chemical Physics*, *142*, 125102. https://doi.org/10.1063/1.4915279

Osakabe, Y., Yamaguchi-Shinozaki, K., Shinozaki, K., & Tran, L.-S.-P. (2013). Sensing the environment: Key roles of membrane-localized kinases in plant perception and response to abiotic stress. *Journal of Experimental Botany*, *64*, 445–458. https://doi.org/10.1093/jxb/ers354

Pietraszewska-Bogiel, A., & Gadella, T. W. J. (2011). FRET microscopy: From principle to routine technology in cell biology. *Journal of Microscopy*, *241*, 111–118. https://doi.org/10.1111/j.1365-2818.2010.03437.x

Rueden, C. T., Schindelin, J., Hiner, M. C., DeZonia, B. E., Walter, A. E., Arena, E. T., & Eliceiri, K. W. (2017). Image J2: ImageJ for the next generation of scientific image data. *BMC Bioinformatics*, *18*, 529. https://doi.org/10.1186/s12859-017-1934-z

Schindelin, J., Arganda-Carreras, I., Frise, E., Kaynig, V., Longair, M., Pietzsch, T., … Cardona, A. (2012). Fiji: An open-source platform for biological-image analysis. *Nature Methods*, *9*, 676–682. https://doi.org/10.1038/nmeth.2019

Shaner, N. C., Lambert, G. G., Chammas, A., Ni, Y., Cranfill, P. J., Baird, M. A., … Wang, J. (2013). A bright monomeric green fluorescent protein derived from Branchiostoma lanceolatum. *Nature Methods*, *10*, 407–409. https://doi.org/10.1038/nmeth.2413

Shcherbo, D., Murphy, C. S., Ermakova, G. V., Solovieva, E. A., Chepurnykh, T. V., Shcheglov, A. S., … Chudakov, D. M. (2009). Far-red fluorescent tags for protein imaging in living tissues. *The Biochemical Journal*, *418*, 567–574. https://doi.org/10.1042/BJ20081949

Snapp, E. L., Hegde, R. S., Francolini, M., Lombardo, F., Colombo, S., Pedrazzini, E., … Lippincott-Schwartz, J. (2003). Formation of stacked ER cisternae by low affinity protein interactions. *Journal of Cell Biology*, *163*, 257–269. https://doi.org/10.1083/jcb.200306020

Somssich, M., Bleckmann, A., & Simon, R. (2016). Shared and distinct functions of the pseudokinase CORYNE (CRN) in shoot and root stem cell maintenance of Arabidopsis. *Journal of Experimental Botany*, *67*, 4901–4915. https://doi.org/10.1093/jxb/erw207

Somssich, M., Ma, Q., Weidtkamp-Peters, S., Stahl, Y., Felekyan, S., Bleckmann, A., … Simon, R. (2015). Real-time dynamics of peptide ligand-dependent receptor complex formation in planta. *Science Signalling*, *8*, ra76. https://doi.org/10.1126/scisignal.aab0598

Somssich, M., & Simon, R. (2017). Studying protein-protein interactions in planta using advanced fluorescence microscopy. *Methods in Molecular Biology*, *1610*, 267–285.

Stryer, L., & Haugland, R. P. (1967). Energy transfer: A spectroscopic ruler. *Proceedings of the National Academy of Sciences of the United States of America*, *58*, 719–726. https://doi.org/10.1073/pnas.58.2.719

Turnbull, D., & Hemsley, P. A. (2017). Fats and function: Protein lipid modifications in plant cell signalling. *Current Opinion in Plant Biology*, *40*, 63–70. https://doi.org/10.1016/j.pbi.2017.07.007

van der Krogt, G. N. M. Ogink, J., Ponsioen, B., & Jalink, K. (2008). A comparison of donor-acceptor pairs for genetically encoded FRET sensors: Application to the Epac cAMP sensor as an example. *PLoS ONE*, *3*, e1916. https://doi.org/10.1371/journal.pone.0001916

Wan, W.-L., Fröhlich, K., Pruitt, R. N., Nürnberger, T., & Zhang, L. (2019). Plant cell surface immune receptor complex signaling. *Current Opinion in Plant Biology*, *50*, 18–28. https://doi.org/10.1016/j.pbi.2019.02.001

Weidtkamp-Peters, S., & Stahl, Y. (2017). The use of FRET/FLIM to study proteins interacting with plant receptor kinases. *Methods in Molecular Biology*, *1621*, 163–175.

Zacharias, D. A., Violin, J. D., Newton, A. C., & Tsien, R. Y. (2002). Partitioning of lipid-modified monomeric GFPs into membrane microdomains of live cells. *Science*, *296*, 913–916. https://doi.org/10.1126/science.1068539

Zapata-Hommer, O., & Griesbeck, O. (2003). Efficiently folding and circularly permuted variants of the Sapphire mutant of GFP. *BMC Biotechnology*, *3*, 5.

Zhu, Y., Wang, Y., Li, R., Song, X., Wang, Q., Huang, S., … Lin, J. (2010). Analysis of interactions among the CLAVATA3 receptors reveals a direct interaction between CLAVATA2 and CORYNE in Arabidopsis. *The Plant Journal*, *61*, 223–233. https://doi.org/10.1111/j.1365-313X.2009.04049.x

Zuo, J., Niu, Q.-W., Frugis, G., & Chua, N.-H. (2002). The WUSCHEL gene promotes vegetative-to-embryonic transition in Arabidopsis. *The Plant Journal*, *30*, 349–359. https://doi.org/10.1046/j.1365-313X.2002.01289.x

SUPPORTING INFORMATION

Additional supporting information may be found online in the Supporting Information section.

How to cite this article: Denay G, Schultz P, Hänsch S, Weidtkamp-Peters S, Simon R. Over the rainbow: A practical guide for fluorescent protein selection in plant FRET experiments. *Plant Direct*. 2019;3:1–14. https://doi.org/10.1002/pld3.189

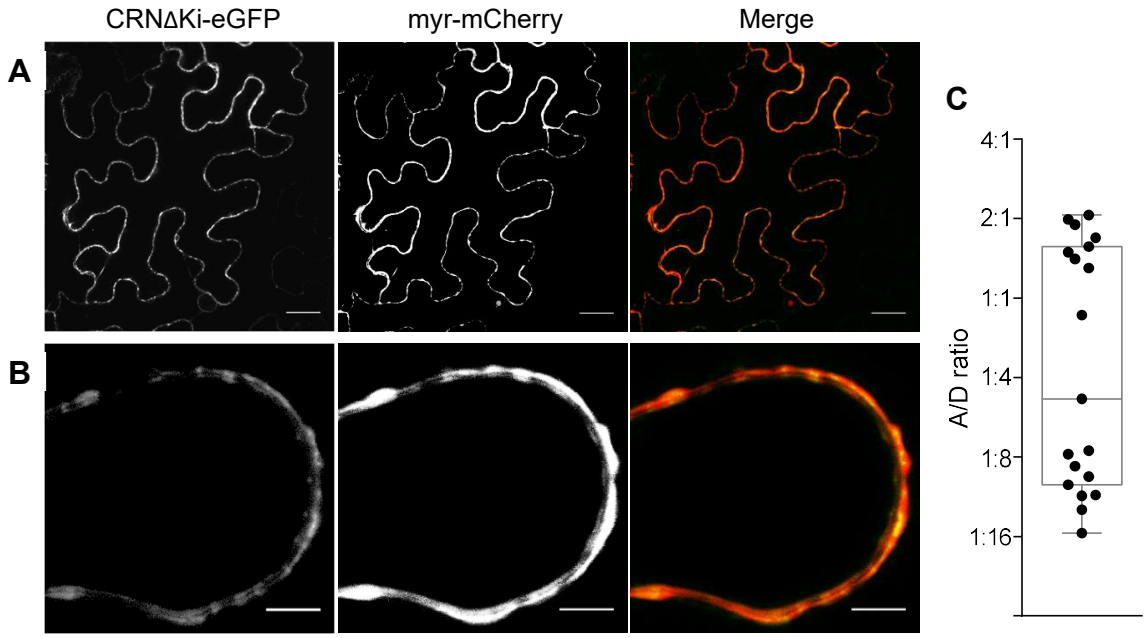

Supplementary figure 1. Myristoylated-mCherry co-localizes with CRNΔKi-eGFP. Confocal microscopy images of Benthamiana epidermis cells co-expressing CRNΔKi-eGFP (left), CLV2-untagged, and myr-mCherry (middle) constructs. False color merged image (right) shows co-localization of both eGFP and mCherry at the plasma-membrane (green: eGFP; red: mCherry) in whole cells (A) and in close-up of a membrane section (B). Scale bar: 25μm (top), 5μm (bottom) (C) Acceptor/Donor intensity ratios in the cells used for fluorescence lifetime measurement.

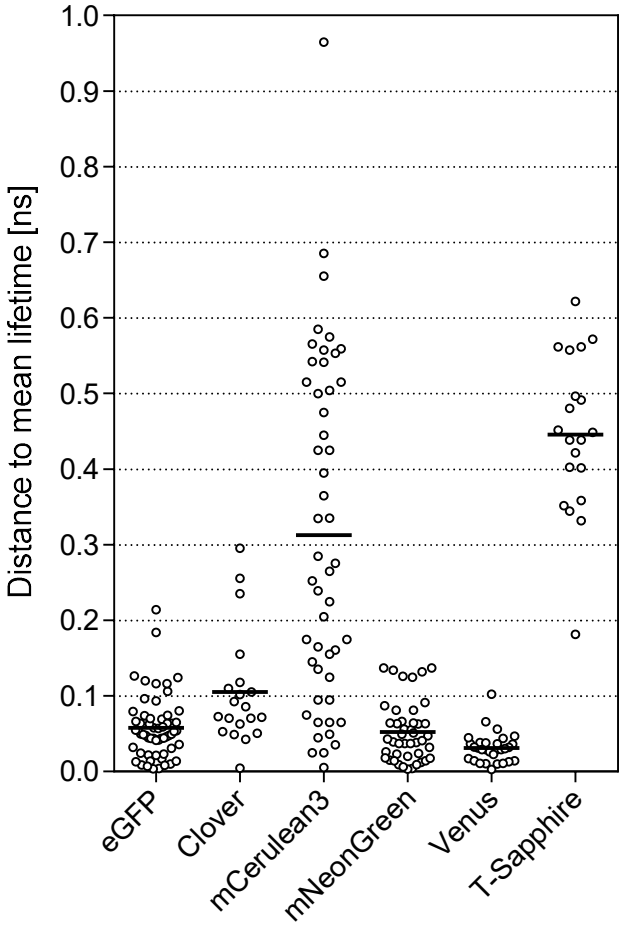

Supplementary figure 2. Lifetime stability for each donor.
Distance of the donor only samples from the population means. Each point represents an individual sample. Bars represent the mean distances.

Supplementary table 1. Oligonucleotides used in this study. [mC] indicates the presence of a 5-methyl-dCytosine.

Name	Target	Sequence
GG_XVE_F	XVE	AAAGGTCTCAGGCTATGAAAGCG
G_XVE_R	XVE	AAACACTGAGACTGTGGCAGGG
PW_XVE_3084_AT_R	XVE	GGAGCGCCAGACGAGTCCAATCATCAGGAT
PW_XVE_3084_TA_F	XVE	ATCCTGATGATTGGACTCGTCTGGCGCTCC
GG_EST_F	LexA-mini35S	AACAGGTCTCAACCTTGCATGCCAGCTTGGGCTGCAGGTCGAGGCT
GG_EST_R	LexA-mini35S	AACAGGTCTCTTGTTCTTCAGCGTGTCCTCTCCAAATGAAATGAA
PS-GG-CDS-Clv2-F	CLV2	AAAGGTCTCAGGCTTAATGATAAAGATTGCAG
PS-GG-CDS-Clv2-R	CLV2	TTTGGTCTCACTGAGAAAGCTGGGTAAG
oGD335	CRNΔKi	AAAGGTCTCAGGCTTAATGAAGCAAAGAAGAAGAAG
oGD336	CRNΔKi	AAAGGTCTCACTGATAACACCAAAGCTGAAACC
oGD339	myr	GGCTCTATGGGAAGAAGAAAAAGAAAACCTAAA
oGD340	myr	CTGATTTAGGTTTTCTTTTTCTTCTTCCCATAG
PW_GG_SV40ori_F	SV40ori	AAAGGTCTCAACTAGGTGTGGAAAGTCCCC
PW_GG_SV40ori_R	SV40ori	AAAGGTCTCAATACGGCCTCCAAAAAAGCC
oGD261	eGFP	AAAGGTCTCATCAGGCAGCGGCTCTGGATCG
oGD262	eGFP	ATAGGGCGAGAATTCGGTCTCAGC
oGD317	Clover, mCerulean3, Venus, T-Sapphire, mTurquoise2	AAAGGTCTCATGCAATGGTGAGCAAGGGCG
oGD318	Clover, mCerulean3, Venus, mOrange, T-Sapphire, mTurquoise2, mRuby3	AAAGGTCTCAGCAGTTACTTGTACAGCTCGTCCATGC
oGD315	D-TGCA linker	TCAGGCAGCGGCTCTGGATCGGCGGCCGC
oGD316	D-TGCA linker	TGCAGCGGCCGCCGATCCAGAGCCGCTGCC
oGD325	mRuby2, mRuby3	AAAGGTCTCATCAGGAATGGTGTCTAAGGGCGAAGAG
oGD326	mRuby2	AAAGGTCTCAGCAGTTACTTGTACAGCTCGTCCATCCC
oGD331	mOrange	TTGTACAAAGTGGTTGATGGG
oGD327	mOrange	AAAGGTCTCATCAGGAATGGTGAGCAAGGGCGAG
oGD343	mNeonGreen	AAAGGTCTCATGCAATGGTGAGCAAGGGAGAG
oGD344	mNeonGreen	AAAGGTCTCAGCAGTTACTTGTAAAGCTCGTCCATTC
RD_GG_mCherry_C-tag_F	mCherry	AAAGGTCTCATCAGCAATGGTGAGCAAGG
RD_GG_mCherry_C-tag_R	mCherry	AAAGGTCTCAGCAGTTACTTGTACAGCTCGTC
RD_GG_mScarlet_C-tag_R	mScarlet	AAAGGTCTCAGCAGTTACTTGTACAGCTC
RD_GG_mScarlet_C-tag_F	mScarlet	AAAGGTCTCATCAGTTATGGTGAGCAAG
RD_mKate2_GG_C-tag_R	mKate2	AAAGGTCTCAGCAGTTAGCGGTGAC
RD_mKate2_GG_C-tag_F	mKate2	AAAGGTCTCATCAGTTATGGTGTCGG
linker_AH_met_F	A-H methylated linker	ACCTACCTTGAGAC[mC]GAAAAGGTGGTCT[mC]A
linker_AH_met_R	A-H methylated linker	CCTATGAGAC[mC]ACCTTTTCGGTCT[mC]AAGGT
linker_HG_met_F	HG methylated linker	TAGGACCTTGAGAC[mC]GAAAAGGTGGTCT[mC]A
linker_HG_met_R	HG methylated linker	ATACTGAGAC[mC]ACCTTTTCGGTCT[mC]AAGGT

Supplementary table 2. Microscope configuration for each FRET pairs.

Donor	Acceptor	Donor Ex/Em peaks	Acceptor Ex/Em peaks	Excitation laser [nm]	Donor band-pass filter	Acceptor band-pass filter	Beamsplitter
eGFP	mCherry	488/507	587/610	485	520/35	607/70	LP560
eGFP	mScarlet	488/507	569/594	485	520/35	607/70	LP560
Clover	mRuby2	505/515	559/600	485	520/35	607/70	LP560
mNeonGreen	mRuby2	506/517	559/600	485	520/35	607/70	LP560
T-Sapphire	mOrange	399/511	548/562	440	520/35	607/70	LP560
Venus	mKate2	515/527	588/633	485	534/30	607/70	LP560
mCerulean3	Venus	433/475	515/527	440	482/35	534/30	LP510
mCerulean3	mNeonGreen	433/475	506/517	440	482/35	520/35	LP510
mTurquoise2	Venus	434/474	515/527	440	482/35	534/30	LP510
mTurquoise2	mNeonGreen	434/474	506/517	440	482/35	520/35	LP510
mNeonGreen	mRuby3	506/517	558/592	485	520/35	607/70	LP560
Venus	mRuby3	515/527	558/592	485	520/35	607/70	LP560

Supplementary table 3. Plasmids available from Addgene. All plasmids are suitable for use with the GreenGate kit (Lampropoulos et al., 2013).

Content	Reference	Backbone
Destination plasmid		
35S:XVE:tRBCS	pGD283	pGGZ001
Entry plasmids		
pLexA-mini35S	pBLAA001	pGGA000
myr	pGD318	pGGC000
eGFP	pGD165	pGGD000
Clover	pGD250	pGGD000
mCerulean3	pGD251	pGGD000
T-Sapphire	pGD252	pGGD000
mRuby2	pGD253	pGGD000
mOrange	pGD254	pGGD000
Venus	pGD255	pGGD000
mCherry	pRD53	pGGD000
mScarlet	pRD134	pGGD000
mKate2	pRD141	pGGD000
mNeonGreen	pGD352	pGGD000
mTurquoise2	pGD425	pGGD000
mRuby3	pGD431	pGGD000

Summary

CLAVATA family (CLVf) receptors are plasma membrane (PM)-located receptor-like kinases (RLKs) with key functions in various signaling pathways of *Arabidopsis thaliana*. CLVf receptors sense extracellular CLV3/EMBRYO SURROUNDING REGION-related (CLE) peptides by forming complexes with co-receptors and proteins like CLAVATA2 (CLV2) and CORYNE (CRN) at the PM. This study contributes to understand how CLE peptide signals are transmitted intracellularly after receptor activation at the PM. Furthermore, the study reveals mechanisms of pathway specificity explaining how the same set of CLVf receptors can mediate distinct signaling outputs in different cellular contexts.

Many RLK-based signaling pathways in plants are highly intertwined and cross-regulated. The review in the first chapter of this thesis presents recently reported principles that guarantee specific signaling within complex informational networks. Thereby, spatio-temporal receptor availability at the PM was identified as one of the main drivers for pathway specificity.

A major advance of this study is the identification of the receptor-like cytoplasmic kinase MAZZA (MAZ) and its homologs as novel interactors of CLVf receptors. MAZ is reversibly PM-associated and shares expression domains with the *CLVf* genes. Genetic analyses revealed that MAZ functions during root meristem development and stomatal patterning. The latter displays a novel place of action of the CLVf receptor pathways.

The study sheds light on the role of the CRN/CLV2 heteromer within root development. Previous reports demonstrated that CLE-triggered root meristem differentiation depends on CRN, which defines PM-localization of CLVf receptors. Tissue-specific *CRN* expression rescue assays in this study revealed that CRN can mediate the same developmental programs from distinct subdomains of the root meristem indicating non-cell-autonomous regulation.

Furthermore, the study comprises new insights how precisely balanced subcellular protein compositions affect CLVf receptor signaling. OCTOPUS (OPS) displays polar localization in developing phloem cells in the root, where it competitively interferes the interaction between CRN/CLV2 and the CLVf receptor BARELY ANY MERISTEM3 (BAM3). Thereby, OPS dampens the pathway dosage-dependently and locally defined, displaying a novel regulatory mechanism for specificity in CLVf receptor signaling.

To improve protein-protein interaction studies in future experiments, this thesis includes a guide for FRET pair selection with high performance at the PM of plant cells.

Together, the thesis comprises several novel concepts on CLVf receptor pathways regulation, signal fine-tuning, and signal transmission. This contributes to the overall understanding of RLK-based informational networks in plants.

Zusammenfassung

Rezeptoren der CLAVATA-Familie (CLVf) haben als Plasmamembran (PM)-lokalisierte Rezeptorkinasen Schlüsselrollen in verschiedenen Signalwegen von *Arabidopsis thaliana*. Durch die Bildung von Signalkomplexen an der PM nehmen CLVf-Rezeptoren zusammen mit Ko-Rezeptoren und weiteren Proteinen, wie CLAVATA2 (CLV2) und CORYNE (CRN), extrazelluläre Peptide der CLV3/EMBRYO SURROUNDING REGION-related (CLE)-Familie wahr. Wie die Signalübertragung nach Rezeptoraktivierung an der PM intrazellulär stattfindet, ist Gegenstand der vorliegenden Arbeit. Außerdem tragen die Studienergebnisse zum Verständnis der Spezifizität von CLVf-Signalwegen in verschiedenen funktionellen Zusammenhängen bei.

Ein aktueller Literaturüberblick verdeutlicht, dass einzelne Elemente pflanzlicher Signalwege teils in unterschiedlichen Signalkaskaden verschiedene Rollen übernehmen. Ein wichtiges Prinzip, um dennoch spezifische Signalantworten zu generieren, ist die dynamische räumliche und zeitliche Kontrolle der Verfügbarkeit von Rezeptoren an der PM.

Um Signalspezifizität im Zusammenhang von CLVf-Rezeptoren zu verstehen, ist die Kenntnis der beteiligten Proteine von zentraler Bedeutung. Im Rahmen der Arbeit wurden deshalb gezielt direkte Interaktionspartner der CLVf-Rezeptoren gesucht. Mit der Identifizierung und Charakterisierung der rezeptor-ähnlichen zytoplasmatischen Kinase MAZZA (MAZ) wurde ein wichtiger Beitrag zur Aufklärung der Signaltransduktion von CLVf-Rezeptoren geleistet. In diesem Zusammenhang konnte auch eine neue Rolle der CLVf-Rezeptoren im Bereich der Entwicklung von Stomata aufgezeigt werden.

Im Wurzelmeristem ist die Perzeption von CLE-Peptid abhängig von einem Heteromer aus CLV2 und CRN, welches vermutlich die PM-Lokalisation bestimmter CLVf-Rezeptoren reguliert. Über Rettungsexperimente von *crn*-Mutanten konnte in dieser Studie gezeigt werden, dass das Protein innerhalb verschiedener Subdomänen seiner nativen Expression zur Induktion der gleichen Signalantwort, nämlich meristematische Zelldifferenzierung, beitragen kann und dabei möglicherweise unterschiedliche CLVf-Rezeptoren beeinflusst.

Wie Signalspezifizität auch auf subzellulärer Ebene vermittelt werden kann, lässt sich innerhalb des sich entwickelnden Phloem-Gewebes beobachten. In der vorliegenden Studie konnte gezeigt werden, dass die Interaktion von CRN mit dem CLVf-Rezeptor BARELY ANY MERISTEM3 (BAM3) in Siebelementen im Übergang zur Differenzierung kompetitiv von

dem polar lokalisiertem Protein OCTOPUS (OPS) gestört wird. Dies stellt einen neuen Mechanismus einer lokalen negativen Regulierung von CLVf-Rezeptoren dar.

Außerdem wurden im Rahmen dieser Arbeit verschiedene Fluorophore bezüglich ihrer Eignung als FRET-Partner im Kontext von PM-lokalisierten Proteinen *in planta* getestet. Dies kann zukünftige Protein-Protein-Interaktionsstudien erleichtern und somit beispielsweise komplexe Signalwege der CLVf-Rezeptoren aufklären.

Insgesamt werden in der vorliegenden Arbeit wichtige neue Konzepte zur Signaltransduktion von CLVf-Rezeptoren vorgestellt. Die Arbeit trägt daher zum allgemeinen Verständnis von rezeptor-basierter Informationsweiterleitung in Pflanzen bei.

Danksagung

Ich möchte mich herzlich bei Prof. Rüdiger Simon für Alles bedanken. Es war eine sehr spannende, lehrreiche, schöne und humorvolle Zeit. Wer von uns den Humor hat, lasse ich jetzt mal offen. Für eine sichere Finanzierung, gute Kritik, offene Diskussionskultur und prägnante Emails bedanke ich mich sehr.

Lieber Prof. Georg Groth, herzlichen Dank für die Übernahme des Zweitgutachtens.

Danke an alle in der AG Simon und darüber hinaus für die gute Atmosphäre, meine Arbeit hätte ich in 3 Jahren fertigbekommen, aber ich wollte einfach nicht weg. Dabei muss ich und will ich natürlich vor allem Jenia nennen, danke für allen Gossip im Lab und unsere Freundschaft. Ich danke auch wirklich allen anderen momentanen und ehemaligen Kollegen aus AG Simon, Klein, Cai und Kollaborationen. Ich muss jetzt los zum Drucken (kein Spaß), deshalb kann ich euch nicht alle persönlich nennen, aber so ist es vielleicht fair, wenn ich jemand vergessen hätte. Ich werde euch ALLE vermissen!

Für einen allerherzlichsten Dank an meine Eltern, Kathrin und die Blümke-Gang muss natürlich noch Zeit sein. Danke, für all die Unterstützung, die man ja leicht als selbstverständlich hinnimmt, ist sie nicht! Danke, dass ihr bis zum Ende gehofft hat, dass diese Arbeit noch jemals fertig wird.

Meiner Frau Anika Danke ich ganz besonders. Das letzte Jahr der Arbeit, das ich länger gebraucht hab als du, widme ich deshalb auch nur dir :D. Ich liebe dich sehr.